Reciprocal regulation of the Fibroblast Growth Factor Receptor 2 (FGFR2) and the Transient Receptor Potential Ankyrin 1 (TRPA1) through their direct interaction

Eleni Kyriakopoulou

Submitted in accordance with the requirements for the degree of
Doctor of Philosophy

The University of Leeds
School of Molecular and Cellular Biology

November, 2019

The candidate confirms that the work submitted is his/her own, except where work which has formed part of jointly-authored publications has been included. The contribution of the candidate and the other authors to this work has been explicitly indicated below. The candidate confirms that appropriate credit has been given within the thesis where reference has been made to the work of others.

Acknowledgements

I would like to thank my supervisor Prof. Nikita Gamper for welcoming me to his group and providing guidance and support for the last 2.5 years of my PhD. I would also like to thank Dr. Zahra Timsah for giving me the opportunity to start this PhD project. Thank you to all past and present members of the Gamper group for their help and support, with a special thank you to Dr. Shihab Shah and Dr. Alexandra Hogea for training me in calcium imaging. I would also like to thank Dr. Steve Milne not only for his assistance in molecular cloning but also for organising the lab/reagents and being there for anything I needed regarding my experiments. Many thanks to Dr. Izzy Jayasinghe for her guidance during expansion microscopy experiments, Tom Sheard for demonstrating the expansion technique and Miriam Hurley for teaching me d-STORM. A special thank you to my friends Safi Masandi and Robert Walmsley for their daily support, intellectual input and company during the long hours of experiments. Of course, I could not forget to thank my best friends Chelsea Wood, Christian Sargent and David Scully for their support since we first met in 2014 in our Master's degree. Lastly, I would like to thank University of Leeds for funding this project.

Abstract

Tyrosine Kinase Receptors (RTKs) regulate fundamental cellular processes including cell proliferation, survival and invasion and thus, dysregulation of their activation is implicated in human malignancies. The canonical mechanism of activation is initiated by receptor activation through ligand-induced dimerization, and autophosphorylation of key tyrosine residues along the C-terminal cytoplasmic domain. It has been demonstrated in the past that FGFR2, an RTK, can dimerise in the absence of ligand resulting in signal activation or inhibition depending on the equilibrium of C-terminal-binding proteins i.e. GRB2 and PLCγ1. This study provided the first indication of a novel direct interaction between FGFR2 and a non-selective cation channel, TRPA1, through the C-terminal domain of FGFR2 and the Ankyrin repeat domain of TRPA1. The interaction was studied by protein interaction techniques in an overexpression system. The FGFR2-TRPA1 complex was also detected in a human lung adenocarcinoma cell line suggesting a possible implication in cancer.

The regulatory effect of TRPA1 on FGFR2 was also investigated. In basal conditions, the interaction with TRPA1 exhibits an inhibitory effect on FGFR2 autophosphorylation which results in downstream PLCγ1 pathway inhibition. Co-immunoprecipitation experiments revealed a decrease in PLCγ1 binding to FGFR2 in the presence of TRPA1 explaining the reduction in the PLCγ1 pathway activation. Upon stimulating conditions, TRPA1-mediated receptor inhibition is raised, as shown by increase in p-FGFR2 however, binding of PLCγ1 to the C-terminal of FGFR2 is still impeded. Finally, a model of TRPA1-mediated regulation of the FGFR2 signalling was proposed in which TRPA1 prevents aberrant basal stimulation of the receptor while maintaining PLCγ1 pathway inhibition even in the presence of ligand. These findings provided the first evidence of direct interaction between an RTK and a TRP channel as well as proposed a novel regulatory mechanism of FGFR2 signalling that can facilitate in the development of therapeutic strategies for FGFR2-related diseases.

Table of Contents

List of Tables

List of Figures

Abbreviations

AITC	allyl-isothiocyanate
ALCL	Anaplastic large cell lymphoma
ALCLs	Anaplastic large celllymphoma
ALK	Anaplastic lymphoma kinase
A-loop	activation-loop
ANKRA	Ankyrin Repeat family-A protein
AR	ankyrin repeat
ARD	ankyrin repeat domain
ASK1	apopostosis signal-related kinase
ATP	Adenosine triphosphate
BH	Bcl-2 homology domain
CA	cinnamaldehyde
Cbl	Casitas B-lineage Lymphoma
CHO	Chinese hamster ovarian cells
c-IAP-1	cellular inhibitor of apoptosis protein-1
CMML	chronic myelomonocytic leukemia
CMML	chronic myelomonocytic leukemia
CREB	cAMP response element-binding protein
DAG	diacylglycerol
DDR	Discoidin domain receptor
DRG	dorsal root ganglion
EGFR	Epidermal growth factor receptor
EML-4	echinoderm microtubule-associated protein-like 4
EMS	myeloproliferative syndrome
EMT	epithelial to mesenchymal transition
EPH	Ephrin receptor
ERK1/2	Extracellular Signal-regulated Kinase-1/2
EVH1	enabled/VASP homology 1 domain
FDA	Food and Drug administration
FGF	Fibroblast Growth Factor
FGFR	Fibroblast growth factor
FHA	fork-head associated
FLT3	FMS-like receptor tyrosine kinase-3
FOX	Forkhead box transcription factors
FRS2	FGFR2-related substrate 2

Gab1	Grb2-associted binding protein
GEF	guanine exchange factor
GIST	gastrointestinal stromal tumours
GRB2	Growth factor receptor-bound protein 2
GSK3β	Glycogen synthase kinase 3
GST	Glutathione S-transferase
GYF	glycine-tyrosine-phenylalanine domain
HEK293T	Human Embryonic Kidney cells
HSPC	Heparin Sulfate Proteoglycans
HSPC	heparin sulphate proteoglycan
HTH	helix-turn-helix
Ig	Immunoglobulin
IP3	Inositol 1,4,5-triphosphate
IR	insulin receptor
IRS	Insulin receptor substrate
LLR	Leucin-rich repeat
LUAD	lung adenocarcinoma
MAPK	mitogen-activated protein kinase
MARCKS	Myristoylated alanine-rich C-kinase substrate
mTORC1	mammalian target of rapamycin complex 1
MuSK	Muscle-Specific Kinase
NF	nucleal factor
NFAT	Nuclear factor of activated T-cells
NPM	nucleophosmin
NSCLC	non-small cell lung cancer
PDGFR	platelet-derived growth factor receptor
PH	plekstrin homology domain
PIP2	phospholipid phosphatidylinositol 4,5-biphosphate
PKA	protein kinase A
PKC	Protein Kinase C
PKD2	polycystic kidney disease-2
PLCγ1	Phospholipase C gamma 1
PPII	Polyproline II helix
PRAS40	proline -rich AKT1 substrate 1
PTB	phosphotyrosine binding
PTK7	Tyrosine-protein kinase-like 7
PxxP	priline-rich motif
ROR	RAR-related orphan receptor

RTK	Tyrosine Kinase receptor
RTKI	receptor tyrosine kinase inhibitor
SCF	Stem Cell Factor
SCLC	small-cell lung cancer
SH2	src-homology domain
SH3	src-homology domain 3
SHP2	SH2-containing tyrosine phosphatase
SOCE	store operated calcium entry
SOS	son-of-sevenless
TIE	angiopoietin receptor
TIM	triosephosphate isomerase
TK	tyrosine kinase
TRP	transient receptor potential
TRPC	transient receptor potential canonical
TRPM	transient receptor potential melastatin
TRPML	transient receptor potential Mycolipidosis
TRPP	transient receptor potential polycystin
TRPV	transient receptor potential vanilloid
TSC2	Tuberous Sclerosis Complex 2
UEV	N-terminal ubiquitin E2 variant
VAMP	vesicle-associated membrane protein
VEGFR	vascular endothelial growth factor receptor
VR-1	vanilliod receptor 1
VRL-1	vanilloid receptor-like 1
WW	tryptophan domain

Chapter 1
Introduction

1.1. Receptor Tyrosine Kinases (RTKs)

1.1.1. Kinases

A wide variety of cellular processes including cell cycle progression, proliferation, differentiation, cell survival, metabolism, transcription and cytoskeleton rearrangement are regulated by specific enzymes called protein kinases and protein phosphatases. These enzymes control the activity of other kinases as well as effector signalling proteins involved in cellular responses (Bhullar et al., 2018; Manning et al., 2002). Protein kinases phosphorylate their substrates by transferring the γ- phosphate group from an ATP molecule to the hydroxyl group of specific tyrosine, serine or threonine residues located on the substrate (Figure 1.1). As a result of this modification substrates are usually activated, a reaction that can be reversed by protein phosphatases which remove phosphate groups from phosphorylated residues (Bhullar et al., 2018; Huse and Kuriyan, 2002). Protein kinase genes account for nearly 2% of the human genome with a total of 518 genes identified so far (Manning et al., 2002). Being key regulators of cellular signalling, mutations on these enzymes that cause aberrant kinase activity are linked to oncogenesis. Subsequently, numerous small-molecule kinase inhibitors have been developed for the treatment of malignancies including breast and lung cancer during the last decades (Bhullar et al., 2018).

Protein tyrosine kinases can be divided into two larger groups: non-receptor (32 genes) and Receptor Tyrosine Kinases (RTKs) (58 genes) (Endicott et al., 2012; Robinson et al., 2000).

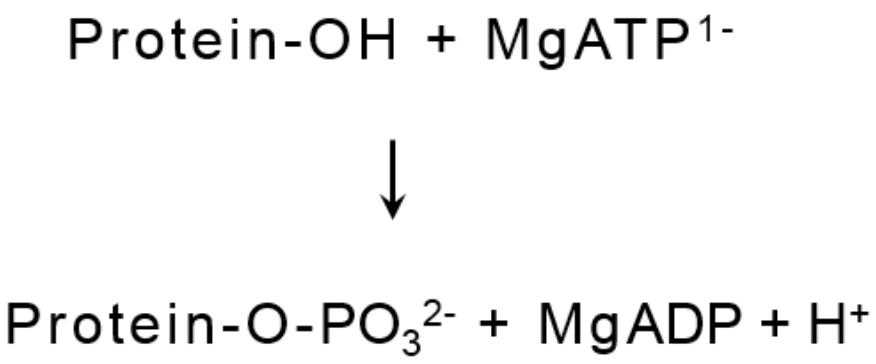

Figure 1. 1: Protein phosphorylation reaction using ATP by kinase enzymes. The γ-phosphate group from the ATP molecule is transferred to the tyrosine, serine, threonine or histidine residues of the protein releasing ADP.

1.1.2. RTK families

Extracellular signals including growth factors, cytokines and hormones are transmitted into the cytoplasm through specific membrane glycoproteins that possess a tyrosine kinase activity. Those transmembrane receptors are named Receptor Tyrosine Kinases or RTKs and are crucial components of cellular signalling in all multicellular eukaryotic organisms. Mutations in these receptors are observed in numerous diseases including cancer, bone disorders and diabetes. There are 58 RTK genes reported in the human genome divided into 20 subfamilies based on ligand specificity, sequence homology and structural features. Those subfamilies include EGFR (Epidermal Growth Factor Receptor), IR (Insulin Receptor), PDGFR (Platelet-derived Growth Factor Receptor), VEGFR (Vascular Endothelial Growth Factor Receptor) , FGFR (Fibroblast Growth Factor Receptor), PTK7 (Tyrosine-protein kinase-like 7), TRK (Tropomyosin Receptor Kinase), ROR (RAR-related Orphan Receptor), MuSK (Muscle-Specific Kinase), MET (Tyrosine protein kinase Met), AXL, TIE (Angiopoietin Receptor), EPH (erythropoietin-producing human hepatocellular receptors), RET (rearranged during transfection), DDR (Discoidin domain receptor), ROS, LMR, ALK (Anaplastic lymphoma kinase)

and STYK1 (Serine/Threonine/Tyrosine Kinase 1) (Figure 1.2). All RTKs share common structural and functional characteristics including the extracellular ligand-binding domain, a single transmembrane domain, a juxtamembrane region and an intracellular kinase domain followed by a C-terminal domain (Schlessinger, 2000).

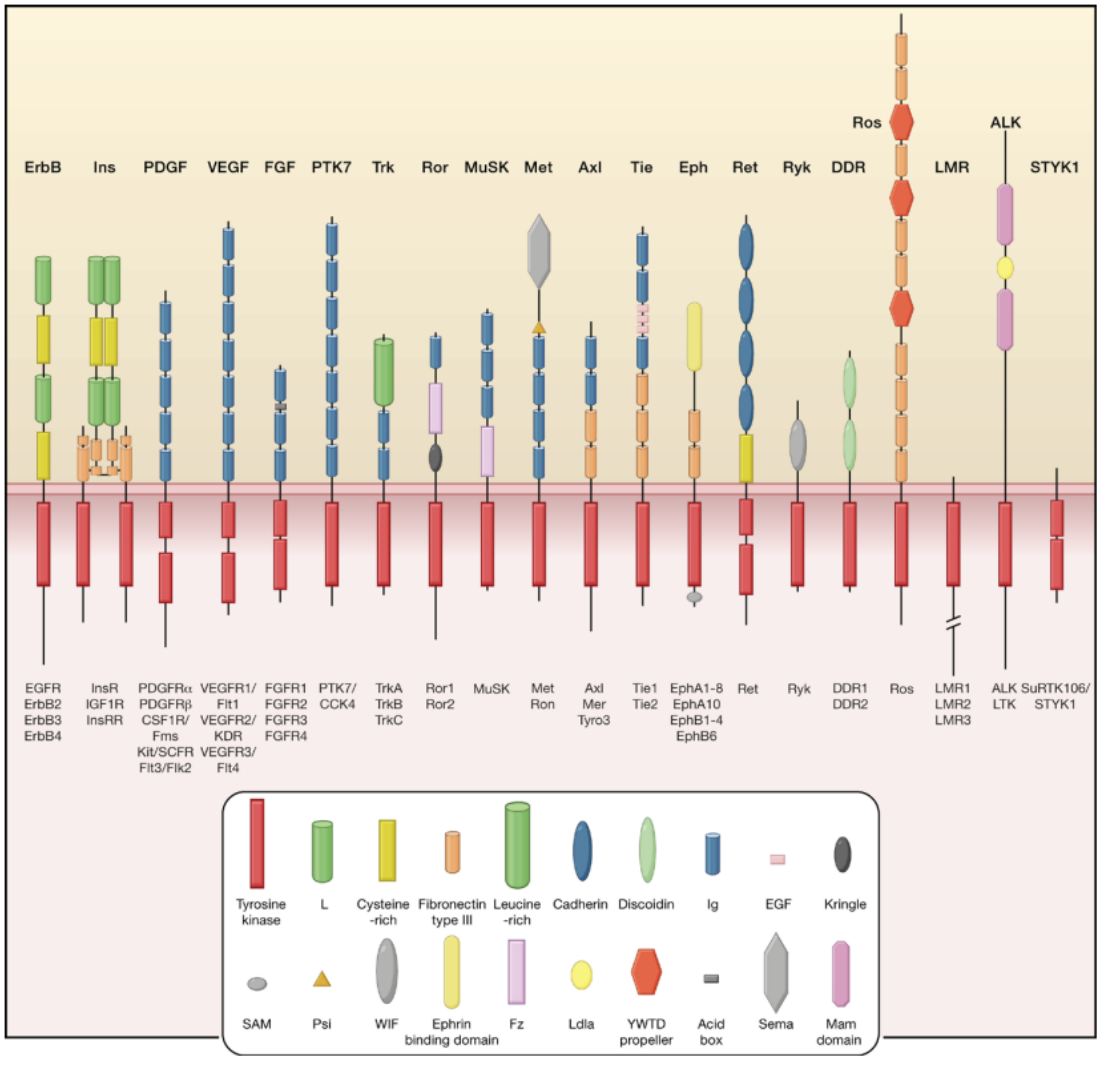

Figure 1. 2: Schematic of the extracellular and intracellular domains of 20 Tyrosine Kinase Receptor Families. (Taken from (Lemmon and Schlessinger, 2010)

1.1.3. RTK structural features

1.1.3.1. The Extracellular domain of RTKs

The N-terminal region of every RTK exists in the extracellular space where it mainly serves as a ligand-binding domain. RTK extracellular domains are rich in intra chain disulphide bonds as well as N-linked glycosylation sites and consist of multiple structural motifs that provide ligand specificity. Most common motif is the Immunoglobulin (Ig) motif which is present in various repeats in 10 RTK subfamilies. For instance, the FGFRs contain two to three Ig-like domains while VEGFR and PTK7 contain up to seven of those motifs. Leucine- and cysteine-rich motifs as well as fibronectin type III are also common among RTK extracellular domains (e.g. EGFR and IR) (Lemmon and Schlessinger, 2010).

Apart from ligand recognition, extracellular domains are also important for receptor dimerization following ligand binding because they participate in receptor-receptor interactions that stabilise the dimeric state. One extreme of this function is the ligand-induced dimerisation of EGFR that is completely receptor mediated and occurs via interactions between the “dimerisation arm” located in the Cysteine-rich motif (domain II) of one receptor with the domain II of the partner receptor (Burgess et al., 2003). Furthermore, extracellular domains can interact with cell surface adhesion molecules. For example, it has been shown that E-cadherin can directly interact with EGFR resulting in receptor inhibition (Qian et al., 2004). Moreover, unlike most RTKs that bind to soluble ligands, Eph receptors recognise membrane-bound ligands called ephrins that are located on the membrane of neighbouring cells. This interaction occurs through the ephrin-binding domains in the extracellular region and serves as point of contact with other cells (Lisabeth et al., 2013).

1.1.3.2. The Transmembrane domain of RTKs

The transmembrane domain connects the extracellular domain with the intracellular kinase domain. The transmembrane domain consists of hydrophobic and basic

residues and contributes to RTK signalling in two manners: thermodynamicly, because it contributes to dimer stability by forming sequence-specific interactions, and structurally, because it controls the orientation of the kinase domain maintaining the active-conformation of the dimer (Li and Hristova, 2010). The importance of the transmembrane domain in signal regulation is highlighted by the fact that mutations in that domain can cause ligand-independent receptor activation, as reported in PDGFR, FGFR and EGFR (Bargmann and Weinberg, 1988; Li et al., 1997; Velghe et al., 2014; Webster and Donoghue, 1996).

1.1.3.3. The kinase domain of RTKs

The kinase domain of RTKs is located at the cytoplasmic region, between the juxtamembrane and the C-terminal region. Like all serine/threonine and tyrosine kinases, the RTK kinase domain adopts a similar architecture with two lobes, one N-terminal and one C-terminal. The conformation of the lobes and interactions between their components dictate the level of catalytic activity of the kinase. The N-lobe consist of 5 β-strands (β1-β5) that form a twisted β-sheet and an αC helix. The primary role of the N-lobe is to facilitate the binding and proper orientation of the ATP. The C-lobe consist of two β-strands (β7 and β8) and five α-helices (αD to αI) that facilitate the substrate binding and catalytic activity. The Activation-loop tyrosine residues whose phosphorylation state regulates the kinase activity are also located in the C-lobe (Wybenga-Groot et al., 2001).

1.1.4. RTK activation

The conserved activation mechanism follows a generalised model that starts with the binding of a growth factor on the extracellular domain causing receptor dimerisation. Subsequent conformational changes release the receptor-specific cis-autoinhibition activating the kinase domain which trans-phosphorylates tyrosine residues along the cytoplasmic domain of the receptor. Phosphotyrosines are crucial for enhancing the tyrosine kinase activity (Activation-loop) as well as serving

as docking areas for phosphotyrosine-binding-motif-containing downstream proteins initiating a cascade of protein interactions and reactions that end in cellular responses (Lemmon and Schlessinger, 2010).

1.1.4.1. Ligand-mediated receptor dimerization

The ligand-mediated mechanism of RTK activation is supported by structures of ligand-bound RTK ectodomains that have been published so far. Even though all RTKs require ligand binding to be activated, the exact mechanism and network of interactions vary among receptor subfamilies.

One case involves a dimeric ligand that simply brings two receptor monomers together into a dimer. For example, one molecule of the dimeric SCF (Stem Cell Factor) interacts with the immunoglobulin-like domains 1, 2 and 3 (D1-3) of one KIT molecule ectodomain and so does the second SCF molecule creating a homodimer with 2:2 stoichiometry. This interaction changes the orientation of the membrane proximal D4 and D5 domains enabling D4:D4 and D5:D5 homotypic interactions that further stabilise the dimer. D4 homotypic affinities are low and the polarised electrostatic surface causes repulsion of proximal receptors preserving the inactive monomeric state. In the presence of SCF, the local receptor concentration is increased and therefore, the D4 affinity becomes adequate to create homotypic interactions and stabilise the complex (Yuzawa et al., 2007). Subsequently, mutations in the D4-D5 domains that increase the dimerisation constant by 250-fold cause ligand-independent receptor dimerisation. Similarly, homotypic interactions occur along the KIT ectodomain (D4-D5) and continue throughout the receptor (transmembrane and intracellular domain) in a “zipper-like” manner creating a network of weak contacts that stabilise the dimer (Reshetnyak et al., 2015). Similar model of receptor dimerisation has been shown for the VEGFR-1/VEGF-A complex. Each VEGFR-1 molecule interacts with both VEGF-A protomers through the D2-D3 binding site. The remaining D4-D7 domains in the extracellular region create

homotypic contacts that further stabilise the dimeric state (Markovic-Mueller et al., 2017). In the cases described above, both receptor-ligand and receptor-receptor interactions are combined in order to form a stable dimer and induce receptor activation.

In the case of the neurotrophin receptor TrkA, receptor-ligand interactions are the only ones that mediate the dimerisation. There are no receptor-receptor interactions between the LRRs (leucine-rich repeat) nor the Ig-like domains along the ectodomain. The dimer interface solely consists of interactions mediated by the Ig-C2 domain of each receptor with both molecules of the NGF (nerve growth factor) dimeric ligand creating a 2:2 complex (Wehrman et al., 2007).

On the contrary, EGFR dimerization interface comprises solely of receptor-receptor interactions, as shown by two crystal structures of EGFR ectodomains bound to TNF-α and EGF ligands (Burgess et al., 2003; Garrett et al., 2002; Ogiso et al., 2002). Since the dimerization is receptor-mediated, autoinhibitory mechanisms are crucial to prevent dimer formation in the absence of ligands. In the monomeric state, intramolecular interactions between domain II and IV (D2, D4) keep EGFR in the tethered conformation which prevents D2 from interacting with respective domains in neighbouring receptors. The autoinhibition is released in the presence of ligand. Each ligand molecule binds to one of the receptor monomers by contacting D1 and D3 of the EGFR ectodomain. This interaction causes D1 re-orientation that releases D2 autoinhibitory contacts and allows intermolecular interactions with neighbouring D2 creating the dimerization interface.

In the case of FGFR, accessory molecules i.e. heparin or heparin sulphate proteoglycans, are involved in the process of receptor dimerisation. Similar to EGFs, FGF ligands are monomeric; however, each FGF binds to D2 and D3 of both FGFR molecules. In a 2:2:2 stoichiometry of an FGFR1c:FGF2:heparin complex there is a network of receptor-ligand, receptor-receptor, receptor-heparin and

ligand-heparin interactions that stabilise the dimeric FGFR (Plotnikov et al., 2000; Schlessinger, 2000).

However, there is evidence that receptors exist in dimeric forms even in the absence of extracellular stimulation. The Insulin Receptor (IR) and IGF-1R are examples of RTK receptors whose monomers are linked with disulphide bonds and form $\alpha\beta_2$ dimers. Moreover, the formation of inactive FGFR2 pre-dimers has also been reported. Binding of ligands to those dimers cause conformational changes that activate the kinase domain of the receptors and fire signalling cascade (Lawrence et al., 2007; Lin et al., 2012; Ward et al., 2007). In general, the inactive state of RTKs, either monomeric or dimeric, requires ligand binding to remove auto-inhibitory molecular interactions and fully activate the receptors.

1.1.4.2. Kinase domain activation

Either monomer or dimeric, RTKs remain inactive (or low activity) until their specific ligand binds to the extracellular domain. Inactivity of free receptors (not ligand-bound) is achieved by cis-autoinhibition mechanisms that are receptor specific. For example, tyrosine Y1162 in the Activation-loop of the Insulin Receptor (IR) completes with tyrosines of the substrate for the active site. This set of interactions between Y1162 and the active site result in ATP access restriction and thus, inhibition of autophosphorylation (Hubbard, 1997). Similar autoinhibition mechanisms involving projection of Activation-loop tyrosines in the active site has been observed in receptors including TrkA and Ror2 (Artim et al., 2012).

However, more than one mechanisms of cis-autoinhibition can be implemented by one receptor. Except for the Activation-loop autoinhibition, IR implements a juxtamembrane-mediated inhibitory effect. Tyrosine Y984 in the juxtamembrane region disrupts the positioning of ATP through interactions with the αC helix which prevents phosphorylation of substrates. Mutation of Y984 to Phenylalanine or

Alanine increased the basal catalytic activity which verifies the inhibitory role for Y984 (Li et al., 2003).

Similar autoinhibitory mechanisms are utilized by juxtamembrane regions of other RTKs including EphB2 receptor, Muscle-specific Kinase Receptor (Musk), KIT receptor and the Fms-like tyrosine kinase 3 (FLT3) receptor (Chan et al., 2003; Griffith et al., 2004; Till et al., 2002). For example, the tyrosines Y604 and Y610 of the EphB2 receptor juxtamembrane domain interact with the αC helix at the N-terminal kinase lobe involved in nucleotide binding which impedes the correct orientation of the ATP. When Tyrosine 788 in the Activation-loop is phosphorylated, the catalytic domain is ordered in a favourable orientation and increases the kinase activity. Upon Y604 and Y610 phosphorylation, contacts with the catalytic domain are lost and the autoinhibitory effect is raised (Wybenga-Groot et al., 2001).

The involvement of the C-terminal domain in receptor regulation at basal states has also been reported. The structure of the Tie2 receptor, for example, revealed that tyrosines in the C-terminal domain form contacts with the kinase domain which result in adoption of inhibitory conformation and obscure substrate binding. Phosphorylation of those tyrosines release the autoinhibitory effects in a manner similar to that of juxtamembrane Tyrosines. Deletion of the Tie2 C-terminal region led to increased autophosphorylation activity and downstream signalling in vitro (Shewchuk et al., 2000). Similarly, PDGFR-β and Ron (Met family) C-terminal domains are shown to inhibit kinase activity in vitro, however, structural details are still to be determined (Chiara et al., 2004; Yokoyama et al., 2005).

1.1.4. RTK-mediated signalling pathways

The first step for an RTK activation is ligand binding to the extracellular domain which results in receptor dimerization and thus, conformational changes that allow autophosphorylations of Tyrosine residues in the Activation-loop. The first substrate of an RTK is the receptor itself and the autophosphorylation of tyrosines along the

cytoplasmic domain occurs in a precise order. The autophosphorylation serves two purposes: to increase the catalytic activity of the kinase as well as to create phosphotyrosine binding sites for downstream docking and effector proteins. For example, FRS2 (FGFR-related substrate 2) and IRS (insulin receptor substrate), that are docking proteins of FGFRs and IR receptors respectively, are bound to and get phosphorylated by the receptors. Phosphotyrosines on the docking proteins are, in turn, recognised by downstream proteins resulting in the formation of signalling complexes. There are three major signalling pathways initiated by RTKs, the MAPK (mitogen-activated protein kinase), PLCγ1 (phospholipase c γ1) and the PI3K (phosphoinositide-3 kinase) pathway which are described in detail in the context of FGFR2 signalling in the section 1.2.4 (Lemmon and Schlessinger, 2010).

1.1.5. RTKs implication in cancer

Based on the latest WHO global statistics, ischaemic heart disease and stroke still remain the leading causes of death accounting for 15 out of 56.4 million of total deaths in 2015 worldwide (WHO, “The top 10 causes of death,”). The next bigger killer is cancer and all cancers combined account for 8.8 million deaths meaning that almost one out of six deaths are cancer-related. Moreover, cancer is one of the most frequent diseases. In 2012, approximately 14 million new cancer cases were recorded worldwide (Torre et al., 2015). Notably, lung cancer is the deadliest cancer of all (1.7 million deaths in 2015), ranking fourth just by itself in the top 10 causes of death following heart disease, strokes and chronic obstructive pulmonary disease (WHO, “The top 10 causes of death,”; Torre et al., 2015). Lung cancer incidents are most frequent among men rather than women. However, lung cancer is the number one cause of cancer-related mortality in men and women after breast cancer (Torre et al., 2015). Lung cancer remains the greatest cancer-related challenge and it is expected to be responsible for 3 million deaths in 2035 (Didkowska et al., 2016).

Lung cancer originates from epithelial cells of the respiratory epithelium and can be divided into two categories based on histological characteristics: small-cell lung cancer (SCLC) accounting for approximately 15% of all lung cancer cases and non-small cell lung cancer (NSCLC) that accounts for the rest of the cases (85%). NSCLC is also divided into further subtypes including the most common lung cancer type called lung adenocarcinoma (LUAD) (38.5%), squamous cell carcinoma (20%) and large cell carcinoma (2.9%) (Dela Cruz et al., 2011). Due to the advanced-stage of diagnosis, the 5-year survival of lung cancer is 18.8% (*SEER*, “Cancer of the Lung and Bronchus - Cancer Stat Facts,”.). At the stage of diagnosis, 16% of the cases are localised, 22% are regional and 57% are distant, having a 5-year survival of 55.6%, 28.9% and 4.5%, respectively. Due to the fact that most cases are diagnosed in advanced stages, lung cancer is usually coupled with metastatic disease that mainly includes brain metastasis. Both SCLC and NSCLC are associated with brain metastasis and nearly 50% of all cases are expected to present secondary brain tumours (Tamura et al., 2015).

Cancer is usually described as the uncontrolled proliferation and accumulation of cells that impairs normal tissue function. However, cancer is not only a mass of proliferating cells but also a sophisticated tissue that in addition to cancer cells, composes of stromal cells, immune cells and vasculature forming the tumour microenvironment. Within a tumour, multiple and complex intracellular interactions occur orchestrating fundamental hallmarks of cancer like cellular proliferation and growth, survival, immortality, angiogenesis and invasion. Those cancer characteristics derive from deregulated signals that otherwise would regulate cellular growth and tissue homeostasis. Most signals are recognised by membrane receptors that are usually overexpressed in cancer cells, increasing responses to minimal stimulation, or mutated and thus ubiquitously activated, initiating signal-independent responses. Downstream signalling components as well as the signals themselves can also be altered in favour of cancer cell growth (Hanahan and

Weinberg, 2011). So far, the tyrosine kinase receptors (RTKs) have been highly implicated in cancer initiation and progression. However, additional types of membrane receptors have been associated with cancer like ion channels whose role is also emerging, possibly characterising cancer as a channelopathy (Litan and Langhans, 2015).

Signalling pathways are extremely fine-tuned processes important for cellular homeostasis. Thus, deregulation of those pathways is highly implicated in several diseases and malignancies. As critical nodes in signalling, RTKs are involved in cancer progression mainly by autocrine stimulation, gene amplification and protein overexpression, activating mutations as well as chromosomal translocations that form fused proteins with altered functions (Lemmon and Schlessinger, 2010).

For example, ErbB2 (HER2) that belongs to the EGFR family of RTKs, is overexpressed in 15-30% of breast cancers and is also associated with poor overall survival. The *ErbB2* gene is amplified 25-50 times creating 40-100 times more protein meaning that there are around 2 million ErbB2 receptors on the surface of breast cancer cells initiating pathways that favour tumour progression (Kallioniemi et al., 1992; Ornitz and Itoh, 2015). The monoclonal antibody Trastuzumab (Herceptin) is approved from the FDA for treatment of HER2-positive breast cancer. Trastuzumab recognises the IV extracellular domain of ErbB2 attenuating signalling, inhibiting angiogenesis and causing antibody-dependent cellular cytotoxicity and demonstrated 33% improvement in overall patient survival. However, some HER2-positive breast cancers acquire resistance to Trastuzumab due to a truncated version of ErbB2 (p95HER2) that misses the extracellular domain but still maintains a functional tyrosine kinase domain. Instead, Lapatinib, an ErbB2 and EGFR tyrosine kinase inhibitor, is more effective in inhibiting p95HER2 phosphorylation and downstream signalling activation in breast cancer cells and is also used in combination therapy against HER2-positive advanced and metastatic breast cancer (Scaltriti et al., 2007). Moreover, ErbB2 is found

overexpressed in other malignancies including gastric, ovarian and endometrial cancers (Kallioniemi et al., 1992). Among others, VEGFR has also been overexpressed in multiple types of cancers promoting angiogenesis and metastasis as well as FGFR1 which has also been found overexpressed in 17% of NSCLC, 6% of SCLC and 15% of hormone-receptor-positive breast cancers (Babina and Turner, 2017; Regad, 2015).

Most cases of RTK fusion proteins are usually found in leukemias. In translocations, RTKs are fused with a dimerising partner that assists in receptor dimerization resulting in constitutively active kinase activity and aberrant signalling. The most common paradigm is the translocation t(2:5)(p23;q35) between ALK (anaplastic lymphoma kinase) and NPM (Nucleophosmin) creating the fusion protein NPM-ALK that is found in 50-60% of all anaplastic large cell lymphoma (ALCLs). Additional examples include the fusion protein ZNF198-FGFR1 found in 48% of 8p11 myeloproliferative syndrome (EMS) and the PDGFRB-ETV6 fusion protein found in n chronic myelomonocytic leukemia (CMML) (Peiris et al., 2019).

Furthermore, activating mutations are very frequent within RTK-related cancers. C-kit, a stem cell factor receptor involved in cell maintenance and differentiation, is highly mutated in many cancers including melanoma, mastocytosis and 80% in GIST (gastrointestinal stromal tumours). The majority of the mutations are located in the juxtamembrane region of the receptor which is responsible for receptor autoinhibition, causing constitutive kinase activation. Mutations in exon 11 (juxtamembrane region) occur in 65% of GIST, while mutations in exon 17 (kinase) often result in hematopoietic malignancies (Abbaspour Babaei et al., 2016). Moreover, mutations that activate the kinase domain and change signalling specificity of PDGFRA also occur in 5% of GIST (Heldin et al., 2018).

The dominant RTK alteration in lung cancer is EGFR mutations occurring in 10-15% of Caucasian and 40% in Asian populations (Lo Russo et al., 2017). These

mutations include deletions in exon 19 and L858R mutation in exon 21 that constitutively activate the receptor and are sensitive to first generation tyrosine kinase inhibitors such as erlotinib and gefetinib used as a treatment for NSCLC (Russo et al., 2017; Tanaka et al., 2017). Mutations in the extracellular domain have also been reported. For instance, M277E is a recently discovered mutation, also sensitive to RTK inhibitors (RTKIs) (Yu et al., 2017). However, more than 50% of the cases acquire resistance to RTKIs. Resistance is also acquired after treatment with afatinib, a second generation irreversible inhibitor within the first year of treatment. Mechanisms of acquired resistance include the secondary mutation T790M which is reported in 50-60% of all cases that are resistant to first and second generation inhibitors. The T790M mutation is located in exon 20 and impairs the ability of inhibitors to bind and inhibit the kinase activity (Pao et al., 2005). D761Y, L747S and L854A are all secondary mutations linked to acquired resistance. Apparently, these mutations are pre-existing in a smaller subpopulation of cancer cells and become the dominant forms of EGFR following RTKI treatment through selection. Likely, third generation RTKIs are under development or clinical trials and seem to be promising in treating NSCLC patients. Osimertinib and Rociletinib are two examples of third generation RTKIs that selectively target mutated EGFRs and not wild type receptors (200 and 22 times higher selectivity for mutated receptors, respectively). The mechanism of action differs from other RTKIs because they recognise and covalently bind to C797 located in the ATP-binding site (Russo et al., 2017).

The translocation between ALK and echinoderm microtubule-associated protein-like 4 (EML-4) genes has been reported in approximately 5% of NSCLC cases as the main oncogenic driver of the disease (Muller et al., 2017; Soda et al., 2007). This translocation creates the EML4-ALK fusion protein that dimerises due to the EML-4 coiled-coil domain resulting in constitutively activated kinase of ALK. Resistance to first generation EML4-ALK inhibitors (crizotinib and cevitinib) has been reported to

22% of the patients and usually originates form secondary ALK mutations that impair drug-binding or even overexpression of EGFR. A more effective second generation inhibitor specifically designed to target EML4-ALK mutations like L1196M is Alectinib, which was approved from the FDA in 2016 (Muller et al., 2017).

1.2. The Fibroblast Growth Factor Receptor 2 (FGFR2)

1.2.1. An overview of the FGFR2 structure

The human Fibroblast Growth Factor Receptor 2 (FGFR2) belongs to the FGFR family of RTKs that consists of FGFR1, FGFR2, FGFR3 and FGFR4 encoded by *FGFR1, FGFR2, FGFR3* and *FGFR4* genes. FGF receptors recognize specific ligands belonging to the Fibroblast Growth Factor (FGF) family of growth factors consisting of 18 members (FGF1 to FGF18) (Ahmad et al., 2012).

All FGFRs share similar structural characteristics. They belong to the immunoglobulin-like superfamily of proteins due to the presence of three extracellular Ig-like domains (D1, D2, D3) (Figure 1.3). D2 and D3 are important for ligand binding and specificity. In more detail, D2 and the D2-D3 linker are responsible for non-specific FGF ligand recognition, while D3 is necessary for ligand specificity (Plotnikov et al., 2000). FGF ligand specificity is established through alternative splicing of the D3 region. As illustrated in Figure 1.4, isoform IIIb includes exon 8 but misses exon 9 whilst, isoform IIIc includes exon 9 but misses exon 8. Residues in that area determine ligand specificity therefore, FGFR2IIIb recognizes FGF-1, -3, -7, -10, -22 while FGFRIIIc recognizes FGF-1, -2, -4, -6, -9, -17 and -18. FGF-1 is a general FGFR ligand that binds to all FGF receptors (Eswarakumar et al., 2005). The first Ig-like domain (D1) and the acidic box (a series of acidic residues) are considered to be involved in the auto-inhibition of the receptor. Based on FGFR3c/FGF1 structures and SPR data, intramolecular interactions between a) the D1-D2 linker and the D2 heparin-binding region and b)

the D1 and the D2-D3 fragment, keep the receptor in a “closed”, auto-inhibitory configuration (Olsen et al., 2004).

The transmembrane (TM) domain is followed by a long, compared to other RTKs, juxtamembrane region consisting of conserved residues that bind to phospho-tyrosine binding (PTB) domains. FGFR-related substrate 2 (FRS2) is a PTB containing adaptor protein that is constitutively bound to the juxtamembrane region of FGFRs, participating in signal transduction (Ong et al., 2000). Each FGF receptor carries a split tyrosine kinase domain and a C-terminal region that are important for receptor activation and signal transduction (Figure 1.3).

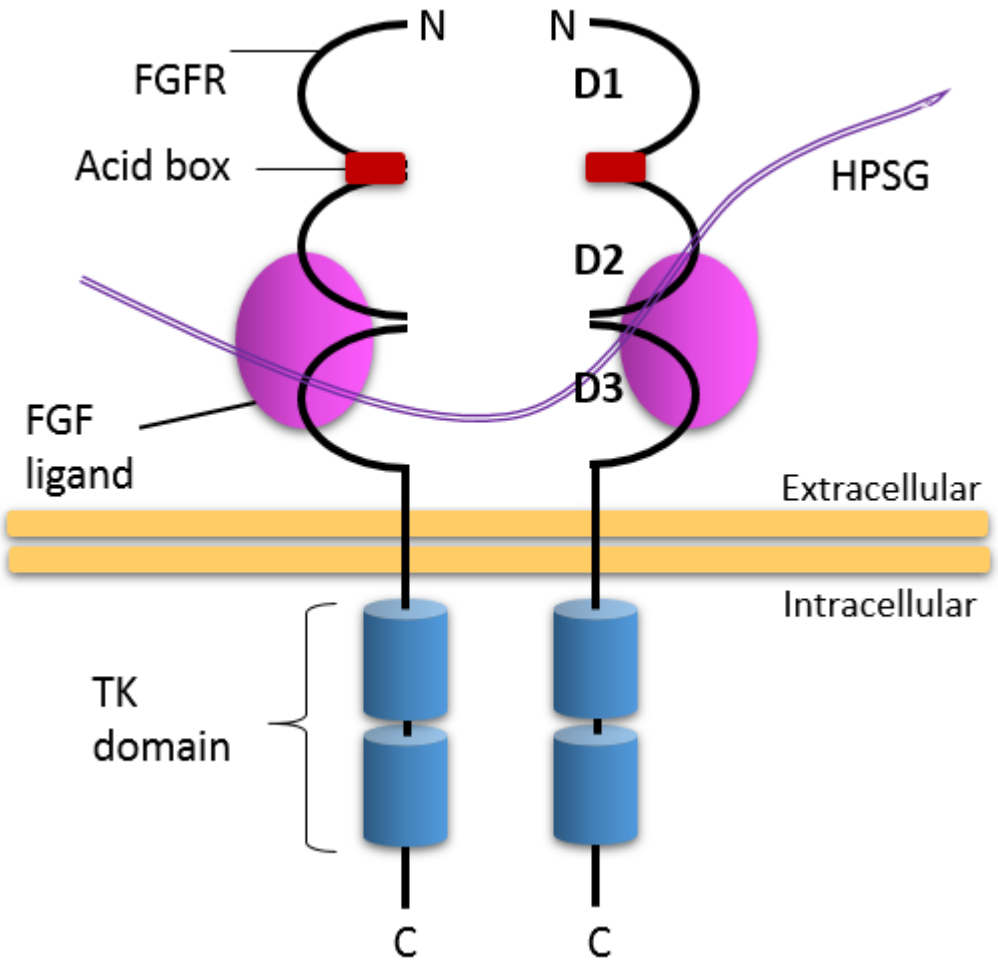

Figure 1. 3: Fibroblast Growth Factor Receptor 2 structure and splicing. Simplified structure of FGFR2. Two FGFR2 monomers dimerise to create a dimer upon FGF/HSPG binding in the D2-D3 extracellular domains. D1 is involved in receptor auto-inhibition and an acid box is located between the first and the second Ig-like domain. Each FGFR2 subunit carries one split intracellular tyrosine kinase domain which is crucial for downstream signalling activation. HSPG = heparin sulphate proteoglycan, TK = tyrosine kinase, FGF = fibroblast growth factor, D1, D2, D3 = immunoglobulin-like domain 1, 2, 3.

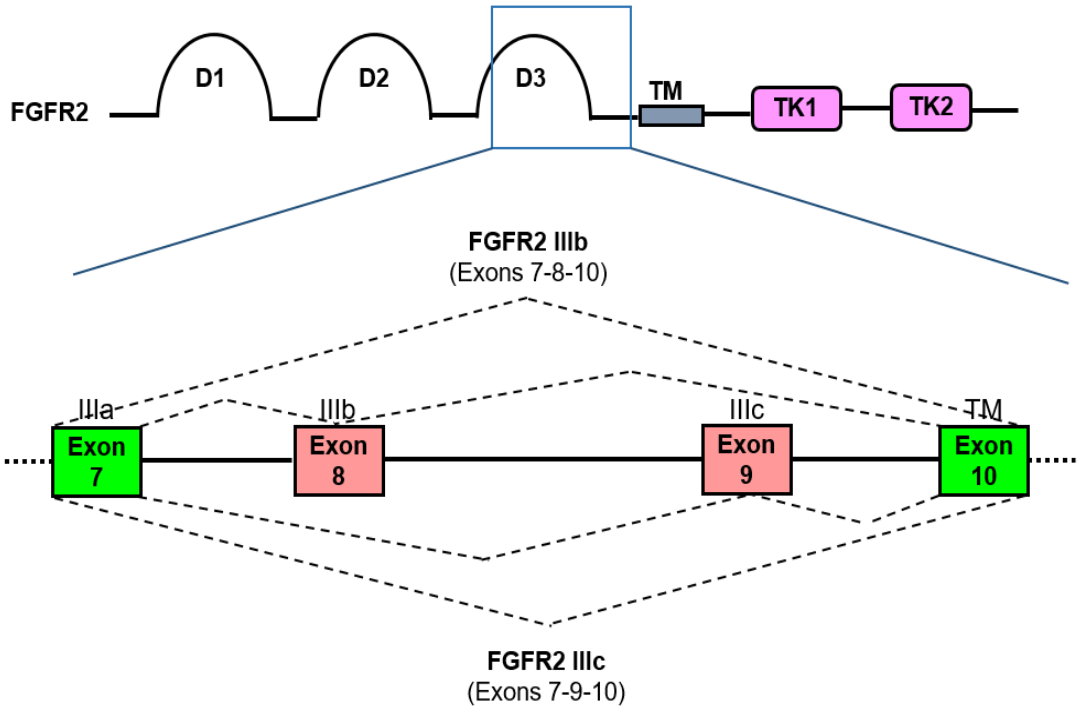

Figure 1. 4: FGFR2 D3 alternative splicing. FGFR isoform IIIb and IIIc are products of alternative splicing of the D3 domain. Isoform IIIb includes exon 8 while in isoform IIIc, exon 8 is replaced by exon 9.

1.2.2. Activation mechanism of FGFR2

Similar to all FGF receptors, FGFR2 is activated upon dimerization of two FGFR2 monomers. Dimerisation is triggered by the binding of FGF ligands to the receptor monomers in combination with Heparin Sulfate Proteoglycans (HSPC) which are also vital components of this interaction that increase the binding affinity and stability between ligand-receptor. X-ray crystallography analysis revealed that in the pentamer of FGFR2-FGF1-hepaprin in a 2:2:1 stoichiometry, the heparin molecule interacting with the dimeric FGF1 that binds to the dimeric FGFR2, binds to only one of the FGFR2 monomers (Pellegrini et al., 2000). Following receptor dimerization, the tyrosine kinase domains of the two monomers come in close proximity enabling trans-phosphorylation on specific tyrosine residues that differ on each receptor. Under non-stimulating conditions, FGFRs have a fine-regulated intrinsic basal kinase activity that is inadequate to trigger FGFR activation without the extracellular signal. Upon ligand binding and subsequent dimerization, the intrinsic kinase phosphorylates primary tyrosine residues of the activation loop that activate the kinase domain on its maximum potential. Next, the fully activated kinase phosphorylates secondary tyrosine residues in the kinase insert, juxtamembrane region and C-termainal domain, which act as binding sites for downstream signalling proteins that are also phosphorylated and activated by the receptor (Chen et al., 2013).

In FGFR1 for instance, Y653 that belongs to the activation loop is phosphorylated first increasing the kinase activity 50-100 fold. Next, the phosphorylation of the rest of the tyrosine residues occurs in a sequential order: Y583 (kinase insert), Y463 (juxtamembrane region), Y585 (kinase insert) and Y766 (C-terminal) are phosphorylated and form docking sites for downstream proteins. Lastly, Y654 located in the activation loop is phosphorylated increasing the kinase activity by 500-1000 fold. (Furdui et al., 2006). Counterpart tyrosine residues on the FGFR2 are shown in Figure 1.5. Y656 and Y657 comprise the activation loop of FGFR2

while, Y466, Y586/Y588 and Y769 are located at the juxtamembrane region, kinase insert and C-terminal region of FGFR2, respectively (Huang et al., 2016; Luo et al., 2009). Phosphotyrosines serve as binding sites for SH2-containing proteins. One of them is PLCγ1 that binds to pY769 of FGFR2 through the cSH2 domain and gets phosphorylated at Y771 and Y783 activating the phospholipase enzymatic activity, as described in the PLCγ1 section (section 1.2.1.4.). In 2016, Huang *et al.* demonstrated that the recruitment and the phosphorylation of the substrate (PLCγ1) by FGFR2 cannot be executed by the same kinase in –*cis*. Notably, the synergistic participation of both monomers is required for succesful substrate phosphorylation. The substrate is recruited by one monomer and then phosphorylated by the other in –*trans* highlighting the importance of receptor dimerization in both kinase activation and substrate phosphorylation during signal transduction (Huang et al., 2016).

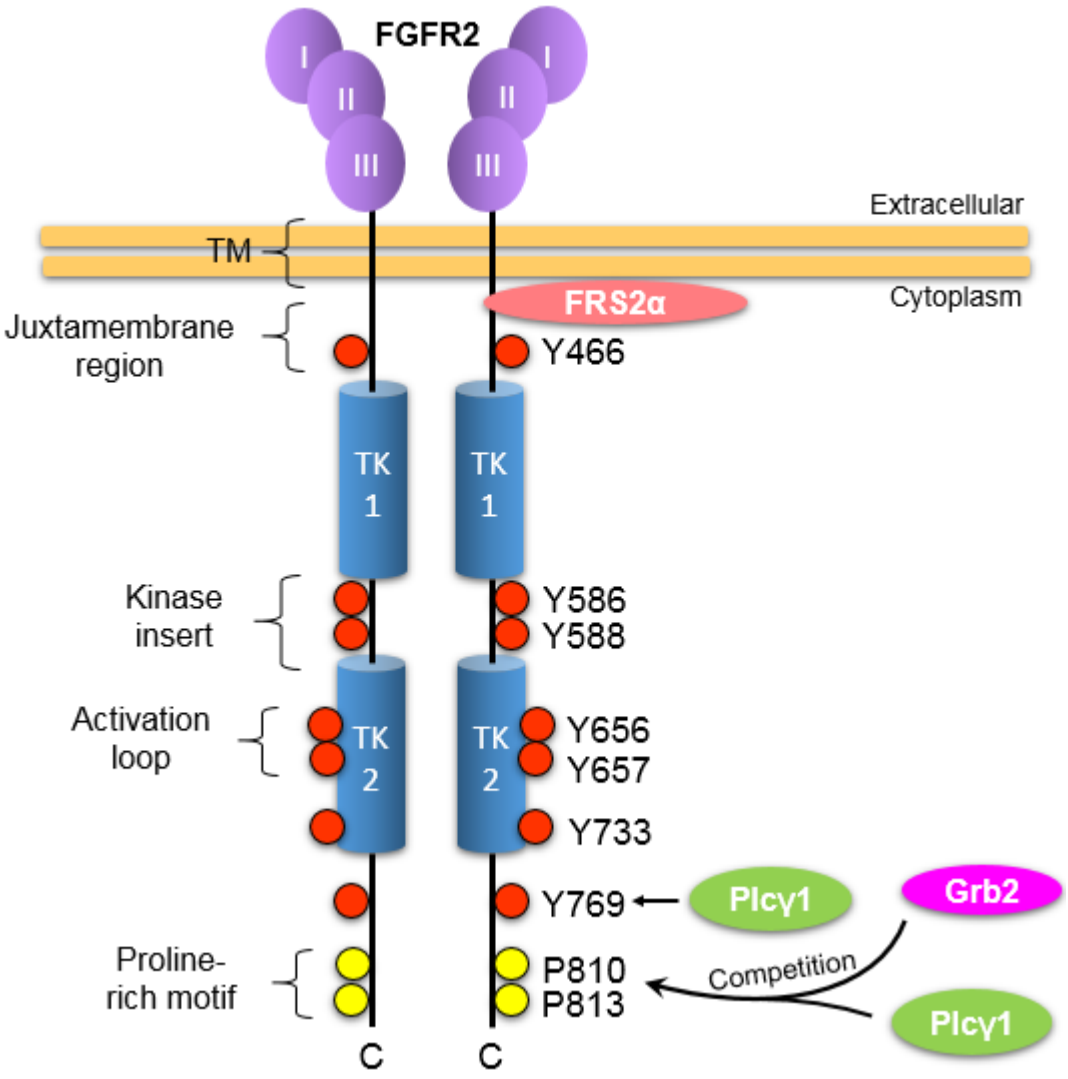

Figure 1. 5: Phosphotyrosine residues on FGFR2. Activated FGFR2 results in auto-phosphorylation of multiple tyrosine residues along the cytoplasmic domain of the receptor. The activation loop consists of phospho-tyrosine 656 and 657 located within the second tyrosine kinase domain. Phospho-tyrosine 466 is located at the juxtamebrane region, phospho-tyrosine 586 and 588 at the kinase insert, phospho-tyrosine 733 at TK2 and finally, phospho-tyrosine 769 at the C-terminal region serving as a docking area for PLCγ1. Proline 810 and 813 belong to the C-terminal proline-rich motif which both Grb2 and PLCγ1 complete for, in non-stimulating conditions.

1.2.3. The kinase autoinhibition mechanism of FGFR2

Solved structures of the wild type, active and inactive FGFR2 kinase domains as well as those that are constitutively active because of point mutations, have revealed an autoinhibitory mechanism that prevents receptor activation prior to phosphorylation of tyrosines in the Activation-loop (Chen et al., 2007).

Upon phosphorylation of the tyrosine Y657 located in the Activation-loop, conformational changes occur because of newly-formed interactions including hydrogen-bonds between pY657, R649 and K569 in the Activation-loop (Chen et al., 2007). At the same time, the inward rotation of the N-lobe brings it closer to the C-lobe resulting in appropriate alignment of the catalytic residues located in the Activation-loop, catalytic-loop and αC-helix. The new rearrangement facilitates the binding of ATP and substrate to their respective binding pockets and enhances the efficiency of the catalysis (Figure 1.6).

According to Chen and colleagues, the molecular autoinhibition prior to Activation-loop phosphorylation is achieved by three residues, E565 (kinase hinge), N549 (loop αC-β4) and K641 (β8), as revealed by structures of mutated and constitutively active FGFR2 kinases (Chen et al., 2007). In a wild type FGFR2 kinase, hydrogen-bonds mediated between these residues stabilise the autoinhibitory conformation by abrogating the inward twist of the N-lobe towards the C-lobe. Phosphorylation of the Activation-loop causes dissociation of those hydrogen-bonds allowing the N-lobe twist and Activation-loop rearrangement, ready for catalysis. Similarly, activating mutations of the FGFR2 kinase domain disrupt the network of hydrogen bonds causing constitutively active kinases.

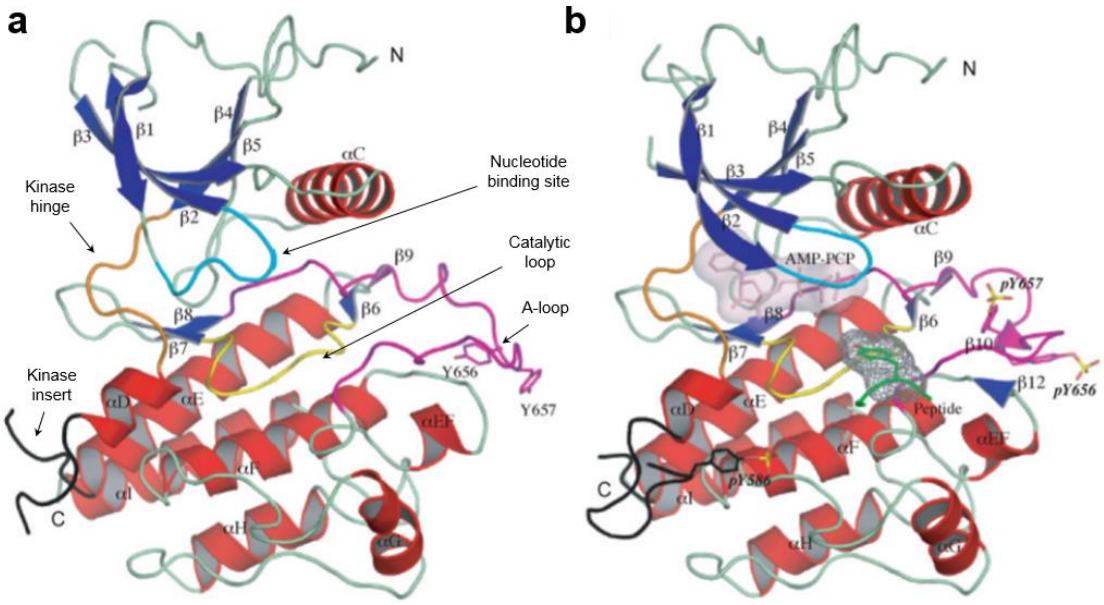

Figure 1. 6: Structure of the wild-type FGFR2 kinase domain in a ribbon diagram. a) Unphosphorylated FGFR2 kinase domain. The kinase insert is shown in black, the kinase hinge region in orange, the nucleotide binding site in blue, the catalytic-loop in yellow and the Activation-loop in purple. b) phosphorylated FGFR2 kinase domain. The non-hydrolysable ATP analog and the substrate are shown in a stick diagram. Adapted from Chen et al., 2007.

1.2.4. FGFR2-induced signalling pathways

1.2.4.1. The PLCgamma1 pathway

PLCγ1 is a phospholipase that belongs to the Phospholipase C –γ subfamily of phospholipases. When activated, PLC enzymes catalyse the hydrolysis of the phospholipid phosphatidylinositol 4,5-biphosphate (PIP2) to Inositol 1,4,5-tri-phosphate (IP3) and diacylglycerol (DAG). IP3 and DAG are second messenger molecules that can trigger downstream signal transduction. The PLCγ1 structure contains a pleckstrin homology domain (PH) followed by an EF hand series, followed by the catalytic domain called triosephosphate isomerase (TIM) barrel and a C2 domain (Figure 1.7). The TIM barrel is divided into X- and Y- boxes which are linked by an extended linker containing an N-terminal and a C-terminal SH2 domain (nSH2 and cSH2) as well as a SH3 domain, all within a split PH domain (Figure 1.7) (Poulin et al., 2005).

The cSH2 domain of PLCγ1 is a critical regulator of the lipase auto-inhibition and activation. In non-stimulating conditions, intramolecular interactions between the cSH2 and the TIM barrel inhibit the phospholipase enzymatic activity. Upon FGFR2 activation by FGF binding to the extracellular domain, tyrosine Y769 on the C-terminal of the receptor gets phosphorylated attracting PLCγ1 that binds to the phospho-tyrosine through the nSH2 domain. As illustrated in Figure 1.8, the outcome of this interaction is the phosphorylation of Y783 located on PLCγ1 X-Y linker, a major residue involved in the phospholipase activation. The auto-inhibition is eliminated when cSH2 engages with the pY783 resulting in conformational changes that release the active site enabling interaction with the substrate (Hajicek et al., 2013).

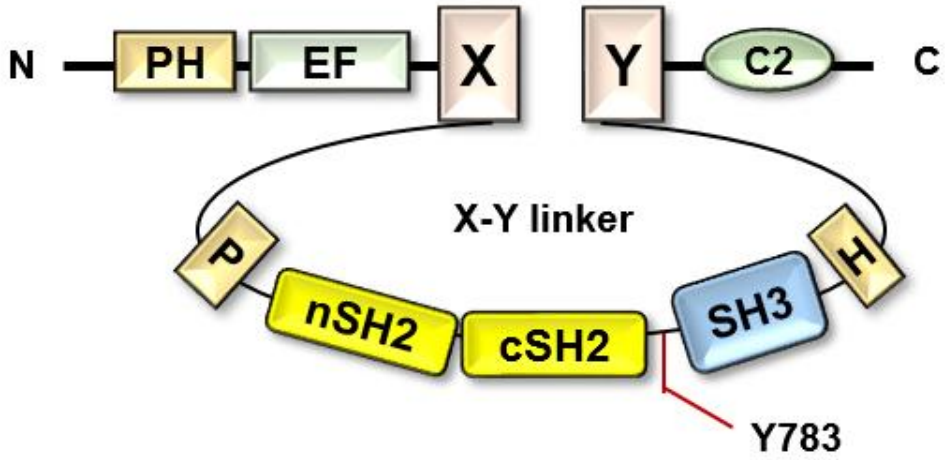

Figure 1. 7: PLCγ1 domains. PLCγ1 is composed of an N-terminal PH domain and a series of EF-hand domains followed by the catalytic domain called triosephosphate isomerase (TIM) barrel, which is followed by a C2 C-terminal domain. The catalytic domain is split into X and Y boxes which are linked by a X-Y linker containing two SH2 and one SH3 domain surrounded by a PH domain (P and H are the split PH domain in the amino acid sequence). Intramolecular interactions between c-SH2 and the X-Y boxes inhibits the enzymatic activity of PLCγ1. PH = plekstrin homology domain, EF = EF-hand,

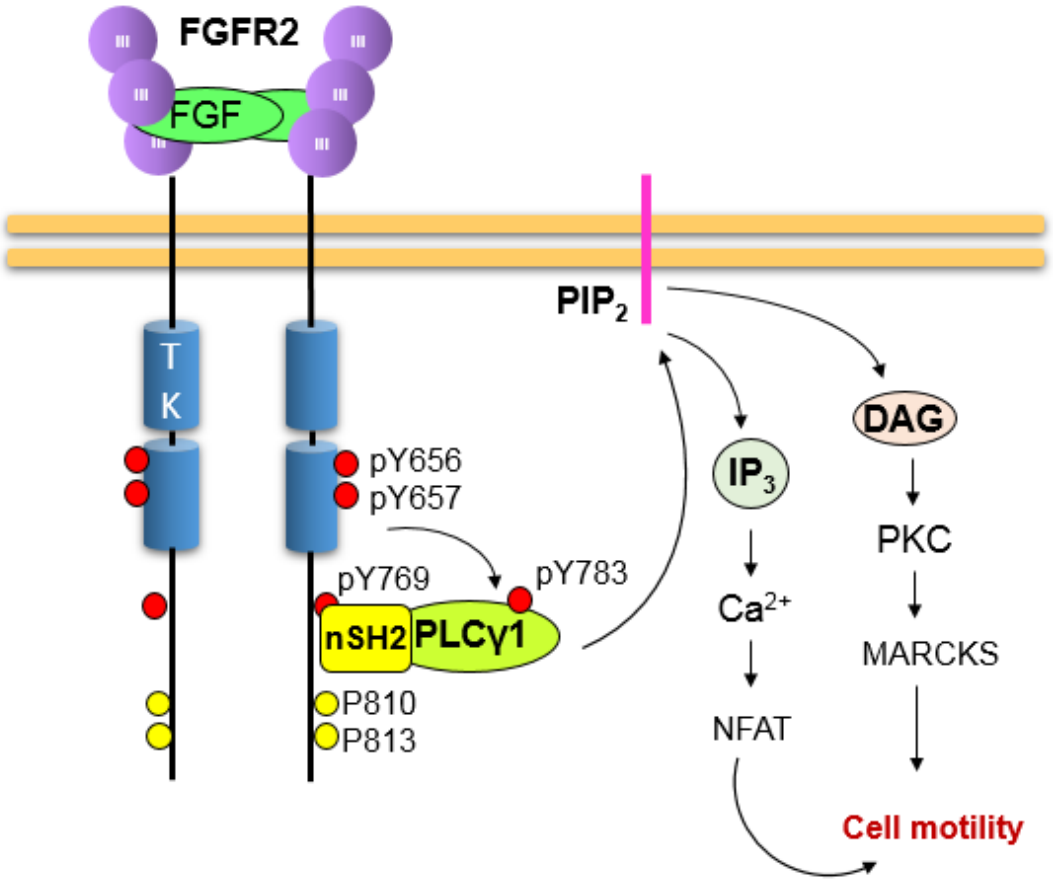

Figure 1. 8: The PLCγ1 pathway. Upon FGFR2 activation by FGF binding, tyrosine 769 is phosphorylated and can be recognized by the n-SH2 domain of PLCγ1. This binding is followed by tyrosine 783 phosphorylation located within the X-Y linker triggering the release of auto-inhibition. PLCγ1 can now hydrolyze PIP2 into IP3 and DAG, second messenger molecules that promote cell motility. nSH2 and cSH2 = N- and C- terminal SH2 domains, PIP2 = phospholipid phosphatidylinositol 4,5-biphosphate, IP3 = Inositol 1,4,5-triphosphate, DAG = diacylglycerol, NFAT= Nuclear factor of activated T-cells, PKC = Protein kinase C, MARCKS = Myristoylated alanine-rich C-kinase substrate

The recruitment of PLCγ1 to the receptor facilitates not only the activation of the enzyme but also places PLCγ1 in close proximity to the membrane where the substrate is located. IP3, one of the two products of the PIP2 hydrolysis, binds to the IP3 receptors in the endoplasmic reticulum triggering Ca2+ release into the cytoplasm which activates calcium-dependent proteins like calcineurin which in turn activates NFAT, a transcription factor that translocates to the nucleus activating the expression of cell motility genes. On the other hand, DAG activates the protein kinase C (PKC) which phosphorylates and activates substrates like the myristoylated Ala-rich C kinase substrate (MARCKS), a regulator of cell motility (Figure 1.8) (Goetz and Mohammadi, 2013). An alternative way of PLCγ1 activation under non-stimulating conditions includes interaction with the FGFR2 receptor through the SH3 domain of PLCγ1 binding to the proline-rich motif of the receptor at the C-terminal domain (Timsah et al., 2014). This phenomenon is explained in the next section.

.

1.2.4.2. The Ras/MAPK and PI3k/Akt pathway

Two additional pathways can be initiated by FGFR2 activation called mitogen-activated protein kinase (MAPK) and PI3k-Akt pathway. The first and most critical component of these pathways is FGFR-related substrate 2 (FRS2). FRS2 is an adaptor protein, meaning that it lacks catalytic activity, and is also a substrate of FGFR2 (the first substrate (FRS1) of FGF receptors is actually PLCγ1). Not all RTKs can bind FRS2 since its PTB domain recognizes residues only on FGFRs, neurotrophin receptors and RET. Both isoforms of FRS2, FRS2α and FRS2β, carry a myristilation sequence at the N-terminal which anchors them to the plasma membrane, a PTB domain that binds to either phosphorylated or non-phosphorylated tyrosine residues on specific RTKs and a series of tyrosines that can be phosphorylated by activated receptors and act as docking sites for

downstream signaling proteins such as GRB2 and Shp2 (Figure 1.9). Both FRS2α and -β have 2 binding sites for SH2-containing tyrosine phosphatase (Shp2). FRS2α also has 4 binding sites for Grb2, another adaptor protein, while FRS2β has three (Gotoh, 2008).

Notably, FRS2 constitutively binds to specific tyrosine residues on the juxtamembrane region of FGFRs that are not phosphorylated, meaning that it is bound to FGFRs even in the absence of extracellular stimulation. However, the binding to RET and neurotrophine receptors is activation-dependent and the binding is mediated through the PTB domain of FRS2 that recognizes phosphotyrosines in the juxtamembrane region of those receptors. When FGFRs are activated, FRS2 is phosphorylated by the receptor at the tyrosine residues creating docking areas for Grb2 and Shp2. Grb2 contains one SH2 domain that uses to bind to the phosphorylated FRS2 and two SH3 domains that interact with downstream proteins such as SOS, Gab1 and Cbl (Figure 1.10) (Gotoh, 2008).

SOS stands for son-of-sevenless and is a guanine nucleotide exchange factor (GEF) for Ras, a GTPase. The binding of SOS to Grb2 through the N-terminal SH3 domain of Grb2 results in SOS activation due to the release of C-terminal inhibition and also brings SOS in close proximity to the membrane-bound Ras, where it can exchange GDP with GTP resulting in Ras-GTP, the activated form of Ras (Zarich et al., 2006). Ras, in turn, activates the first kinase of the pathway called Raf, which is a serine/threonine kinase, initiating a cascade of kinase phosphorylation and activation. MEK1/2 phosphorylation and activation by Raf is followed by MEK1/2-mediated ERK1/2 activation. ERK1/2 can translocate to the nucleus where it phosphorylates transcription factors like c-Fos that regulate gene expression promoting cell proliferation (Figure 1.10) (Dhillon et al., 2007).

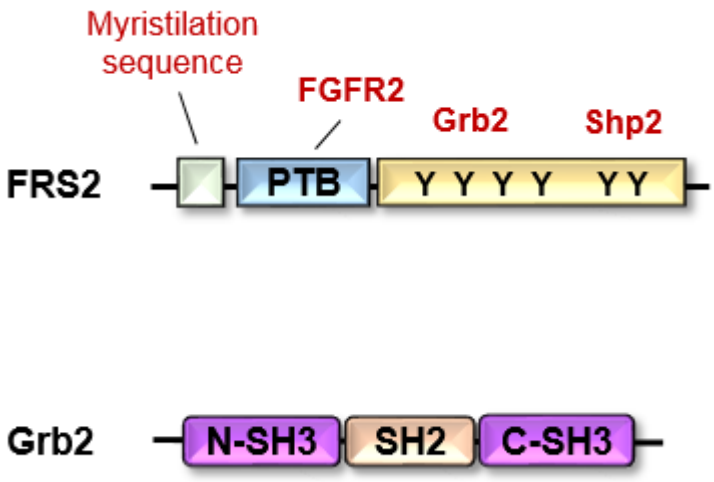

Figure 1. 9: Figure 1.4: FRS2 and Grb2 adaptor proteins. FRS2 contains a myristilation sequence that uses to anchor to the cell membrane, a PTB domain that recognises residues in the juxtamembrane region of FGFR2 and a series of phospho-tyrosines responsible for Grb2 and Shp2 recruitment through SH2 domains. Grb2 contains a single SH2 domain surrounded by two SH3 domains.

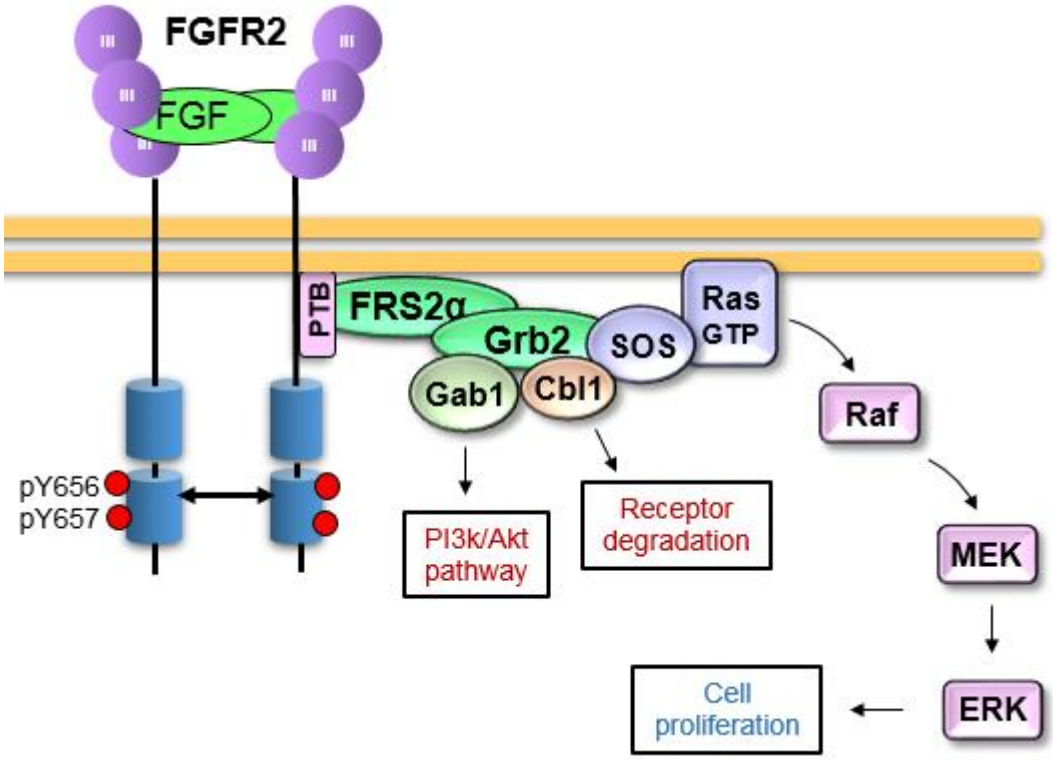

Figure 1. 10: The MAPK pathway. A stimulated receptor phosphorylates tyrosine residues on FRS2 which interact with Grb2. Grb2, in turn, interacts with Gab1, that initiates the PI3k/Akt pathway, Cbl1, that triggers receptor degradation and SOS, which activates the Ras/Raf/MAPK pathway.

Gab1 stands for Grb2-associated binding protein 1 and is another adaptor protein that binds to the C-terminal SH3 domain of Grb2 triggering the PI3k-Akt pathway as illustrated in Figure 1.11. Upon receptor activation the formation of the complex FRS2/Grb2/Gab1 causes phosphorylation of Gab1 recruiting the phosphatidylinositol-4,5-bisphosphate 3-kinase (PI3k) that produces PIP3. PIP3 is recognized by plekstrin (PH) domains contained in proteins like Akt (or PKB for Protein Kinase B) and phosphoinositide-dependent kinase-1 (PDK-1). As a first step, the binding of Akt to PIP3 releases the auto-inhibition caused by intermolecular interactions between the PH domain and the kinase domain. The complete activation of Akt occurs following phosphorylation of the threonine 308 by the also membrane-recruited PDK-1 and the phosphorylation of serine 473 by mTOR complex 2 (mTORC2). Negative regulation of the PI3k-Akt pathway is mediated by the Phosphatase and tensin homolog (PTEN) which reverses the production of PIP3 by PI3k as well as by two phosphatases named Protein phosphatase 2 (PP2A) and PH domain and Leucine rich repeat Protein Phosphatases (PHLPP) that dephosphorylate thr308 and Ser473 on Akt, respectively, resulting in Akt inhibition (Hers et al., 2011).

Activated Akt phosphorylates a variety of downstream effector proteins regulating cell survival and apoptosis pathways, metabolism and cell proliferation (Figure 1.11). Akt positively regulates glucose transportation through negative phosphorylation of PTP11B, a downstream effector that inhibits insulin signalling. Metabolism is also regulated by phosphorylation of GSK3-β which inhibits the kinase activity resulting in the activation of the glycogen synthase enzyme and subsequently increase in the glycogen synthesis by the cell. GSK3 also stimulates cyclin D1 and E as well as c-jun and c-myc degradation and therefore, phosphorylation and inhibition by Akt promotes cell proliferation. Moreover, Akt regulates cell survival by phosphorylating pro-apoptotic Bcl-2 homology domain (BH3)-only proteins that inactivate pro-survival proteins like the Bcl-2 members. The

phosphorylation of BH3-only proteins inhibits their ability to inactivate pro-survival proteins promoting cell survival. Another Akt effector is ASK1 (apoptosis signal related kinase), whose phosphorylation prevents apoptosis. Furthermore, Akt promotes cell survival by regulating effectors in a transcriptional level. Akt negatively phosphorylates transcription factors of the FOXO (forkhead box) family preventing BH3-only proteins and Fas-ligand expression and subsequent apoptosis signalling pathways. Except for negative regulation, Akt positively phosphorylates transcription factors like CREB and NF-κB that activate the expression of Bcl-2 proteins and c-IAP1 & 2, respectively, triggering cell survival. Lastly, Akt positively regulates the mTORC1 pathway that stimulates cellular growth as well as negatively phosphorylates TSC2 (Tuberous Sclerosis Complex 2) and PRAS40 (Proline-rich AKT1 substrate 1), inhibitors of mTORC1 (Hers et al., 2011).

However, the adaptor protein FRS2 triggers both positive and negative signals. The binding of Cbl (Casitas B-lineage Lymphoma) to the complex of FGFR/FRS2/Grb2 causes ubiquitination and subsequently degradation of the receptor as a form of signal elimination (Kaabeche et al., 2004).

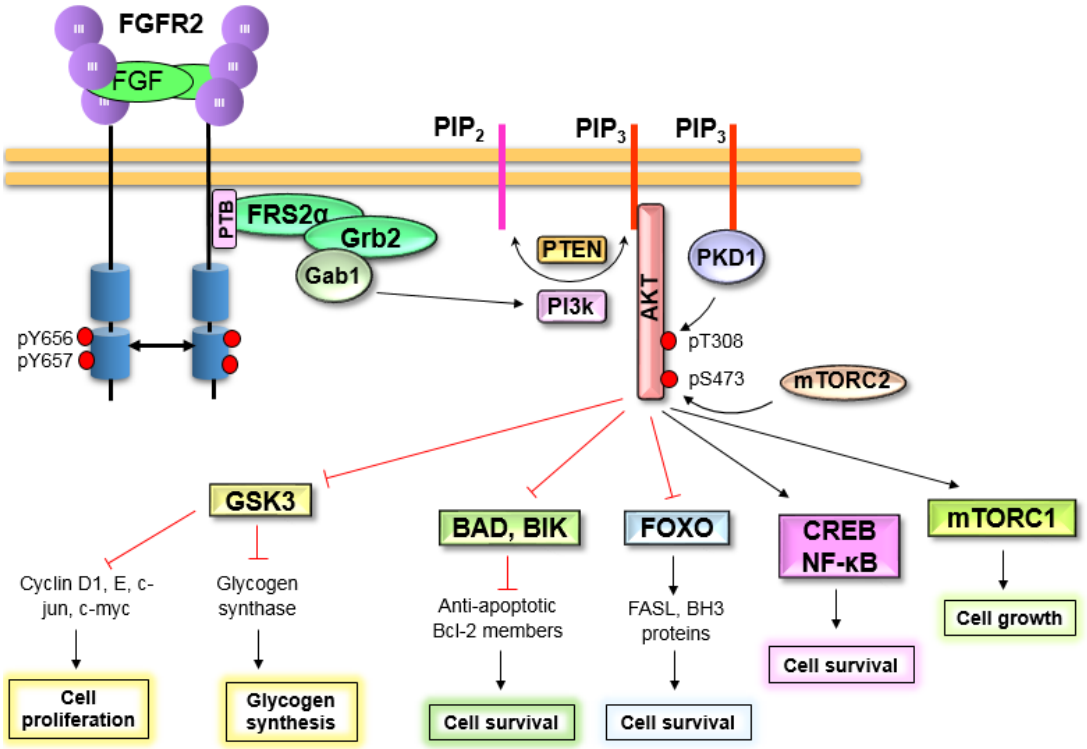

Figure 1. 11: FGFR2-mediated Akt/PI3k pathway. A stimulated FGFR2 receptor recruits the Grb2-Gab1 complex through FRS2. Gab1 activates PI3k that converts PIP2 to PIP3 which is in turn recognised by Akt and PDK1 through its plekstrin domain. In this way, Akt is recruited to the cell membrane where it gets phosphorylated by PKD1 in threonine 308 and by mTORC2 in serine 473. The phosphorylation causes Akt kinase upregulation which phosphorylates a series of targets like GSK3, the anti-apoptotic proteins BAD and BIK, the transcription factors of the FOXO family, CREB and NF-Kb and mTORC1 promoting cell proliferation, glycogen synthesis, cell survival and cell growth.

1.2.5. Importance of Proline-rich motifs in signal transduction

The most common type of protein motif found in eukaryotic cells is the proline-rich motif which frequently includes a sequence of mainly proline residues with additional flanking residues that form a special secondary structure called left-handed Polyproline II helix (PPII) (Rubin et al., 2000). The PPII helix features a pseudo-symmetry of three residues per turn, explaining the observed proline-rich motif patterns in proteins which are 1) PxxPxxP and 2) xPPxPPx, where x represents any other residue. Only six different types of proline-rich motif-binding domains have been described so far; SH3, WW, EVH1, GYF, UEV domain and the single-domain profiling proteins (Ball et al., 2005).

Proline-rich motifs are great binding targets for protein interactions due to several characteristics. The low entropic binding of proline-rich motifs to binding sites facilitates a relatively strong and stable binding. Polyproline peptides have an incredibly limited mobility (and thus entropy), coming from the fact that prolines have restricted degrees of rotational freedom, which is reduced even more upon interaction with proline-rich binding domains stabilizing the interaction. Therefore, the binding is stronger compared to an interaction involving a regular, more flexible polypeptide. An additional advantage originates from the fact that the backbone of the polyproline peptides lacks intramolecular hydrogen bond formation due to the unavailability of the amide of the prolines, making the carbonyl groups available for intermolecular hydrogen bonding. Similarly, carbonyl groups of prolines are electron-rich due to the interaction of the methyl group with the amide nitrogen, causing prolines to be good hydrogen bond acceptors rather

than donors, as other amino acids are. An interesting feature of PPII helices is that the side chains and the carbonyl groups of the backbone are pointed outward to the solvent at regular intervals (C2 pseudo-symmetry) explaining the property of binding sites to interact in two directions; the forward and reverse orientation (Ball et al., 2005; Williamson, 1994; Zarrinpar et al., 2003).

Notably, there is a wide range of proteins carrying proline-rich motifs. Firstly, hydroxylated polyproline motifs have a more structural rather than a binding/interaction role. They exist in proteins like collagen, the most abundant protein in animals, whose triple-stranded helix consists of three PPII helices in which proline residues stabilize the collagen structure. Additional examples of proline-rich motifs with structural role are the blood complement protein C1q as well as the plant cell wall proteins called extensins. Apart from the structural role, proline-rich motifs are generally involved in protein interactions necessary for different processes. One example is the salivary proline-rich proteins whose sequence is mainly constituted of proline-rich motifs. These proteins account for the 70% of all the proteins in the saliva and use the proline-rich motifs to bind to dietary polyphenols in order to eliminate the toxic effects. Mutual proline-rich interactions are also crucial for transcription processes. RNA Pol II possesses a series of repeated proline-rich motifs at the C-terminal domain which is speculated that it is involved in the assembly of multiple transcriptional activators forming transcription complexes. Furthermore, proline-rich motifs are also implicated in synaptic vesicle release process. Syntaxin-1, for instance, carries proline-rich motifs that uses to interact with membrane-bound proteins like VAMP-1 and synaptophysin, also proline-rich

proteins, activating vesicle release at synapses. A final type of proline-rich proteins that has also attracted a lot of interest due to the involvement in signal transduction is the proteins that bind to SH3 domains. SH3-containing proteins can have a catalytic activity like PLCγ1, Src, Abl or can be adaptor proteins like Grb2 (Williamson, 1994).

SH3 domains are sequences of around 60 residues long that bind to the PxxP motif in two orientations and thus, they are divided into two classes. SH3 Class I binds in the forward orientation (N- to C-) and recognizes the motif (R/K)xxPxxP, where R = Arginine and K = Lysine and SH3 Class II binds in reverse orientation (C- to N-) and recognizes the motif PxxPx(R/K). SH3 domains form two anti-parallel β-sheets and two loops, named RT and c-Src loop. The interaction occurs when aromatic residues of the SH3 domain (Tyrosine and Tryptophan) that form hydrophobic groves, form hydrogen bonds with the backbone carbonyl groups of the PPII. The exposed side chains of the prolines 1 and 4 (periodic turn every 3 residues) enter the hydrophobic pockets of the SH3 surface just like ridges and groves. Specificity is accomplished by residues in the surrounding loops flanking the core binding area that interact with opposite flanking residues on the PPII helix of the proline-rich motif (Ball et al., 2005; Zarrinpar et al., 2003).

SH3 domains can have a recruitment as well as a regulatory role. For instance upon stimulation, FGFR2 is activated and phosphorylates FRS2 creating phosphotyrosine binding sites for the SH2 domain of Grb2. Grb2 is already bound to SOS through the nSH3 domain that recognizes the proline-rich motif (VPPPVPPRRR peptide) on SOS, the activator of Ras. As Ras is

myristoylated and membrane-bound, Grb2 brings SOS in membrane vicinity resulting in co-localisation with Ras and subsequent activation of the GTPase (Terasawa et al., 1994). In this case, interaction between SH3 domains and proline-rich motifs connects the activation of receptor tyrosine kinases with the Ras-Raf-MAPK pathway. In other cases, SH3 domains regulate protein activity such as the SH3 domain in src kinase that once bound to targets, releases the inhibitory effect that was established by intramolecular interactions with the src SH2 domain (113).

Apart from adaptor and effector proteins, proline-rich motifs exist in the C-terminal domain of tyrosine kinase receptors. The proline-rich motif of FGFR2 has been proved to be involved in signal transduction regulation via protein-protein interactions. The first binding partner was identified in 2010 by Ahmed *et al* who described the direct interaction between the proline-rich motif of FGFR2 with the c-SH3 domain of the adaptor protein Grb2. In basal conditions, dimeric Grb2 binds to FGFR2 causing dimerization and basal auto-phosphorylation activity, yet no downstream signalling pathway is activated. The binding covers tyrosine residues inhibiting phosphorylation and complete activation of the receptor (Figure 1.12a). Upregulation of the kinase activity occurs when the receptor is stimulated by an FGF ligand resulting in Grb2 phosphorylation in tyrosine Y209. Grb2 is no longer capable of binding to FGFR2, enabling the receptor to get fully activated and trigger downstream signalling pathways (Figure 1.12b) (Ahmed et al., 2010). The second binding partner was identified in 2014 by Timsah *et al*, who demonstrated that PLCγ1 can interact with the proline-rich motif of FGFR2 via its SH3 domain. In basal conditions. PLCγ1 auto-inhibition prevails and the pathway is inactive. PLCγ1 auto-inhibition is released upon binding to

the proline-rich motif of the receptor resulting in pathway activation and increased cellular invasion. Notably, the interaction with FGFR2 depends on protein concentration since Grb2 is also competing for the binding site (Figure 1.12c) (Timsah et al., 2014). Nevertheless, PLCγ1 can also be “canonically” activated by interacting with phospho-tyrosines on stimulated FGFR2 via its SH2 domain, as described in the PLCγ1 section.

Both of these cases highlight the importance of receptor-proline rich motifs in signal transduction regulation under non-stimulating conditions, either by inhibiting receptor activation or by regulating pathways depending on protein equilibrium. However, not all the binding partners have been identified. SH3-containing proteins are more prominent because they are known to recognise proline-rich motifs. So far, both Grb2 and PLCγ1 interact with FGFR2 through their SH3 domains. Interestingly, there is evidence of direct interaction between proline-rich motifs and Ankyrin repeat domains, another common protein motif explained in detail in the TRPA1 section. According to Rader *et al*, the mouse Ankyrin-repeat family A protein (ANKRA) interacts with the proline-rich motif-containing cytoplasmic domain of rat megalin (a low-density lipoprotein receptor found in epithelial kidney cells) through its ankyrin repeats (Rader et al., 2000). Based on this evidence, there could be possible ankyrin repeat containing binding partners for the proline-rich motif of FGFR2. One of them is the ion channel TRPA1 which is described in section 1.3 and studied in this project.

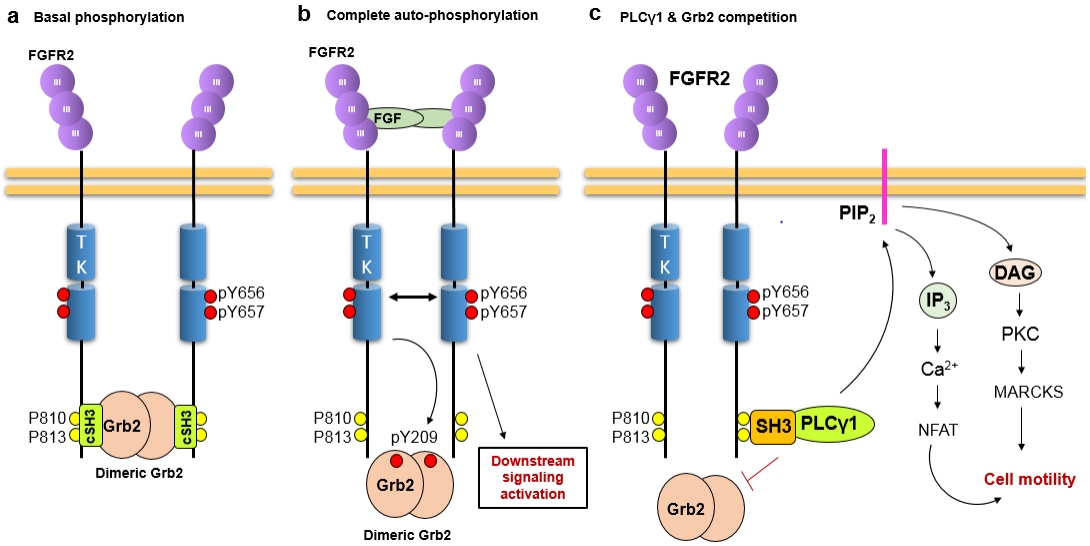

Figure 1. 12: FGFR2 proline-rich motif protein interactions and role in signal transduction. **a.** Dimeric Grb2 regulates the basal FGFR2 phosphorylation levels by interacting with the C-terminal proline-rich motif of the receptor through its cSH3 domain. **b.** Under stimulating conditions, FGFR2 kinase activity is upregulated and phosphorylates Grb2 in tyrosine 209 resulting in Grb2 dissociation and activation of downstream pathways. **c.** PLCγ1 competes with Grb2 for the proline-rich motif of FGFR2. Under non-stimulating conditions and low Grb2 concentrations, PLCγ1 binds to the receptor and gets activated resulting in PLCγ1 pathway activation and increased cell invasion.

1.2.6. FGFR2 implication in cancer

Aberrant FGFR signalling is responsible for various skeletal disorders as well as numerous carcinomas. Aberrant signalling can originate from gene amplification, protein overexpression, activating mutations or chromosomal translocations that all result in enhanced receptor activity and downstream signalling (Hallinan et al., 2016).

Out of all FGFRs, gene amplifications are more frequent in FGFR1 gene and have been reported in 16% of squamous NSCLC, 15% of ER-positive and 4.1% of triple-negative breast cancers (Lee et al., 2014; Schildhaus et al., 2013, p. 1). However, FGFR2 gene and protein are also amplified/elevated in 4.7% and 12.8% of triple-negative breast cancers, respectively, and FGFR2 SNPs have been associated with increased breast cancer risk (Campbell et al., 2016; Lee et al., 2014). Moreover, FGFR2 is found overexpressed in approximately 4-9% of gastric cancers and is associated with aggressive tumours and poor prognosis (Ahn et al., 2016; Deng et al., 2012). Inhibition of FGFR2 with PD173074 in FGFR2–amplified gastric cell lines resulted in decreased cell proliferation and increased apoptosis. Concomitant with the enhanced FGFR2 signalling, increased phosphorylated EGFR, Her2 and Erbb3 levels were observed which conferred resistance to anti-EGFR treatment and were FGFR2-dependent (Kunii et al., 2008). Interestingly, overexpression of FGFR2 in those cancers is accompanied by the overexpression of the FGFR2-IIIb C3 isoform that has a shorter C-terminal region and lacks specific tyrosine and leucine residues important for receptor internalisation. The C3 isoform confers more stability and increased activity to the receptor promoting tumorigenic levels

of signalling (Cha et al., 2009). FGFR2 protein levels are also increased in 11.1% of hepatocellular carcinoma and associated with poorer overall survival (Lee et al., 2015) Increased FGFR2 protein levels also occur in 12.9% of NSLC and 52% of pancreatic cancer cases in which are correlated with advanced stages (Matsuda et al., 2014; Theelen et al., 2016). On the other hand, FGFR2 down-regulation has also been reported. Both main FGFR2 isoforms (IIIb and IIIc) are decreased in thyroid cancer suggesting the use of FGFR2 expression levels as a marker for early diagnosis (Redler et al., 2013).

In contrast, FGFR2 activating mutations are more common in cancers. FGFR2 mutations similar to germline mutations responsible for skeletal syndromes are present in 10-16% of endometrial carcinoma including the most common S252W mutation that affects the D2-D3 extracellular ligand-binding domain that enhances ligand affinity and alters specificity (Pollock et al., 2007; Yu et al., 2000). Inhibition of FGFR2 by PD173074 or shRNA reduced endometrial cell lines proliferation and induced apoptosis (Byron et al., 2008). FGFR2 mutations also occur in 2.7-5% of squamous NSCLC and 2.2% of total NSCLC cases (Hibi et al., 2016; Liao et al., 2013). Most of these mutations are located in the extracellular domain increasing ligand-binding or receptor dimerisation and activation. However, tyrosine kinase domain mutations also occur and are capable of promoting cellular transformation in xenografts which can be reversed by FGFR2 inhibitors (Liao et al., 2013; Tchaicha et al., 2014).

FGFR2 fusion proteins are rare in cancers. However, FGFR2 fusions have been found in NSCLC (FGFR2-KIAA1967), breast cancer (FGFR2-AFF3),

prostate (SLC45A3-FGFR2) and thyroid cancer (FGFR2-OFD1), where the FGFR2-binding partner promotes receptor dimerization and kinase activation (Wu et al., 2013). The most common FGFR2 fusion is found in cholangiocarcinoma with the FGFR2-PPHLN1 fusion present in 16% of the cases (Sia et al., 2015).

Moreover, FGFR2 isoform switch (IIIb to IIIc) is implicated in epithelial to mesenchymal transition (EMT) and cancer progression. FGFR2IIIb is characterised as an epithelial isoform due to involvement in epithelial cell differentiation while FGFR2IIIc is a mesenchymal isoform which is often overexpressed in epithelial tumours. Ranieri *et al* 2016 showed that human keratinocytes overexpressing IIIc instead of IIIb demonstrated morphological and cytoskeletal changes that favour invasive phenotypes like anchorage-independent cell growth and expression of mesenchymal markers (Ranieri et al., 2015b). The phenotype actually occurs following FGF2 treatment indicating that stimulation is still required for activation of the receptor and EMT initiation. However, the two isoforms have different specificity and affinity for ligands thus, microenvironment signals are interpreted in different ways. The FGFR2IIIb-mediated keratinocyte invasiveness is also supported by the fact that E5 human papilloma virus 16 protein (16E5) was able to alter the FGFR2 splicing machinery in keratinocytes so that the IIIc isoform is produced, a switch necessary for EMT initiation in the early stages of carcinogenesis (Ranieri et al., 2015a). Similarly, the isoform switch to IIIc was observed in 90% of renal carcinomas and associated with a mesenchymal cell phenotype (Zhao et al., 2013). Presence of the IIIc isoform is also found in 27% of colorectal cancer cases and is associated with distant metastasis and poor prognosis. Colorectal cancer cell lines

overexpressing IIIc isoform demonstrated increased growth and invasion as well as increased formation of larger tumours in mice. These results were reversed by an FGFR2IIIc-specific antibody suggesting the FGFR2 isoform targeted therapy (Matsuda et al., 2012). Numerous studies have suggested the role of FGR2IIIc in tumour progression and EMT in various cancers like breast, cervical and prostate cancer (Cha et al., 2008; Kawase et al., 2010; Shoji et al., 2014). Despite this evidence, the role of IIIc remains elusive since it is also involved in mesenchymal to epithelial transition (MET) as reported in bladder cancer cell lines (Chaffer et al., 2006).

1.3. The Transient Receptor Potential Ankyrin Repeat 1 (TRPA1)

1.3.1. The TRP channels

TRP (Transient Receptor Potential) channels are non-selective cation channels, meaning that they are permeable to monovalent (Na^+, K^+) and divalent (Ca^{2+}, Mg^{2+}) cations, with higher selectivity to Ca^{2+}. Not all the structures of the known TRP channels have been elucidated yet, but they all seem to share the same membrane topology of six transmembrane domains (S1-S6) with a central pore formed by the pore helixes between S5 and S6. A functional channel is composed of four subunits forming homotetramers (Venkatachalam and Montell, 2007). However, heterotetramers have also been found within members of the same family like the TRPC family (Cioffi et al., 2012; Strübing et al., 2001; Woo et al., 2014) as well as members of different families (Kobori et al., 2009; Stewart et al., 2010).

TRP channels are distinctive from the similar topology voltage-gated K^+ channels due to the absence of charged residues in the S4 domain; thus

TRP channels are non-voltage-gated ion channels that are mainly expressed in sensory neurons. Conservation between species reveals the critical role of TRP channels in sensing environmental cues, from thermosensation all the way to noxious pain sensation (Venkatachalam and Montell, 2007). The implication of TRP channels into several sensations like heat and cold sensing, vision, hearing, olfaction, taste, touch and pain have been reported in the past however, the exact mechanism of action remains most of the times unknown (Bautista et al., 2007; Caterina et al., 1997; Cuajungco et al., 2007; Grandl et al., 2010; Jin et al., 2017; Julius, 2013; Montell, 2005; Pyrski et al., 2017). Despite the identical membrane topology, diversity in the activity between TRP channels is noticed due to differences in the amino acid sequence of the N- and C-terminal domains, which both happen to be intracellular and carry variable motifs like Ankyrin repeats, coiled coil regions, TRP box, EF-hand, Ca^{2+}/calmodulin binding sites, enzymatic activities and more (Voets et al., 2005).

1.3.1.1. The trp mutant

In 1969, Cosens D.J. and Manning A. discovered a new Drosophila Melanogaster mutant with impaired visual system based on behavioural tests. They described the mutant as nearly blind since the electroterinogram (ERG) response to a continuous bright light decreases after a period of 10 to 15 seconds, followed by a recovery period during which the fly cannot respond to any light stimuli. They located this Mendelian factor in the third chromosome and identified it as a recessive mutation (Cosens and Manning, 1969). Later on, in 1975, Minke, B. and colleagues named this D. Melanogaster mutant as transient receptor potential mutant (trp) due to the

fact that unlike wild-type flies, there was a transient large initial response to intense light that decays to the baseline, steady state potential that represents the response to dim light (Minke et al., 1975). During that time, the role of the trp locus was unknown, until 1989 when the trp gene was cloned. The trp RNA is 4.1kb long and produces a 1275 amino acid transmembrane protein with 8 putative TM domains that was not similar to any known protein in that time (Minke et al., 1975). However, it was believed that the TRP protein was involved in light signal transduction subsequent to the production of IP3 by PLC (PLC is activated by G-proteins activated by rhodopsin, a light-sensitive receptor in flies) (Montell and Rubin, 1989).

The first evidence suggesting that the TRP protein is a calcium (Ca^{2+}) channel came from experiments using the fly Calliphora in which Lathanum (La^{3+}), a non-selective Ca^{2+} transporter blocker, was applied to the retina of the wild type fly. Similar to the Drosophilatrp mutant, the response to intense light stimulation was decreased after a short period of high receptor potential (Hochstrate, 1989). Soon enough, Suss Toby et al., verified the previous results and described that La^{3+} application caused a trp-like response in wild type flies but not in the trp mutant homologue in those flies, indicating that the TRP protein is a putative Ca^{2+} transporter that can be blocked by La^{3+} (Suss-Toby et al., 1991).

In 1992, Hardie and Minke demonstrated that the TRP protein is indeed a non-voltage-gated Ca^{2+} channel that is absent in the trp mutant and tried to explain the trp phenotype based on that hypothesis. They proposed that there are at least two classes of light-sensitive Ca^{2+} channels involved in the phototransduction system of the fly and that TRP is the high Ca^{2+}

permeability one which is missing in the trp mutant. However, the stable-plateau state is sustained by the second class of ion channels. They also explained that the TRP Ca^{2+} channel is indirectly activated by IP3 to initiate Ca^{2+} influx into the cell that is important for excitation during intense light stimulation (Hardie and Minke, 1992). At the same time, another group of researchers identified a trp homologue in the Drosophila genome with a 74% transmembrane amino acid sequence similarity that they named transient receptor potential-like (trpl) gene. The TRPL protein has 2 calmodulin-binding sites, has 6 transmembrane domains and carries Ankyrin-like repeats. The group proposed that the TRPL protein is also a Ca^{2+} channel, expressed in rhabdomeres like the TRP protein, verifying the Hardie and Minke's hypothesis of two separate classes of Ca^{2+} channels mediating the wild type response in intense light illumination (Phillips et al., 1992).

1.3.1.2. The discovery of mammalian TRP channels

After the discovery of TRP channels in arthropods, studies were focused on identifying the existence of those channels in vertebrate organisms. Since the first TRP channel in Drosophila, more than 100 homologues have been identified in several animals. In total, 28 channels have been found in mammals and only 27 channels, grouped in 6 families, have been found in humans; TRPC (canonical), TRPV (vanilloid), TRPM (melastatin), TRPP (polycystin), TRPML (mucolipin) and TRPA (ankyrin) (Nilius and Owsianik, 2011).

The first human trp homologue was discovered in 1995. It was named Human trp-1 (Htrp-1) and it was almost 40% identical to the invertebrate trp (Zhu et al., 1995). The same year, another group identified a family of

human TRP channel genes named TRPC1-3 for transient receptor potential channel-related protein 1-3. Only the TRPC1 and 3 were actually expressed into proteins; TRPC2 is a pseudogene. These channels were widely expressed in human tissues (mainly brain, testis, ovaries and heart) and characterised as non-voltage gated ion channels due to the absence of charged residues in the S4 transmembrane domain. These discoveries revealed that trp proteins are conserved within species and mediate an important role in calcium replenishment. Another important observation is the conservation of Ankyrin repeats in the N-terminal domain of trp channels, suggesting a regulatory role in channels activation or signal transduction through the cytoskeleton (Wes et al., 1995). The next year, 7 TRP channels were identified in the mouse genome (Mtrp-1-6 and TRP7) (Okada et al., 1999; Zhu et al., 1996). The mammalian TRP channels, had high similarity to the original Drosophila trp and later were grouped in the same category of TRP-canonical (TRPC) ion channels consisting of 7 members in humans (Montell et al., 2002).

The next human trp channel was discovered in 1997 by David Julius group in an attempt to identify capsasin receptors (capsasin is the active ingredient in “hot” chilli peppers). A functional assay was performed based on the fact that capsasin stimulation results to Ca^{2+} influx in sensory neurons. The assay was designed to detect Ca^{2+} influx followed by capsasin treatment of non-neuronal cells transfected with cDNA clones from dorsal root ganglia neurons (DRG) library, thinking that the expression of the receptor-coding cDNA would mediate non-neuronal cell stimulation. The new receptor was named vanilliod receptor 1 (VR1) and was also heat-activated. VR1 was expressed in small diameter sensory neurons. Homology studies revealed

that VR1 was similar to other human TRPs and the original trp channels in Drosophila underlying the diverse role of trp channels (Caterina et al., 1997). Two years later, the vanilloid receptor-like protein 1 (VRL1) was cloned by the same group based on sequence similarity with VR1. The new protein was not activated by capsasin but noxious heat (52^{o}C), was 66% identical to VR1 and seemed to belong to the trp family of ion channels (Caterina et al., 1999). Within the next years, more ion channels similar to VR1 were identified and grouped in the same family of transient receptor potential vanilloid (TRPV) channels (Hoenderop et al., 2001; Montell et al., 2002; Smith et al., 2002). The TRPV family consists of 6 TRP ion channels in humans (Nilius and Owsianik, 2011).

Melastatin was the founding member of the TRPM family of ion channels, first characterised in 1998 (Hunter et al., 1998; Montell et al., 2002). Only 8 members of the TRPM family are expressed in the human genome . The founding member of the TRPP family is PKD2 (polycystic kidney disease-2) or Polycystin-2, a protein involved in Polycystic kidney disease. The human TRPP family consists of three members: TRPP2 (PKD2), TRPP3 (PKD2L1) and TRPP5 (PKD2L2) (Koulen et al., 2002; Nilius and Owsianik, 2011; Veldhuisen et al., 1999). The gene named MCOLN1 that is involved in Mycolipidosis IV, a degenerative disorder, encodes for the protein mucolipin, the founding member of the TRPML family of ion channels that consists of three channels in total (Nilius and Owsianik, 2011; Sun et al., 2000). The most recently discovered family of TRP channels is the TRPA family with the TRP-Ankyrin 1 (TRPA1) being the one and only member of this family in humans (Jaquemar et al., 1999).

1.3.1.3. The discovery and characterisation of TRPA1

TRPA1 was discovered in 1999 by D. Jaquemar et al. in an attempt to identify proteins with altered expression following oncogenic transformation (Jaquemar et al., 1999). It was found that TRPA1 was one of the transformation-sensitive proteins that were repressed in SV40-trasnformed human lung fibroblasts. This novel Ankyrin repeat-containing protein was named p120, was 1119 amino acid long and 127.5kDa. The gene is located at chromosome 8 in the region 8q13. p120 was expressed in very low levels in human tissues and mainly in lung fibroblasts and liposarcoma cells. Based on its amino acid sequence, p120 could be divided into two parts: an N-terminal domain containing 14-18 ankyrin repeats resembling the cytoskeletal protein Ankyrin and, a C-terminal domain containing 6 hydrophobic segments that could be transmembrane domains. Full length p120 could not be overexpressed in mammalian cells despite numerous attempts. High levels of the protein appeared to be toxic and abolished healthy cell growth. The function of the novel protein remained unknown, however it was noted that its topology was very similar to the TRP-like proteins, characterising it as putative ion exchanger which is involved in signal transduction (Jaquemar et al., 1999).

Generally, TRP channels are involved in thermosensation and can be activated at different temperature thresholds like the heat-activated TRPV1 at 43^{o}C, TRPV3 at 33^{o}C, TRPV2 at 55^{o}C and the cool temperature- and menthol- activated TRPM8 (25oC) (Bautista et al., 2007; Bender et al., 2005; Grandl et al., 2010; Moqrich et al., 2005). In 2003, Story et al. identified TRPA1 as a cold-activated TRP channel after screening for proteins that

resemble TRP channels and could be involved in thermosensation (Story et al., 2003). The first evidence originated from the fact that TRPA1 was expressed in a small population of mouse DRG neurons including the non-myelinated C and αδ fibres as well as Calcitonin gene-related peptide (CGRP) and substance P (SP)- positive neurons, which are also involved in sensing temperature and noxious cues. TRPA1 was further found to be co-expressed with the heat-activated TRPV1-prositive neurons at 30%, while 97% of the TRPA1-positive neurons expressed TRPV1 at the same time. By performing a series of calcium imaging and patch clamp experiments on TRPA1-transfected CHO and HEK cells as well as utilising Xenopus oocytes, Story et al. introduced that TRPA1 is a cold temperature-activated non-selective cation channel with a temperature threshold of approximately 17^{o}C. However, TRPA1 was not co-expressed with the cold-activated TRPM8, suggesting at least three distinct subpopulations of neurons: TRPV1+/TRPA1+/TRPM8- which can be activated at cold temperatures (~15oC) (as well as hot temperatures), TRPV1-/TRPA1-/TRPM8+ which can be activated at cool temperatures (~24^{o}C) and menthol and lastly, TRPV1+/TRPA1-/TRPM8- activated at hot temperatures (Story et al., 2003).

Following the discovery of TRPA1 thermosensitivity, a series of plant-based natural compounds were also identified as TRPA1 agonists including allyl-isothiocyanate (mustard oil), cinnamaldehyde (cinnamon), gingerol (ginger), eugenol (cloves), methyl salicylate (wintergrass), D9-tetrahydrocannabinol (THC) and cannabinol (cannabis), describing TRPA1 as a noxious compound chemosensor of DRG and trigeminal ganglia neurons (Bandell et al., 2004; Jordt et al., 2004). Moreover, a panel of isothiocyanates (chemical group –N=C=S) known to cause skin irritation and inflammation were also

identified as TRPA1 specific agonists. Apart from the allyl-isothiocyanate found in mustard oil, this panel included benzyl-isothiocyanate (yellow mustard), phenylethyl-isothiocyanate (Brussel sprouts), isopropyl-isothiocyanate (nasturtium seeds) and methyl-isothiocyantate (capers) (Jordt et al., 2004). Furthermore, it was demonstrated that TRPA1 can also be activated indirectly by bradykinin (a pain- and inflammation-inducing reagent) through B2R (bradykinin receptor) and the downstream activation of PLC effectors, supporting the nociceptive role of TRPA1. However, the exact mechanism of activation is not known yet (Bandell et al., 2004). Interestingly, Jordt et al. (2004) were the first to demonstrate that human TRPA1 is not a cold-sensitive channel, initiating the still ongoing controversy regarding the ability of the human TRPA1 to detect and be activated by cold temperatures.

1.3.2. TRPA1 structure

The structure of the human TRPA1 was determined in 2015 by David Julius' group to approximately 4Å by electron cryo-EM-microscopy (Paulsen et al., 2015). A functional TRPA1 channel consists of four subunits forming a homotetramer. Each subunit carries a cytoplasmic N-terminal domain consisting of 16 ankyrin repeats, six α-helices forming the transmembrane domain and a cytoplasmic C-terminal domain folded in a coiled-coil secondary structure (Figure 1.13 and 1.14). The most distinctive feature of TRPA1 is the extended N-terminal domain, which combined with the C-terminal domain, comprises 80% of the whole channel mass (Paulsen et al., 2015).

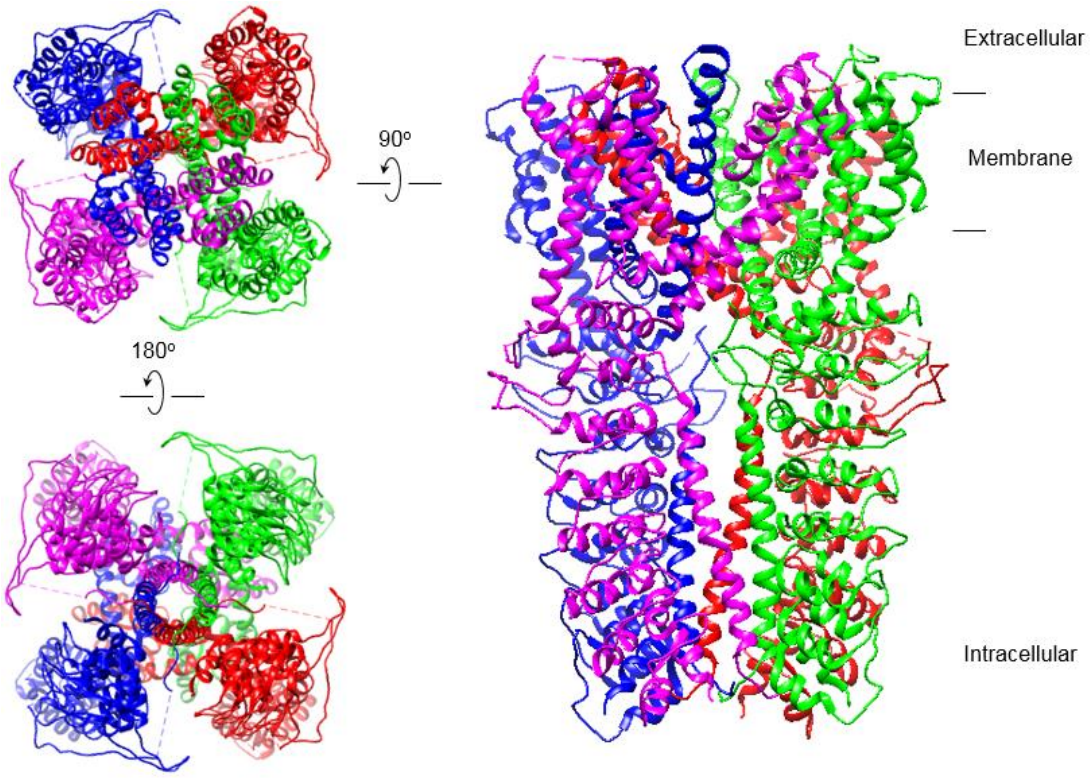

Figure 1. 13: The structure of a TRPA1 tetramer as solved by Paulsen et al 2015. Each subunit is represented in a colour-coded ribbon diagram. The extracellular view (top left), cytosolic view (bottom left) and side view (right) are shown and include the residues 446-1078. Unstructured regions including the AR1-11 are excluded from this representation. The structures were made using the Chimera software and the data obtained from PDB 3J9P.

In more detail, the tetrameric C-terminal coiled-coil structure is located right underneath the channel's pore and is crucial for inter-subunit interactions and channel assembly (Figure 1.13). It appears that stabilising factors like polyphosphates (inositol hexakisphosphate – InsP6) bind to this area supporting channel's function and integrity. An additional stabilising element at this location is a group of five Ankyrin repeats (ANK12-ANK16) of the N-terminal domain of each subunit surrounding the tetrameric coiled-coil providing extra support and all together forming the "stem" of the channel (Figure 1.13). The configuration of the remaining 11 ankyrin repeats is poorly determined however, it is speculated that this group of ankyrin repeats of each subunit forms a crescent shape and all four crescent-shaped wings adopt a "propeller" structure right at the bottom of the channel located in the cytoplasmic area (Paulsen et al., 2015).

Right above the "stem" of the channel and adjacent to the transmembrane domain, there is a complex network of multiple interactions between different structural elements of the channel that allosterically regulate the pore gating. Following the 16th ankyrin repeat, a pre-S1 region joins the ankyrin repeat domain (ARD) with the first transmembrane α-helix (S1) (Figure 1.14). The pre-S1 region also contains a linker with two helix-turn-helix (HTH) motifs connected by two β-strands. On the other hand, a TRP-like domain which follows the sixth transmembrane α-helix (S6) and is parallel to the lipid bilayer, creates a series of interactions with the α-helices of the two HTH motifs and the β-strands of the pre-S1 linker. The TRP-like domain of TRPA1 is crucial for allosteric modulation since it interconnects with multiple structural elements including the pre-S1 region and linker as well as the S4-S5 linker via hydrophobic interactions. Important cysteine and lysine

residues for electrophilic interactions with agonistic compounds are located in the pre-S1 region and linker (C621, C641, C665 and L710) causing conformational changes and mechanical forces all the way to the TRP-like domain which translate into the channel's gating. However, the AITC-binding site bound to the agonist has not been solved yet and no particular interactions and structural changes have been described so far (Paulsen et al., 2015).

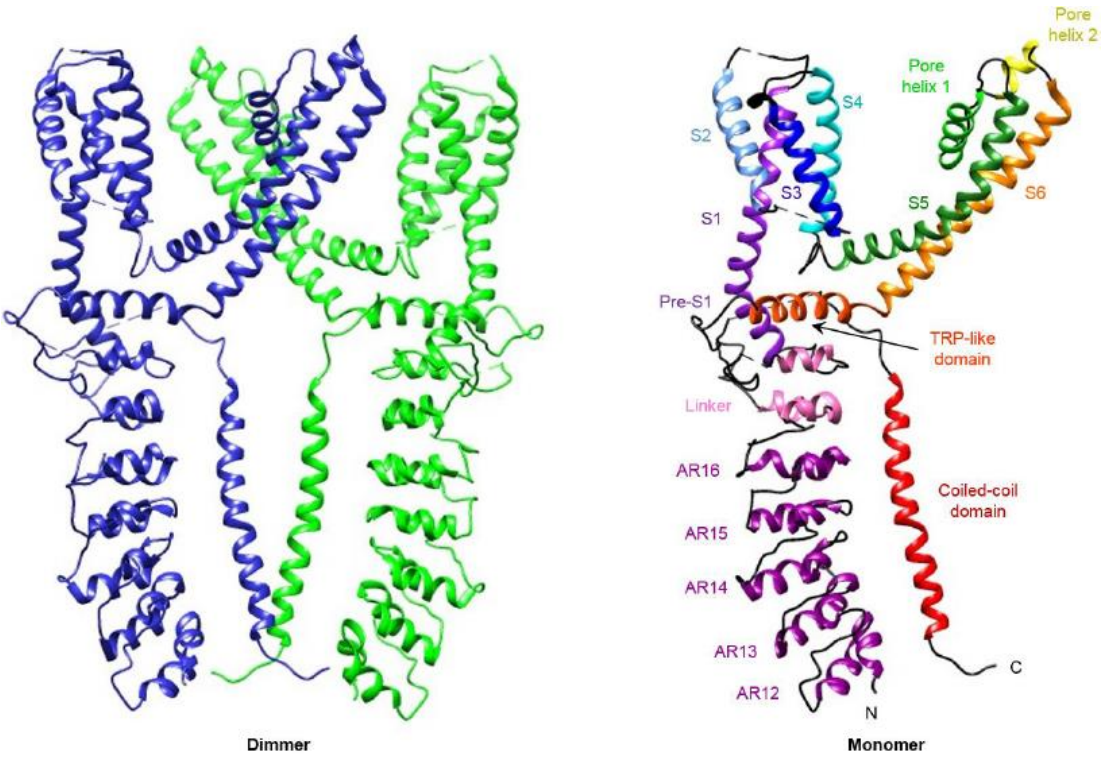

Figure 1. 14: Structure of TRPA1 dimer and monomer in ribbon diagrams (186). AR 12-16 interacting with the C-terminal coild-coil form the “stem” of the channel, as shown in the dimer representation. More detailed structural domains are shown in colour-coded ribon diagrams (monomer). The structures were made using the Chimera software and the data obtained from PDB 3J9P.S

Although TRPA1 pore resembles that of TRPV1 for having two major constrictions sites, the TRPA1 pore is formed by two pore helices between S5 and S6, compared to one helix of TRPV1 (Paulsen et al., 2015). A series of current recordings on human wild type TRPA1 and pore-residue mutants reveal the key amino acids that modulate pore selectivity. The first step for ion conductance is attracting cations to the mouth of the channel while repelling anions at the same time. Glutamate at position 920 (E920) is the master regulator of attracting cations to the pore due to its negative charge. The more distant E924 and E930 are also involved in attracting cations, yet to a lesser extent. The charge-neutralising mutation E920 to Alanine (E920A) decreased the inward current of Cs^{+} compared to the wild type, as well as abolished the channel's blockage by Ba^{2+}, indicating E920 role in cation collection. Further deeper into the pore, aspartate 915 (D915) comprises the first constriction site, as firstly described by D. Julius (Paulsen et al., 2015). Permeant ions partially lose waters of hydration and the negatively-charged side chains of D915 make up for those interactions forming a tight selectivity filter. It is estimated that the diameter of an open pore at this site is at least 8.2Å, based on a screening for multiple-sized organic cations currents, which is relatively small compared to other cation channels. D915E mutation caused a reduced ion conductance due to the bulkier side group of glutamate creating steric hindrance that impedes ion permeation. On the other hand, altering the charge of the residue by using the D915N mutation also weakened inward currents indicating that the negative charge also facilitates permeation. At the deepest site of the pore a second constriction site is formed by two hydrophobic residues, Ile957 and Val96. This is the narrowest point of the pore with a diameter of

approximately 6Å that hinders permeation of rehydrated ions. Moreover, a recent study also proposes the involvement of the first extracellular loop (S1-S2 linker) as a key player in pore opening regulation (Marsakova et al., 2017).

Two most common TRPA1 inhibitors include HC-030031 and A-967079. Although D. Julius attempted to solve the inhibitor-bound state of the channel, only A-967079 appeared to be successful. A-967079 binding site is located between the S5, S6 and the first pore helix and the most implicated residue at this site is Phe909. It is speculated that the inhibition is mediated through hindering the lower pore gate which is mostly formed by S5 and S6. Mutations affecting A-967079 binding did not change HC-030031 inhibition suggesting a separate binding site which still remains unknown. In 2016, chimeric studies involving human and frog TRPA1 as well as point mutations showed that HC-030031 binds to the aspartate N855 located between S4 and S5 via hydrogen bonds and the binding is stabilised by hydrophobic interactions between the hydrophobic part of HC-030031 and the hydrophobic pocket adjacent to N855 (Gupta et al., 2016).

1.3.3. TRPA1 modulation

One of the most well-studied activation mechanisms of TRPA1 is that of activation by covalent interactions with ligands. Most of these compounds share the common feature of eletrophilicity meaning that they carry a highly carbon moiety that interacts with thiol groups of specific Cysteine residues located on the linker region of TRPA1 (connecting Ankyrin repeats with the transmembrane domain) forming products called Michael adducts (Bang and Hwang, 2009). This method of activation differs from the usual receptor-

ligand mechanism that requires high specificity and transient binding. Interestingly, the TRPA1 unconventional and probably primitive way of activation allows for a variety of structurally diverse electrophiles to covalently interact and activate fast responses to noxious stimuli (Hinman et al., 2006; Macpherson et al., 2007; Macpherson and Patapoutian, 2010).

So far, numerous plant-derived natural compounds have been found to activate TRPA1 by covalent electrophilic attack including isothiocyanates (e.g. AITC), cinnamaldehyde (CA) and allicin found in garlic (Bautista et al., 2007; Brône et al., 2008; Hinman et al., 2006; Macpherson et al., 2007, 2005). However, there are many synthetic electrophilic compounds, mostly environmental pollutants and toxic inhalants that can also activate TRPA1 through covalent modification such as tear gas (dibenz[b,f][1,4]oxazepine (CR), 1-chloroacetophenone (CN), 2-chlorobenzylidene malononitrile (CS)) and acrolein (found in cigarette smoke) (Bautista et al., 2006; Brône et al., 2008). Although many N-terminal cysteine residues of TRPA1 have been proposed to participate in ligand binding, the exact cysteines involved and the actual mechanism of channel activation remains unknown (Paulsen et al., 2015). Hinman et al. in 2006 proposed that C619, C639, C663 and K708 are sufficient to induce channel activation by exogenous electrophilic ligands based on amino acid substitution experiments, while Takahashi et al. (2008) suggested that C421 and C621 are important for TRPA1 activation by endogenous inflammatory reagents like 15-deoxy- Δ12,14-prostaglandin J2 (15d-PGJ2), NO, H_2O_2, which are also electrophilic compounds (Hinman et al., 2006; Takahashi et al., 2008). A more recent study identifies C621 as a highly reactive residue that reacts 6,000 times faster than any other TRPA1 cysteine. Although C621 mutants demonstrate a reduced channel activation,

C621 per se cannot activate TRPA1. Notably, TRPA1 activation requires C665. Replacement of C665 completely abolished channel activation. Moreover, a lysine adjacent to the reactive C621 (K620) also assists in TRPA1 activation by most likely decreasing C621's pKα which increases its reactivity (Bahia et al., 2016). Interestingly, the rattlesnake TRPA1 is insensitive to electrophiles even though it has similar cysteine residues indicating that activation by electrophiles is not solely dependent on cysteine modification but also by other subcellular cofactors and subsequent structural changes in the TRPA1 molecule (Bahia et al., 2016; Cordero-Morales et al., 2011).

While specific cysteine mutations abrogate TRPA1 activation by electrophiles, TRPA1 still maintains its sensitivity to other structurally distinct compounds like cannabinoids and the cooling reagent icilin, suggesting multiple ways of activation (probably by the conventional receptor-ligand mechanism) (Bahia et al., 2016; Bang and Hwang, 2009). Other natural agonists of TRPA1 include thymol (thyme), carvacrol (oregano) and oleocanthal (olive oil) which are not capable of activating TRPA1 by cysteine modification (Alvarenga et al., 2016; Gachons et al., 2011; Lee et al., 2008). It has also been shown that anti-inflammatory drugs and anesthetics can also activate TRPA1 such as ibuprofen and lidocaine (Gachons et al., 2011; Piao et al., 2009). However, not all agonists are TRPA1-specific. For instance, carvacrol, thymol and ethyl vanillin (synthetic vanilla) are also agonists of TRPV3, both TRPA1 and TRPV1 can be activated by garlic compounds but so far, AITC and CA have been proposed as solely TRPA1-specific agonists (Wu et al., 2017; H. Xu et al., 2006).

Two independent studies have also proposed TRPA1 direct activation by calcium ions which is consistent with the presence of an EF-hand domain located at the N-terminal Ankyrin repeat domain of the channel (Doerner et al., 2007; Zurborg et al., 2007). In fact, TRP channel regulation by calcium is not rare. TRPM2, TRPM5, TRPM8 and TRPC4 have all been found to be regulated by intracellular calcium concentrations (Chuang et al., 2004; Du et al., 2009, p. 2; Prawitt et al., 2003; Watanabe et al., 2003). Doerneret al. first demonstrated that the presence of extracellular calcium potentiates AITC, CA and carvacrol responses and introduced the mechanism of dose-dependent direct activation by intracellular calcium that binds to the putative EF-hand (Asp468-Leu480) of TRPA1. It was proposed that specifically Leu474 was highly involved in the interaction with calcium ions and that no cytosolic factors like calmodulin, a calcium-dependent protein regulator, or PLC pathways, also described to activate TRPA1, were involved in the mechanism (Doerner et al., 2007). Similar data were obtained by another research group which also suggested a mechanism of indirect cold-activation through the subsequent intracellular calcium increase following cooling. The finding was supported by the fact that calcium-insensitive TRPA1 mutants had similar responses to cold temperatures with the control cells. Together these data indicate that TRPA1 could be activated by any stimulus that increases calcium influx in the cytosol serving as a signal amplifier. Calclium-insensitive mutants did not potentiate the calcium influx in response to carbachol (cholinergic agonist) compared to wild type TRPA1, suggesting that calcium binding is a requirement for TRPA1 activation by PLC pathways (Zurborg et al., 2007). However, the presence of an EF-hand has not been verified yet. The idea of an interaction with the putative EF-

hand was excluded in another study in which mutations of previously proposed calcium-interacting residues did not affect channel's potentiation (Y. Y. Wang et al., 2008). The same study described that TRPA1 is also inactivated by calcium following potentiation, two mechanisms that appear to be independent. TRPA1 potentiation by calcium also explains the positive synergistic effect of TRPA1 and TRPV1 following simultaneous activation in sensory neurons (Hsu and Lee, 2015). Surprisingly, a 2017 study proposes for the first time the calmodulin-dependent mechanism of calcium potentiation and inactivation suggesting that the C-terminal rather than the N-terminal possesses a non-canonical calmodulin binding site of 17 amino acids (L995-N1011) (Hasan et al., 2017).

Furthermore, TRPA1 serves as a signal amplifier since it can be activated indirectly through activation of other receptors. Numerous studies have shown that TRPA1 is activated by G protein-coupled receptors (GPCRs) which are involved in various cellular responses including inflammation and itch. GPCRs form complexes with heterotetramic G proteins (G-α, -β, -γ) which dissociate after receptor activation and subsequent exchange of GDP to GTP. Activated G proteins can generate second messengers like c-AMP and stimulate PLC pathway (Tuteja, 2009). TRPA1 was initially found to be activated by bradykinin through B2R which is a GPCR introducing PLC signalling as an essential mediator of TRPA1 activation (Bandell et al., 2004). Bradykinin treatment caused increased calcium responses mediated by TRPA1 in either CHO or HEK cells co-expressing both receptors, compared to the single transfected cells, while the use of U-73122, a PLC inhibitor, decreased those responses (Bandell et al., 2004; Hinman et al., 2006). The exact mechanism that potentiates TRPA1 is not known but the

increase of intracellular calcium could be a possible explanation since elevated intracellular calcium levels have been shown to potentiate TRPA1 (Bandell et al., 2004; Y. Y. Wang et al., 2008). However, there is evidence that PLC can act by releasing the inhibition by PIP2, a potential TRPA1 inhibitor (Dai et al., 2007). Another study proposed B2R-mediated TRPA1 activation through the PKA and cAMP pathway, also GPCR-inducible, due to the fact that PKA activators mimic while inhibitors decrease Bradykinin-potentiated AITC responses (S. Wang et al., 2008). Additional GPCRs that have been reported to activate TRPA1 include m1 muscarinic acetylcholine receptor (m1AchR), protease-activated receptor-2 (PAR2), the bile acid receptor (TGR5), the Thymic Stromal Lymphopoietin receptor (TSLPR) and the Mas-related G-coupled receptors MrgprA3 and MrgprC11 (Dai et al., 2007; Hinman et al., 2006; Lieu et al., 2014; Wilson et al., 2013, 2011). MrgprA3 and MrgprC11 are involved in histamine-independent itch and can be activated by two pruritogens, chloroquine and BAM, respectively. Although MrgpC11-induced TRPA1 activation requires Gαq/11 and activation of the downstream PLC pathway following BAM treatment, Gβ/γ pathway seems to be essential for MrgprA3-induced TRPA1 activation (Wilson et al., 2011).

In 2011, Takahashi et al. presented a novel role of TRPA1 as an oxygen sensor in DRG neurons (Takahashi et al., 2011). The ability of TRPA1 to sense oxygen molecules is facilitated by reactive cysteine residues (C633 and C856) in the N-terminal domain that interact with O2. Their model of action states that in normoxic conditions TRPA1 is inhibited by O2-dependent PHDs (proline-hydroxylases) that hydroxylate P394 in the N-terminal domain of TRPA1. When the oxygen levels drop (hypoxia), the

PHD-mediated TRPA1 inhibition is relieved resulting in TRPA1 activation. During increased O2 levels (hyperoxia), reactive cysteines are firstly oxidised forming sulfenic acid that can be easily reversed by cellular glutathione. In the second state, more stable intramolecular or intermolecular disulfide bonds are formed between the reactive cysteines activating the channel. The mechanism of activation involving reactive cysteines has been extensively studied for electrophilic agonists, as described above. However, the difference between the two types of agonists (O2 and electrophiles) is more likely due to the different stability of the end products. Michael adducts formed by electrophilic attack are more stable than the unstable and easily reversible oxidised products formed by interaction with O2. Since pain can also be induced by hypoxic conditions, the physiological role of TRPA1 in pain sensation can also be supported by the mechanism of hypoxia-mediated TRPA1 activation. Concomitant with this observation, in vivo studies verify the above model of activation and link pain with TRPA1 activation by hypoxia (So et al., 2016).

1.3.4. The importance of the TRPA1 N-terminal domain

The N-terminal domain of TRPA1 consists of 720 amino acids and accounts for 57% of the total protein (Hynkova et al., 2016). Based on the solved structure of TRPA1, the N-terminal domain is comprised of an Ankyrin repeat domain (ARD) which includes 16 tandem ankyrin repeats, and a pre-S1 region that is connected to the ARD via a linker. The unusual large size of the N-terminal domain (more than half of the whole protein) predicts its involvement in the channel's regulation and function. Indeed, chemo- ,

thermo- and mechano-sensation as well as pore gating and channel assembly are all functions attributed to this domain (Paulsen et al., 2015).

The N-terminal has been proposed to be a polymodal sensor of environmental stimuli which translates cues into channel gating. The vast majority of the TRPA1 agonists activate TRPA1 by cysteine modification on cysteine residues located within the ARD or the linker and pre-S1 region. Those include exogenous as well as endogenous inflammatory electrophilic compounds or even O2, as described earlier (Hinman et al., 2006; Takahashi et al., 2011, 2008). The agonist-involved residues are in close proximity to the TRP-like domain of TRPA1, a known allosteric modulator of the channel, suggesting a possible activation mechanism (Paulsen et al., 2015). Moreover, a putative EF-hand located at the AR12 has been suggested to modulate TRPA1 based on the intracellular calcium levels (Y. Y. Wang et al., 2008). Other N-terminal-binding agonists include Zn^{2+} whose binding site was proposed to consist of both N- and C- terminal cysteine and histidine residues (Cordero-Morales et al., 2011).

The larger part of the N-terminus consists of 16 ankyrin repeats (ARs), amino acids 1-688. Despite the numerous attempts to identify specific functions, the role of the human TRPA1 ARD still remains largely unknown. A study utilising different chimeric TRPA1 channels created by the human and the rattlesnake orthologues proposed the importance of the ARD domain in chemical and heat sensitivity (Cordero-Morales et al., 2011). The rattlesnake AR3-8 and AR10-15 conferred heat sensitivity to the heat-insensitive human TRPA1 while conserving AITC-sensitivity, suggesting the role of specific ARs in thermosensation rather than the need for a particular

number of repeats. Cordero Morales and colleagues also highlighted the role of AR11-16 in chemical sensitivity as well as identified AR11 as an important locus for TRPA1 calcium desensitisation. Moreover, they recommended the division of the ARD into two modules (AR3-8 involved in signal recognition and AR10-15 serving as an enhancer region), a finding that agrees with the solved structure of TRPA1 which describes a group of five Ankyrin repeats (AR12-16) parallel to the C-terminal coiled-coil and close to the membrane portion of the channel and a second group of 11 ARs which form a crescent shape underneath the channel (Cordero-Morales et al., 2011; Paulsen et al., 2015).

The conserved tetrapeptide T/SPLH found in five of the ARs (AR2, AR6 and AR11-13) is important for sustaining the AR conformational integrity and mutations on key residues alter TRPA1 sensitivity to chemical, calcium and voltage changes (Hynkova et al., 2016). Destabilising mutations on AR2 and AR6 for example, disrupted the voltage-dependent regulation of TRPA1 and mutations on AR6 affected calcium-regulation and channel gating (Hynkova et al., 2016). Although TRPA1 is not a voltage-gated channel, it presents voltage-dependency. Indeed, another study has shown that the pore helix residue Leucine 906 is involved in voltage-dependent gating of the pore and it serves as a gate keeper rather than a voltage-sensor (Wan et al., 2014). Moreover, AR11-13 are shown to be crucial for the channel's function due to the fact that T/SPLH mutations disrupt responses to stimuli (Hynkova et al., 2016). This hypothesis is supported by the 3-dimensional positioning of the AR12-16 and the TRP-like domain allowing for an extended network of interactions that eventually regulate the pore opening (Paulsen et al., 2015).

The same study also proposed that the threonine and serine residues on the ARD are potential candidates for phosphorylation by different cellular kinases (Hynkova et al., 2016). In support to that, Meents et al. in 2016 introduced a new mechanism of TRPA1 sensitisation by GPCRs involving activation of Protein Kinase A (PKA) and subsequent phosphorylation and sensitisation of TRPA1 (Meents et al., 2017). Forskolin (FSK), a PKA activator, increased TRPA1 responses after carvacrol-pulse-treatment-induced desensitisation. The responses were also inhibited by H89 treatment (PKA inhibitor) using Calcium imaging and whole-cell patch clamp experiments. After a series of point mutations on Serine and Threonine residues it became apparent that S86, S317 and S428, all located in the ARD region, are phosphorylation sites for PKA (Meents et al., 2017). TRPA1 direct phosphorylation by PKA was also supported by another study which introduced an additional player in this process, A-kinase anchoring Protein 79/150 (AKAP), which is a scaffold protein assisting in phosphorylation of membrane receptors by PKA and PKC (Brackley et al., 2017). However, Brackley et al. proposed S87 as a PKA phosphorylation site as well as S119, T281 and T529 as PKC phosphorylation sites (Brackley et al., 2017). Taken together these data highlight the role of ARD in regulation of TRPA1 function and gating of the channel. Nevertheless, contradictory studies exclude the involvement of the ARD domain in thermal and chemical sensitivity and describe the ability of TRPA1 to respond to cold and other chemical agonists (electrophilic or not) even in the absence of the ARD (Moparthi et al., 2014). A higher resolution structure of the complete ARD domain may reveal novel interactions and functions that modulate TRPA1.

Alternative ARD functions may arise from the intrinsic role of Ankyrin repeats as protein-protein interaction motifs. Each Ankyrin repeat usually consists of approximately 33 amino acids adopting a canonical Helix-Turn-Helix (HTH) orientation which extends in a loop forming a hairpin-like-beta-sheet with adjacent loops (Mosavi et al., 2004). The number of Ankyrin repeats within a protein varies from 2-34 and are named after the cytoskeletal protein Ankyrin that has 24 repeats. All ARs are linearly stalked in a helix bundle that adopts a concave shape which is usually described as a hand with a palm (inner helices) and fingers (loops). Inter- and intra- repeat hydrophobic interactions and hydrogen bonds are important for the stability of the bundle and the surface-exposed residues are involved in protein recognition. So far, ARDs are known to mediate protein-protein interactions and are present in a variety of proteins like membrane receptors (TRP channels, Notch), cell cycle regulatory proteins (INK4), transcription factor inhibitors (IkBa) and cytoskeletal proteins (Ankyrin). Due to the wide variety of proteins that can interact with an ARD, there are no universal characteristics that can describe those interactions. However, some generalisations could be made including the fact that AR binding sites are usually extended to a wider area of the protein-target rather than a short motif like SH3 or SH2 motifs bind to, as well as the fact that the palm and the fingers on the concave surface are mostly involved in the interactions with the target. Although ARs share the same structure and most of the residues are conserved, the loop residues and some located at the inner helix have been found to be involved in ligand recognition and ligand specificity (Mosavi et al., 2004; Voronin and Kiseleva, 2008).

The ARD is not a unique characteristic of TRPA1. The TRPC and TRPV family also possess an N-terminal ARD, even though the number of repeats are limited to 4-6. To date, no protein-based ligands have been found to interact with any of the TRP ARDs. In fact, only calmodulin has been proposed to bind to TRPV1 ARD (Lishko et al., 2007). Instead, several non-protein ligands have been shown to bind and regulate TRP channels. For instance, both TRPV1 and TRPV4 ARD have an ATP binding site, TRPV4 ARD also binds β-D-glucose and glycerol, while TRPV2 ARD binds acetic acid (Inada et al., 2012; Jin et al., 2006; Lishko et al., 2007). The most common role of the ARD is electrophilic ligand recognition through cysteine residues. Even though no protein-based ligands have been reported so far, it is possible for TRPA1 to interact with other membrane proteins (Paulsen et al., 2015).

Further information can be obtained from the non-mammalian TRPN channels that have the longest N-terminal ARD consisting of 29 repeats. TRPN channels have been extensively involved in mechanosensation (hearing and touch) and characterised as force-gated channels (Wilson and Corey, 2010). This hypothesis is favoured by the recently solved structure of the D. Melanogaster TRPN1 analogue, NOMPC (no mechanoreceptor potential) (Jin et al., 2017). The authors presented that the ARD of each subunit is shaped in a helical spring interacting with neighbouring ARDs in two major positions.

The inter-subunit interactions, important for the integrity of the structure, involve three to four ARs of each subunit and are mediated by polar and charged residues located on those ARs. They also described three different

classes of the channel with differences in ARD confirmation which suggests that the N-terminal domain is very flexible allowing for movements in the ARD. Structural analysis of the rest of the channel revealed that a network of interactions involving the ARD, the pre-S1 elbow, and the linker region could possibly evoke the movement of the S6 that enlarges the lower restriction site, opening the channel. Jin and coleagues proposed that mechanical forces that displace the ARD spring (linked to cytoskeletal microtubules) are translated into pore opening, favouring the role of NOMPC as a mechanosensitive channel. Nevertheless, TRPN family of channels do not exist in mammals and the discovery of mammalian mechanosensory channels involved in hearing is still an ongoing process (Jin et al., 2017). TRPA1 has been proposed to serve as a mammalian mechanosensor, a feature that can be supported by the long ARD (Corey et al., 2004; Nagata et al., 2005; Zhang et al., 2008) However, the role of TRPA1 in mechanical sensitivity still remains largely unsolved (Kwan et al., 2006).

1.3.5. Calcium channels in cancer

Intracellular calcium is one of the most crucial second messengers and a major component of signalling pathways that regulate fundamental cellular processes including cell proliferation, survival, differentiation and motility. Due to its increased complexity, calcium signalling is still not completely understood. However, calcium-mediated signalling cascades usually modulate the activity of calcium-dependent proteins like Ca2+/calmodulin-dependent protein kinase II (CaMKII), calmodulin, calpain and the transcription factors like NF-KB and NFAT altering gene expression and thus cellular responses. The ability of calcium signalling to alter the expression of

cyclins, also make it an important cell cycle regulator. Moreover, the spatial and temporal localisation of calcium also determines responses including cellular movement highlighting the complex but at the same time fine-orchestrated calcium signalling (Cui et al., 2017). Consequently, deregulation of calcium signals originating from calcium transporters are implicated in malignancies (Leanza et al., 2016).

Intracellular calcium levels are controlled by calcium homeostasis components: calcium pumps, exchangers and channels which have been reported to be modified in cancers. Calcium can be released form the endoplasmic reticulum (ER) into the cytoplasm through the IP3 receptor (IP3R) or ryanodine receptor (RyR) while it can return back to the ER through ER-Ca^{2+} ATPases (SERCA) that use the energy from the hydrolysis of ATP to move Ca2+ molecules against the gradient. Other organelles like mitochondria and Golgi also possess similar mechanisms of Ca^{2+} transportation including channels, ATPases and calcium exchangers like the Na^{+}/Ca^{2+} exchangers that move calcium ions against the gradient taking advantage of the Na^{+} gradient. Calcium levels are also controlled by plasma membrane calcium transporters which regulate calcium influx and efflux to/from extracellular space/cytosol. Apart from plasma membrane Na^{+}/Ca^{2+} exchangers and Ca^{2+} ATPases, calcium influx is supported by a diverse array of channels. Those include the voltage-gated calcium channels (Cav), ligand-gated calcium channels like P2X, transient receptor potential channels (TRP) and the store-operated channels Orai (Cui et al., 2017; Monteith et al., 2017).

Voltage-gated calcium channels (subfamilies Cav1-3) are characteristic of excitable cells as they are regulated by membrane depolarisation (Buchanan and McCloskey, 2016). However, some of these channels like Cav1.2 and Cav3.2 have been found overexpressed in cancer cells too (Martínez-Delgado and Felix, 2017). Zhang *et al* (2017) found increased expression of Cav3.2 in glioblastoma patients which was also correlated with poor prognosis. Downregulation of Cav3.2 by RNAi or pharmacological inhibition by mibefradil (an FDA-approved hypertension drug) abolished cancer cell growth and increased survival via a mechanism that supresses survival pathways (AKT/mTOR) while enhancing pro-apoptotic pathways (BAX proteins) as well as by altering gene expression. Similar anti-tumorigenic results were obtained by *in vivo* studies after treatment with mibefradil, suggesting that targeting calcium channels can also be considered as a cancer therapy (Y. Zhang et al., 2017). The role of Cav3 channels have also been investigated in breast cancer cell lines in which they are usually found overexpressed, yet the exact effect still remains to be elucidated. For instance, the tumour suppressor role of Cav3.1 has been observed in MCF-7 breast cancer cells while the role of Cav3.2 seems to be cell type-dependent (Ohkubo and Yamazaki, 2012; Pera et al., 2016; S. Zhang et al., 2017). The effect of Cav3.2 overexpression has also been examined in prostate cancer in which complex formation with potassium channels has also been observed (Gackière et al., 2013; Ohkubo and Yamazaki, 2012).

Furthermore, several TRP channels, mostly TRPC, TRPV and TRPM members, are overexpressed in cancers (Shapovalov et al., 2016). TRPC5 is overexpressed in colorectal cancer and has been correlated with increased metastasis, decreased cancer cell differentiation, tumour grading

and poorer overall patient survival (Chen et al., 2017b, 2017a; Zhang et al., 2016). Up-regulated TRPC5 results in elevated calcium influx which in turn results in decreased E-cadherin (epithelial marker) and increased mesenchymal markers enhancing cancer cell proliferation, migration and invasion. The mechanism of TRPC5-mediated epithelial-to-mesenchymal transition (EMT) involves upregulation of HIF-1α/Twist signalling pathway while cancer cell differentiation is regulated by Wnt5α/β-cat pathway that increases the stemness of the cells (Chen et al., 2017b, 2017a). Importantly, TRPC5 is also involved in drug resistance in colon as well as breast cancer (Wang et al., 2017a). TRPC5 has been proposed as a non-invasive marker for breast cancer chemoresistance as it is found in resistant-cancer-cell-derived exosomes (Wang et al., 2017b). Overexpression of TRPC1, TRPC3, TRPC4 and TRPC6 in NSCLC patients has been correlated with tumour grading while inhibition of TRPC channels in A549 cells abolished cancer cell proliferation (Jiang et al., 2013; Wang et al., 2017a). Silencing of TRPC1, in particular, causes cell cycle arrest in G(0)/G(1) of NSCLC cells and subsequent inhibition of cell growth and decreased cyclin D1 and D3 expression (Tajeddine and Gailly, 2012). Simultaneously, EGFR-mediated signalling is also decreased. Tajeddine *et al* proposed the positive interaction loop between EGFR signalling and TRPC1 in NSCLC which includes TRPC1 activation by EGFR-mediated calcium entry and in turn, EGFR activation by TRPC1 calcium influx promoting NSCLC progression (Tajeddine and Gailly, 2012). TRPC1 has also been implicated in proliferation of hepatocellular carcinoma cells, drug resistance in ovarian cancer as well as breast cancer progression in which it functionally cooperates with calcium-activated potassium channels (Kca3.1) and

correlates with poor survival (Faouzi et al., 2016; Liu et al., 2016; Selli et al., 2015). Other TRPC channels include TRPC6, reported in prostate, lung and pancreatic cancer as well as TRPC4, involved in meduloblastoma invasion (Bernichtein et al., 2017; Nielsen et al., 2017; Wei et al., 2017; Yang et al., 2016).

Among the TRPV family members, TRPV6 implication in prostate cancer has been highly studied. TRPV6 is found overexpressed in prostate cancer cell lines and patient tissues and is correlated with advance stages and poor survival (Fixemer et al., 2003; Lehen'Kyi et al., 2007). Silencing of TRPV6 in prostate cancer cell lines reduced cellular proliferation and increased apoptosis via a TRPV6-mediated Ca2+-dependent mechanism (NFAT activation) suggesting the direct role of TRPV6 in prostate cancer progression. Moreover, TRPV6 is a constitutively active calcium channel highly selective for calcium ions that mediates continuous calcium entry in prostate cells promoting proliferation (Lehen'Kyi et al., 2007, p. 6). TRPV6 upregulation has been attributed to its translocation to the plasma membrane through a mechanism that involves the Orai/TRPC1 signalling pathway (Raphaël et al., 2014). Overexpression in pancreatic cancer cell lines has also been observed and TRPV6-mediated cellular proliferation occurs via NFAT activation (Lehen'Kyi et al., 2007; Skrzypski et al., 2016). TRPV6 channels have also been implicated in SCLC and breast cancer carcinogenesis (Guilbert et al., 2011; Lau et al., 2014; Peters et al., 2012; Skrzypski et al., 2016). Furthermore, TRPV3 is overexpressed in 67% of all lung cancer cases and correlates with tumour staging and poor patient survival. *In vitro* studies using lung cancer cell lines revealed that TRPV3 promotes proliferation through calcium influx that assists in G1 to S phase

transition via activating CaMKII, upregulation of cyclin A, D1 and E as well as downregulation of the cell cycle suppressor p27 (Li et al., 2016). On the other hand, TRPV4 is responsible for breast cancer cell metastasis mediated by activation of AKT and FAK pathways and downregulation of E-cadherin and beta-catenin (epithelial markers) (Lee et al., 2017).

Among the TRPM family members, TRPM8 has been implicated in various cancers including pancreatic, prostate, bladder and colorectal cancer (Borrelli et al., 2014; Xiao et al., 2014; Yee, 2016). However, the exact role of action is still unknown (Yee, 2015). It was recently shown that the glycosylation state of TRPM8 determines cancer progression in pancreatic cancer and that the splice variant TRPM8α increases invasion and regulates apoptosis in (LNCaP) pancreatic cancer cells (Peng et al., 2015; Ulăreanu et al., 2017). On the other hand, the protective effect of TRPM8 has also been observed in prostate cancer. Androgen-dependent early stages of prostate cancer are accompanied by TRPM8 overexpression which is decreased after anti-androgen therapy or transition to androgen-independent states suggesting that loss of TRPM8 expression is associate with advanced cancer stages. In fact, TRPM8 transcription is regulated by AR (androgen receptor) due to ARE-I binding sites however, the protein levels are negatively regulated due to increased ubiquitination and degradation of the channel. Inhibition of ubiquitination increased channel activity resulting in increased apoptosis, p53 and caspase 9 activity supporting the anti-tumour effect of TRPM8 (Asuthkar et al., 2015). Moreover, TRPM8 anti-metastatic role in prostate cancer has also been reported. TRPM8 is highly expressed in prostate cancer-derived endothelial cells in which it represses cell motility by a mechanism involving direct interaction and inhibition of GDP-RAP1

(GTPase), a protein involved in integrin signalling pathways. In this way, both *in vitro* would healing and vascular tubulogenesis was impaired indicating the anti-metastatic role of TRPM8 in prostate cancer (Genova et al., 2017). The overexpression of TRPM7 has also been reported in bladder, glioblastoma, pancreatic and breast cancer where it is involved in increasing cancer cell proliferation and invasion via activating various pathways (Cao et al., 2016; Gao et al., 2017; Nakashima et al., 2017; Rybarczyk et al., 2017; Wong et al., 2017; Yee, 2017). Importantly, the kinase activity of TRPM7 is also involved in phosphorylating substrates like myosin IIA regulating cytoskeleton and thus, cell motility (Song et al., 2017).

Store-operated calcium entry (SOCE) is a key process in calcium signalling. SOCE is initiated when activated GPCRs activate PLC pathways that result in increased IP3 levels which causes IP3R-mediated calcium influx from the ER to the cytosol. This reduced ER calcium concentration is sensed by Stromal interaction molecules (STIM) membrane proteins which oligomerise and translocate closer to the plasma membrane where they form complexes with Orai receptors and initiate the store-operated calcium entry. There are 2 isoforms of STIM proteins (STIM1 and STIM2) and three of Orai (Orai1, 2 and 3) (Vashisht et al., 2015). As calcium signalling components, Orai/STIM complexes are also implicated in cancers. Among the three isoforms Orai3 has been mostly implicated in malignancies like lung adenocarcinoma and breast cancer where it is overexpressed and proposed as a marker of poor prognosis. Silencing or inhibition of Orai3 in those cancer cell lines causes decrease in cell proliferation, arrest in G1 phase and reduction in cyclin D, E, CDK 2 and 4 as well as increase in cell cycle inhibitors (Ay et al., 2013, p. 3; Benzerdjeb et al., 2016; Faouzi et al., 2013, 2011; Motiani et al., 2010).

Increased Orai3 levels in prostate cancer cells cause heteromeric Orai1/Orai3 channels which have been suggested to mediate store-independent Ca2+ entry and promote cancer progression (Dubois et al., 2014). Orai1 channels have also been implicated in cancers like glioblastoma and gastric cancer and complexes consisting of Orai1, TRPC1 and SK3 channels (small conductance calcium-activated potassium channel 3) have also been implicated in colon cancer metastasis (Guéguinou et al., 2016; Gui et al., 2016; Motiani et al., 2013; Xia et al., 2016).

1.3.6. The role of TRPA1 in cancer

Although several TRP channels have been shown to be dysregulated in a number of human cancers and thus proposed as novel pharmacological targets and possible prognostic markers, very little information exists regarding the role of TRPA1 in cancer progression. An expression profile study in 2016 showed that TRPA1 protein levels were elevated in nasopharyngeal carcinoma tissues and negatively correlated with patients survival presenting TRPA1 as a novel indicator of poor prognosis in nasopharyngeal carcinoma (Wu et al., 2016). It is important to note that TRPA1 can be upregulated as well as downregulated in cancers and the outcome of this alteration is cancer-type specific. For instance, another data-driven study found that TRPA1 gene expression was substantially increased in kidney cancer and this change was correlated with better overall survival. C-index analysis revealed that TRPA1 is a great prognostic marker for kidney cancer especially when combined with other TRP channels including TRPC4, TRPM3 and TRPP1. On the other hand, the same study found

decreased TRPA1 gene expression in prostate cancer, highlighting the complex role of TRPA1 in cancer progression (Y. R. Park et al., 2016).

So far, very little is known about the direct role of TRPA1 in lung cancer in a more detailed and mechanistic way. In 2013, TRPA1 levels were found elevated in small-cell lung cancer cell lines which demonstrated increased calcium influx and ERK1/2-mediated cell proliferation following AITC treatments. Increased cell viability was observed after administration of non-toxic doses of AITC while TRPA1 downregulation by siRNA inhibited cell growth (Schaefer et al., 2013). Another study showed that the combination of TRPA1 and TRPM8 overexpression in Lewis lung cancer cells rather than the overexpression of the single channels promotes cell adhesion and invasion as well as resistance to cytotoxic T lymphocytes and chemotherapy (Derouiche et al., 2017; Du et al., 2014, p. 8). Both studies implicate the involvement of TRPA1 in lung cancer yet the exact mechanism of action still remains unsolved. Notably, no TRPA1 mutations have been linked to cancer so far, indicating that elevated levels of the channel rather than a decrease or increase in activation can be capable of promoting malignancies.

Recent studies also highlight the indirect role of TRPA1 in prostate cancer which involves regulation of the tumour microenvironment (TME). While TRPA1 is absent in prostate cancer cells, overexpression in prostate stromal cells can regulate their paracrine effect and promote cancer progression (Derouiche et al., 2017). In early 2017, Roudbaraki’s group investigated the TRPA1 agonist triclosan (TCS), an antibacterial agent commonly used in cosmetics and hygiene products, in prostate stromal cells and showed that TCS treatment increased calcium influx which was blocked by TRPA1

inhibitors as well as TRPA1 siRNA knock down and promoted VEGF secretion. TCS-induced VEGF production was inhibited by HC-030031, a TRPA1 inhibitor, indicating the role of TRPA1 in the paracrine regulation of prostate cancer cells by the TME (Derouiche et al., 2017). Very recently, the same group verified the role of TRPA1 in the prostate cancer TME by studying an anti-cancer plant-derived compound, resveratrol (RES), which surprisingly activates TRPA1 expressed in prostate cancer-associated fibroblasts (CAFs). The prostate CAF cell line PS30 and primary CAFs produced HGF and VEGF following treatment with RES, an outcome that was prevented by TRPA1 inhibition or knock down. Moreover, prostate cancer cells and CAFs co-culture reduced RES-mediated cancer cell apoptosis which was rescued by simultaneous treatment with a TRPA1 inhibitor. These results indicate that activation of CAF-expressed TRPA1 by RES promotes cancer progression by inducing HGF and VEGF expression regulating the TME. In contrast, RES acted as an inhibitor of wild type TRPA1, transiently expressed in HEK cells. In addition to that, RES responses were reduced in prostate CAFs co-expressing wild type TRPA1 indicating a different version of TRPA1 in prostate CAFs. Sequencing analysis revealed a K539R mutation and two SNPs (Y69C and K186N), all located within the ARD of TRPA1, introducing for the first time the role of TRPA1 point mutations in cancer regulation. Indeed, those two polymorphisms have been associated with higher sensitivity to agonists (Vancauwenberghe et al., 2017).

On the contrary, TRPA1 has also been associated with tumour prevention. Another study in 2016 that investigated the inflammation in the TME showed that methyl syrignate (MS), a TRPA1 activator, causes COX-2

downregulation in the lung cancer cell line A549. Hypoxic conditions that prevail in the TME of solid tumours induce increased levels of prostaglandins and COX-2 which eventually promote cellular migration and invasion. MS treatment reduced A549 invasion which was rescued by the use on TRPA1 inhibitors suggesting the antitumor effect of TRPA1 (J. Park et al., 2016).

Since TRPA1 is naturally involved in pain pathways, its role in cancer pain has also been noticed. Based on studies using oral squamous cell carcinoma mouse models, increased NGF is associated with cancer-related inflammation and NGF blockage reversed the effects by decreasing the expression of TRPV1 and TRPA1 in trigeminal ganglion neurons (Ye et al., 2011). Similarly, elevated amounts of TRP-activating lipids in the saliva of oral cancer patients have been shown to induce pain-related behaviours in rat paws which were reversed by TRPV1 and TRPA1 inhibition (Ruparel et al., 2015). Lastly, chemotherapy-induced peripheral neuropathy (CIPN) has been linked to TRPA1 hypersensitivity by oxidative stress products. TRPA1 antagonist systemic administration in mice prior to chemotherapy reversed TRPA1 hypersensitivity and alleviated pain suggesting TRPA1 antagonists as a novel strategy against CIPN (Trevisan et al., 2013).

1.4. Aims and Objectives

Taken together, previous work has revealed the importance of the FGFR2 C-terminal domain in FGFR2 signalling regulation through protein-protein interactions. Preliminary bioinformatics data by Dr. Zahra Timsah's group proposed TRPA1 as a putative binding partner for the C-terminal domain of FGFR2. The aim of this project is to characterise the potential interaction between FGFR2 and TRPA1 and investigate the effects of this interaction on FGFR2 signalling. Thus, the specific objectives of this study are:

1. to investigate the interaction between FGFR2 and TRPA1 in HEK293T cells
2. to investigate the interaction in a Lung Adenocarcinoma (LUAD) cell line
3. to map the binding sites on both proteins
4. to determine the complex stoichiometry
5. to examine the effect of TRPA1 binding on FGFR2 signalling

2. Chapter 2
Material and Methods

2.1. Mammalian cell culture

2.1.1. Maintenance of cell lines, passaging, freezing and thawing

All cell lines (Table 2.1) were cultured in Dulbecco's modified Eagle's high-glucose medium (DMEM), supplemented with 1% Gibco® Antibiotic-Antimycotic (Life Technologies™) and 10% v/v Gibco® foetal bovine serum (FBS, Life Technologies™). All cells were cultured in 75 or 25 cm^3 flasks and incubated at 37^oC and 5% CO_2.

Table 2. 1: List of cell lines used in the project

CELL LINE	PROVIDER	DESCRIPTION
HEK-293T (CRL-3216™)	ATCC®	Human embryonic kidney cells expressing the T-antigen of adenovirus SV40
CCL-204 (CCD-16Lu™)	ATCC®	Normal human lung fibroblasts
HCC-44 (CSC-0C542)	Creative Bioarray	Human Lung adenocarcinoma
HCC-515	Dr. Ignacio I. Wistuba	Human Lung adenocarcinoma

At 90% confluency, the cells were passaged to new flasks. Old medium was aspirated and the cells were detached by incubation with 1 x TrypLE™ Express (GIBCO, UK) for ~3 minutes in the incubator (2ml for T-75, 1ml for T-25). Once all the cells were detached, trypsin was deactivated upon addition of fresh complete medium (at least 2 times the volume of trypsin) and the cell suspension was transferred to a 15ml tube. The cells were collected by centrifugation for 5 minutes at 600rpm. The supernatant was discarded and the cell pellet re-suspended in

warmed fresh medium (5-10ml depending on the passage ratio). Usually 0.5-1ml of re-suspended cells were added in a new flask containing fresh medium.

For long term cell storage, 0.5ml of the cell suspension was mixed with 0.5ml of freezing medium (10% DMSO in DMEM) in cryovial tubes which were placed in Mr. Frosty box and kept in -80^{o}C for 1-2 days prior to transferring into a liquid nitrogen tank.

Recovery of cells involves quick thawing and transferring of cell suspension into a new flask with warmed fresh medium.

2.1.2. Transient transfection

The cells were seeded in 6-well plates after passaging and cultured at 37^{o}C and 5% CO_2. At 80% confluence the cells were ready for transfection. Metafectene (Biontex) was used as a transfection reagent in 1:3 ratio (metafectene:DNA). Thus, 2µg of DNA was mixed with Opti-MEM medium (100ul total volume) while 6ul of metafecten reagent was mixed in Opti-MEM medium (100ul total volume). The DNA mixture was added on top of metafectene drop by drop and incubated for 20 minutes in room temperature (200ul total/per well). After the time elapsed, the DNA-metafectene mixture was added to each well of the plate drop by drop. The plate was transferred into the incubator and 16-24h later the medium was replaced with fresh one.

For the FGFR2 si-RNA knock down, RNAiMAX (Thermo Fisher) was used to transfect HEK-293T cells with FGFR2 si-RNAs (Assay ID: 118292, 1215, negative control ID: AM4611, Thermo Fisher). For a 6-well plate format, 30pmol of si-RNA and 9µL of RNAiMAX were diluted in 150µL OptiMEM and then combined in a total volume of 300µL per well. After 5 minute incubation the mixture was added to the cells.

2.1.3. Cell treatments

The cells were serum starved (medium without FBS) for 2 hours prior to any treatment. Whenever needed, the cells were treated with 20ng/ml FGF9 for 30 minutes, 100μM AITC for 5 minutes and 50μM HC-030031 for 5 minutes.

2.1.4. Cell lysis

Treated or just serum starved cells were washed 2 times with PBS and then mechanically lysed using the back of a pipette tip in 200ul of lysis buffer (Table 2.2). The mixture was transferred into an Eppendorf tube and centrifuged for 10 minutes at 13,000rpm to precipitate all the debris. The supernatant was transferred into a clean tube and used right after or kept in -80^{o}C for future use.

Table 2. 2: Cell Lysis Buffer recipe

Reagent	Final Concentration
HEPES	50mM
NaCl	150mM
NaVO3	1mM
NaF	10mM
Glycerol	10%
NP-40	1%

2.2. Molecular Cloning techniques

2.2.1. Bacterial transformation

NEB® 5-alpha Competent *E. coli* High Efficiency bacteria were used for transformation based on the manufacturer's instructions. BL21 bacteria were transformed in case protein expression and purification was needed. 1pg-100ng of plasmid DNA was added to an aliquot of bacteria and incubated on ice for 30 minutes without vortex. Next, bacteria underwent a heatshock step for 30 seconds

at 42°C and then incubated on ice again for 5 minutes, prior to recovery on warm growth media for 1 hour at 37°C. Different amounts of bacteria suspension (100-300µl) were spread on agar plates containing appropriate antibiotic and incubated overnight at 37°C. The next morning, bacteria colonies were screened for carrying the correct insert by plasmid purification and agarose gel electrophoresis.

2.2.2. Agarose gel electrophoresis

DNA agarose gel electrophoresis was used to detect correct PCR, digestion and miniprep product sizes and quality. Different percentage of agarose was used based on the DNA size that was being tested. For smaller fragments <1kb, 2% agarose was used while fragments >1kb were analysed in 1% agarose gels. Agarose was dissolved in 1x TAE buffer (MP Biomedicals). SYBR Safe (Invitrogen) was used to visualise DNA fragments in 1:10,000 dilution. The gels were left to set in the gel apparatus provided and then placed in the gel tank containing 1x TAE buffer. DNA samples were diluted in 6x Gel loading dye Blue (New England Bioloabs) prior to loading and 1kb or 100bp DNA ladder was also loaded on the gel as a size reference. Samples were run at 100V for approximately 1 hour.

2.2.3. DNA gel extraction

DNA fragments of interest were extracted from agarose gels using the GeneJet Gel Extraction kit (Thermo Fisher) following the manufacturer's manual. In brief, the band of interest was removed from the gel using a scalpel under the UV light. The excised gel band was kept in an Eppendorf tube and weighed. Next, the binding buffer was added in a ratio of 1:1 (volume in µL : weight of gel band in mg), and incubated at 50-60°C with occasional vortexing until the gel is completely dissolved. The mixture was passed through a GeneJet purification column by centrifugation for 1 minute. Another 100µL of Binding Buffer was passed through the column to improve the purity of the extracted DNA. The column was washed with 700µL Wash Buffer and then, centrifuged for an extra 1 minute to remove any excess buffer

remained in the column. The dried column was transferred into a clean Eppendorf tube and the DNA fragment was eluted with 50µL Elution buffer. The concentration of the extracted DNA was measured with a Nanodrop equipment.

2.2.4. Small scale plasmid DNA extraction (miniprep)

Recombinant plasmids from transformed DH5α bacteria (NEB® 5-alpha Competent *E. coli* High Efficiency) were purified using the QIAprep Spin Miniprep Kit (QIAGEN). Following bacterial transformation, single colonies were selected and inoculated into 5ml of dYT growth media containing appropriate antibiotic (ampicillin 10µg/ml, kanamycin 50µg/ml) and incubated overnight at 37^{o}C and 200rpm. Bacteria pellets were resuspended in 250µl P1 buffer, then lysed in 250µl P2 lysis buffer and then neutralised by adding 350µl P3 neutralisation buffer. The mixture was centrifuged at 13,000 rpm for 10 minutes and the supernatant was applied onto spin columns which bind the plasmid while other cellular components are eluted in the flow through. The spin columns were washed with ethanol containing wash buffer and lastly, the plasmids were eluted in 50µl Elution buffer. Plasmid concentration was measured using a Nanodrop spectrophotometer.

2.2.5. Plasmids used in this project

Table 2. 3: List of DNA plasmids

Protein	Construct	Provider
TRPA1	pCMV6-AC-GFP	Origene
FGFR2-FLAG tag	pCMV3-FGFR2-Flag	Sino Biologicals
TRPA1-Δ10	pCMV6-AC-GFP	YouBio, Hunan, China
FGFR2-C-58	pGEX4T1	Dr. Chin-Chuan Lin, University of Leeds
FGFR2-STREP Tag	pcDNA6B	Dr. Chin-Chuan Lin, University of Leeds
e-GFP	pGFP-N3	Clontech
FLAG Negative control	pCMV3-C-FLAG	Sino Biologicals

vector		

2.1.1. TRPA1 truncations

The pCMV6-AC-GFP vector from Origene (NM_007332, RG219290 clone) was used for full length TRPA1 mammalian cell expression. TRPA1-Δ10 (deletion of AR 1-10) and TRPA1-Δ5 (deletion of AR 1-5) were made by YouBio, Hunan, China.

2.2.6. C-58 mutations

The C-58 Proline to Alanine mutations were introduced into the pGEX4T1-C58 vector by using the Q5 site-direct mutagenesis kit (New England Biolabs). The pGEX4T1-C58 vector was kindly provided by Dr. Chin-Chuan Lin, Ladbury's group. Firstly, PCR was performed to generate the mutants by using the appropriate primer pairs containing the single nucleotide mutations (Table 2.4). Primer sets were generated using the online tool "NEBaseChanger" from New England Biolabs (https://nebasechanger.neb.com/).

Table 2. 4: PCR primer list used for site directed mutagenesis of the C-58 fragment (Proline to Alanine)

Primer	Sequence 5'-3'	Base substitution
C58-P804A-Fw	AGACCCCATGGCTTACGAACC	CCT to GCT (C to G)
C58-P804A-Rv	GGAGAAAAAACAGAATCATCTCCTG	n/a
C58-P810A-Fw	ACCATGCCTTGCTCAGTATCC	CCT to GCT (C to G)
C58-P810A-Rv	TCGTAAGGCATGGGGTCT	n/a
C58-P813A-Fw	TCCTCAGTATGCACACATAAACG	CCA to GCA (C to G)
C58-P813A-Rv	AGGCATGGTTCGTAAGGC	n/a

The PCR reaction mix and the cycling conditions used are shown below:

Table 2. 5: PCR reaction

Reagent	Working concentration
Reverse Primer	0.5µM
Forward primer	0.5µM
Q5 Hot Start High-Fidelity 2X Master Mix	1x
Template DNA (1–25 ng/µl)	1-25 ng
dNTPs	200µM
Nuclease-free water	Up to 10µL

Table 2. 6: Cycling conditions

Step	Temperature	Time
Initial Denaturation	98°C	30sec
Denaturation	98°C	10sec
Annealing	*	30sec
Extension 35x cycles	72°C	2.5min
Final extension	72°C	2min

* Appropriate annealing temperatures were used according to the Tm values of the primer pairs.

PCR efficiency was verified by agarose electrophoresis and the appropriate DNA fragment was extracted and purified using the GeneJET Gel Extraction Kit (Thermo Scientific) – see section 2.2.3. Following gel extraction, the PCR products were

incubated at room temperature for 5 minutes in a KLD reaction containing a mix of kinase, ligase and Dpn1 enzymes (Table 2.7). In this step, linear products are phosphorylated and ligated into circular plasmids. The initial template is removed by Dpn1 which targets methylated DNA.

Table 2. 7: KLD reaction

Reagent	Volume (10µl)
PCR product	1µl
2X KLD reaction buffer	5µl
10X KLD Enzyme Mix	1µl
Nuclease-free water	3µl

The last step includes bacteria transformation using the KLD reaction products (see 2.2.1 section). The mutated plasmids were obtained by MiniPrep (section 2.2.4) and send for sequencing using appropriate primers to ensure the mutated sites were correct and the reading frame was intact.

2.3. Immunofluorescence (IF)

Cells were cultured on 10mm glass coverslips in 24-well plates and transfected or treated appropriately depending on the experiment. Fixation step was performed using 4% paraforlamdehyde (PFA) in PBS for 20 minutes at room temperature. The cells were washed 4 times with PBS and then blocked for 1 hour at room temperature with blocking buffer containing 8% Fetal Bovine Serum (FBS) and 0.5% NP-40 in PBS prior to overnight incubation with primary antibodies (1:250) diluted in the same buffer at 4^{o}C. After washing 3 times with PBS the cells were incubated with secondary antibodies conjugated with AlexaFluor fluorophores of the appropriate wavelength for 1 hours at room temperature in the dark. Next, the cells

were washed 3 times with PBS. The coverslips were lifted and placed with the cells facing down onto glass slides using mounting medium containing DAPI and sealed with nail polish. Fluorescent images were obtained using a confocal microscope.

2.4. Protein biochemistry

2.4.1. Protein expression and purification of C-58 WT and mutants

The GST-tagged C-58 fragment of FGFR2 was expressed in BL21(DE3) strain of *E. coli*. This strain carries the T7 RNA polymerase gene which is regulated by the *lacUV5* promoter and can be expressed followed IPTG stimulation. Once expressed, T7 RNA Polymerase can transcribe any gene under the control of the T7 promoter e.g. the gene of interest in the pGEX4T1 vector (Studier and Moffatt, 1986).

2.4.1.1. Recombinant protein expression in bacteria

BL21(DE3) cells were firstly transformed with C-58 constructs and the colonies were screened to determine whether they were successfully transformed by performing diagnostic digestion with *BamH1* on isolated plasmid DNA. The colonies whose DNA digestion produced the correct fragment size (successful transformation) could be used for further culture and induction of protein expression as well as stored in glycerol stocks for future use.

Appropriately transformed BL21(DE3) bacteria from an overnight 5ml culture were inoculated in 250ml of dYT media containing ampicillin and cultured until optical density OD_{600}=0.6. At this point, 300μM of isopropyl-β-D-thiogalactopyranoside (IPTG) were used to induce the recombinant protein expression for 12h at 20^{o}C. Next, the bacteria were pelleted at 4,000xg for 20 min at room temperature and stored at -20^{o}C for future use.

2.4.1.2. GST-tagged recombinant protein batch purification

Pelleted BL21(DE3) cells expressing the recombinant protein were re-suspended in Lysis buffer (50mM Tris pH 8, 100mM NaCl, 1mM β-mercaptoethanol and 0.1mM PMSF) prior to lysing with sonication (10sec x 5). The sonicated cells were centrifuged at 13,000xg at 4^{o}C for 1 hour and the supernatant was applied onto 400µl Glutathione Sepharose 4B GST-tagged beads (GE Healthcare) for 30 min at room temperature. GST beads have been washed in PBS to remove storage buffer and equilibrated with Lysis buffer. All bead centrifugations are performed at 500xg for 5 min. After 30 minutes, the beads were washed with 10 times bed volume lysis buffer 3 times and the protein of interest was eluted in 20mM glutathione in 50mM Tris-HCl. 20µl samples from each step were stored and analysed by SDS-PAGE.

2.4.1.3. C-58-GST-beads production

Purified C-58 FGFR2 fragments (wild type and 3 proline mutants) were incubated with washed and equilibrated GST beads for 2 hours at room temperature. Next, the C-58-GST-beads were washed 3 times in 10x bed volume 1x PBS and stored in PBS (50% beads) for future use in GST pull down assays.

2.4.2. Determining protein concentration

Following cell lysis (section 1.1.4), the total protein concentration contained in the cell lysates was determined by using the Bio-Rad Protein Assay Dye Reagent Concentrate (Biorad) which is based on the Bradford method. In brief, the acidic dye Coomassie Brilliant Blue G-250 binds to proteins present in the solution and changes absorbance from 465nm to 595nm. The detected absorbance is proportional to the protein concentration within a range. Bovine Serum Albumin (BSA) was used as a protein standard (linear range 0.2-0.9mg/mL) and the relative protein concentration of the samples can be determined by comparing with that of

the BSA standards. The Dye Reagent concentrate (Bio-Rad) was diluted 1:5 with deionised water and 1mL of the diluted dye was added in cuvettes (BRAND® UV cuvettes semi-micro, chamber volume 1.5). 2µL of the protein sample was added in the cuvette, mixed and then measured at 595nm.

2.4.3. Sodium Dodecyl Sulphate–Polyacrylamide Gel (SDS-PAGE)

SDS-PAGE was used to separate proteins from lysates based on molecular weight. The Biorad Mini-PROTEAN II System and the Tris-Glycine 4-20% pre-cast gels were used for SDS-PAGE. The protein samples were mixed with appropriate volume of 4x Laemmli SDS sample buffer and denatured at 95^{o}C for 5 minutes. 50µg of total protein were loaded for each sample on the gel together with a Pre-stained Precision Plus Protein standards (Biorad) as a protein size marker. The samples were run in 1x Running buffer (0.025M Tris, 0.192M glycine and 0.1% SDS) at 120V for 1 hour and 15 minutes. Following electrophoresis, the gels were stained with Coomassie blue G-250 for 1 hour with gentle agitation to visualise all proteins. Alternatively, the gels were used in Western blots.

2.4.4. Western blot

Proteins separated in an SDS-PAGE gel were transfected onto PVDF membranes by semi-dry transfer. The equipment used for semi-dry transfer was the Trans-Blot® Turbo™ Blotting System from Bio-Rad. Pre-packed top and bottom stacks were purchased from Bio-Rad (Trans-Blot Turbo Transfer System Transfer pack – mini). Proteins were transferred from the gel to the membrane by running the pre-set standard protocol for all molecular weight proteins (25V for 30min).

After the transfer was complete, the membranes were blocked in Blocking Buffer (5% non-fat dry Milk in Wash Buffer) for 1 hour at room temperature on a shaking platform. Next, the membranes were incubated with primary antibodies (1:1000 in Blocking Buffer) for 2 hours at room temperature or overnight at 4^{o}C. The

membranes were then washed 3 times for 10 minutes with Wash Buffer (Table 2.8) and incubated with secondary antibodies (1:1000 in Blocking Buffer) for 1 hour at room temperature. The membranes were washed again 3 times for 10 minutes with Wash Buffer prior to imaging with chemiluminescence. SuperSignal™ West Pico PLUS Chemiluminescent Substrate (Thermo Scientific) was applied to the membranes for 1 minute and the results were imaged by a G-box machine from Syngene.

Table 2. 8: Recipe for 1L of 10X Wash buffer

10X Wash Buffer (TBS-T) 1L	
Tris-HCl	63.04g
Tris-Base	12.11g
NaCl	87.99g
1mM EDTA	2.92g

2.4.5. Quantification of western blots

Western blot images were analysed by densitometry with Image J. A rectangle was drawn closely surrounding the band of interest and the signal intensity was determined with the “measure” function. The same rectangle was moved over the next band keeping the same surface area and the intensity of all protein bands was also determined. The output was copied to Excel or SPSS or Graph Pad where it was statistically analysed by Student’s t-test or Analysis of Variance (ANOVA).

2.4.6. Membrane protein isolation

HCC-515 cells from a T-75 flask were resuspended in 0.5ml of Solubilisation buffer (200 mM NaCl, 20 mM Tris.HCl, 1 mM PMSF, Protease Inhibitor Cocktail, pH 8). The cells were then sonicated for 5 seconds at 60% amplitude followed by a 10-second break for 4 times. 10µL were kept for Western blot analysis. Next, the whole

cell lysate was centrifuged at 20,000 x g for 20 minutes at 4°C. The supernatant was collected and the pellet was resuspended in 100µL Solubilisation Buffer and sonicated again. After the centrifugation step, the supernatants were combined and centrifuged in an ultracentrifuge at 100,000 x g for 1 hour at 4°C to pellet the insoluble material. 10µL of the supernatant (soluble/cytoplasmic fraction) were kept for Western blot analysis. The pelleted membranes were resuspended and incubated in 100 µL of Solubilisation Buffer containing 1% DDM (n-Dodecyl-B-D-Maltoside) for 2 hours at 4°C. The solubilised membranes were then ultracentrifuged at 100,000 x g for 1 hour at 4°C and the supernatant was collected as the solubilised membrane fraction. All samples were analysed by Western blot (section 2.4.3 and 2.4.4).

2.4.7. List of Antibodies used in this project

Table 2. 9: List of primary and secondary antibodies

Antibody	Raised in	Company	Cat. No.
Anti-TRPA1	mouse	Santa Cruz	Sc-166469
Anti-FGFR2	rabbit	Santa Cruz	Sc-122
Anti-FGFR2	rabbit	Protein Tech	13042-1-AP
Anti-TRPA1	rabbit	Protein Tech	19124-1-AP
Anti-TRPA1	rabbit	MIllipore	ABN1009
Anti-pERK	rabbit	Cell Signalling	9101
Anti-ERK	rabbit	Cell Signalling	4695
Anti-β-actin	rabbit	Cell Signalling	4970
Anti-p-PLCγ1	rabbit	Cell Signalling	14008
Anti-PLCγ1	mouse	BD biosciences	610027
Anti-mouse HRP	Goat	Cell Signalling	7076
Anti-rabbit HRP	Goat	Cell signalling	7074
Anti-mouse AlexaFluor555/488	Goat, donkey	Thermo Scientific	A11029, A21202
Anti-rabbit AlexaFluor555/488/594	goat	Thermo Scientific	A11034, A11029, A11012

2.5. Protein interaction techniques

2.5.1. Co-immunoprecipitation

500-1000µg of total protein contained in 500µl of cell lysate were mixed with 20µl of Protein A/G plus Agarose beads (Santa Cruz) for 30 minutes at 4^{o}C upon agitation to pre-clear the lysates from non-specific protein interaction with the beads. The beads were then spun down at 500 x g for 5 minutes and the supernatant was transferred into a clean 1.5ml tube where 5µl of the protein “prey” antibody was added (1:100) and incubated at 4^{o}C for 1 hour under agitation. Next, 50µl of Protein A/G beads were added in the tubes and left overnight to incubate at 4^{o}C under agitation. A step of 3 washes with 1ml 1x PBS was performed and after removing the last supernatant, 50µl of SDS sample buffer was added to the beads. The samples were boiled at 95^{o}C for 5 minutes and the results were analysed by SDS-PAGE and western blot.

2.5.2. GST-pull down

For GST pull down assay, 500µg of total protein contained in HEK cell lysate, wild type or overexpressing TRPA1, were mixed with 50µl of GST-C58 beads (25µl bed volume) overnight at 4^{o}C. The beads were spun down at 600 x g for 5 minutes and the supernatant was discarded prior to washing with 1ml 1x PBS 3 times to avoid non-specific protein binding to the beads. After removing the last supernatant, the beads were mixed with 40µl of 4x Laemmli SDS sample buffer and boiled at 95^{o}C for 5 minutes to break any protein interactions and denature protein structures. The results were analysed by SDS-PAGE followed by western blot.

2.5.3. Microscale thermophoresis (MST)

To investigate the direct interaction between FGFR2 and TRPA1, Microscale Thermophoresis (MST) was performed. The MST method utilises the

thermophoretic properties of molecules in order to determine binding affinities. Thermophoresis is the movement of molecules through a temperature gradient and it depends on the shape, charge and solvation energy of the molecule. MST is used for binding affinity determination for protein-protein, protein-small molecules, protein-DNA and enzyme-substrate interactions. MST offers great advantages over other methods (ITC – Isothermal Titration Colorimetry and SPR – Surface Plasmon Resonance) because 1) it allows for analysis of interactions in biological liquids such as blood or cell lysate which is closer to native conditions, 2) allows for analysis of strong interactions with a K_d as low as 1pM, and 3) does not require high sample consumption or molecule immobilisation on surfaces (Jerabek-Willemsen et al., 2014).

The MST principle is described in Figure 2.1. We used the NanoTemper NT.115 equipment located at the Faculty of Biological Sciences, Astbury Building with the help of Dr Iain Manfield. Purified full length TRPA1 and ΔN (Δ1-688 TRPA1, deletion of the N-terminal Ankyrin Repeat Domain), were kindly provided by Prof. Peter Zygmunt, Sweden. Purified human full length FGFR2 was bought from Origene (TP317098). Full length TRPA1 and ΔN were labelled with Alexa-Fluor488, passed through a NAP-5 column (GE Healthcare) to eliminate unincorporated dye and used at a constant concentration of 83nM. Purified FGFR2 was used in an increasing concentration. The FGFR2 titration series ranged from 0.1nM to 1.8µM (serial 1:1 dilution with PBS which was supplemented with 0.014% F-14 to keep membrane proteins solubilised). 10µL of 83nM TRPA1 or ΔN were mixed with 10 µL of FGFR2 (serial concentrations) and incubated for 30 minutes prior to loading into the capillaries (4 µL). The experiment was performed at 10-50% LED and 40-80% MST power. The data were analysed by Dr. Zahra Timsah using the the Monolith Software and GraphPAd Prism.

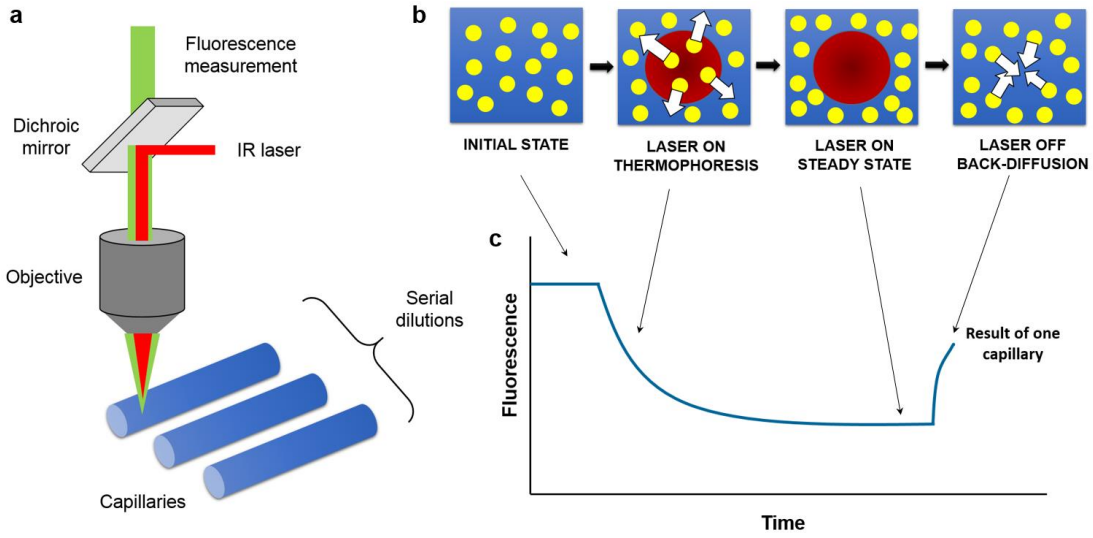

Figure 2. 1: Schematic of MST Principle. FGFR2 and TRPA1 mixtures are loaded into capillaries (4µl). The IR laser is focused on each capillary causing a localised temperature increase that makes the molecules move away (thermophoresis). Labelled TRPA1 is also excited by the IR laser emitting fluorescence signal. Initially, the molecules are equally diffused within the capillary and the fluorescent signal is steady. Thermophoresis is caused when the laser is turned on and a reduction in the fluorescence signal is detected. A steady fluorescence signal follows during which the molecules do not return to that initial location. When the laser is off, the molecules diffuse back increasing the fluorescence signal again. Thermophoresis depends on properties including shape, charge and size of the molecules. The binding of FGFR2 to TRPA1 changes the TRPA1 thermophoretic properties which are translated into changes in fluorescence and depend on the concentration of FGFR2 (different capillaries).

2.5.4. Proximity ligation assay

The Proximity Ligation Assay (PLA) is used to study protein interactions *in situ* based on a template DNA amplification step that can be successful only if the 2 protein targets are located within 40nm from each other (Söderberg et al., 2006). The Duolink® kit from Sigma was used for this experiment.

This assay involves targeting of proteins of interest with primary antibodies raised in different species, followed by incubation with secondary antibodies specifically modified to carry an oligonucleotide DNA sequence, one “+” and the other one “-“. The next step involves the addition of connecting DNA sequences that hybridize to the PLA probes placed on the secondary antibodies, only if the 2 probes are located within 40nm (Figure 2.2). A ligase enzyme also added to the reaction ligates the sequence into a circular DNA template that can be amplified up to 1000-fold through rolling-circle amplification by a DNA polymerase. The PLA probes serve as primers for the amplification step. Additional fluorescently-tagged oligonucleotides hybridise to amplified repeated sequences allowing the detection and localisation of the signal that is visualised as discrete spots using a confocal microscope.

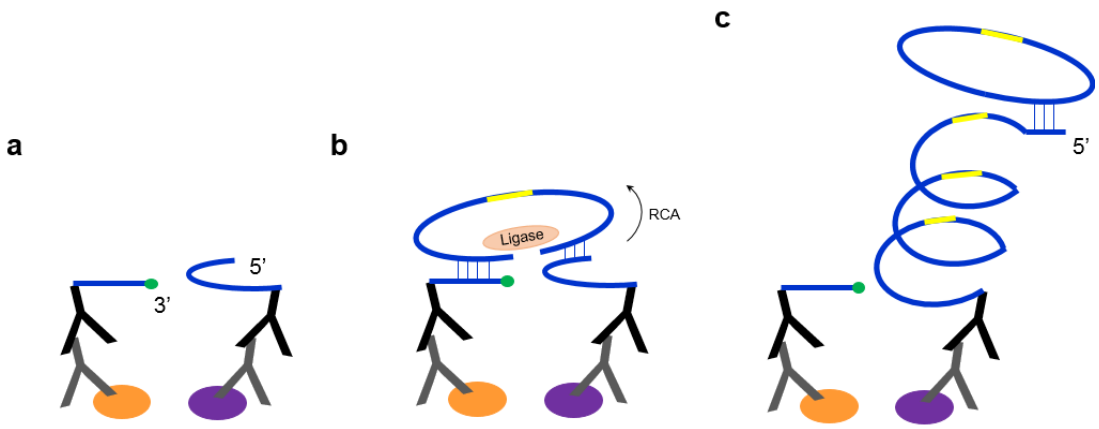

Figure 2. 2: Schematic representation of PLA principle. a) binding of secondary antibodies that carry DNA sequences. b) Addition of DNA oligos complementary to DNA sequences conjugated to secondary antibodies. The Ligase enzyme ligates the oligos into a circular DNA template. DNA sequences serve as primers for a rolling cycle amplification by a DNA pol. c) Fluorescent probes complementary to a specific amplified sequence hybridise to it and generate the PLA signal (yellow).

Cells (HEK283T or HCC-515) were cultured in 10mm glass coverslips and stained with primary antibodies overnight following the regular immunofluorescence protocol. For the secondary antibody incubation, PLA(+) and PLA(-) probes were incubated for 1 hour in a humidified incubator. For each reaction (40ul) 8ul of PLA(+) and 8ul of PLA(-) were mixed in 24ul blocking buffer and placed on one 10mm coverslip. Next, the cells were washed 3 times with PLA wash buffer A and incubated with the ligation reaction (40ul) that included 8ul ligation buffer and 1ul Ligase in 31ul dH_2O for 30 min in a humidified incubator. The cells were washed 3 times with PLA wash buffer A, and then incubated with the amplification reaction (40ul) that included 8ul amplification buffer and 0.5ul DNA polymerase in 31.5ul dH_2O for 100 minutes in a humidified incubator. Lastly, the cells were washed 3 times with PLA wash buffer A and 0.01% PLA wash buffer B for 10min. The coverslips were mounted in glass slides using a mounting medium containing DAPI. The results were visualised in a confocal microscope.

Following image acquisition, PLA signals from each positive cell were manually counted for each condition and statistically analysed in SPSS. Normality test showed that the data was non-parametric thus, Kruskal Wallis, a non-parametric ANOVA test, and Mann Whitney (non-parametric post hoc) statistical analysis were performed.

2.6. Calcium imaging

Calcium Imaging experiments were performed with the help of Alex Hogea and Shihab Shah (members of Gamper Group). Calcium imaging was used as a functional assay for TRPA1 activity. HCC-44 or HCC-515 cells that were cultured on coverslips, were serum starved for 2 hours prior to imaging. Next, the cells were incubated with 1 µM Fura-2-AM (calcium indicator) and 0.01% pluronic acid in EC solution (160 mM NaCl, 2.5 mM KCl, 1 mM $MgCl_2$, 2 mM $CaCl_2$, 10 mM Hepes, and

10 mM Glucose) at 37 °C for 45 to 60 minutes. Following placement of coverslip chips in the perfusion chamber, the cells were washed with EC solution for 2 minutes. Next, the cells were perfused with 100µM AITC for 5 minutes to activate TRPA1 channels prior to washing with EC for another 2 minutes. Ionomycin (Thermo Fisher Scientific) was used at the end of each recording as a positive control for calcium detection. HC-030031 was used at 50µM for 5 minutes before treatment with AITC to pre-block TRPA1 channels. Fura-2 was alternatingly excited at 340nm (calcium bound) and 380nm (calcium free) every 2 seconds and 510nm emission recordings were monitored. The calcium response was indicated by the ratio of fluorescence at 340nm/380nm (F340/F380).

Experiments were performed in triplicates with 20-40 cells each. Firstly, all the data points were normalised against the first baseline value to overcome baseline variation between cells. The calcium response was calculated by subtracting the baseline (first EC wash right before stimulation) by the maximum response detected within the 5 minutes of AITC stimulation.

An inverted Nikon Eclipse TE-2000 microscope, Polychrome V monochromator, IMAGO CCD camera, and TILLvision 4.5 software were utilised for this calcium imaging.

2.7. Super resolution microscopy

Image resolution using a regular confocal microscope is restricted to approximately half the size of the wavelength used, due to the diffraction limit of light. This results in a resolution limit of maximum 200nm laterally and 500nm axially that prevents detailed analysis of single molecules and cellular structures. An increase of 1.7 times (max. 140nm laterally, 400nm axially) in resolution can be achieved by Airyscan imaging (Huff, 2015). Regular confocal imaging utilises a pinhole of 1 A.U. (Airy unit) because pinholes with diameter smaller than 1 A.U, even though achieve

higher resolution (0.2 A.U. = 1.4x resolution increase), result in signal loss up to 95%. Airyscan utilises a novel detector composed of 32 smaller pinholes of 0.2 A.U. each, that combines the higher detection of a 1.25 A.U. pinhole with the resolution of a 0.2 pinhole, resulting in increased signal to noise ratio too (Huff, 2015). However, the 140nm maximum resolution is still way bigger than the size of biological complexes and molecules.

The development of super resolution microscopy techniques such as d-STORM (direct-Stochastic Optical Reconstruction Microscopy) and PALM (PhotoActivated Localisation Microscopy) has managed to overcome the resolution limit by taking advantage of the photo-switchable properties of fluorophores (Schermelleh et al., 2019). In brief, only a portion of the fluorophores are stochastically activated or “switched off” in sequential acquisitions. This results in separation of signals both in space as well as time. Superimposition of all the frames reconstructs the final image that can achieve resolution up to 20nm.

An alternative method to overcome the diffraction limit of light and achieve higher resolution is Expansion Microscopy (ExM). ExM involves the physical expansion and thus magnification of the sample which is embedded into a swellable gel, resulting in separation of molecules and increase in resolution (Figure 2.3). In comparison to single-molecule super resolution microscopy techniques, ExM offers advantages such as use of inexpensive materials and equipment, simple and quick protocols as well as 3D imaging of thick specimens. However, due to the nature of the technique, live imaging is not feasible (Wassie et al., 2019).

2.7.1. Expansion microscopy

The Expansion microscopy experiments were performed in collaboration with Dr. Izzy Jayasinghe and Tom Sheard that provided an already validated protocol and assisted with data analysis. The ExM protocol involves a series of chemical reactions aiming to expand the sample isotropically (Figure 2.3). First, fluorophores

conjugated to secondary antibodies are attached to Acrylol X (AcX) which acts as a linker between the fluorophores and the polymer. Next, the samples are incubated with the Monomer solution that consists among others of Sodium Acrylate (monomer) and DMA (cross-linker). During polymerisation, a mesh of Solium PolyAcrylate is generated that is attached to the fluorophores through the anchors of AcX. Isotropic expansion requires digestion of the biological material through incubation with Proteinase K. Proteinase K digests all molecules, destroying any cellular structures. As a result, isotropic expansion of the swellable gel is achieved upon incubation in water due to osmosis and high charge of the electrolyte mesh. A 4x expanded gel increases in volume 100 times. The expansion factor depends on the chemistry of the monomer solution and the concentration of the cross-linker (N,N′-Methylenebisacrylamide, DMA). For a 10X ExM, lower concentrations of DMA are used which results in greater expansion but also higher gel fragility (Wassie et al., 2019). The resolution depends on the expansion factor. A 4x expanded gel imaged with Airyscan confocal can achieve a resolution of 35nm, while a 10x expanded gel can achieve a resolution of 14nm.

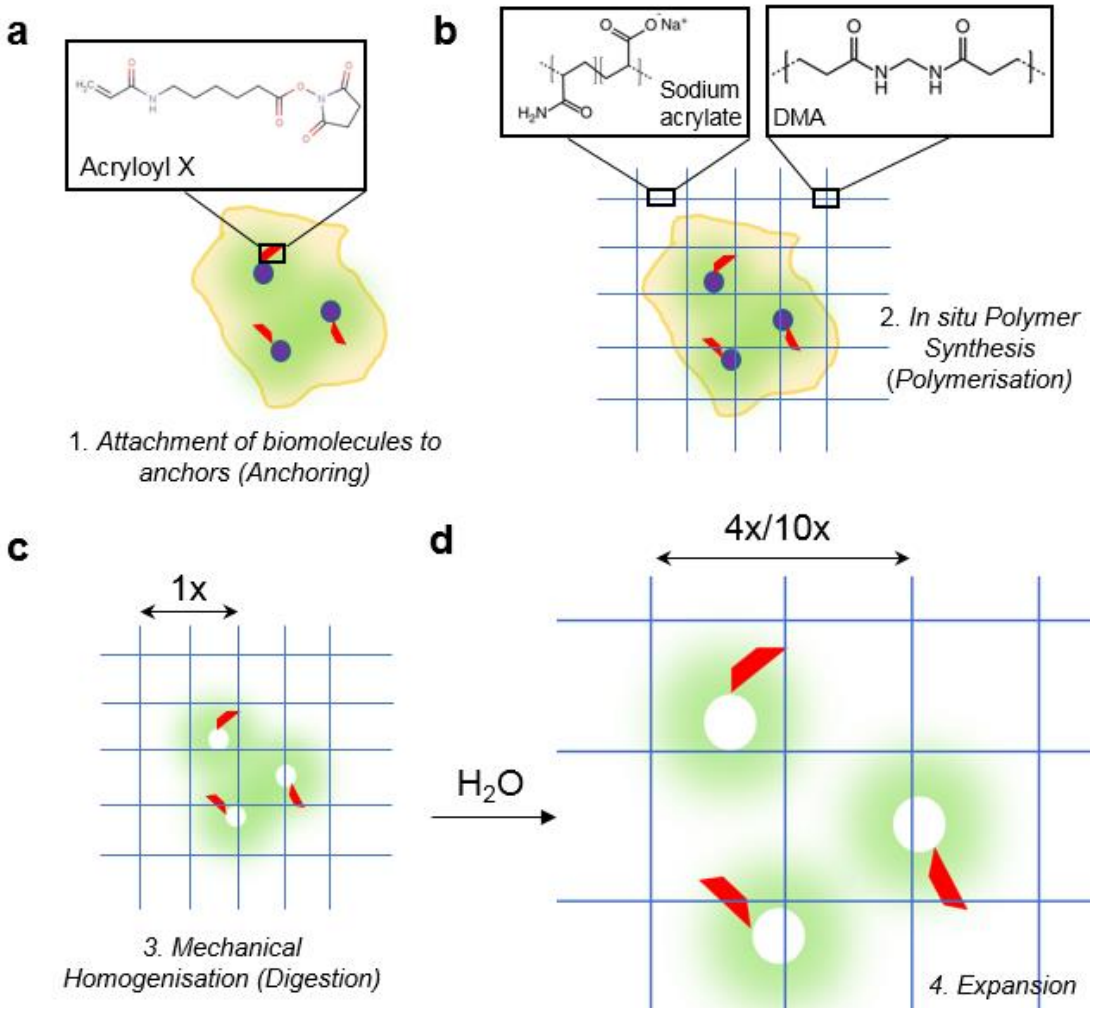

Figure 2. 3: Schematic representation of Expansion Microscopy protocol. a) Anchoring step: Fluorophores (green), conjugated to antibodies targeting molecules (blue spheres), attach to anchors of Acryloyl X (AcX). b) Polymerisation step: Monomer solution containing the monomer (Sodium Acrylate) and the cross-liker (DMA) is applied to the sample. Upon APS (initiator) and TEMED (accelerator), Sodium Acrylate starts to polymerise and create a hydrogel mesh. AcX anchors attach fluorophores to the hydrogel mesh. c) Digestion step: the biological material is removed by digestion with Proteinase K that digests proteins. d) Physical expansion of the gel following incubation in water.

However, the fluorophores remain attached to the mesh. d) Upon water immersion, the gel is expanded. The attached fluorophores are now further apart and can be resolved under a confocal microscope.

2.7.1.1. Immunofluorescence staining

Cells were cultured in square glass coverslips (22mm x 22cm) within wells of a 6-well plate and stained with primary and secondary antibodies following a regular immunofluorescence protocol (section 2.3). Alexa-Fluor488 and Alexa-Fluor594 conjugated secondary antibodies were used for expansion since Dr Izzy Jayasinghe's group has successfully been using those fluorophores in expansion microscopy. Next, the coverslips were attached to slides to create square chambers and imaged in a regular confocal microscope (Airyscan mode) to obtain pre-expansion images of the cells.

2.7.1.2. Anchoring

Following PBS washes of the secondary antibody and pre-expansion imaging, the PBS is removed and replaced with the Anchoring Solution. The Anchoring Solution consists of Acryloyl X (AcX) in a final working concentration of 0.1mg/mL in PBS. Aliquots of 10mg/mL (1mg of AcX in 100µL DMSO) were diluted 1:100 in PBS and approximately 300µL were applied onto the cells overnight at 4^{o}C. The slides were kept in a humidified box to keep cells from drying out. This anchoring method is the same for both the 4X and 10X expansion protocols.

2.7.1.3. Monomer polymerization

<u>ExM 4X:</u>

The next day, the cells were washed with PBS and then incubated with Polymer Solution for 2 hours at 37^{o}C. In brief, 282µL of (1.06% strength – Table 2.10) Polymer Solution was mixed with 12µL PBS, 3µL of Ammonium persulfate (APS, 0.1% working concentration) and 3µL of N,N,N',N'-Tetramethylethylenediamine

(TEMED, 0.1% working concentration) to make 1x of 300µL final Volume. The solution was mixed avoiding air bubbles. Firstly, the coverslips were detached from the slides. New coverslips were cut lengthwise to create strips and placed on the two edges of the coverslips (with the cells) to serve as walls. The Polymer Solution was then applied to the cells and a new full-size coverslip was placed on top to seal the "chamber".

Table 2. 10: polymer recipe for ExM 4X

Reagent	Stock (g/100mL)	Volume	Working concentration (g/100ml)
Sodium acrylate	38	0.5625	8.6
Acrylamide	50	0.125	2.5
N,N'-Methylenebisacrylamide	2	0.1875	0.15
Sodium chloride	29.2	1	11.7
PBS	10x	0.25	1x
Water	n/a	0.225	n/a
Total Volume	n/a	2.35mL	n/a

ExM 10X:

The Polymer Solution for ExM 10X consists of 0.15875g Sodium acrylate (SA) and 666µL Dimethylacrylamide (DMA) in water of 2.5mL total Volume (33% DMA and SA). The solution was bubbled with nitrogen gas for 1 hour at 4°C. 333µL of Potassium Persulfate (KPS, 27mg/mL stock concentration) was added in 2.166mL of Polymer Solution and bubbled with nitrogen gas for another 15 minutes.in the meantime, the cells were washed with PBS and coverslip walls were in place. 375µL of Polymer Solution containing KPS were mixed with 1.5µL TEMED (0.4% working concentration) and applied to the cells. A new coverslip was placed on top

to seal the “chamber”. The cells were incubated with the Polymer Solution overnight at room temperature.

2.7.1.4. Digestion

Following Polymerisation, the remaining tissue embedded in the gel is dissolved with a Proteinase K incubation step which is the same for both 4X and 10X expansion protocols. Firstly, the gel is removed from the chamber by carefully separating the coverslips and cutting excess gel. The shape and dimensions of the gel are recorded. Next, the gel was placed in a well of a 6-well plate and 2mL of Digestion Solution (Table 2.11) is applied. 100uL of Proteinase K (8units/mL working concentration) was mixed with 10mL of Digestion Solution (1:100) and the gel was incubated for 12-16hours overnight at room temperature.

Table 2. 11: Digestion Buffer recipe for 100mL

Reagent	Stock	Working concentration	Amount used
EDTA	01M	1mM	1mL
Tris pH 8	1M	50mM	5mL
Triton X-100	100%	0.5%	0.5mL
Guanidine HCl	n/a	0.8M	7.6424g
Water	n/a	n/a	Up to 100mL
HCl	10%	n/a	Up to pH 8

2.7.1.5. Expansion

The next day, the Digestion Solution was removed and the gel was transferred to a container that was big enough to fit the expanded gel. The gel was incubated with 30-100mL of deionised water which was changed every 30 minutes to 1 hour until

the expansion plateaued. At this point, the new dimensions of the gel were recorded and divided by the initial dimensions to determine the expansion factor. All the incubations were performed in a dark room to avoid photobleaching.

2.7.1.6. Imaging and analysis

The gel was cut into squares that would fit in square chamber slides for imaging. To avoid gel drifting while imaging, the square chamber slides were coated with 0.1% poly-L-lysine for 30 minutes and then washed with water prior to placing the gel. A few drops of PBS were added on top of the gel to prevent it from drying and shrinking during imaging. Fluorescent images were obtained at 63x magnification and by using the Airyscan mode in a confocal microscope. Airyscan processed images were inserted into Image J. A threshold (usually “ISODATA” was applied to areas of interest and the images were analysed with the Mander’s Colocalisation Analysis. The obtained values were copied to Excel and statistically analysed.

2.8. Statistical Analysis

Statistical analysis was performed on data obtained from at least three repetitions. Throughout the thesis, the data are presented in bar graphs as the average of all repetitions. The error bars represent the S.E.M. (standard error of the mean). Statistical significance between 2 groups and more than 2 groups was analysed by Student’s t-test in Excel and ANOVA (analysis of variance) in SPSS or GraphPad, respectively. Statistical significance is shown by asterisks (*).

3. Chapter 3
Characterisation of the FGFR2-TRPA1 complex

3.1. Introduction

Protein-protein interactions are necessary for multiple cellular processes, including signal transduction. Intermolecular and intramolecular protein interactions are mediated through specific recognition and reversible binding between structural motifs found on the protein molecules. There are numerous protein domains that are implicated in target recognition based on protein motifs. The SH2 domains, for instance, bind to phosphorylated tyrosine residues on target proteins and the FHA (Fork-head Associated) domains recognize phosphorylated threonine and serine residues on targets (Ball et al., 2005).

As a Tyrosine Kinase Receptor, FGFR2 forms direct interactions with downstream adaptor and effector proteins (substrates for phosphorylation) resulting in signalling cascades. One of the most significant protein interactions involves recognition of FGFR2 phospho-tyrosine residues by SH2-containing proteins. The n-SH2 domain of PLCγ1, for instance, recognises phospho-tyrosine 769 (pY769) on the FGFR2 C-terminal region which results in PLCγ1 phosphorylation and activation by the receptor (Huang et al., 2016). Another substrate of FGFR is FRS2 (FGFR-related substrate-2) which is constitutively bound and interacts through its PTB domain (phospho-tyrosine binding domain) that recognises non-phosphorylated residues on the FGFRs juxtamembrane region (residues 419, 422, 423 and 425 of human FGFR1) (Gotoh, 2008). There is evidence that phosphorylated serine residues on FGFR2 (S779) can also serve as interaction sites for the 13-4-4 group of proteins which can activate pathways including the MAPK however, the specific mechanism of signalling activation through phospho-serines remains elusive (Lonic et al., 2008).

An additional form of interaction that is shown to be vital for the FGFR2 signal regulation, especially under non-stimulating conditions, occurs through its C-terminal proline-rich motif. In general, Proline-rich motifs are recognised by SH3 domains and so far, there are two SH3-containing binding partners that have been described for FGFR2: the adaptor protein GRB2 and the phospholipase PLCγ1 (Ahmed et al., 2010; Timsah et al., 2014).

There is evidence of a direct interaction between proline-rich motifs and Ankyrin repeat domains (ARD), another common protein motif. According to Rader et al, the mouse Ankyrin-repeat family A protein (ANKRA) interacts with the proline-rich motif-containing cytoplasmic domain of the rat megalin (a low-densitty lipoprotein receptor found in epithelial kidney cells) through its ankyrin repeats (Rader et al., 2000). Based on this evidence, there could be other possible ankyrin repeat-containing binding partners for the proline-rich motif of FGFR2. Following bioinformatics analysis performed by Dr. Zahra Timsah's group (unpublished data), one of those potential binding partners is the ion channel TRPA1.

TRPA1 is a non-selective cation channel with an extended N-terminal domain that carries 16 ankyrin repeats. The primary module of the TRPA1 ARD (AR12-16) is responsible for electrophilic ligand recognition which mainly includes Cysteine 621, 641 and 665, however, no protein-based ligand has been proven to bind directly on the ARD so far. This raises the question of what is the actual function of the rest of the ARs (Paulsen et al., 2015). Given the large number of ARs compared to other TRP channels, TRPA1 could interact with other membrane-bound or cytoplasmic proteins. For example, Tmem100, a two-transmembrane protein, forms complexes with both TRPA1 and TRPV1, individually, regulating TRPA1 activation. However, the binding region on either of the channels has not been further determined.

To the best of our knowledge, the direct interaction between a TRP channel and an RTK has never been reported, especially in the context of cancer. This Chapter

aims to characterise the possible interaction between FGFR2 and TRPA1 in a cellular overexpression system as well as map the interaction sites on both proteins by utilising protein interaction techniques including pull-downs, PLA and biophysical methods. Physiological complex formation is also studied in a human LUAD cell line. Further characterisation and stoichiometry of the FGFR2-TRPA1 complex is studied by Expansion Microscopy, a super-resolution microscopy technique.

This set of data led to a publication in 2017 by Dr Zahra Timsah's group (Berrout et al., 2017) however, additional controls, repeats and further experiments have been conducted and included in the present chapter.

3.2. Results

3.2.1. FGFR2-TRPA1 complex formation in transfected HEK-293T cells

To assess the binding between FGFR2 and TRPA1, HEK-293T cells transiently transfected with plasmids containing tagged proteins (tGFP-TRPA1 and FGFR2-FLAG), (tGFP = turbo GFP), were lysed and used for co-IP experiments. It was crucial to incubate the cells in serum-free media for 2 hours prior to lysis to avoid any stimulation of FGFR2. Transfection efficiency and simultaneous expression was confirmed by Immunofluorescence staining using anti-FGFR2 and anti-TRPA1 antibodies (Figure 3.1). The expression of both proteins in HEK-273T cells confirms both plasmids are functional, and that this system can be utilised for studying the interaction between FGFR2 and TRPA1

Lysates from HEK-293T cells transfected with tGFP-TRPA1 and/or FGFR2-FLAG were used in co-IP experiments in which either FGFR2 (Figure 3.2a) or TRPA1 (Figure 3.2b) served as "bait" protein and the results were analysed by western blot. FGFR2 successfully pulled down TRPA1 (a, lane 4) and vice versa, TRPA1 pulled down FGFR2 (b, lane 3) suggesting complex formation between the two proteins.

Minimal amounts of protein were detected in negative control cells expressing only the protein “prey” verifying the specificity of the results (a and b lane 2).

Even though the tGFP tag is connected to the N-terminal of TRPA1 and the FLAG tag is linked to the C-terminal of FGFR2, both regions are located in the cytoplasm. In order to eliminate the possibility of interaction through the tags, co-IP experiments were performed in HEK-293T cells expressing negative control vectors. The ability of tags to pull down the protein “bait” was examined in western blots (Figure 3.3). Firstly, the anti-FLAG antibody was not able to pull down TRPA1 in the absence of FGFR2 (Figure 3.3a, lane 2, tGFP-TRPA1+empty FLAG vector) excluding the possibility of interaction through the FLAG tag of the receptor. However, the anti-FLAG antibody pulled down TRPA1 when the cells were double transfected with tGFP-TRPA1 and FGFR2-FLAG confirming the interaction between the two proteins once again.

Similarly, an anti-FGFR2 antibody on HEK-293T cells co-expressing FGFR2-FLAG and an empty GFP vector failed to precipitate GFP (Figure 3.3b, lane 1) eliminating the possibility of interaction of FGFR2 with GFP tag. However, the pGFP-N3 vector (Clontech) was used in this co-IP due to lack of tGFP (turboGFP) negative control vector. Nevertheless, this experiment showed that there was no interaction between FGFR2 and GFP, confirming the specificity of FGFR2-TRPA1 interaction (at least in the context of the above controls). TRPA1 could not be recognised by a regular anti-GFP antibody in the presence of FGFR2, neither in the co-IP nor the lysates blot (Figure 3.3b, lanes 2 and 4), even though it was recognised by the anti-TRPA1 antibody (same lanes). This is because a specific anti-tGFP antibody is required for tGFP recognition.

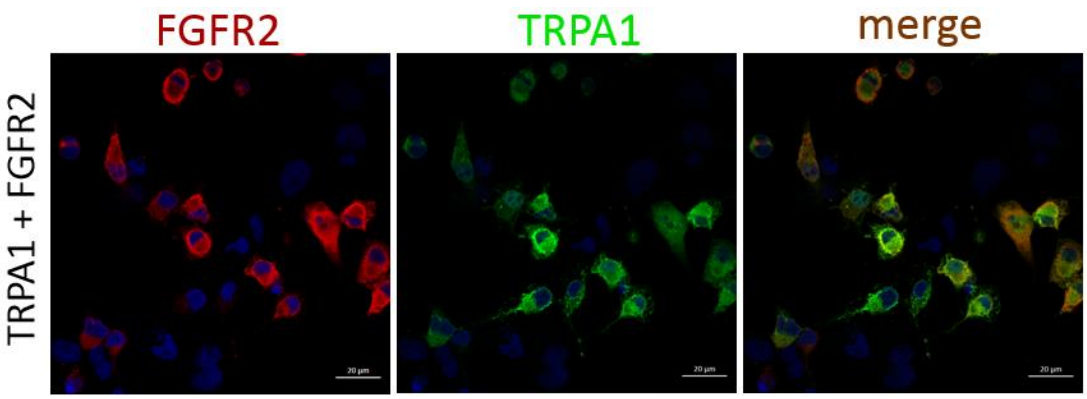

Figure 3. 1: Efficiency of transfection for FGFR2 and TRPA1 in HEK-293T cells. Immunofluorescence staining with anti-FGFR2 (Santa Cruz) and anti-TRPA1 (Santa Cruz) antibodies to verify successful expression of the proteins in HEK-293T cells. Scale bar equals 20µm.

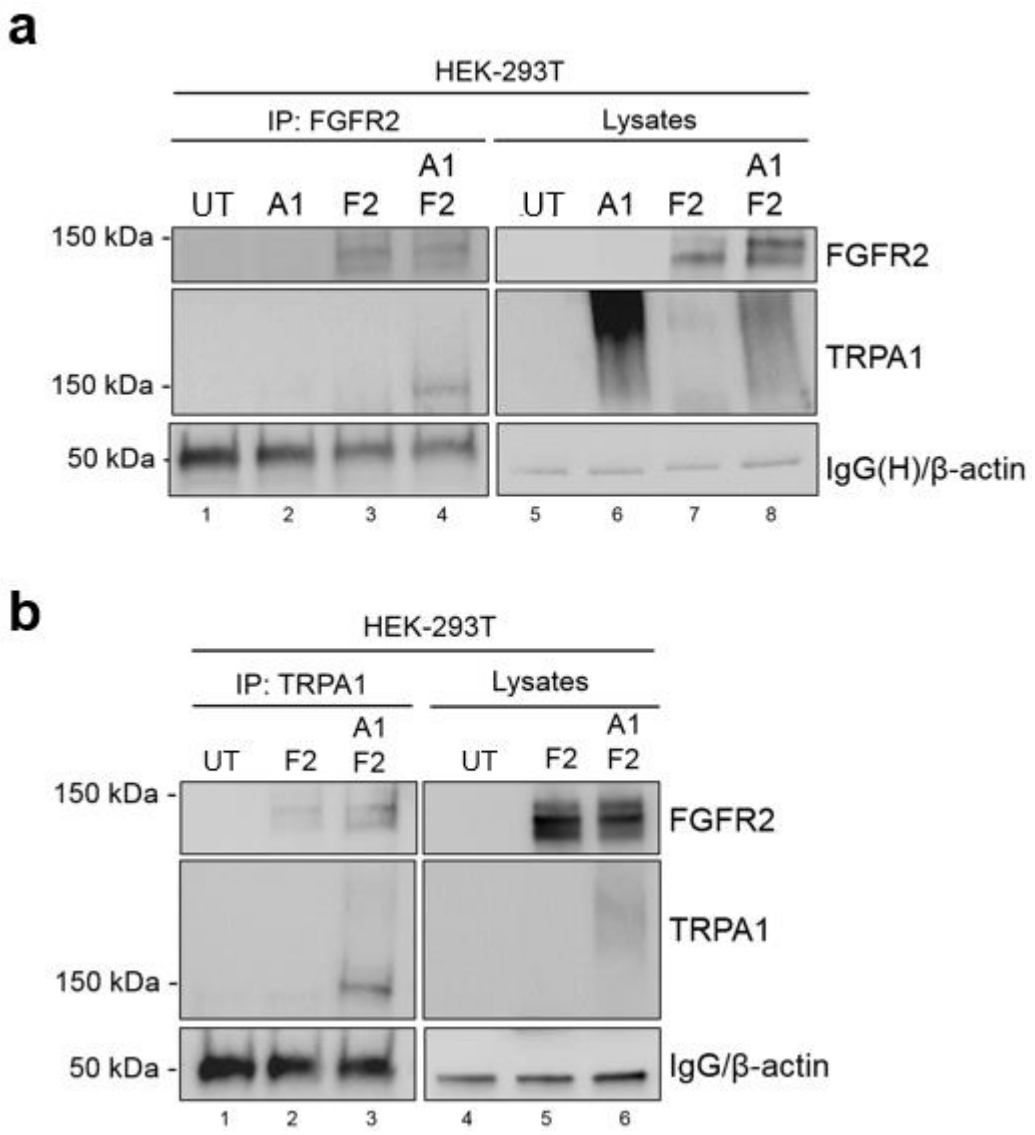

Figure 3. 2: Co-Immunoprecipitation experiments confirming the interaction between overexpressed FGFR2 and TRPA1 in HEK-293T cells. a) Co-IP with anti-FGFR2 antibody (Santa Cruz) and b) with anti-TRPA1 antibody (Santa Cruz) on HEK-293T cells transfected with FGFR2-FLAG and tGFP-TRPA1. Un-transfected (UT), tGFP-TRPA1- and FGFR2-FLAG-transfected cells were used as negative controls. Left panels = co-IP, right panels = expression levels for the proteins of interest. The IgG heavy chain band and β-actin are used as loading controls for the IP and Western blot, respectively. Representative blots are shown (n=3).

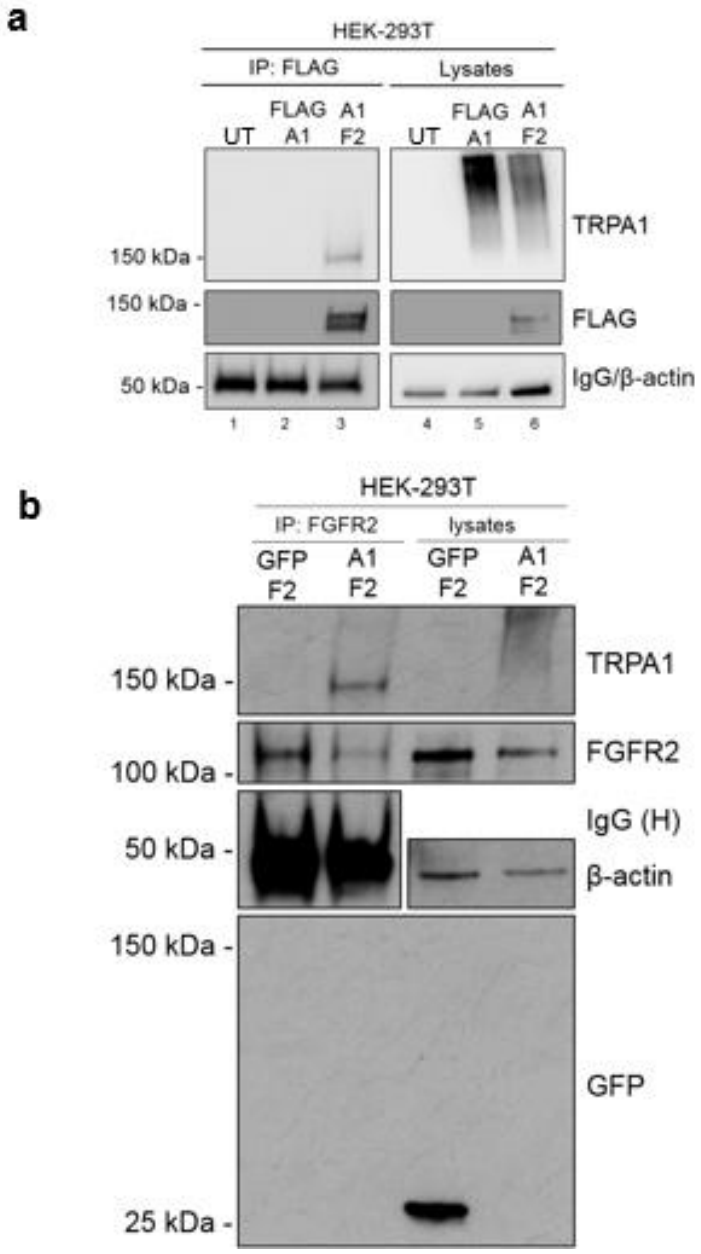

Figure 3. 3: Co-Immunoprecipitation experiments to control for binding through the epitope tags. a) Co-IP with the anti-FLAG antibody on HEK-293T cells transfected with FGFR2-FLAG + tGFP-TRPA1 (positive control), Un-transfected (UT) and tGFP-TRPA1+FLAG vector (negative controls). b) Co-IP with the anti-FGFR2 antibody (Santa Cruz) on HEK-293T cells overexpressing FGFR2-FLAG + tGFP-TRPA1 (positive control) and FGFR2-FLAG + GFP (negative control). Left panels = co-IP, right panels = expression levels for the proteins of interest. The IgG heavy chain band and β-actin are used as a loading controls for the IP and Western blot, respectively. Representative blots are shown (n=3).

In the next series of experiments, Proximity ligation assay (PLA, see Chapter 2 for details) was also performed to confirm the interaction between overexpressed FGFR2 and TRPA1 in HEK-293T cells. The PLA assay was performed using antibodies against FGFR2 and TRPA1 proteins.

Confocal analysis of the PLA experiment showed that the PLA signal was significantly higher ($p<0.05$, Mann Whittney, mean = 23 puncta per cell) in cells overexpressing FGFR2-FLAG and t-GFP-TRPA1 compared to cells overexpressing only tGFP-TRPA1 (mean = 4.7 puncta per cell) which served as a biological negative control because only one of the proteins was overexpressed (Figure 3.4 and 3.5). PLA signal is created only when the two PLA probes are located within 40nm apart which suggests a high chance of physical interaction between FGFR2 and TRPA1, therefore, verifying the co-IP results.

Interestingly, a low PLA signal was observed in un-transfected cells (mean = 2 puncta per cell), which could be the result of either a “noise” signal created by the “by chance” colocalization of non-specifically bound antibodies or interactions between endogenous FGFR2 and TRPA1 proteins, potentially expressed in HEK-923T cells at low levels, or even a combination of the above. The tGFP-TRPA1-expressing cells in which FGFR2 was not over-expressed had a significantly higher TRPA1-FGFR2 PLA signal compared to the wild type cells (Figure 3.5). This increase in PLA signal upon over-expression of TRPA1 could be due to interactions between exogenous TRPA1 and minimal amounts of endogenous FGFR2.

Nevertheless, the PLA signal was significantly higher in double- compared to single-transfected cells indicating signal specificity. As an additional negative control, PLA was performed without primary antibodies added to double transfected cells, which showed no PLA signal. Two TRPA1 antibodies raised in different

species were used as a technical positive control in cells overexpressing only tGFP-TRPA1 (mean = 9.5 puncta per cell) (Figure 3.4).

TRPA1 is fluorescently tagged, which facilitates the visualisation and confirmation of protein presence in the examined cells. On the other hand, there was no fluorescent tag for FGFR2 - thus, the presence of the protein could not be verified at the time of PLA imaging. However, based on the PLA principle, to visualise a PLA signal the proteins should be expressed in the same cell, so PLA signal was automatically linked to double expression. Indeed, the PLA signal was present in GFP cells (co-expressing FGFR2) and not in non-GFP cells (wild type or only FGFR2 expression) (Figure 3.4). It was also observed that the PLA signal varied from 6 to 72 in 127 cells overexpressing both proteins which can be explained by the differences in protein expression levels between cells following transfection.

Next, to eliminate the possibility of increased PLA signal because of protein overexpression and “random” co-localisation due to abundance, rather than due to actual physical association of the targets, an additional PLA assay was performed on cells transfected with a negative control empty GFP vector and FGFR2-FLAG. In theory, this combination should not have higher PLA signal than the FGFR2-FLAG and tGFP-TRPA1 combination because GFP does not interact with FGFR2 or FLAG. PLA signal was significantly higher in this negative control (mean = 62 puncta per cell) compared to the FGFR2+TRPA1 condition (Figure 3.6). In this experiment, **a different pair of antibodies had to be used: anti-GFP and anti-FLAG, which means that this is not an “ideal” negative control**. However, it shows that PLA can be affected by protein over-expression.

Therefore, the PLA experiment in Figure 3.5 is an indication of FGFR2 and TRPA1 close proximity / physical association and not a definite proof of interaction due to the fact that the proteins were overexpressed and as a result present at high levels.

Further interpretation of PLA results is considered in the Discussion section of this chapter.

Taken together, both co-IP and PLA experiments could suggest complex formation between TRPA1 and FGFR2 in overexpressing HEK-293T cells.

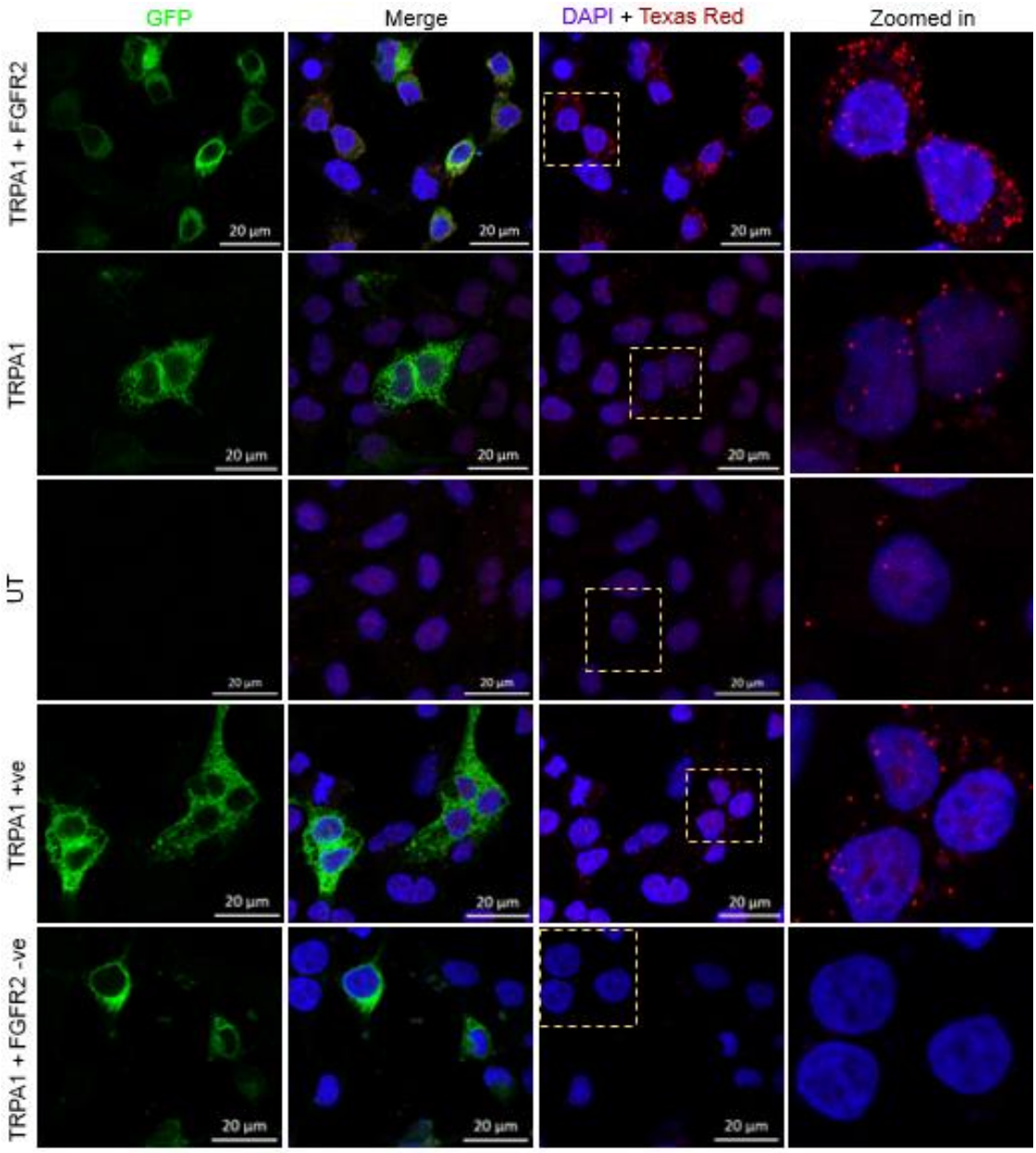

Figure 3. 4: PLA assay on transfected HEK-293T suggests close proximity of FGFR2 and TRPA1. Protein overexpression is indicated on the left and each row represents a different assay condition. 'TRPA1+FGFR2-ve' = no primary antibodies. 'TRPA1+ve' = TRPA1-transfected cells and the use of two TRPA1 antibodies raised in different species (Santa Cruz and Protein Tech). 'UT' = Un-transfected. TRPA1 is tGFP-tagged and FGFR2 is FLAG-tagged. TRPA1 presence is verified with GFP. PLA signal is visualised with Texas Red. DAPI stain is used for nuclear staining. Representative images are shown (n=4). 'Merge' for DAPI, GFP and Texas Red.

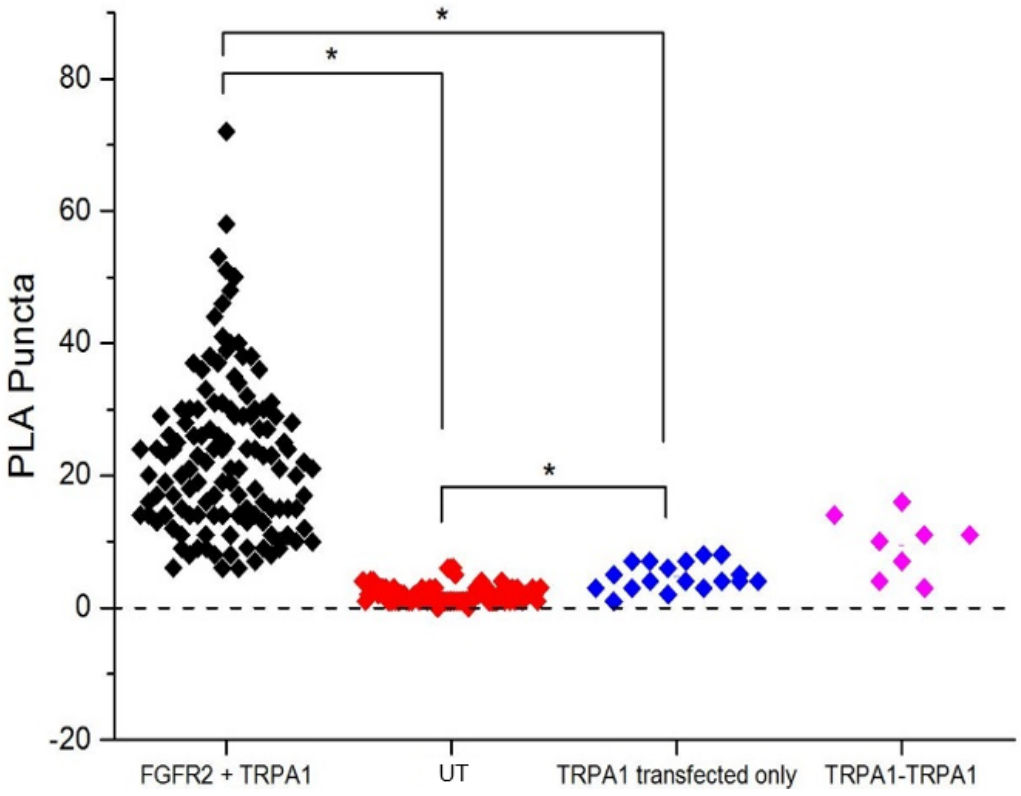

Figure 3. 5: PLA quantification. Scatter plot illustrating PLA puncta per cell in four different conditions. There was a significant difference between the groups as analysed with non-parametric Kruskal Wallis test on OriginPRO. Significant differences are shown as * ($p \leq 0.05$, Mann Whitney, non-parametric post hoc). FGFR2-FLAG + tGFP-TRPA1 = 127 cells and mean = 23 puncta per cell, UT = 74 cells and mean = 2 puncta per cell, TRPA1-only (negative control) = 18 cells and mean = 4.7 puncta per cells, TRPA1-TRPA1 (positive control) = 8 cells and mean = 9.5 puncta per cell. Statistical analysis of Figure 3.4. UT = Un-transfected.

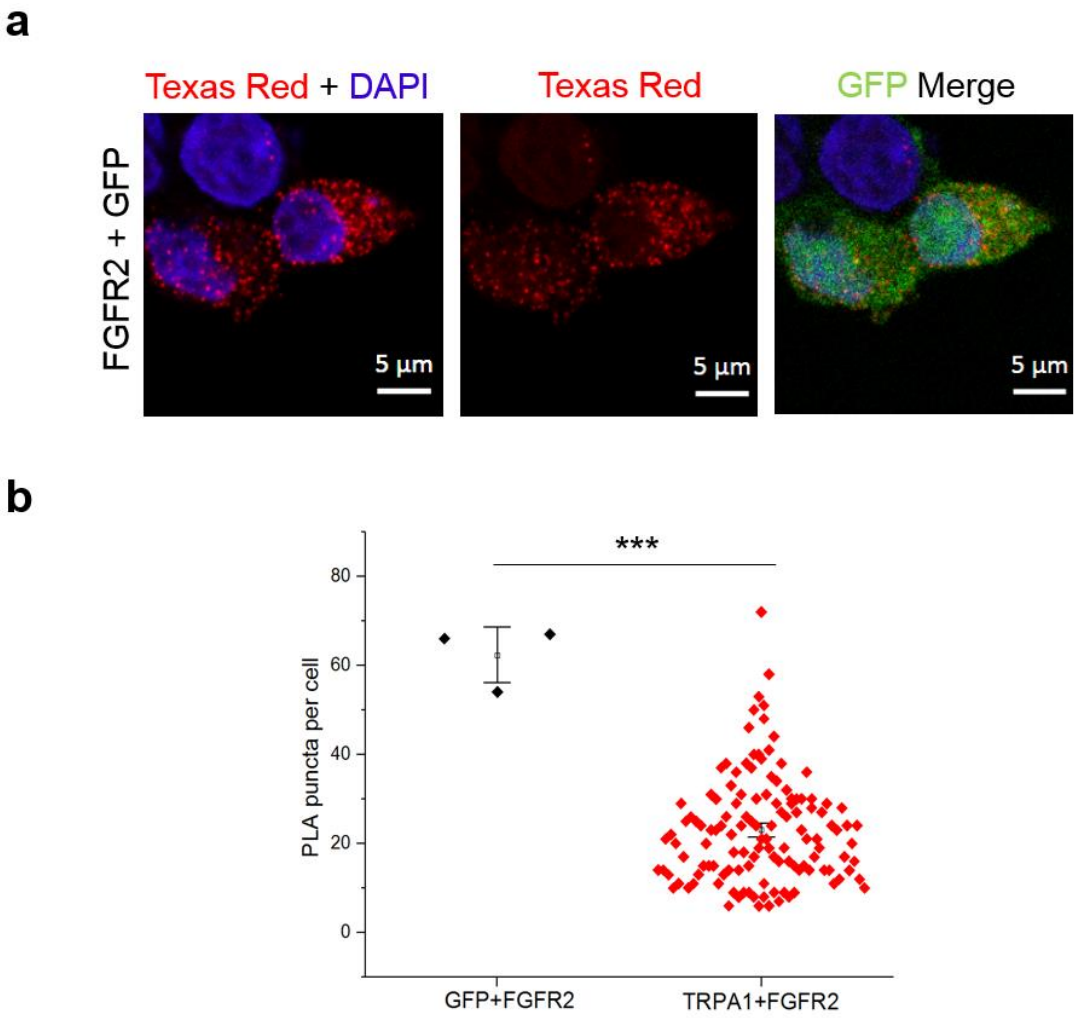

Figure 3. 6: PLA signal is affected by protein abundance. a) Representative images of PLA assay on HEK-293T cells transfected with FGFR2-FLAG + GFP as a negative control. TRPA1 = GFP, PLA = Texas Red, cell nuclei = DAPI. b) Statistical analysis. Scatter plot illustrating the PLA puncta per cell in two groups. FGFR2-FLAG + GFP = 3 cells, FGFR2-FLAG + tGFP-TRPA1 = 127 cells. Significant differences are shown as *** ($p \leq 0.001$, Mann Whitney, non-parametric, OriginPRO). Error bars of the mean are shown in black.

3.2.2. TRPA1 directly binds to FGFR2 through the Ankyrin Repeat Domain (ARD)

At this point, co-IP and PLA experiments suggest complex formation between FGFR2 and TRPA1. However, direct interaction between the two proteins has not been confirmed. For this reason, a biophysical method called Microscale Thermophoresis (MST) was performed using purified proteins to study protein interaction *in vitro*. Purified TRPA1 labelled with Alexa-Fluor488 was used at a constant concentration of 83 nM while purified FGFR2 was used in an increasing concentration (0.1-1800 nM). A binding curve was constructed after raw data analysis using the Monolith software, performed by Dr. Zahra Timsah, which revealed protein interaction between the proteins. The dissociation constant (K_d) was calculated as 122.8 ± 23.4 nM that indicates the concentration at which the two proteins exist in an equilibrium of bound and unbound state (Figure 3.7b).

The N-terminal Ankyrin Repeat Domain (ARD) of TRPA1 is an appropriate candidate for protein interactions since ARD are involved in protein interactions. To investigate the potential role of the ARD in the interaction with FGFR2, MST was performed with a truncated version of TRPA1 (Δ1-688 or Δ16) in which the 16 N-terminal Ankyrin repeats have been deleted (Figure 3.7a). In this case, a binding curve could not be created suggesting that TRPA1 cannot interact with FGFR2 in the absence of the ARD domain (Figure 3.7b).

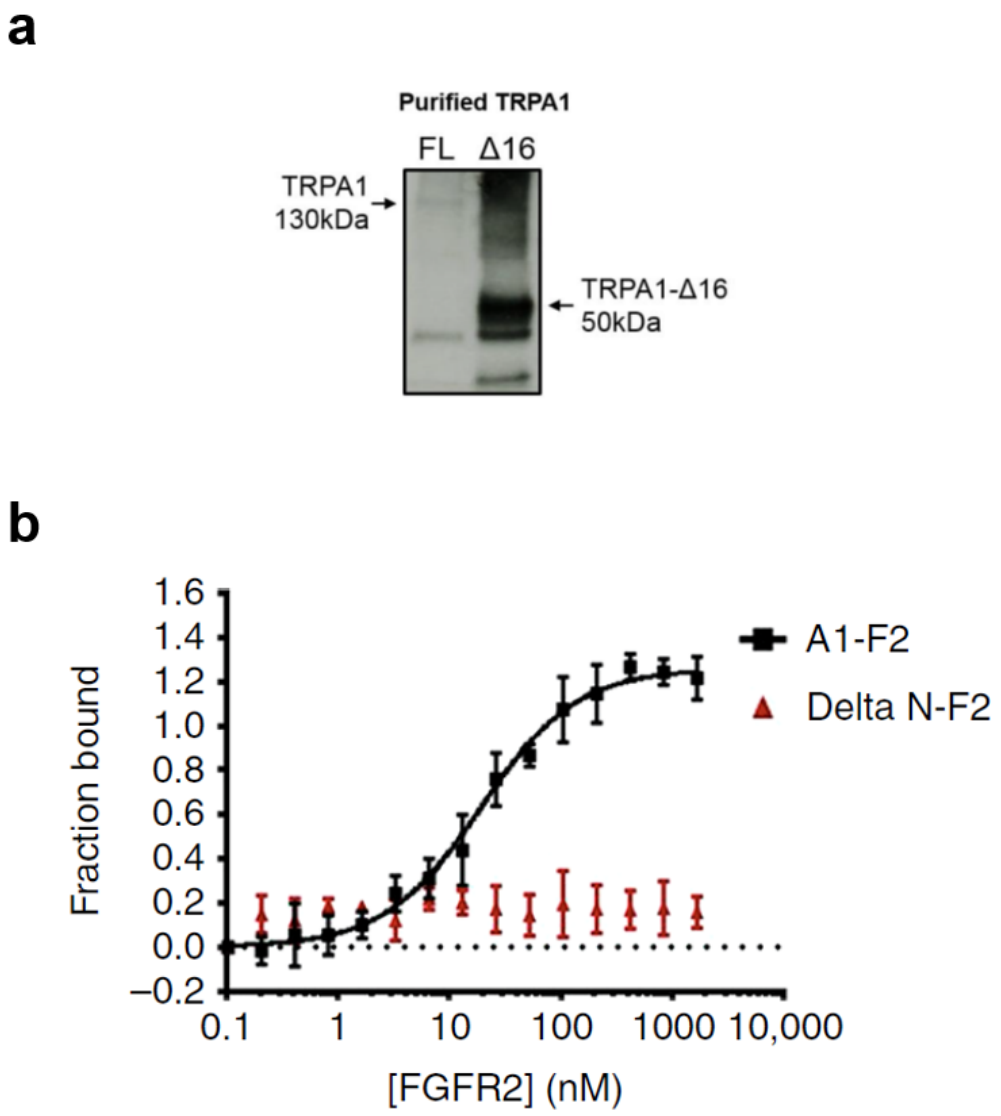

Figure 3. 7: Direct interaction of FGFR2 and TRPA1 through the ARD as suggested by MST analysis of purified proteins. a) Western blot of purified samples of TRPA1 full length (FL) and Δ16. Bands of interest are specified with arrows. TRPA1 full length = 130 kDa and TRPA1-Δ16 = 50 kDa. Purified TRPA1 and Δ16 were kindly provided by Prof. Peter Zygmunt, Sweden. b) Dose-response curve of TRPA1 bound to increasing concentrations of FGFR2. Error bars = standard error of the mean (n = 7). Delta N-F2 = Δ16. Dissociation constant K_D = 122.8 ± 22.4 nM.

To further examine the involvement of the TRPA1 ARD domain in the interaction with FGFR2 within cells, truncated versions of TRPA1 missing either the first 10 (Δ10) or the first 5 (Δ5) ankyrin repeats were co-expressed with FGFR2 in HEK-293T cells and protein interactions were studied by co-IP (Figure 3.8 and 3.9). Firstly, the transfection efficiency of the Δ10 and Δ5 constructs in HEK-293T cells was examined by western blot using an anti-TRPA1 antibody that recognises epitopes outside the ARD. As shown in Figure 3.8a, the Δ10 construct was successfully transfected and expressed in HEK-293T cells. The predicted molecular weight of 124 kDa matches the weight of the Δ10 band. Unfortunately, the transfection of the Δ5 construct was not successful after a number of attempts, therefore making the further analysis of the role of specific repeats between 1 and 10 not feasible (Figure 3.8a).

Interestingly, co-expression of Δ10 with FGFR2 was difficult. When transfected together, the expression levels of both proteins were significantly lower (Figure 3.9a, lane 3) compared to the full length TRPA1 and FGFR2 combination (Figure 3.8b). Δ10 protein levels are absent in double-transfected cells compared to lane 2 in which cells were transfected with Δ10 only. An example of an inconclusive co-IP experiment is shown in Figure 3.9b. The fact that Δ10 did not pull down FGFR2 (lane 3) like full length TRPA1 did (positive control - lane 2), could be due to the failed co-expression of FGFR2. Therefore, co-IP experiments could not be performed accurately (Figure 3.9b).

To solve this complication, GST pull-down assays were performed instead, which are explained in the next section.

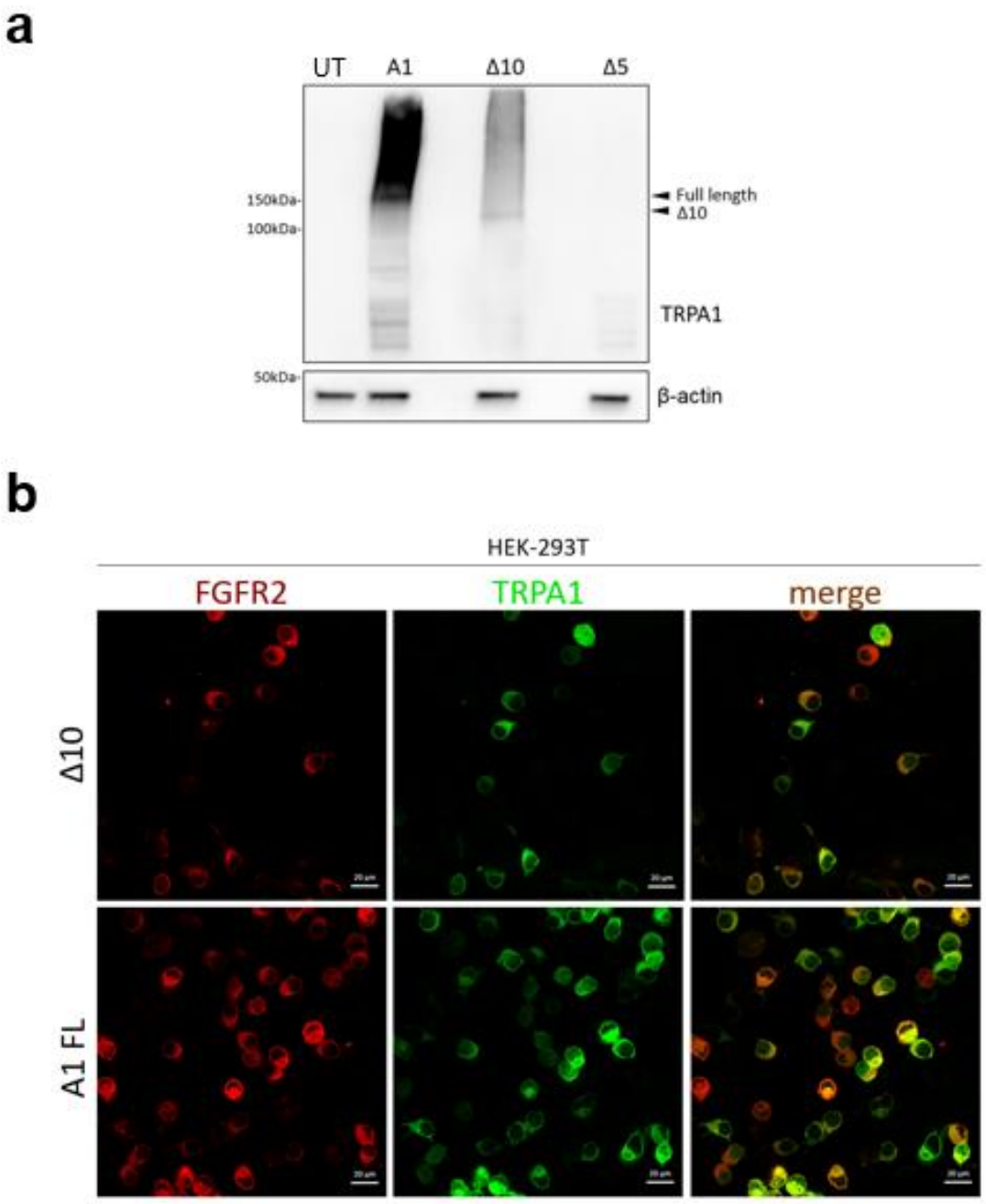

Figure 3. 8: Protein expression of full length, Δ10 and Δ5 TRPA1 by western blot and immunofluorescence. a) Western blot analysis of un-transfected (UT), TRPA1 full length, TRPA1 Δ10- and Δ5-transfected cells. Full length TRPA1 = 150 kDa. Δ10 = 124 kDa. Δ5 = 143 kDa. β-actin was used as a loading control. b) Immunofluorescence staining on FGFR2-FLAG + tGFP-TRPA1 full length or Δ10. FGFR2 = red. TRPA1 = green. (Anti-TRPA1 and anti-FGFR2 antibodies from Santa Cruz)

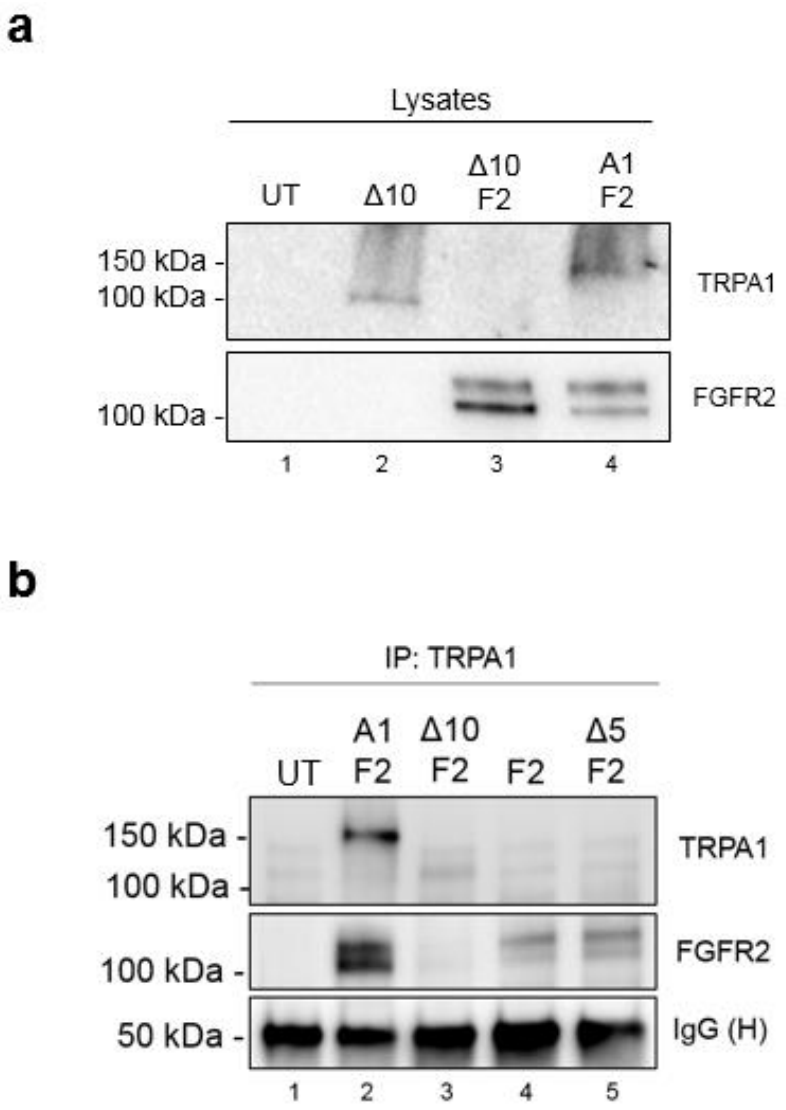

Figure 3. 9: Co-IP experiment to examine the binding capacity of Δ10 to FGFR2. a) Western blot analysis to verify the co-expression efficiency of FGFR2-FLAG and tGFP-TRPA1-Δ10 (Santa Cruz antibodies). b) Co-IP experiment with anti-TRPA1 antibody (Santa Cruz) on HEK-293T cells. FGFR2-FLAG + tGFP-TRPA1 cells were used as positive control. FGFR2-FLAG-transfected cells were used as negative control. tGFP-TRPA1-Δ5 was not expressed at all. IgG heavy chain was used as loading control. UT = un-transfected cells.

3.2.3. The FGFR2 C-terminal domain mediates direct interaction with the TRPA1 ARD

The C-terminal region of FGFR2 has been implicated in protein-protein interactions with downstream signalling proteins and therefore it was hypothesised that it could also be involved in the interaction with TRPA1. To examine the role of the FGFR2 C-terminal region in this interaction, a fragment containing the last 58 amino acids of FGFR2 (C-58) was tagged with GST (34 kDa total molecular weight), expressed in *E.coli* and purified by GST affinity purification (Figure 3.10a).

Cell lysates were prepared from un-transfected HEK-293T cells as well as cells transfected with the TRPA1 construct. These lysates were then utilised in pull-down assays using the GST-C-58 conjugated beads and the results were visualised by western blot (Figure 3.11a,b, lane 2). Furthermore, the un-transfected HEK-293T lysate was mixed with standard GST beads as a control for non-specific binding (Figure 3.11b, lane 1). As shown in Figure 3.11b, TRPA1 was pulled down by the C-58 fragment but not by the empty GST beads suggesting that the last 58 C-terminal residues of the receptor are involved in the interaction with TRPA1. The ability of C-58 to pull down endogenous PLCγ1 was used a positive control since the interaction between the two has been reported before (Timsah et al., 2014). As expected, PLCγ1 was pulled down both in wild type and TRPA1-expressing cells (lane 2, 3).

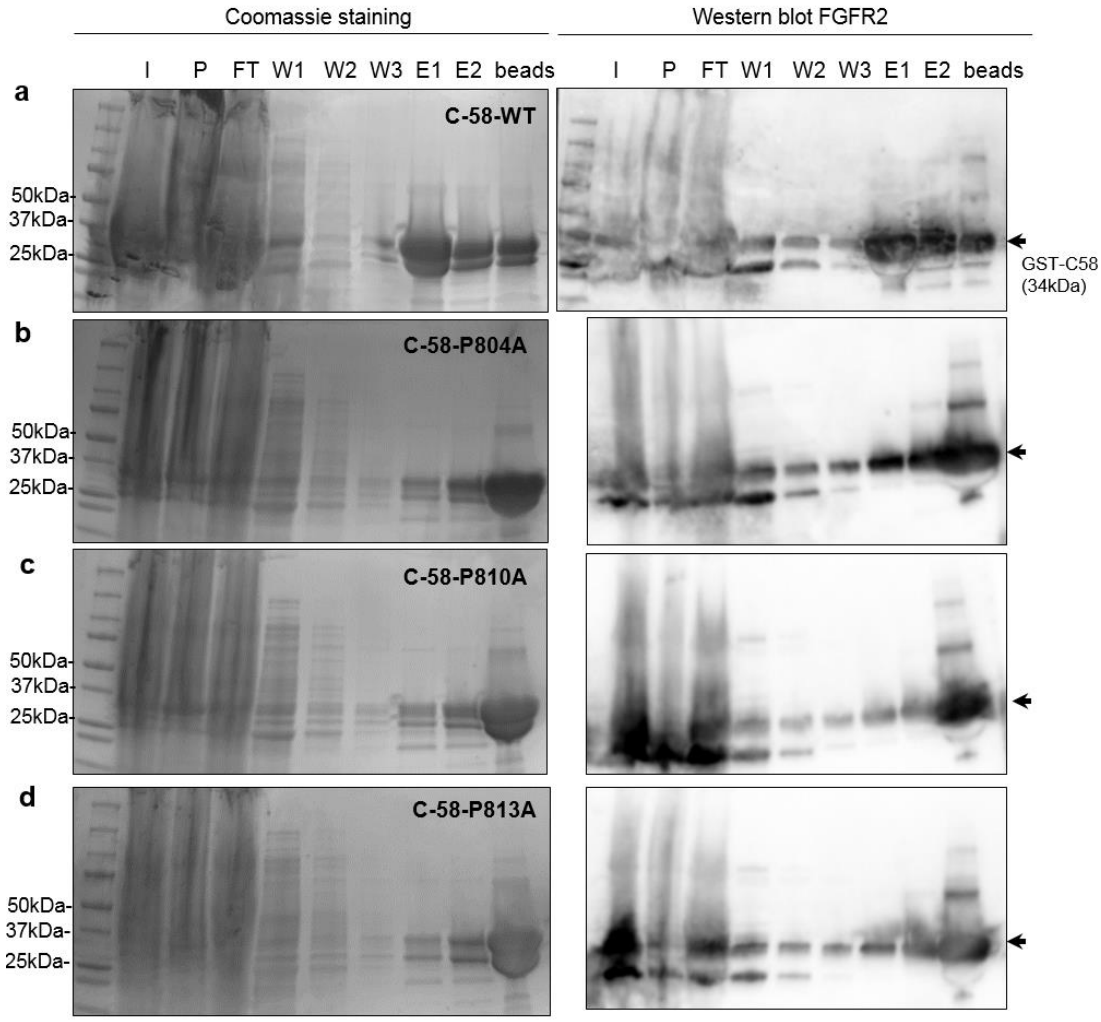

Figure 3. 10: C58 fragment purification. SDS-PAGE stained with Coomassie staining (left panels) and Western blots probed for total FGFR2 antibody (Protein Tech) (right panels). Samples from different stages of the purification process were loaded: Input (I), Pellet (P), Flow Through (FT), Wash 1,2 and 3 (W1,2,3), Elution 1 and 2 (E1 and 2) and beads. a) C58-WT. Proline (P) to Alanine (A) mutation on sites b) 804, c) 810 and d) 813. Purified corresponding bands are indicated with arrows. The molecular size of GST-C58 fragments is 34 kDa (26 kDa GST + 8 kDa C58).

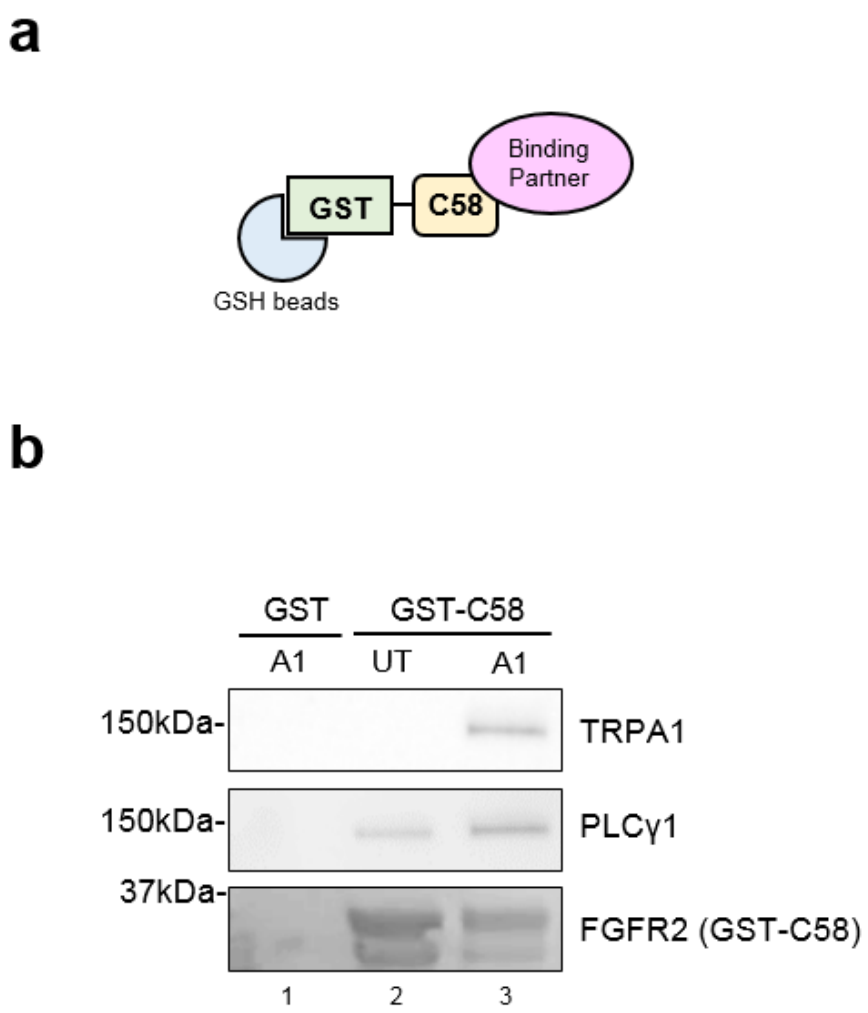

Figure 3. 11: TRPA1 binds to the C-terminal domain of FGFR2. a) Schematic representation of the GST pull-down assay. GST-tagged C-58 fragment is attached to the Glutathione beads and pulls down binding partners that are detected by western blot. b) GST pull down assay to assess the interaction of TRPA1 with the C-terminal 58 amino acids of FGFR2. Lysates from tGFP-TRPA1-transfected cells were mixed with the GST-C58 beads as well as uncoupled GST-beads (negative control). Un-transfected (UT) cell lysate mixed with GST-C58 beads was used as a negative control. C-58 FGFR2 levels were used as a loading control (ponceau staining). PLCγ1 binds to the C-terminal domain of FGFR2 and therefore it was used as a positive control. A representative blot is shown here (n=4). GST = Glutathione S-transferase.

Following some difficulties in co-express TRPA1-Δ10 and FGFR2 constructs, GST pull down assays were performed instead to examine the role of the ankyrin repeats in the interaction (Figure 3.12). Lysates from HEK-293T cells expressing full length TRPA1 or Δ10 were subject to pull down assay with GST-C-58 beads and the ability of C-58 to pull down Δ10 was compared to the full length protein. Indeed, Δ10 was pulled down approximately 80% less than the full length TRPA1 (0.23 ± 0.06 a.u., p = 0.0002, Student t-test) which indicates that the first ten ankyrin repeats of TRPA1 are crucial for the binding to the FGFR2 C-terminal fragment (Figure 3.12).

To further determine the specific binding site on FGFR2, site-directed mutants of the C-58 fragment were constructed. The proline-rich motif at the C-terminal of FGFR2 is involved in protein-protein interactions with SH3-domain-containing downstream proteins (Ahmed *et al*., 2010, Timsah *et al*., 2014). Even though TRPA1 does not contain SH3 domains, the ability to bind to the proline-rich motif was still investigated. Three purified C-58 mutants (Proline to Alanine) were used in GST pull down assays: P804A, P810A and P813A (Figure 3.10b, c, d). Endogenous PLCγ1 pull down was used as a positive control since it interacts with that proline-rich motif through the SH3 domain. Indeed, PLCγ1 pull down was reduced when P810 and P813 were mutated (n = 1). However, there was no decrease in the ability to pull down TRPA1 between the wild type and mutant fragments in this set of experiments (n = 2) (Figure 3.13).

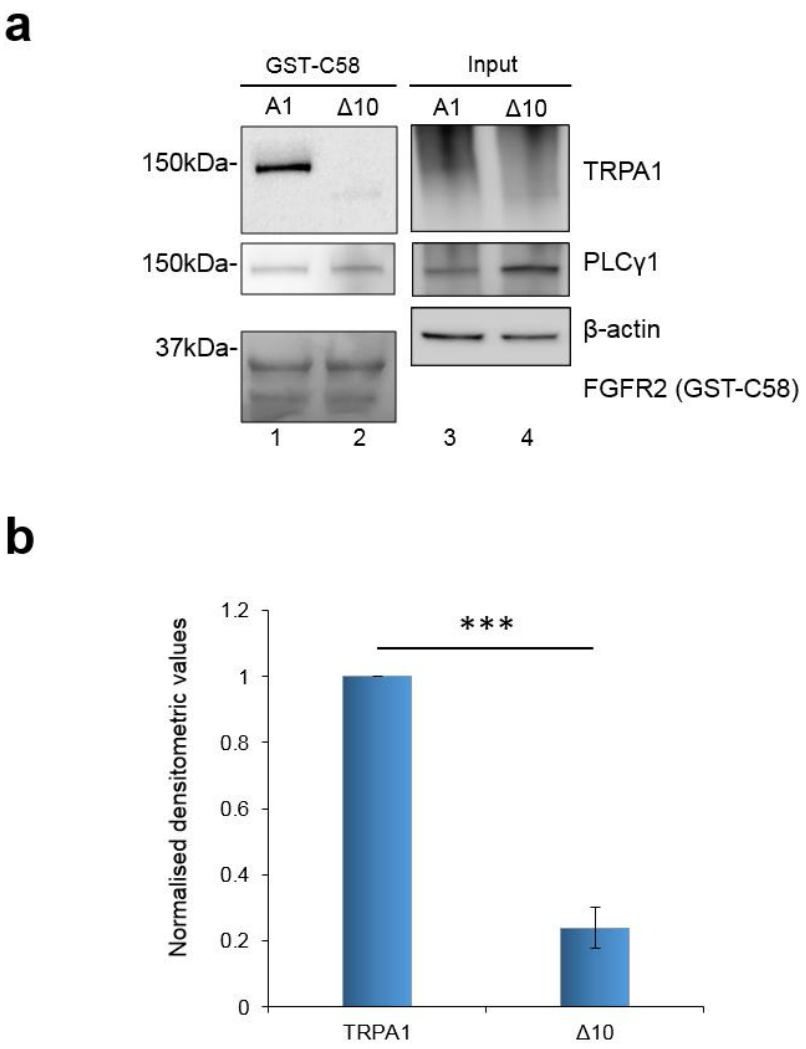

Figure 3. 12: Mapping out the FGFR2 binding site on TRPA1 by GST pull down. a) TRPA1 full length and Δ10-expressing cell lysates were subject to GST pull down assay with GST-C58 beads. GST pull down (left panel) and Western blot to determine protein expression (right panel). C-58 levels were used as a loading control (Ponceau staining). PLCγ1 binds to the C-terminal domain of FGFR2 and therefore it was used as a positive control. b) Quantification of the GST pull down by densitometry on ImageJ. Bar graph showing the normalised densitometry values of TRPA1 and Δ10 conditions against TRPA1. Densitometry values were initially normalised against C58 (loading control). A significant difference is indicated by *** ($p \leq 0.001$, Student t-test). Error bars represent the standard error of the mean (n = 3). GST = Glutathione S-transferase.

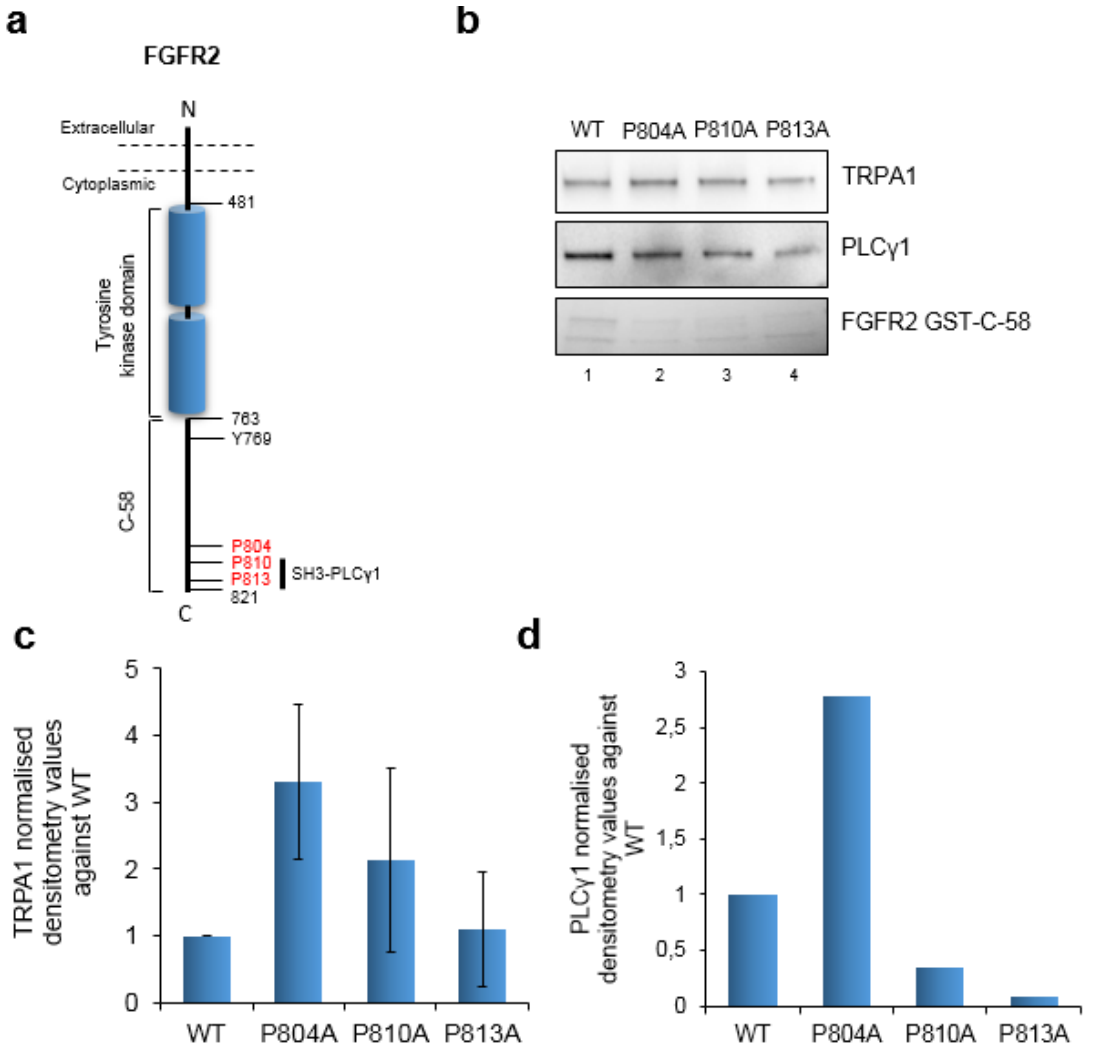

Figure 3. 13: Mapping out the binding site on FGFR2 C-terminal domain. a) schematic representation of FGFR2 cytoplasmic domain. C-58 consists of residues 763 to 821. Mutated Prolines are indicated in red. PLCγ1 binds to prolines P810 and P813 through the SH3 domain. Phosphorylated Tyrosine 769 (pY769) is the binding site for PLCγ1 SH2 domain. b) GST pull down assays with tGFP-TRPA1-expressing cell lysates and wild type and three individual Proline mutations of C-58. PLCγ1 was used as a positive control and GST-C58 was used as a loading control (ponceau staining). c) and d) Quantification of the GST pull down by densitometry on ImageJ. Bar graphs showing the normalised densitometry values of TRPA1 (n = 2) and PLCγ1 (n = 1) in four conditions against the wild type C58. Densitometry values were initially normalised against C58 (loading control). Error bars in c represent the standard error of the mean (n = 2). GST = Glutathione S-transferase.

3.2.4. Endogenous FGFR2-TRPA1 complex formation in HCC-515 LUAD cells

Hitherto, I have established that FGFR2 and TRPA1 can interact when overexpressed. However, in order for this interaction to play a physiological role, it is crucial to show that the interaction of endogenous FGFR2 and TRPA1 proteins occurs in a physiologically relevant system like cancer cells. The FGFR2 role in Lung Adenocarcinoma progression through protein-protein interactions has already been described before (Timsah *et al*., 2015) and thus, LUAD cell lines were selected as a tool to assess the interaction in cancer.

Firstly, the protein expression pattern of FGFR2 and TRPA1 in human LUAD tissues was determined by immunohistochemistry, performed by Michael Shires (St. James's Hospital, Leeds). A commercially available tissue microarray (TMA, Pantomics, Richmond, USA) with 102 normal and LUAD tissue sections was utilised and stained with anti-FGFR2 and anti-TRPA1 antibodies. The expression levels were semi-quantified by a specialised pathologist, Mihai Gagea (MD Anderson, USA), using a scoring system from zero 0 to 3+ (arbitrary units), with 0 representing absence of protein expression and 3+ representing maximum protein expression. As shown in Figure 3.14, both FGFR2 and TRPA1 are overexpressed in LUAD compared to the healthy tissue, with approximately 70% of all LUAD tissues being scored as 3+ for both proteins.

Next, the protein levels of FGFR2 and TRPA1 were studied by western blot in two human LUAD cell lines (HCC-44 and HCC-515) and one normal lung fibroblast cell line (CCL-204). HCC-515 cells express both proteins of interest (Figure 3.15, lane 3) and therefore, it was chosen for further interaction experiments. HCC-44 cells express only FGFR2 (Figure 3.15, lane 2) and CCL-204 normal lung fibroblasts express neither FGFR2 or TRPA1 (Figure 3.15, lane 1). Protein expression was also verified by immunofluorescence (Figure 3.16) to ensure PLA experiments could be performed.

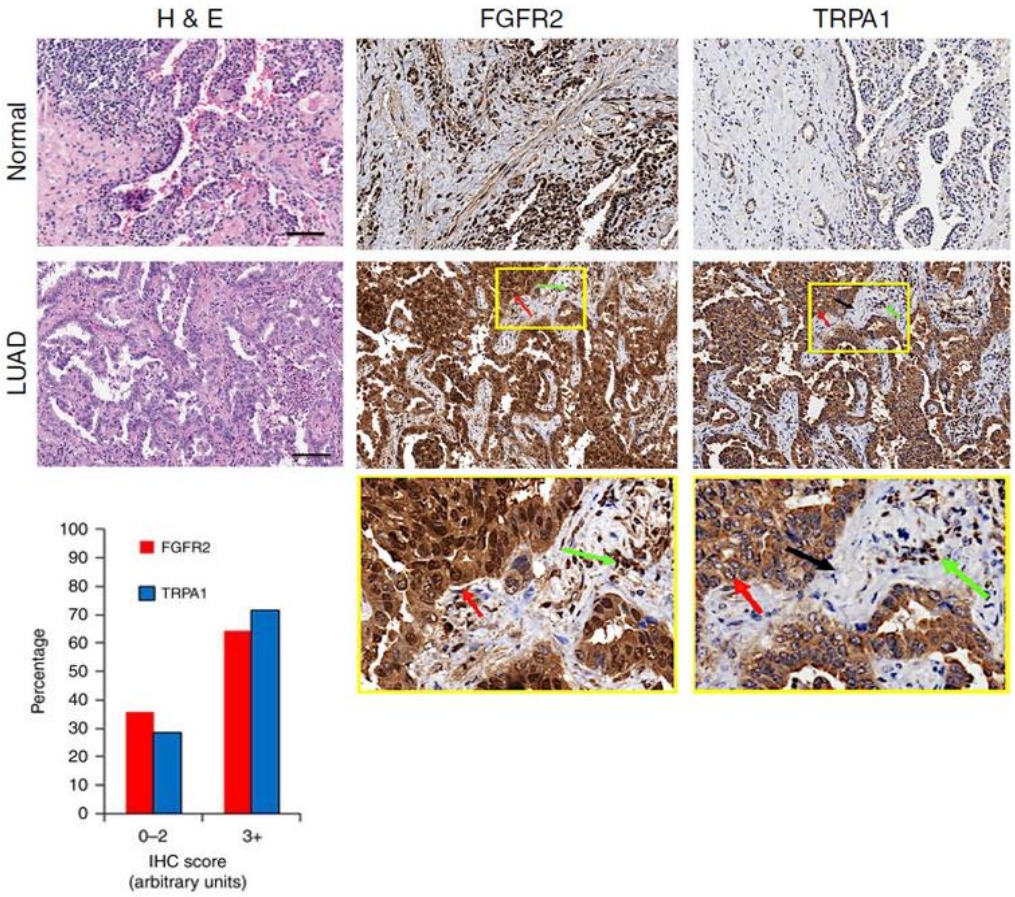

Figure 3. 14: Protein expression of FGFR2 and TRPA1 in human healthy and LUAD tissue microarray analysed by Immunohistochemistry. Hematoxylene and Eosin (H&E) staining on normal and LUAD tissue (left panels). Representative images of IHC staining with anti-FGFR2 and anti-TRPA1 antibodies show increased protein expression in LUAD tissues for both proteins. (scale bar=10µm). Protein levels are shown as brown staining. Yellow boxes show details on different cell types: red arrows indicate neoplastic cells which are strongly positive for both proteins, green arrows indicate infiltrated inflammatory cells which are also positive for both proteins and the black arrow indicates the supporting stroma that is negative for both proteins. The bar graph illustrates the semi-quantified results of IHC. Around 70% of LUAD tissues express high levels of FGFR2 and TRPA1 as scored by a specialised pathologist, Mihai Gagea (MD Adnerson Cancer Centre, Houston, USA). IHC was performed by Michael Shires (St. James's Univeristy Hospital, Leeds, UK). Figure taken from our publication (Berrout et al., 2017).

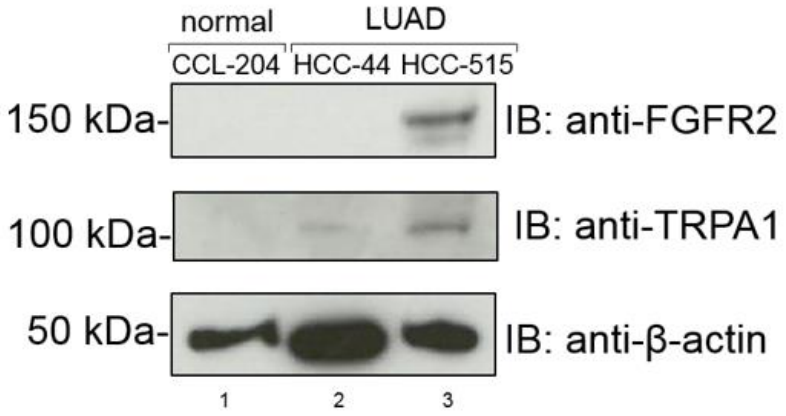

Figure 3. 15: Protein expression levels of TRPA1 and FGFR2 in normal and LUAD cell lines. Western blot analysis of the endogenous expression of FGFR2 (Santa Cruz) and TRPA1 (Millipore) in normal CCL-204 and LUAD HCC-515 and HCC-44 cells. Band density was quantified by ImageJ and the values were normalised against β-actin (loading control). Representative western blot is showing (n=3).

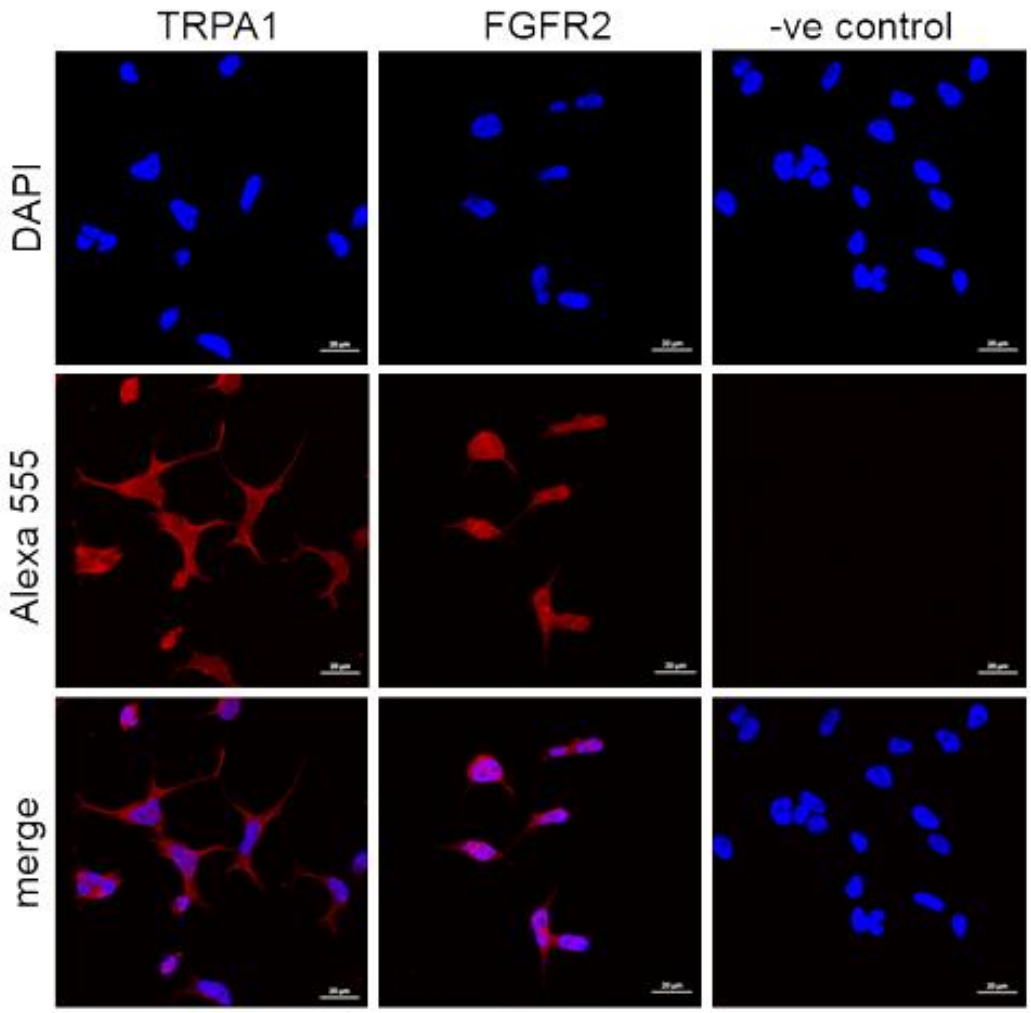

Figure 3. 16: Immunofluorescence staining for FGFR2 and TRPA1 in HCC-515 cells. Specific antibodies for each protein were used in independent staining experiments. Alexa_Fluor555-conjugated secondary antibodies were used to visualise the staining. Primary antibodies were excluded from the negative controls. Anti-TRPA1 from Protein Tech, anti-FGFR2 from Santa Cruz.

The presence of FGFR2 and TRPA1 proteins on the plasma membrane of HCC-515 cells was verified by cellular fractionation. Both FGFR2 and TRPA1 were detected in the membrane fraction (Figure 3.17a). The FGFR2–TRPA1 interaction was confirmed in HCC-515 cells by Co-IP experiments in which FGFR2, protein “bait”, successfully pulled down TRPA1 (protein “prey”) (Figure 3.17b, lane 2).

PLA experiments in HCC-515 cells further supported complex formation. In these experiments, FGFR2 was knocked down with siRNA and the efficiency of knock down was verified by western blot at 35% (Figure 3.18b). PLA levels of FGFR2 knock-down cells was significantly lower compared to scrambled siRNA / control cells (p-value = 0.000001) suggesting that endogenous FGFR2 and TRPA1 proteins are in close proximity in HCC-515 cells and could be physically associated (Figure 3.18c). Due to the lack of time, this PLA experiment was only performed once.

To further investigate the activity of TRPA1 in the LUAD cell lines used in this chapter, calcium imaging experiments were performed using AITC as a TRPA1 agonist. As shown in Figure 3.19a, b and c, HCC-515 cells had a borderline response to AITC while HCC-44 cells had a much higher response. When HCC-44 cells were pre-treated with HC-030031, a specific TRPA1 inhibitor, there was a nearly 7-fold reduction in the calcium response indicating the signal detected in these cells was specific to TRPA1 (Figure 3.19d and e).

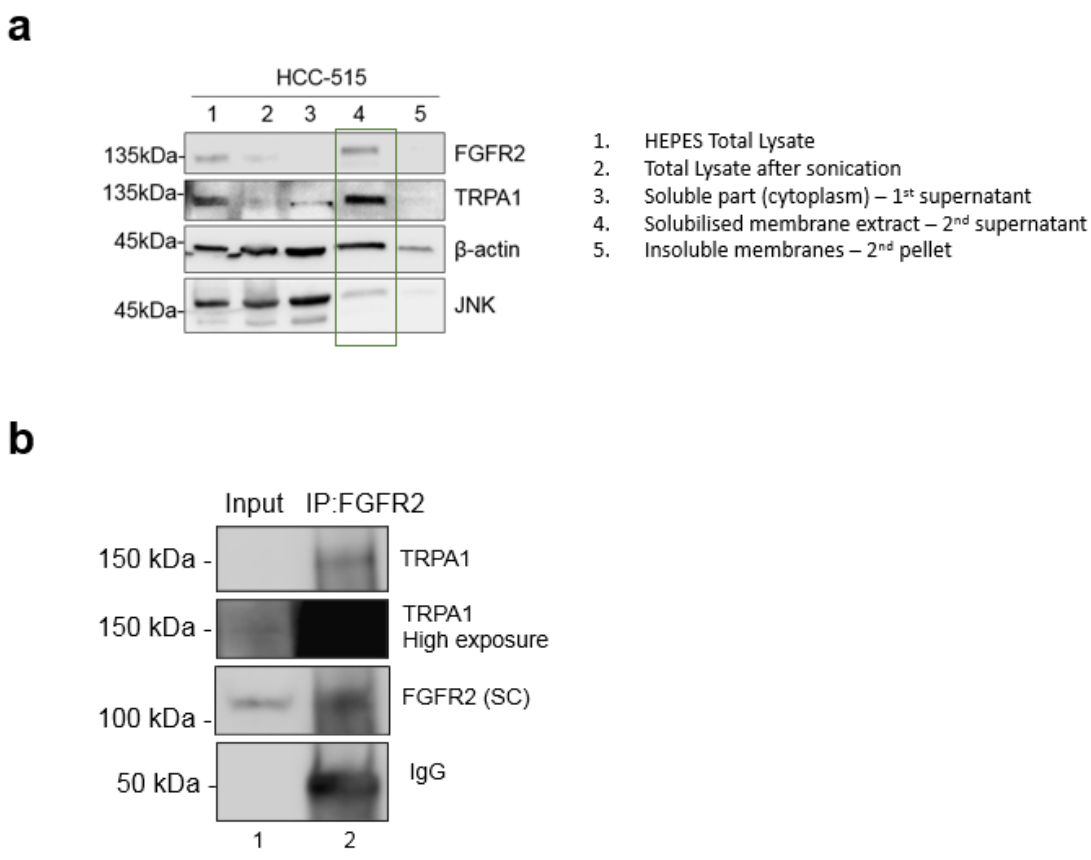

Figure 3. 17: Co-IP experiment suggesting FGFR2 and TRPA1 complex formation in HCC-515 cells. a) Western blot analysis of the FGFR2 (Protein Tech) and TRPA1 (Protein Tech) protein levels in a membrane fraction and total cell lysate. Proteins of interest are present in the membrane fraction, as expected. JNK and β-actin were used as a control for the cytosolic fraction. b) co-IP experiment to determine complex formation between FGFR2 and TRPA1 in HCC-515 cells. An anti-FGFR2 (Santa Cruz) antibody was used to precipitate FGFR2 and the presence of TRPA1 (Protein Tech) was detected by western blot. Total cell lysate was loaded on the left as a verification of correct band sizing. TRPA1 band in the cell lysate was visible only in higher exposure times that overexposed/saturated the band in the IP lane. (SC = Santa Cruz)

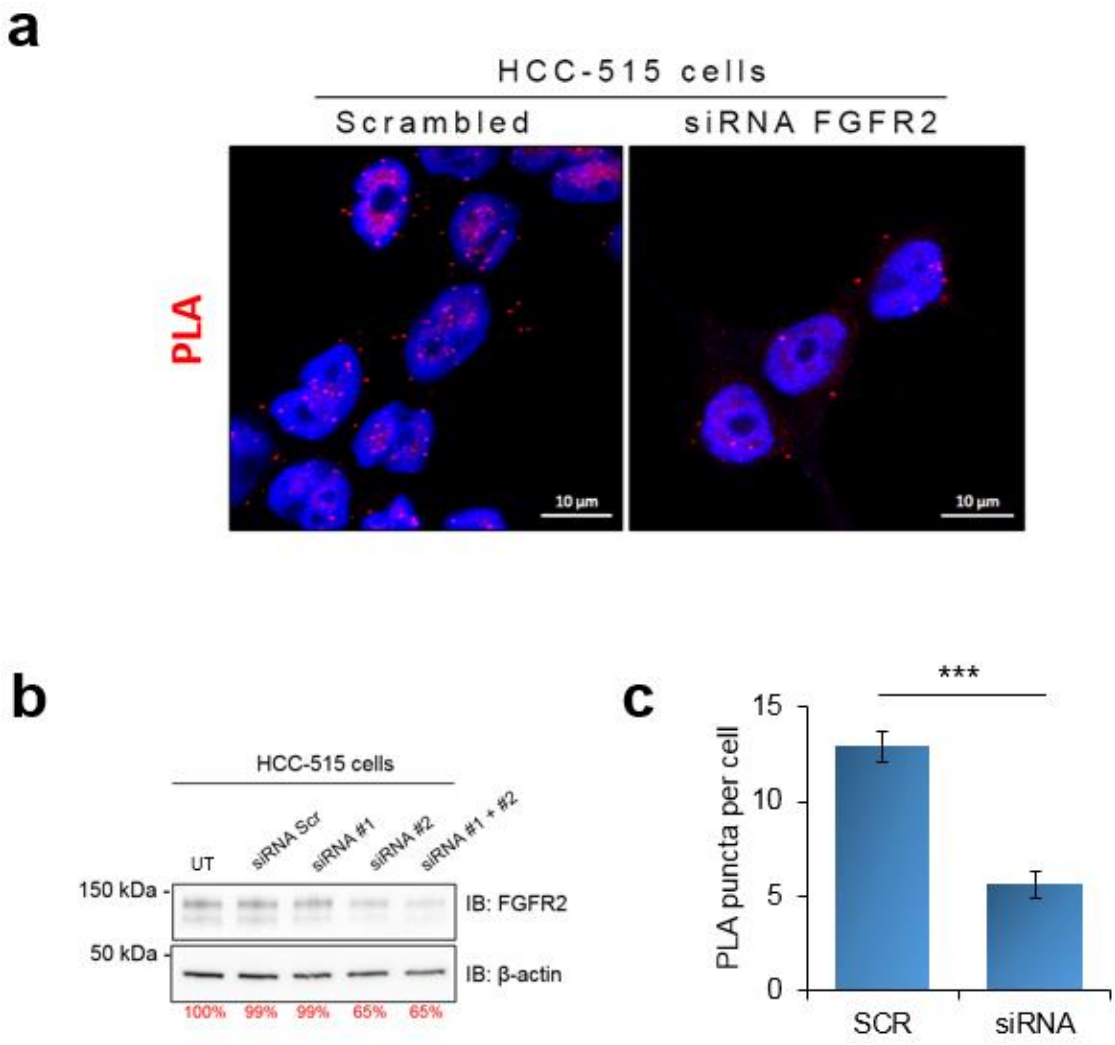

Figure 3. 18: PLA experiment on scrambled and FGFR2 siRNA-tranfected HCC-515 cells. a) Representative PLA images in scrambled and siRNA HCC-515 cells. b) Western blot verifying the efficiency of FGFR2 knock-down in HCC-515 cells used for PLA experiments. Protein levels were quantified by densitometry on Image J. β-actin was used as a loading control. siRNA#2 decreased FGFR2 protein levels by 35%. UT = un-transfected. c) Bar graph illustrating the PLA puncta per cell in scrambled (SCR) and FGFR2 knock down cells. Error bars = S.E.M. SCR n = 12 cells, siRNA n = 10 cells. N = 1. Significant differences are shown as *** (p-value ≤ 0.001 with unpaired students t-test).

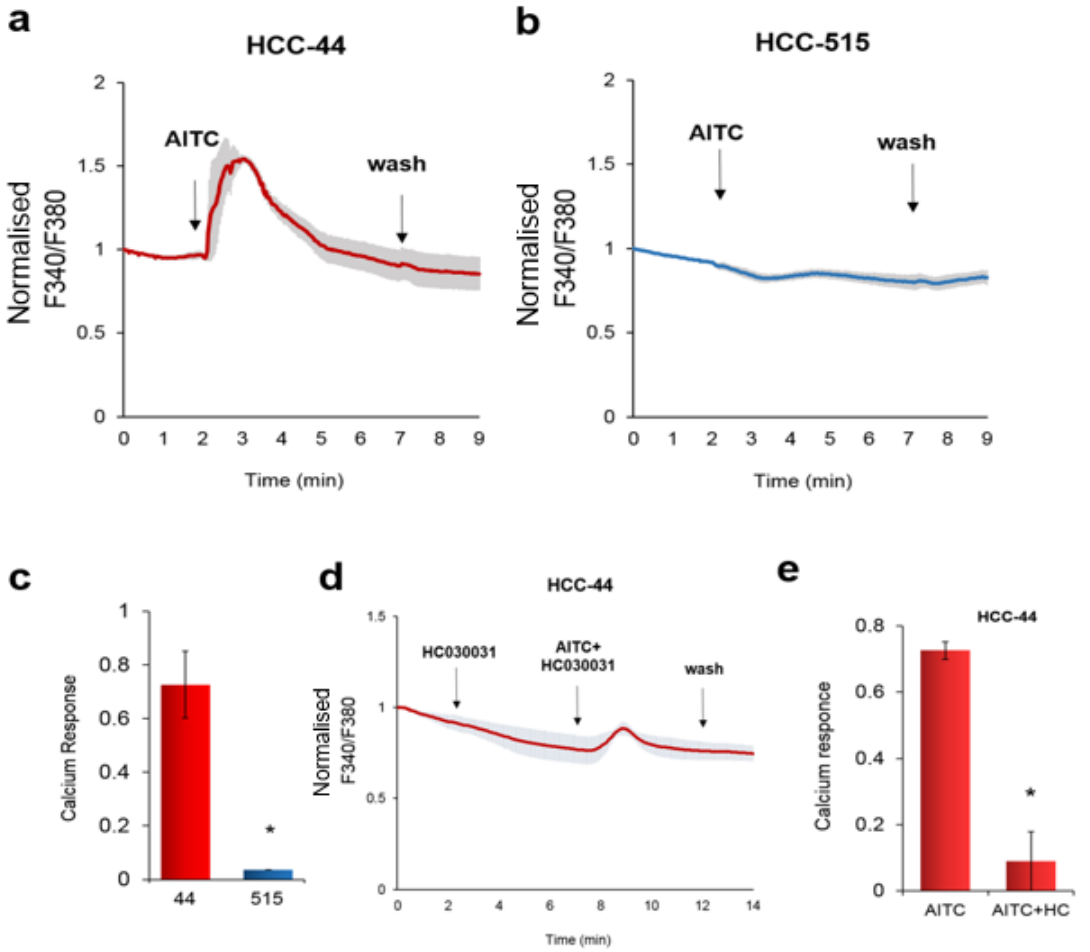

Figure 3. 19: Calcium imaging experiments on LUAD cell lines. a) and b) Normalised to baseline average calcium response after a 5-minute AITC perfusion shown as a ratio of Fura-2 fluorescence intensity at 340/380 nm. Error bars = S.E.M (n = 4). (Absolute baseline fluorescence ratio: HCC-44 = 709 ± 50.6, HCC-515 = 699.6 ± 7). c) Quantification of maximum calcium response from a and b. HCC-44 cells had a significantly higher response ($p \leq 0.05$ by Student's T-test) compared to HCC-515 cells. Error bars = S.E.M. d) Normalised average calcium response after a 5-minute HC030031 followed by an AITC + HC030031 perfusion shown as a ratio of Fura-2 fluorescence intensity at 340/380 nm. Error bars = S.E.M (n = 3). e) Bar graph representing the calcium response of HCC-44 cells after AITC perfusion in the absence and presence of HC030031. Calcium response is calculated as the difference between the maximum F340/F380 within the 5 minutes of AITC perfusion and the F340/F380 prior to perfusion initiation (baseline). Error bars = S.E.M and $p = 0.0119$ (*) by student's t-test, n = 3.

3.2.5. FGFR2-TRPA1 complex characterisation by Expansion Microscopy (ExM)

To further characterise the FGFR2-TRPA1 interaction in the nanometre scale, Expansion Microscopy (ExM) was performed on HEK-293T cells that were transfected with FGFR2 and TRPA1 constructs. ExM allows for super-resolution image acquisition and therefore, detailed analysis of molecules of interest. Firstly, FGFR2-FLAG + tGFP-TRPA1-expressing cells underwent a 4-times and a 10-times expansion (Figure 3.20). The expansion factor was calculated by manual measurement of the gel size right before image acquisition (final size divided by initial size). For the 4x expansion, the expansion factor was exactly 4, while for the 10x expansion, the expansion factor was calculated to be approximatelly 8.5. Considering the maximal Airyscan lateral resolution is 140 nm (480 nm laser), a 4x and an 8.5x expanded sample will give a theoretical resolution of 35 nm and 16.4 nm, respectively which enables the visualisation of individual protein complexes (Fouquet *et al*., 2015, Sheard *et al*., 2019, Truckenbrodt *et al.*, 2018). Figure 3.20 illustrates the increase in the resolution as the expansion factor increases from 1x to 10x. It looks like both FGFR2 and TRPA1 are located in membrane structures such as the plasma membrane and the Endoplasmic Reticulum however, this is not certain since no membrane markers were used in this experiment.

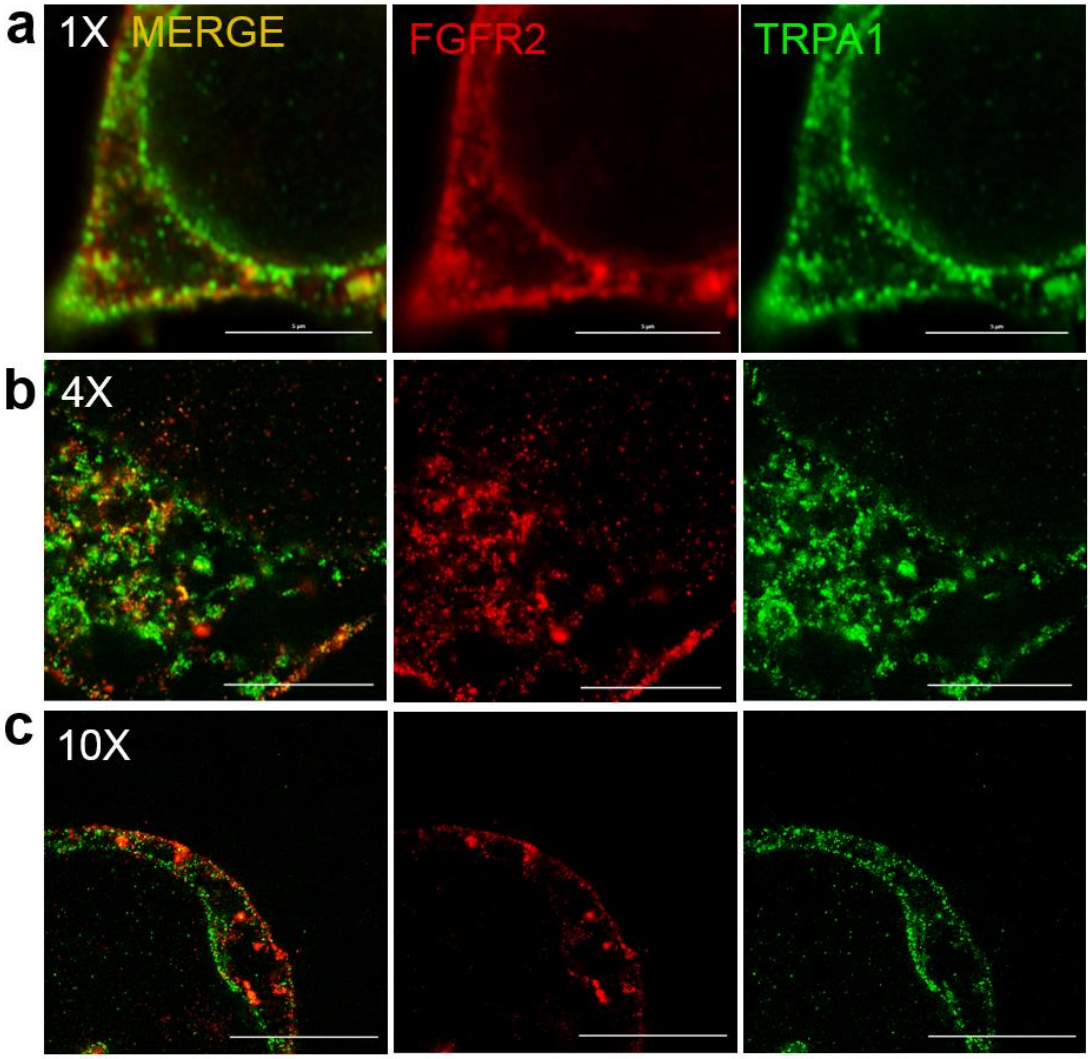

Figure 3. 20: Improvement in optical resolution as obtained by increasing the expansion factor. a) Regular Airyscan confocal image (estimated resolution 140 nm) b) ExM 4x (estimated resolution 35 nm), c) ExM 10x (estimated resolution 16.5 nm). All scale bars indicate 5 μm.

Next, images of 4x expanded cells were obtained from two different focal planes and analysed for FGFR2 and TRPA1 co-localisation by ImageJ. Since the area of interest for the FGFR2 and TRPA1 interaction is the plasma membrane, the two focal planes were focused on membrane areas. Focal level 1 includes images of a flat membrane surface and away from the nucleus (edge of the cell) and focal level 2 includes images above the membrane surface (cell interior) (Figure 3.21). Due to lack of membrane markers, the bottom membrane surface was considered to be the first plane in which signal was detected. Co-localisation was quantified by performing a Mander's co-localisation analysis which calculates the Mander's values M1 and M2 that represent the percentage of co-localisation for each protein (Zinchuk *et al*., 2007). Analysis of images similar to these shown Figure 3.20 revealed that, 31.2% ± 5.7% of FGFR2 molecules co-localise with TRPA1 and 49.3% ± 3.1% of TRPA1 co-localise with FGFR2 on a vertical membrane area – cell periphery (above bottom surface – Figure 3.22a). On the other hand, FGFR2 M1 equals 18.8% ± 3.9% and TRPA1 M2 equals 33.1% ± 6.5% on a flat membrane surface (Figure 3.22b). The percentages of co-localisation do not significantly differ between the two focal planes, suggesting consistency in data acquisition. However, the focal plane 1 was chosen as a more suitable way of analysing co-localisation due to the higher amount of molecules that can be detected in one surface area. Moreover, the theoretical resolution in this 4x ExM experiment is around 35nm, meaning that objects located in a shorter distance could not be separated. The fact that FGFR2 co-localises with TRPA1 indicates that they are in close proximity (less than 35 nm apart).

Next, a 10x ExM images were analysed. The 10x Mander's co-localisation values were compared to the 4x ones. In 10x, FGFR2 M1 was reduced to 11.2% ± 1.1% (~60% reduction) and TRPA1 M2 was reduced to 23.7% ± 3.6% (~30% reduction) (Figure 3.23). When imaging close to single molecule level, Pauli's exclusion law, stating that two molecules cannot be at the same spot at the same time, should be

taken into consideration (Aaron *et al*., 2018). Therefore, this result would be expected as the resolution has been increased to 16.4 nm, visibly separating all molecules further (even those that interact), resulting in lower co-localisation signal.

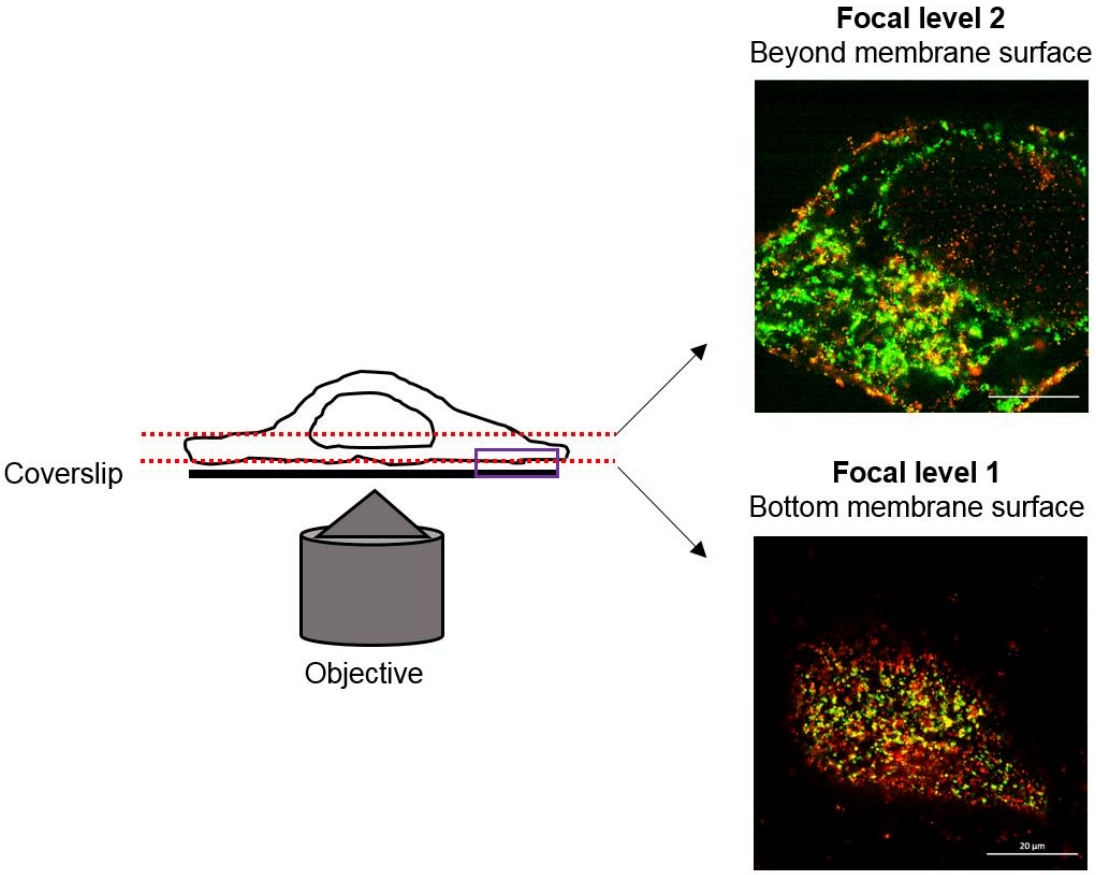

Figure 3. 21: Schematic illustrating the two membrane focal planes analysed in ExM 4x. Focal level 1 is located right at the bottom cell surface that is attached to the coverslip creating a relatively flat membrane. Focal level 2 is located above the bottom membrane surface and includes cellular compartments such as ER, organelles and nucleus. In this plane, the plasma membrane signals originate form a line of membrane that surrounds the cell.

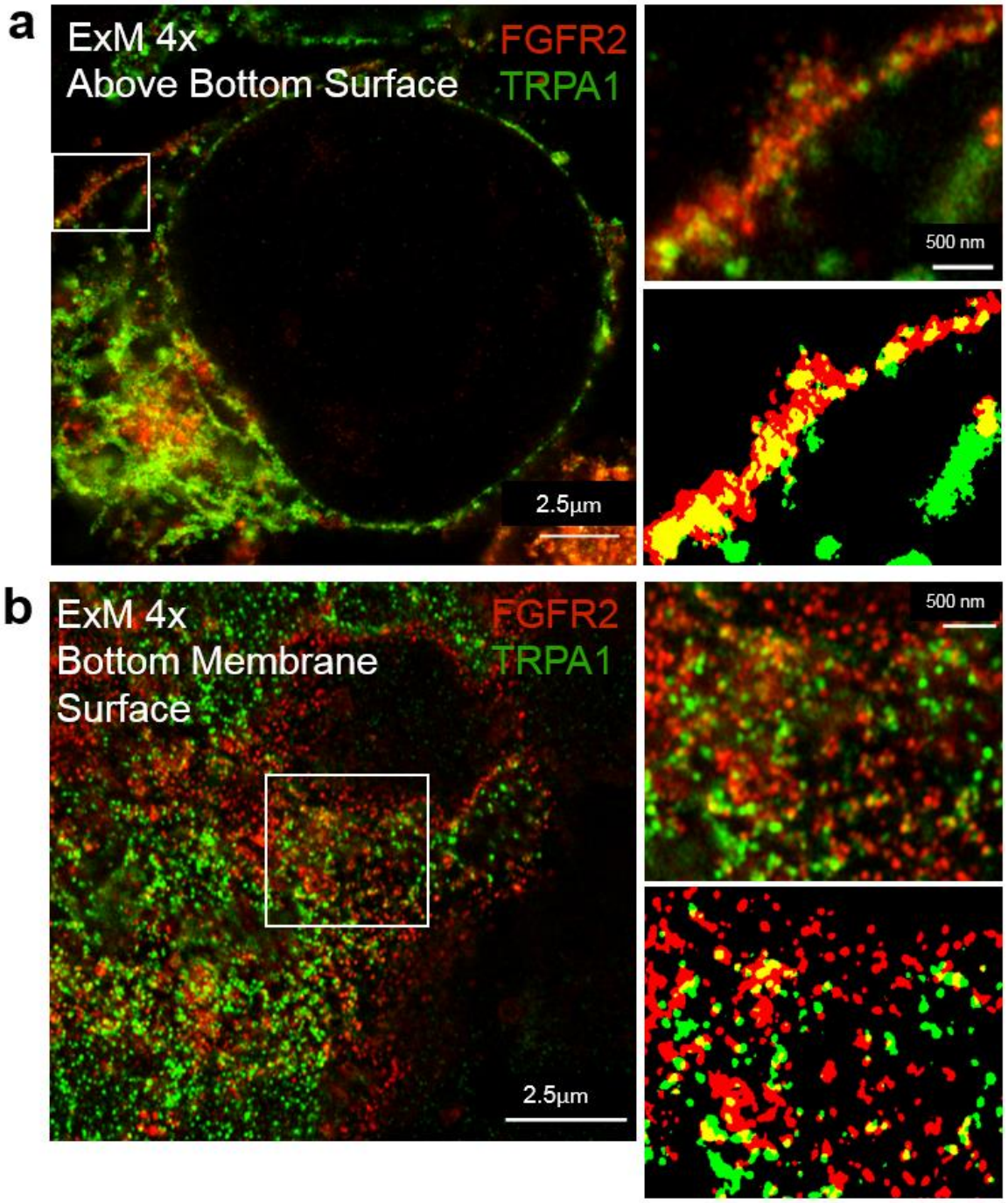
a
ExM 4x
Above Bottom Surface
FGFR2
TRPA1
2.5µm
500 nm
b
ExM 4x
Bottom Membrane
Surface
FGFR2
TRPA1
2.5µm
500 nm

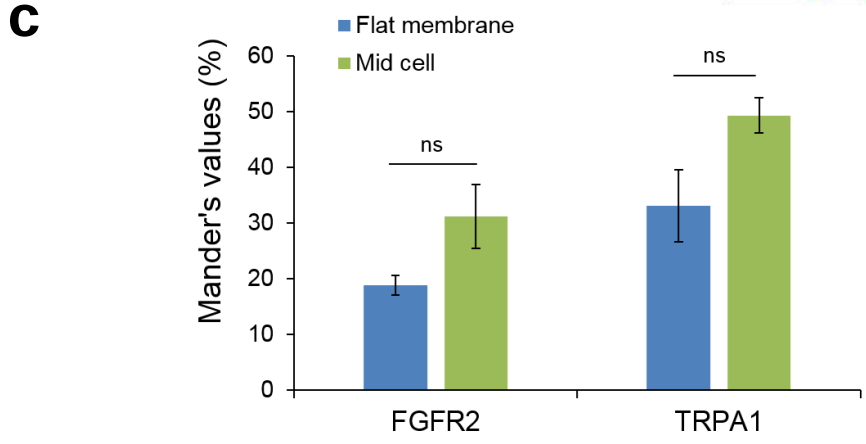
c
Flat membrane
Mid cell
Mander's values (%)
60
50
40
30
20
10
0
ns
ns
FGFR2
TRPA1

Figure 3. 22: Mander's values from FGFR2 and TRPA1 co-localisation analysis do not differ in two different focal planes. Representative image of a 4x expanded cell in focal plane 2 (a) and focal plane 1 (b) (left). White boxes indicate representative analysed areas. Zoomed in area that was used in the analysis (right top) and image after threshold (right bottom). FGFR2 = red, TRPA1 = green. c) Quantification of Mander's M1 and M2. No significant difference was observed between the groups (p-value = 0.242 and 0.597 for FGFR2 and TRPA1, respectively).

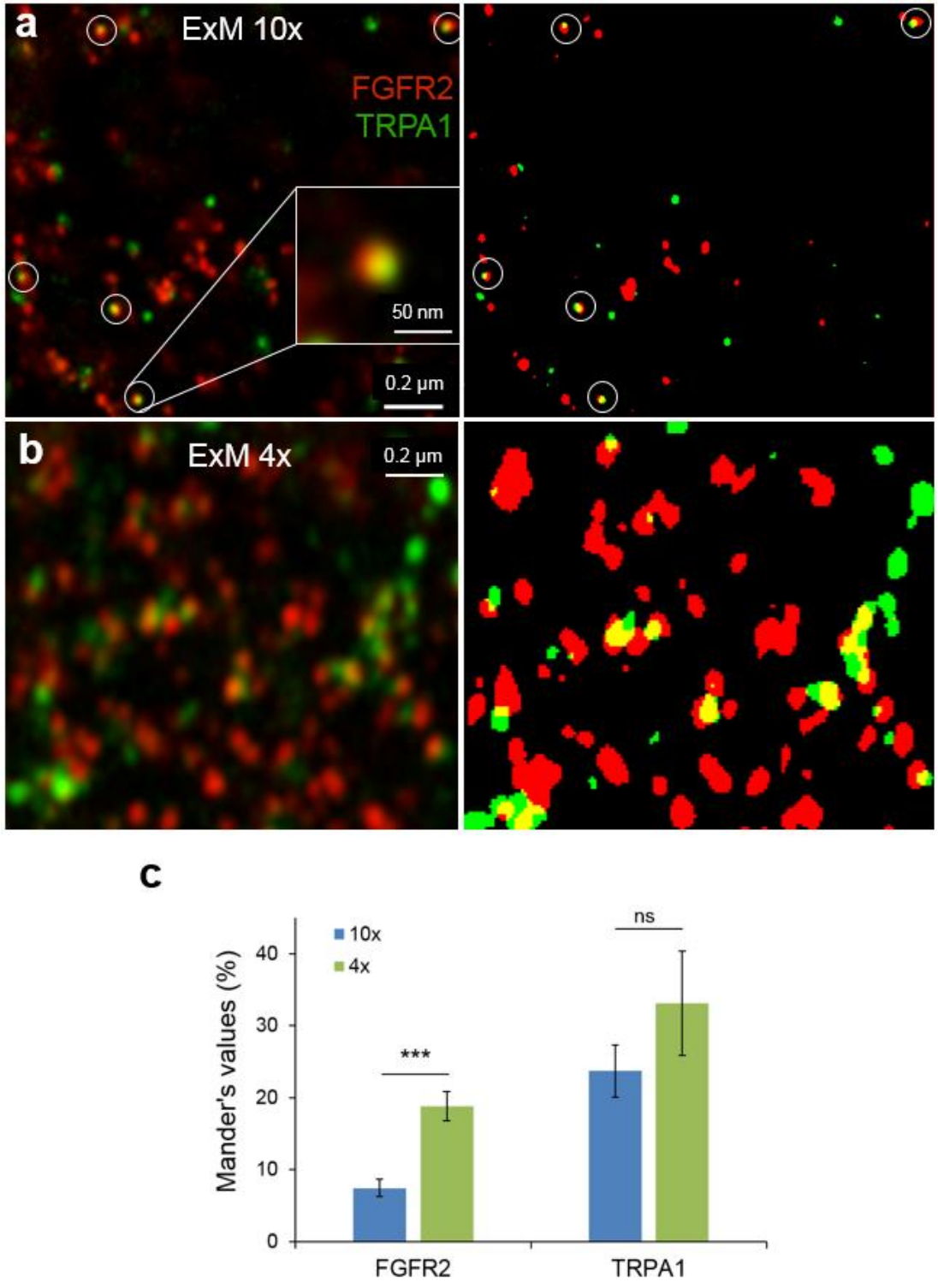

Figure 3. 23: Reduced Mander's co-localisation values in 10x compared to 4x ExM. Representative image of a (a) 10x ExM and (b) 4x ExM for FGFR2 (red) and TRPA1 (green) at 16.4nm and 35nm resolution, respectively (left). Same image following threshold implementation (right). White circles indicate co-localisation events at 10x. White box indicates enlargement of one co-localisation event.

Detailed observation of complexes detected in 10x ExM would be beneficial to understand the complex formation between FGFR2 and TRPA1 as well as for future attempts to determine the stoichiometry of the complex. For this reason, it was crucial to set some nanoscale measurements and determine protein and theoretical complex sizes.

The TRPA1 channel (4 subunits) is 10.4 nm wide (parallel to membrane) and 12.3 nm long (vertical size) as revealed by the cryo-EM structure (Paulsen *et al*., 2015). The orientation of the ARD remains unresolved yet, the estimated size (AR1-11) is around 10nm each, increasing the radius of TRPA1 at 10 nm. Thus, the total TRPA1 channel diameter could be estimated at 20 nm minimum (Figure 3.24a) which is higher than the estimated resolution of 16.4 nm indicating that individual TRPA1 channels can be resolved. Moreover, a monoclonal antibody recognising the C-terminal region of TRPA1 was used in this experiment. Based on the location of the C-terminal domains, it could be speculated that only one antibody would have access to this area due to limited space.

The size of the FGFR2 dimer in complex with FGF9 ligand is around 5nm meaning that a single FGFR2 molecule has a width of 2.5 nm (Goetz and Mohammadi, 2013). These measurements represent the width of the complex in the extracellular space however, it would be expected that the FGFR2 dimer would have a similar size in the intracellular C-terminal region (Figure 3.24b and c). A polyclonal antibody against the C-terminal region of FGFR2 was used in this experiment, which, in combination with the secondary antibody, adds 20-30 nm to the size of the receptor complex visualised via the immunofluorescence

Furthermore, the error generated by the detection method, i.e. primary and secondary antibodies, should also be calculated and taken into consideration. An antibody average size is between 10-15 nm, which sets the error to 20-30 nm for

primary and secondary antibody combined (Figure 3.24) (Sheard et al., 2019). In other words, the spot at which a fluorescent signal is detected, does not represent the actual location of the molecule, which, in reality, can be located anywhere around a 30 nm radius.

Taken together, by summing up the error generated by the detection of both FGFR2 and TRPA1, the estimated maximum size of a complex would be in the range of 50-70 nm. This is because the interaction occurs through the ARD of TRPA1 which is 10 nm long, plus 2-times the antibody error (Figure 3.24d). Representative images of FGFR2-TRPA1 “complexes” within 70 nm are shown in Figure 3.25 and Appendix.

Based on observations on the “complexes”, it appears that TRPA1 exists in complex with one or two FGFR2 molecules at a time (Figure 3.25a and b, Appendix). However, it is not possible to determine whether both FGFR2 molecules are in direct contact with the channel or whether they form a dimer that interacts with TRPA1 through one of them. The resolution of two FGFR2 molecules within a dimer is possible by 10x ExM because the secondary antibodies labelling each molecule would be at least 20 nm apart. This means that each red signal represents one FGFR2 molecule, in theory. However, placing two FGFR2 molecules close together could initiate their dimerization anyway, assuming that interactions through the ARD are flexible enough to allow these movements.

The interaction of TRPA1 with 3, 4 or more FGFR2 molecules has not been clearly observed, suggesting that it probably creates complexes in 1:1 or 1:2 (single or dimers) stoichiometry. However, the possibility of TRPA1 to form higher order complexes by interactions with multiple FGFR2 molecules cannot be completely excluded at present. There have been locations with higher density of molecules that cannot be fully interpreted (Figure 3.25c). An additional point to consider is the

fact that these are 2D images thus, molecules from different planes that are projected into the 2D image result in artefacts.

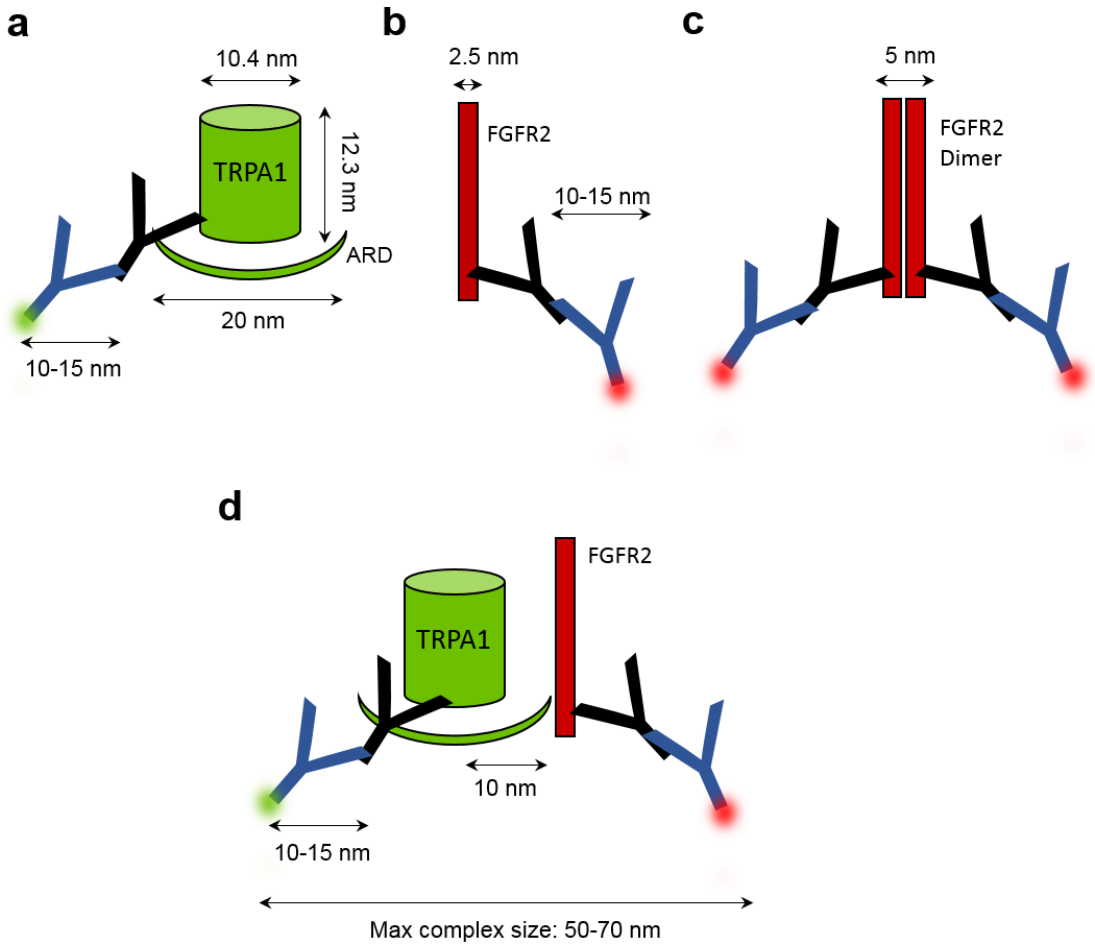

Figure 3. 24: Schematic representation of estimated distances in FGFR2 and TRPA1 complex. a) TRPA1 tetrameric channel dimensions with antibody error. ARD = Ankyrin Repeat Domain. b) monomeric FGFR2 dimensions with antibody error. c) dimeric FGFR2 with antibody error. d) Maximum distance between green (TRPA1) and red (FGFR2) signal in which an interaction can theoretically occur including antibody error.

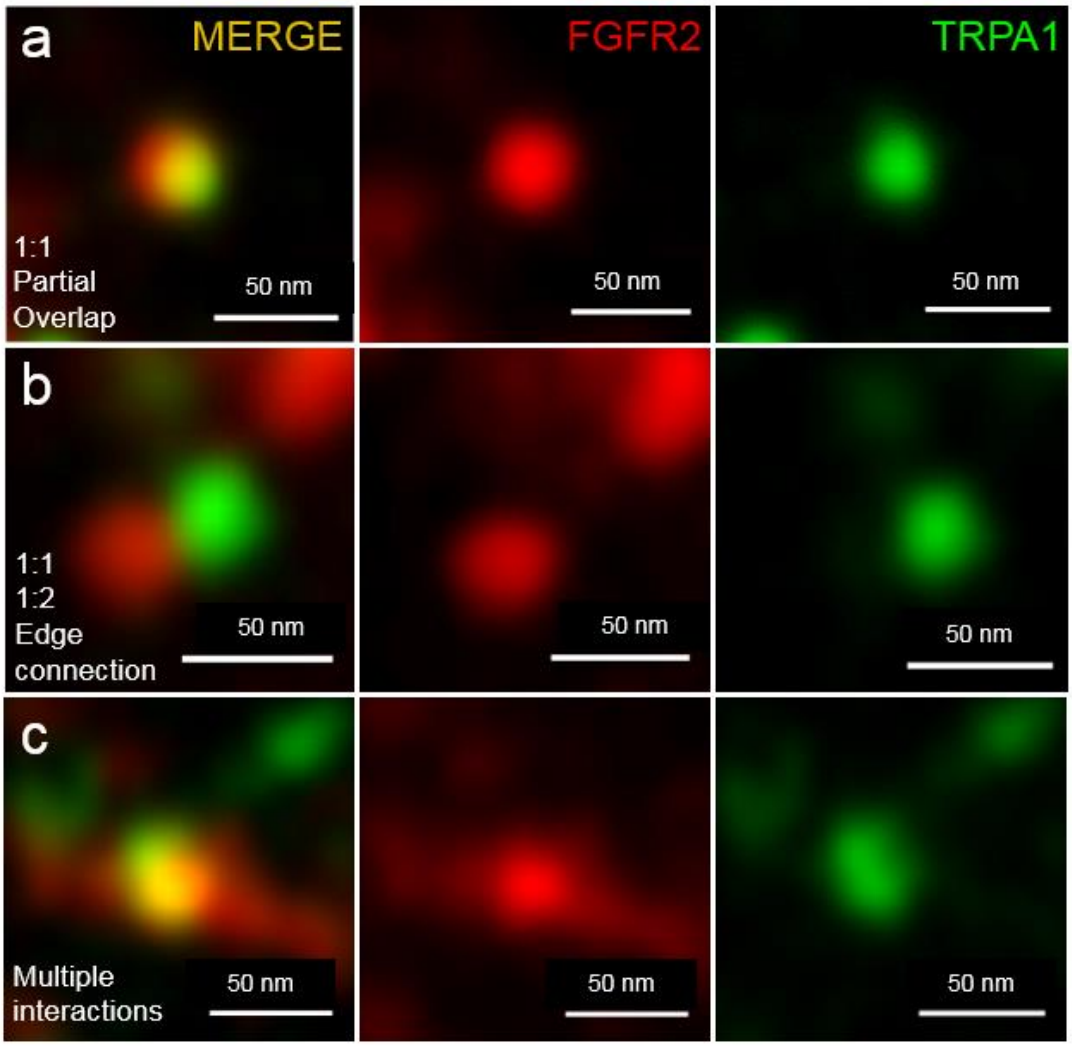

Figure 3. 25: Representative images of FGFR2 and TRPA1 complexes as obtained by ExM 10x in transfected HEK-293T cells. a) FGFR2-TRPA1 complex in 1:1 stoichiometry. Signals partially overlap. b) FGFR2-TRPA1 complex in 1:1 or possibly 2:1 stoichiometry. Signals do not overlap but are located within maximum complex distance of 50-70 nm. c) Higher density of FGFR2 and TRPA1 signals in a localised area. Chance of higher order complexes. Representative images are shown.

3.3. Discussion

3.3.1. Complex formation between FGFR2 and TRPA1

3.3.1.1. Co-Immunoprecipitation (Co-IP) controls

Co-IP results in this chapter suggest for the first time that TRPA1 is a novel interaction partner for FGFR2. Since the proteins of interest were tagged and overexpressed in HEK-293T cells, the use of appropriate controls was attempted to discard the possibility of interaction through the tags (Figure 3.2 and 3.3).

First, an empty FLAG tag (negative control) was not able to pull down TRPA1 eliminating the possibility of interaction of the FLAG tag with TRPA1 or the TurboGFP tag of TRPA1 (Figure 3.3a, lane 2). However, due to the small size of the FLAG tag (8 amino acids = 1kDa estimated), no band was visible in the western blot (lane 5) and thus, the efficiency of transfection for the negative vector was not verified.

On the other hand, the appropriate TurboGFP negative control vector was not available at the time and therefore, an empty eGFP vector was used instead as an alternative option to eliminate the possibility of interaction occurring through the TurboGFP tag of TRPA1 and indeed, eGFP did not precipitate FGFR2. TurboGFP is an optimised variant of ppluGFP (from *Pontellina Plumata*) that is brighter and has faster maturation kinetics compared to eGFP and therefore, it is highly applicable in gene expression analysis (Evdokimov et al., 2006).

TurboGFP-tagged proteins have been used in Co-IP experiments in the past that showed no interaction through the tag, indicating that TurboGFP tags are suitable for protein interaction experiments (Lu *et al*., 2014, Penicud and Behrens, 2014). Additionally, FLAG tag proteins have repeatedly been used in interaction experiments and have been shown to be suitable for Co-IP (Hu *et al*., 2018, Sun *et al*., 2011). All this evidence suggests that the observed TRPA1-FGFR2 interaction is highly unlikely occurred through the epitope tags. This conclusion is additionally

supported by the pull-down assays and biophysical methods (MST) utilising purified proteins (Figures 3.7 and 11).

3.3.1.2. Proximity Ligation Assay (PLA) limitations

PLA experiments were utilised as an additional method to investigate FGFR2 and TRPA1 complex formation. PLA was introduced as a simple and easy modification of a conventional immunofluorescence method to assess protein proximity/interaction for any pairs of antigens for which specific antibodies can be produced (Soderberg et al., 2006). This flexibility allows the investigation of not only protein complexes but also receptor dimerization and post-transcriptional protein modifications like phosphorylation (Chen *et al*., 2013, Elfineh *et al*., 2014, Gajadhar and Guha, 2010, Gomes *et al*., 2016, Iwabuchi *et al*., 2017). By principle, PLA signal is generated only when the PLA probes are located within maximum of 40nm (suggesting close proximity and possible interaction) which is lower than the optical resolution limit allowing for localisation analysis in the nanometre scale. As shown in Figure 3.4 and 3.5, significantly higher PLA signal was observed in the presence of both proteins of interest compared to negative controls (omission of primary antibodies and overexpression of only one of the proteins). However, these data should be interpreted with caution because PLA can produce “false positive” signal (Alsemarz *et al*., 2018), (see below).

One of the most significant limitations of PLA is the use of appropriate controls that not only reference for antibody specificity but also for proximity specificity. Regular negative controls such as omission of primary antibodies or absence of one of the epitopes (e.g. si-RNA knock down) correct only for the non-specific binding of the secondary antibodies, which is generally low, and therefore controls like that always produce negligible amounts of signal (as seen in Figure 3.4 and 3.5). Last year, Alsemarz, A., *et al*., proposed that PLA is prone to false positive signal that is roughly proportionate to the antibody density/abundance of antigens by comparing signals from antigens that are known to be interacting as well as non-interacting

proteins. At high protein abundance, the PLA signal was not significantly different in cases of non-interacting proteins (e.g. E-cadherin/membranous-GFP, E-cadherin/soluble-GFP, β-tubulin/soluble GFP) compared to known interacting proteins (e.g. E-cadherin/β-catenin). These data suggest that significant PLA signal can be detected provided that the primary antibodies have bound close enough, in other words, high abundance of the two antigens in a localised area (e.g. membrane or microtubules) which generates the “specificity” artefact (Alsemarz *et al*., 2018).

As an attempt to correct for any exaggerated signal due to the overexpression of the proteins in HEK-293T cells, FGFR2-FLAG + eGFP expressing cells were utilised as a negative overexpression control. Considering that a different pair of antibodies was used in this negative control (anti-GFP and anti-FLAG), a comparison with PLA signal generated by the anti-TRPA1 and anti-FGFR2 pair would not be fair. Therefore, even though FGFR2-FLAG+eGFP cells had higher PLA signal compared to FGFR2-FLAG+TRPA1-tGFP (Figure 3.6), it does not indicate that PLA generated by FGFR2 and TRPA1 antibodies is an artefact. In order to compare between PLA results, the same set of primary and secondary antibodies should be utilised.

Nevertheless, PLA can be an informative tool, given the proper experimental design and uses of appropriate controls. Gajadhar, A., *et al*., for instance, studied the ligand-induced EGFR dimerization in cells overexpressing two different epitope-tagged EGFRs. In this example, both antibody specificity (primary antibody omission or lack of one of the antigens) and proximity specificity controls (dimerization mutant) were implemented. The dimerization mutant showed similar localisation and expression levels compared to the wild type version and therefore, would be an appropriate negative control for this PLA experiment (Gajadhar and Guha, 2010).

In the present study, a mutated variant of TRPA1 or FGFR2 that impairs the interaction would be an acceptable negative control. However, as mentioned in the results section, TRPA1-Δ10 and full length TRPA1 were not expressed in similar levels especially when co-expressed with FGFR2 and therefore, PLA experiments would still remain inconclusive (Figure 3.9a).

In conclusion, PLA results in Figures 3.4,5 and 6 are not a conclusive evidence of an interaction but rather an indication of close proximity between FGFR2 and TRPA1.

3.3.2. The C-terminal region of FGFR2 directly interacts with the Ankyrin Repeats 6-10 of TRPA1

3.3.2.1. Direct interaction between FGFR2 and TRPA1 ARD as shown by MST

Co-IP and PLA experiments suggest a protein interaction between FGFR2 and TRPA1; however, this approach could not verify the direct binding of the two proteins. To investigate whether FGFR2 and TRPA1 interact directly and to further characterise the binding affinity and identify the TRPA1-binding site, a biophysical method, Microscale Thermophoresis (MST), was performed. The output from the MST assays is a binding curve. The dissociation constant is defined as the concentration in which the first protein occupies half of the sites on the second protein in equilibrium. Subsequently, the lower the dissociation constant (K_d), the higher the binding affinity is (Kastritis and Bonvin, 2013). For instance, the dissociation constant of monoclonal antibodies, that are very specific and show high affinity for their target antigens, has been measured to be in the range of 20 to 200 pM which is very strong (Landry et al., 2015).

Indeed, MST revealed that FGFR2 and TRPA1 interact directly with a dissociation constant (K_d) of 122.8 ± 23 nM. It also revealed that the interaction is mediated

through the ankyrin repeat domain of TRPA1 since no binding curve was acquired with the TRPA1-Δ16 truncation.

It could be agreed that a *Kd* of 122 nM is a relatively strong interaction and is in the range observed for other FGFR2 interactions. The cSH2 domain of PLCγ1, for example, interacts with the pY769 of FGFR2 with a dissociation constant of 100nM, as measured by Surface Plasmon Resonance (SPR) (Huang et al., 2016). The SH3 domain of PLCγ1 binds to the C-terminal 23 amino acid fragment of FGFR2 with a dissociation constant of 40 µM and the SH3 domain of GRB2 binds to the same site with a dissociation constant of 100 nM for a 2:1 complex and 25 µM for a 2:2 complex (by ITC) (Timsah *et al*., 2014, Lin *et al*., 2012). Notably, differences up to 4-fold are expected when comparing dissociation constants as measured by different methods (Landry *et al*., 2015). In general, interactions studied with full length proteins (like here) are more accurate, as fragments do not represent the original folding in synergy with the rest of the protein.

This MST experiment shows for the first time the involvement of the TRPA1 ARD in the interaction with FGFR2. The *Kd* of this interaction (122 nM) also lies between the range of previously reported interactions mediated by ARDs. For example, the ankyrin repeat domain of the oncoprotein gankyrin binds to the C-terminal portion of the S6 ATPase from the 26S proteasome with a dissociation constant of 67 nM, the first two repeats of the ARD of Iκ-Bα interacts with the N-terminal domain of NF-κB with a *Kd* of 40 pM and the p53-BP2 ARD binds to the L2 loop of p53 with a *Kd* of 0.5-5 µM (Chapman *et al*., 2014, Patel *et al*., 2008, Bergqvist *et al*., 2009).

Further studies to identify the binding site contained in the TRPA1 ARD by Co-IP were not accomplished in this study because, upon co-expression, the protein levels of TRPA1-Δ10 and FGFR2 were very low (Figure 3.10). The decrease in protein levels could be explained as possible competition for the transcriptional machinery since both genes are under the control of pCMV promoters. The TRPA1-

Δ10 efficiency of transfection is much lower than the full length TRPA1 and this could have magnified the effect of this competition. Due to protein expression level problems, the Co-IP between full length and truncated TRPA1 would not be a fair comparison. To overcome this issue, GST-pull down assays were performed as discussed below.

3.3.2.2. FGFR2 and TRPA1 interaction is mediated through the C-terminal domain of FGFR2

Firstly, the evidence that the C-terminal Proline-rich fragment of FGFR2 is involved in the interaction with the ARD binding site of TRPA1 came from additional GST-pull down assays (Figure 3.11b). The bacterial expression system for FGFR2-C58 was chosen due to higher protein yield compared to mammalian systems. Moreover, the absence of post-transcriptional modifications on the fragment allows for use of bacterial expression systems. Appropriate negative controls, including empty beads or use of wild type cell lysate, failed to pull down TRPA1 which verifies the specificity of the signal. However, these controls do not test for the possibility of interaction through the GST tag and therefore, an additional control with GST-conjugated beads would be more suitable to eliminate this likelihood.

GST-pull down assays with amino acid substitution mutations from Proline to Alanine located in the C-terminal region of FGFR2 did not show any reduced binding between C58 and TRPA1 (Figure 3.13). That was an attempt to map the specific residues involved in the interaction with the TRPA1 ARD. The reason behind mutating these particular residues comes from previous studies on FGFR2 C-terminal interactions with SH3-contaning proteins which reveal Proline 810 and 813 as a Proline-rich binding site (Ahmed *et al*., 2010, Lin *et al.*, 2012, Timsah *et al*., 2014). The data presented here (Figure 3.13) could suggest that P810 and P813 are not involved in the interaction with TRPA1 however, additional repeats are needed to achieve certainty in regards to the involvement of the prolines in question. The PLCγ1 positive control was performed in one replicate and showed

reduction of PLCγ1 binding to P810 and P813, as shown in the literature, however, this control should be implemented in all GST pull down experiments involving proline mutations to ensure the validity of the experiment.

Based on the published study from our lab, Proline 810 and 813 are involved in the interaction with the ARD. Notably, these substitutions did not entirely abolish the binding; some TRPA1 binding was still detectable, suggesting that Proline 810 and 813 are not the only residues comprising the FGFR2 binding site. In fact, ARDs differ from other common motifs like SH2 or SH3, which bind to a well determined sequence, because they can recognise a wide variety of sequences. ARD-mediated interactions involve diverse targets in which discontinuous areas of residues along the interaction interface are recognised. A number of factors regulate the specificity of ARDs. Even though ankyrin repeats are highly conserved (e.g. TPLH tetrapeptide in the first helix), several amino acid substitutions confer target specificity. The number of repeats can also affect the recognition since the higher the number of repeats the more concave and compact the interaction surface becomes. The specificity can also be influenced by the presence of additional domains in the protein (Li *et al*., 2006, Islam *et al.*, 2018). Therefore, the possibility of a more extended binding site on the FGFR2 C-terminal region cannot be excluded.

3.3.2.3. AR 6-10 mediate the interaction between TRPA1 and C-terminal domain of FGFR2

Using FGFR2-C58 conjugated GST beads determined that the FGFR2-binding site of TRPA1 is located within the first ten ankyrin repeats, since TRPA1-Δ10 showed an approximately 80% reduction in interacting with FGFR2-C58 (Figure 3.12). Based on the cryo-EM structure of TRPA1, the last five ankyrin repeats (12-16) are fully resolved and incorporated into the “stem” of the channel together with the C-terminal Coiled-coil domains. The remaining 11 ankyrin repeats (1-11), that form a crescent-shaped density around the “stem” of the channel, are not fully resolved

because their positions are more flexible. However, a “propeller” orientation is more favourable. This structural conformation and flexibility would make the first eleven ankyrin repeats more accessible and facilitate protein interactions (Paulsen *et al*., 2015).

Serial ankyrin repeat truncations and subsequent amino acid substitutions are needed to completely map the exact binding site within the first ten ankyrin repeats of TRPA1.

At this point it is crucial to ensure that the truncated TRPA1 is still a functional membrane channel and that the decrease in the interaction with FGFR2 C-terminal domain is not due to membrane traffic failure. Therefore, calcium imaging experiments to assess the activity of the transfected full length TRPA1 as well as Δ10 would be ideal to ensure proper membrane localisation and function of the channels. Notably, TRPA1 has been found to be fully functional and respond to cold temperatures as well as electrophilic compounds even in the absence of the N-terminal ARD (Moparthi *et al*., 2014) suggesting that Δ10 is more likely to also be functional in the present study.

3.3.2.4. Interplay between TRP channels and RTKs

This study is the first to document a direct interaction between FGFR2 and TRPA1. In general, crosstalk between TRP channels and RTKs has been investigated before yet, the exact mechanisms remain elusive. Those mechanisms usually involve PLC proteins or additional mediators like calcium (Tajeddine and Gailly, 2012, Veldhuis *et al*., 2015).

In 2016, the role of TRPC3 in indirect EGFR activation (transactivation) was described and implicated in hypertension-induced vascular smooth muscle cell (VSMC) growth and the subsequent possibility of stroke. Angiotensin II, a vasoconstrictor and VSMC growth activator, transactivates EGFR through activating ADAM17, a metalloproteinase involved in ectodomain shedding of pro-

HB-EGF (pro-heparin-binding epidermal growth factor). ADAM17 activity is calcium-dependent and complex formation between ADAM17 and TRPC3 results in its activation due to localised calcium influx indicating the role of TRPC3 in EGFR transactivation and cerebrovascular remodelling (Wang *et al*., 2016).

Notably, there is evidence of complex formation between TRP channels and RTKs however, detailed follow-up studies have not been performed. Firstly, in 1999, Wang and colleagues showed that TRPC3 and the neurotrophic receptor TrkB (an RTK) share common spatial and temporal expression in the central nervous system of foetal and neonatal rats and that TRPC3 was co-immunoprecipitated with Trk receptors, possibly forming a complex that explains the Calcium-dependent current after BDNF treatment (Li *et al*., 1999).

Another example is the functional interaction between TRPV3 and EGFR in keratinocyte differentiation and hair formation (Cheng *et al*., 2010). In this study, TRPV3 and EGFR co-immunoprecipitated. Interestingly, TRPV3 was not immunoprecipitated with either FGFR2 or ADAM17, a known metalloprotease responsible for TNF-α shedding (EGFR ligand). EGFR is involved in epidermis renewal by controlling keratinocyte proliferation and terminal differentiation thus, EGFR deficiency is coupled with the wavy hair phenotype and skin problems. Similarly, TRPV3 knock-out mice demonstrated the same phenotypes. Cheng and colleagues (Cheng *et al*., 2010) suggested a model, whereby unknown signals (most likely 32^{o}C on skin surface) activate TRPV3 in basal levels that cause calcium influx and activation of metalloproteinases and glutaminases (ADAM17 and TGase1, 2) that increase TNF-α/EGFR activation and downstream signalling pathways including PLCγ, MAPK and PI3K. Activation of EGFR potentiates TRPV3 either by the direct interaction (TRPV3 phosphorylation) or through PLCγ and ERK, creating a positive feedback loop that enhances EGFR signalling even more.

These examples use co-immunoprecipitation experiments to suggest complex formation, yet direct interactions between the components have not been investigated in these studies. Nevertheless, they implicate TRP and RTK interplay in physiological processes. So far, TRP/RTK complex formation has not been described in the context of cancer. The present study investigates the direct interaction between FGFR2 and TRPA1 and their implications in cancer signaling.

Taken together, the fact that TRPA1 interacts with the C-terminal domain of FGFR2 and more likely masks specific key residues for signalling raises questions such as possible competition with PLCγ1 and GRB2 which share the same Proline-rich binding site and subsequent effects on general FGFR2 signalling. This automatically highlights the role of TRPA1 in FGFR2-related skeletal diseases and cancer (Ornitz and Marie, 2015). The effect of this interaction on FGFR2 signalling is investigated in Chapter 4.

3.3.3. FGFR2 and TRPA1 complex formation in LUAD

3.3.3.1. Overexpression of FGFR2 and TRPA1 in human LUAD tissues

Apart from the over-expression system, the FGFR2-TRPA1 interaction was also studied in a physiologically relevant system to confirm that the interaction occurs in native conditions such as within cancer cells. Dysregulated FGFR2 signalling has been implicated in malignancies and therefore, cancer cells would be a suitable system to confirm TRPA1 interactions that could affect FGFR2 signalling (Sme Theelen *et al*., 2016, Timsah *et al*., 2015). Firstly, IHC staining confirmed that TRPA1, as well as FGFR2, are overexpressed in human LUAD compared to healthy tissues which is consistent with previous studies. For instance, Takahashi, *et al*, in 2018, investigated the protein expression of TRPA1 in a series of cancer types and revealed that TRPA1 levels were significantly elevated in a panel of Breast and Lung cancer (LUSC and LUAD) tissues by IHC as well as in selected

cell lines by western blot (Takahashi *et al*., 2018). Moreover, high levels of FGFR2 have also been detected in lung malignancies including squamous cell carcinoma and adenocarcinoma and have been associated with overall survival and recurrence-free survival (Chang *et al*., 2014, Behrens *et al.*, 2008, Timsah *et al*., 2015). Therefore, LUAD cell lines were utilised to investigate the interaction in a native system.

3.3.32. FGFR2-TRPA1 complex formation in HCC-515 cells

Western blot analysis and immunofluorescence experiments have verified the expression of both proteins in the HCC-515 human LUAD cell line (Figure 3.15 and 16). In particular, immunofluorescence images show a dense nuclear localisation of FGFR2, a phenomenon that has been described in the past for FGFR1,2 and 3 yet, little is known about their actual mechanism of action in the nucleus (Salva *et al*., 2019, Zhou *et al*., 2015). Studies seem to converge on the transcriptional role of FGFRs which, in turn, have an effect on cancer cell phenotype. For instance, the intracellular domain of FGFR1 is cleaved following FGF10 stimulation in breast cancer cells and translocates to the nucleus where it orchestrates an invasive gene expression signature (Chioni and Grose, 2012). On the other hand, FGFR2 has been found to translocate to the nucleus and physically interact with and negatively regulate HIF-1 and HIF-2 inhibiting hypoxia-induced cell invasion in pancreatic cancer cells (Lee *et al*., 2019). The presence of FGFR2 in the nucleus of HCC-515 cells has been acknowledged but not investigated further as it exceeds the objectives of this study. However, isolation of membrane proteins and analysis by western blot confirmed the localisation of both FGFR2 and TRPA1 at the cellular plasma membrane of HCC-515 cells and therefore, FGFR2-TRPA1 membrane complex formation could be studied (Figure 3.17a).

Co-IP experiments with an anti-FGFR2 antibody confirmed that endogenous FGFR2 can pull down endogenous TRPA1 and that this interaction can occur

naturally in cells (Figure 3.17b). An additional sample utilising a cell line that expresses only one of the proteins such as the HCC-44 cells would be an ideal negative control in this situation. PLA experiments were also performed as supporting evidence in which PLA signal from wild type and FGFR2-siRNA knock-down cells were compared (Figure 3.18). Indeed, the PLA signal was significantly lower in the knock-down cells. However, treatment of cells with an interaction inhibitor, for instance, would be a more suitable negative control. An inhibitor could be anything that blocks the interaction or competes with the binding sites such as overexpressed soluble C-terminal FGFR2 fragments that could bind to the ARD of TRPA1 or vice versa. Nevertheless, the fact that the PLA signal was detected in HCC-515 cells indicates close proximity between FGFR2 and TRPA1 (endogenous levels) and supports the Co-IP results.

3.3.3.3. FGFR2-mediated regulation of TRPA1

Notably, hardly any calcium response could be detected in HCC-515 cells, which express higher levels of TRPA1 compared to HCC-44 cells, by calcium imaging experiments using AITC as an agonist indicating a non-functional TRPA1 channel. In contrast, HCC-44 cells, expressing very low levels of TRPA1, had a high calcium response upon AITC treatment which was specific to TRPA1 because the response was reduced in the presence of a TRPA1 specific inhibitor (Figure 3.18). Additional experiments such as calcium imaging on FGFR2-transfected HCC-44 cells which exhibited lower calcium response to AITC, are included in our publication (Berrout *et al*., 2017). These data suggest FGFR2-mediated inhibition of TRPA1, possibly via conformational changes in the ARD that translate into pore opening regulation.

The observation that TRPA1 activation can be influenced by physical association with other proteins is not new. Previously, it has been shown that TRPA1 complex formation with TRPV1 causes inhibition of TRPA1 both in overexpression systems as well as in sensory neurons (Weng *et al.*, 2015). In this study, Hao-Jui Weng, and

colleagues described that the C-terminal domain of Tmem100 (a membrane protein) containing the KRR sequence binds to TRPA1 and increases its activation in the presence of TRPV1 by weakening the TRPA1-TRPV1 interaction. The authors also propose that individual interaction sites on each component of the complex are responsible for the interaction and thus, channel modulation however, no specific domains of the channels were investigated.

3.3.4. FGFR2-TRPA1 complex exists in 1:1 and 2:1 stoichiometry and can possibly form higher order complexes based on Expansion Microscopy data.

3.3.4.1. Molecular counting in Super-resolution microscopy

ExM 10x was performed as an attempt to determine the complex stoichiometry in FGFR2 and TRPA1 complexes. The use of single-molecule super-resolution microscopy methods for molecular counting has been described before however, there are certain challenges related to over-counting, due to fluorophore blinking or under-counting, due to limited detection efficiency. Despite those challenges, scientists developed strategies to quantify molecules, including RAF kinase multimers, the bacterial Flagellar Motor Protein FLIM and PIP3 content in endosomes, by super-resolution techniques such as STORM and PALM (Deschout et al., 2014; Nan et al., 2013; Puchner et al., 2013).

In contrast, ExM 10x provides a much simpler platform to perform molecular counting since no photoswitching-derived challenges are faced. For example, Sheard, *et al*., were able to count single RyR molecules (Ryanodine receptors) within clusters in nanodomains of rat cardiac myocytes as well as match them to phosphorylated RyR by two-colour imaging. Centroids of individual RyRs were calculated and matched to any phospho-RYR signal within a radius of 30nm (localisation error) (Sheard et al., 2019). Similar approach was followed in the

present ExM 10x experiment in which 30nm error for each molecule was taken into consideration when estimating the maximum distance between FGFR2 and TRPA1 required to form a complex (Figure 3.23).

3.3.4.2. ExM limitations in this study

The present preliminary ExM experiments have certain limitations. To begin with, the calculated expansion factor depends on a crude measurement of the gel pre- and post-expansion in the macroscopic scale. The macroscopic swelling of the gel does not always represent the true expansion of intracellular structures in the microscopic scale. Another limitation to consider is whether the expansion is occurring homogenously and isotropically throughout the gel resulting in a uniform expansion factor.

A relatively new approach designed to overcome these issues proposes the use of nanorulers as a calibration tool to quantify the microscopic expansion factor. Nanorulers are utilising the DNA origami technology to create a DNA platform of a determined size in which two marks, separated by a set distance (e.g. 80nm), are linked to fluorophores. Conventional confocal microscopy will not be able to separate the two points of the nanoruler. Following ExM, the two points will be separated, and the microscopic expansion factor will be determined as the ratio of distance between the two fluorophores post-expansion divided by distance pre-expansion (determined nanoruler size). Interestingly, it has been shown that the microscopic expansion factor can deviate from the macroscopic one. This deviation is probably derived from the fact that the nanorulers are initially attached to the coverslip and the friction generated between the coverslip and the swellable gel is preventing full expansion, which ultimately highlights that the gel is expanding un-isotropically (Scheible and Tinnefeld, 2018).

An alternative approach is to utilise cellular ultrastructures of known size as a calibration tool such as α-actinin lattices, peroxisomes and centrioles (Gambarotto

et al., 2018; Sheard et al., 2019; Truckenbrodt et al., 2018). Sheard and colleagues performed ExM 10x and proved consistent and isotropic expansion by comparing the 2-strand morphology of α-actinin lattices (z-discs) and z-disc width (sarcomeric length) in cardiomyocytes, respectively (Sheard et al., 2019). The same optimised and validated protocol was implemented in the present ExM 10x experiment and thus, isotropic expansion was expected in our samples.

An additional issue emerging from this ExM experiment is the lack of a membrane marker that would ensure imaging of the membrane surface. However, this would necessitate the use of a third fluorophore which would increase the complication of the experiment. Imaging in TIRF (Total Internal Reflection Fluorescence) in which only fluorophores within approximately 100nm above the coverslip surface are imaged, would also facilitate cell membrane imaging (Fish, 2009). However, a TIRF imaging set up was not available and therefore, an alternative approach had to be implemented. Since FGFR2 and TRPA1 are membrane proteins and cells are mostly flat on the coverslip, images were obtained at the lower focal plane (flat, near-surface) in which FGFR2 and TRPA1 fluorophores were present.

Furthermore, the ExM experiments were performed on overexpressed proteins which can generate artefacts due to protein abundance. HCC-515 cells would be the optimal system for ExM since FGFR2 and TRPA1 are endogenously expressed and complex formation between the two proteins has been shown (Figure 3.17).

Mander's co-localisation analysis of 10x ExM images showed that 11.2% of FGFR2 co-localises with TRPA1 and 23.7% of TRPA1 co-localises with FGFR2 (Figure 3.23). However, there was no other condition to compare these percentages to. Cells over-expressing FGFR2 and TRPA1-Δ10 would be an ideal negative control, since TRPA1-Δ10 does not interact with FGFR2 as effectively (Figure 3.12).

3.3.4.3. Stoichiometry of the FGFR2 and TRPA1 complex

Preliminary ExM 10x experiments performed on FGFR2 and TRPA1 expressing HEK293T cells revealed physical association between the two proteins and suggest a putative complex stoichiometry of 1:1 and 2:1 (Figure 3.24). The use of regular antibodies for detecting the two proteins generated a localisation error of 20-30nm per molecule. Smaller localisation error can be achieved by an alternative detection method utilising nanobodies (fragments of monomeric variable domains of antibodies). Nanobodies confer a more accurate signal localisation because of their smaller size (1.5 x 2.5 nm, 13 kDa) compared to regular antibodies (10-15 nm, 150 kDa). The smaller size also facilitates access to restricted areas that antibodies cannot reach due to steric hindrance and therefore, the detected signal is more specific in regard to the true number and location of labelled proteins (Ries et al., 2012).

Based on the interaction mechanism, which involves the binding of the TRPA1 ARD to the C-terminal domain of FGFR2, a theoretical stoichiometry model could be constructed: TRPA1 is a homotetramer meaning that each channel possesses four ARDs which can potentially interact with four different FGFR2 molecules (4:1 stoichiometry). However, as observed by ExM 10x, it is more likely for FGFR2-TRPA1 complexes to be present in 1:1 and 2:1 stoichiometry.

There are three possible explanations for this observed phenomenon. A possible explanation would be that not all antigen sites are occupied by an antibody due to steric hindrance. Secondly, (for the 2:1 model) two adjacent ARDs could be interacting with the same FGFR2 molecule and thus, all ARDs are actually occupied. Thirdly, this is a “pre-complex” in which not all ARD sites have been occupied by FGFR2 yet. Interestingly, areas with higher signal density were also detected raising the possibility of higher order c+omplexes. However, those images

were blurry most likely due to signals from different focal planes and therefore, z-stacks would be more informative regarding 3D interactions.

Moreover, it is still not clear whether the two FGFR2 molecules in the 2:1 model are individual monomers interacting with one ARD each or act as a dimer that is connected to one or two adjacent ARDs. At this stage, it is fairly difficult to express with certainty the exact complex composition, since specific details regarding the interaction are still elusive. For example, can more than one FGFR2 molecules bind to one ARD (multiple interaction sites) ?, Can two ARDs bind to a single FGFR2 molecule ?, Can an FGFR2 dimer bind to a single ARD ?

Taken together, even though ExM 10x provided information regarding the possible number of molecules comprising the complex, it is not able to characterise the network of interactions between those molecules which could potentially determine the fate of the downstream FGFR2 signalling. The FGFR2 signalling upon TRPA1 interaction is studied in the next chapter (Chapter 4).

4. Chapter 4
Investigation of the function of the FGFR2-TRPA1 complex

4.1. Introduction

It has been shown that the basal FGFR2 signalling is regulated by protein-protein interactions occurring at the proline-rich motif which is located at the C-terminal domain of the receptor. Those interactions in combination with the expression levels of the components dictate which downstream pathway prevails and regulate cellular behaviour (Lin et al., 2012; Timsah et al., 2015, 2014).

Dimeric GRB2 binds to the proline-rich motif causing FGFR2 pre-dimer formation and phosphorylation of A-loop tyrosine residues, in non-stimulating conditions. However, these pre-dimers are inactive since GRB2 covers regions on the C-terminal domain which are important for signal transduction. Upon stimulation, FGFR2 becomes fully activated and phosphorylates GRB2 resulting in dissociation which enables FGFR2 signalling (Lin et al., 2012) (see Figure 1.12).

PLCγ1 recognises pY769 on a stimulated FGFR2 molecule and becomes active upon FGFR2-mediated phosphorylation (Huang et al., 2016). However, PLCγ1 also binds to the same region on FGFR2 as GRB2 and becomes activated even in non-stimulating conditions. PLCγ1 and GRB2 compete for the binding site on FGFR2 and therefore, the protein equilibrium dictates the fate of FGFR2 signalling (Timsah et al., 2014) (see Figure 1.12).

In Chapter 3, it was suggested that TRPA1 directly binds to the FGFR2 C-terminal domain which implies a potential competition between the other 2 components (GRB2 and PLCγ1) as well as a regulatory action of TRPA1 towards the FGFR2 signalling. In this chapter, we investigate the effect of TRPA1 binding on FGFR2 dimerisation, phosphorylation and downstream signalling activation.

4.2. Results

4.2.1. The FGFR2-TRPA1 interaction affects the FGFR2 basal level signalling

To investigate the effect of FGFR2-TRPA1 complex on FGFR2 activity and signalling, western blots were performed to detect activity levels of FGFR2 as well as downstream signalling proteins (Figure 4.1). Phosphorylated levels of FGFR2, PLCγ1 and ERK were used as an indicator of protein activity and therefore, pathway activation in a series of conditions. HEK293T cells were transfected with FGFR2-FLAG and/or tGFP-TRPA1 and remained serum starved or treated with FGF9. FGF9 was used as a positive control because it is an FGFR2 ligand and activator of the FGFR2 signalling pathway (Wing et al., 2005). Quantification analysis involved the normalisation of the phosphorylated against the total levels of each protein.

As shown by the western blot, p-FGFR levels were increased after FGFR2 overexpression (lane 3) and that indicates the basal level of FGFR2 activity in non-stimulating conditions. When the cells were also transfected with TRPA1, p-FGFR2 basal levels were decreased by approximately 50% (0.51 ± 0.04, p-value = 0.042 by Tukey's post-hoc) compared to the FGFR2-

expressing cells suggesting that the binding of TRPA1 causes inhibition (direct or indirect) of the FGFR2 kinase.

Basal p-PLCγ1 and p-ERK levels were increased when cells were transfected with FGFR2 by 48 ± 9.2 (p-value = 0.000004 by Tukey's post hoc) and 12 ± 2.2 times (p-value = 0.018 by Tukey's post hoc) compared to the un-transfected sample, respectively. Considering the lower activity of FGFR2 in the presence of TRPA1, it would be expected that signalling proteins like PLCγ1 (substrate of FGFR2) and ERK (downstream of FGFR2) would also have lower phosphorylation levels. Indeed, p-PLCγ1 basal levels were decreased in the FGFR2+TRPA1 cells (lane 5) by approximately 60% (0.40 ± 0.03, p-value = 0.002 by Tukey's post-hoc) compared to the FGFR2-expressing cells (lane 3). However, p-ERK basal levels were not significantly different between FGFR2- and FGFR2+TRPA1-expressing cells, suggesting that the binding of TRPA1 to FGFR2 does not affect the MAPK pathway.

Notably, except for p-ERK (increased by 2.2-fold ± 0.1, p-value = 0.001 by Tukey's post hoc), p-FGFR and p-PLCγ1 were not increased under FGF9 stimulation (lane 4) as it would be expected (further discussed in section 4.3.1).

The same experiment was performed with a strep-tagged FGFR2 construct to demonstrate reproducibility. Firstly, the interaction between FGFR2-STREP and tGFP-TRPA1 was confirmed by Co-IP using an anti-TRPA1 antibody (Figure 4.2a). Indeed, consistent results were obtained by using a different construct of FGFR2 containing a different tag. Both p-FGFR and p-PLCγ1 levels were decreased in the presence of TRPA1 while p-ERK levels were not changed. This experiment was performed once.

Next, just to verify that the p-FGFR bands in the western blot belong to p-FGFR2 specifically and not to any other phosphorylated FGF receptor, a Co-IP was performed using an anti-FGFR2 antibody to precipitate total FGFR2 and then probed for p-FGFR to specifically detect phosphorylated levels of FGFR2. As shown in Figure 4.3, p-FGFR2 was decreased approximately 55% as similarly observed in the previous western blots with FGFR2-FLAG (Figure 4.1).

To further investigate if the MAPK pathway is also regulated by TRPA1, a western blot was performed to detect levels of p-ERK in cells that were TRPA1-transfected and kept serum starved or treated with AITC (TRPA1 agonist) and/or HC030031 (TRPA1 specific inhibitor) (Figure 4.4). The results show that there was a nearly 2-fold increase in the p-ERK levels in the presence of TRPA1 (lane 2). The p-ERK levels were further increased by another 2-fold in TRPA1-expressing cells that were also treated with AITC (lane 3). However, AITC was capable of increasing p-ERK by approximately 3-fold in HEK cells that were not transfected with TRPA1 compared to untreated cells (Figure 4.4, lane 1 and 4). To further understand whether the detected increase was due to TRPA1-mediated calcium signalling or due to an alternative mechanism, TRPA1-transfected cells that were serum starved or treated with AITC in the presence of the TRPA1 specific inhibitor HC030031 (prior to and during AITC treatment). The addition of HC030031 (lane 5 and 6) did not alter the p-ERK levels compared to non-HC030031-treated cells, suggesting that this effect of TRPA1 may not be mediated by the channel’s activity. Due to time limitations this experiment was performed once.

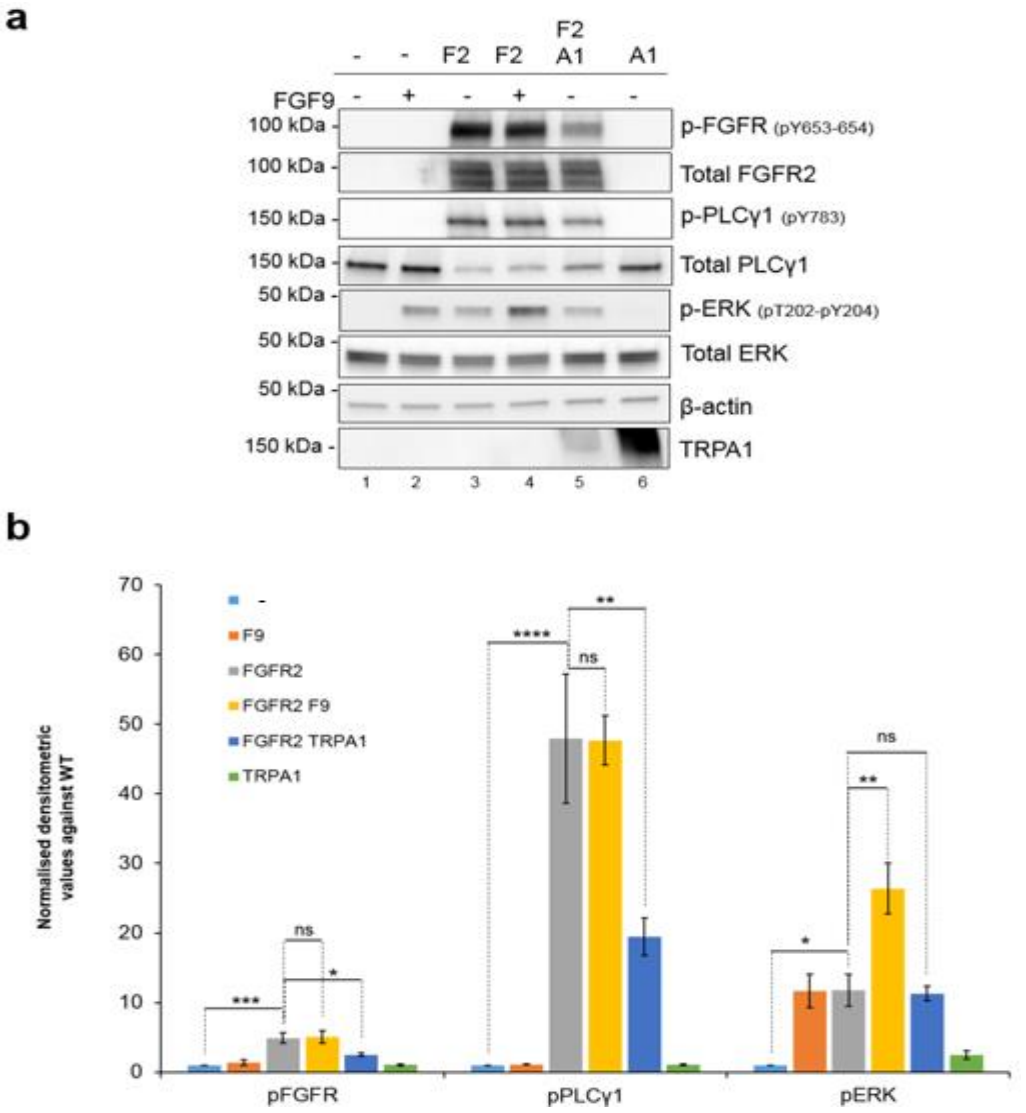

Figure 4. 1: Western blot analysis of FGFR2 signalling using FGFR2-FLAG. a) Western blot on un-transfected and FGFR2-FLAG and/or tGFP-TRPA1-transfected HEK-293T cells using the antibodies against the indicated proteins (anti-TRPA1 and anti-FGFR2 from Santa Cruz). The cells were serum starved for 2 hours prior to any treatment and lysis. β-actin was used as a loading control. b) Quantification of the western blot by densitometry using ImageJ. All densitometry values were normalised to β-actin. The bar graph illustrates the ratio of phosphorylated divided by total protein levels as normalised by the un-transfected control. F2 = FGFR2-FLAG, A1 = tGFP-TRPA1, F9 = FGF9. ns = non-significant. One-way ANOVA with Tukey's post hoc analysis, n = 4, Error bars = S.E.M.

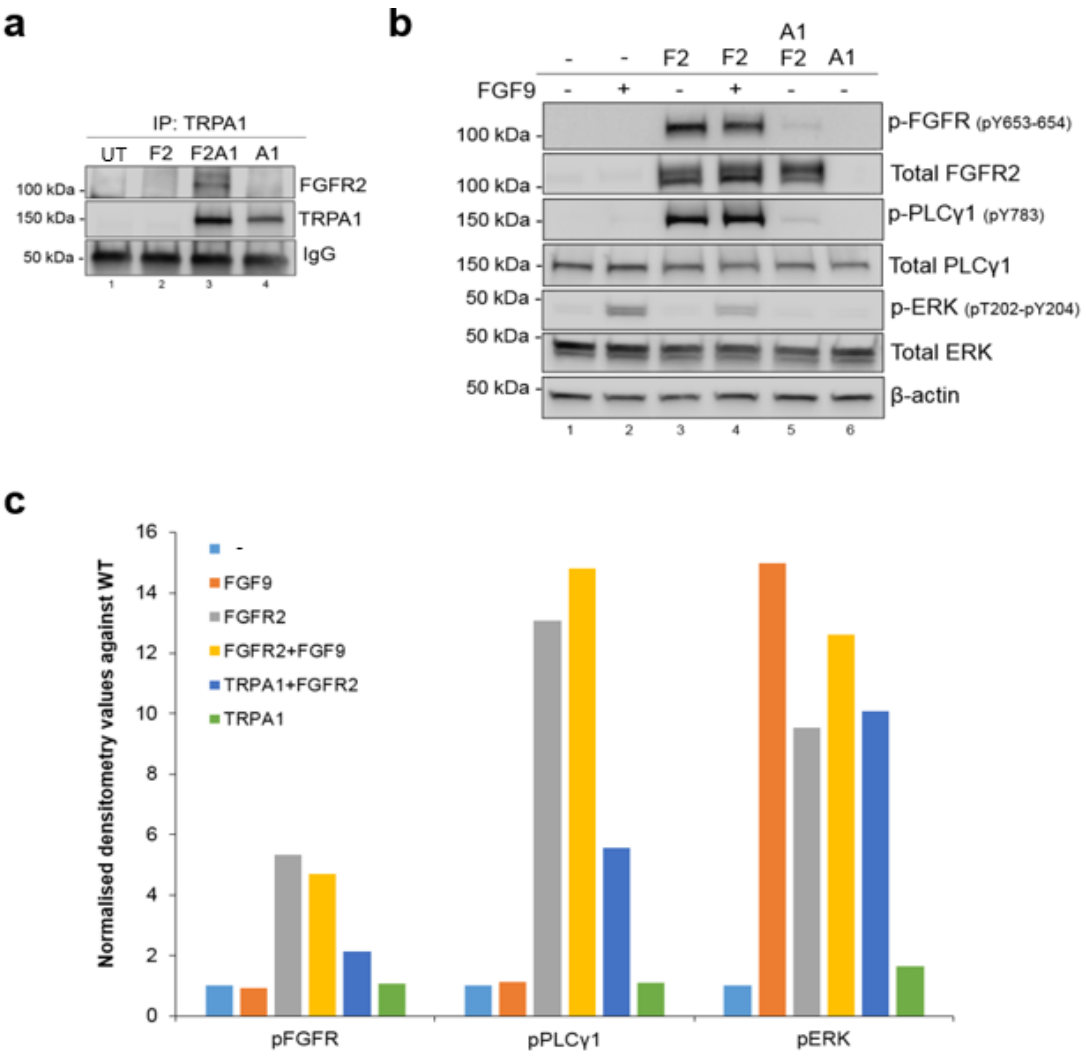

Figure 4. 2: Western blot analysis of FGFR2 signalling using FGFR2-STREP. a) Co-IP experiment using an anti-TRPA1 antibody (Santa Cruz) on lysates from un-transfected (UT) and FGFR2-STREP and/or tGFP-TRPA1-transfected cells. b) Western blot on un-transfected FGFR2-STREP and/or tGFP-TRPA1-transfected HEK-293T cells using antibodies against the indicated proteins (anti-TRPA1 and anti-FGFR2 from Santa Cruz). The cells were serum starved for 2 hours prior to any treatment or lysis. β-actin was used as a loading control. c) Quantification of the western blot by densitometry using ImageJ. All densitometry values were normalised to β-actin. The bar graph illustrates the ratio of phosphorylated divided by total

protein levels as normalised by the wild type control (n = 1). F2 = FGFR2-FLAG, A1 = TRPA1-tGFP, F9 = FGF9.

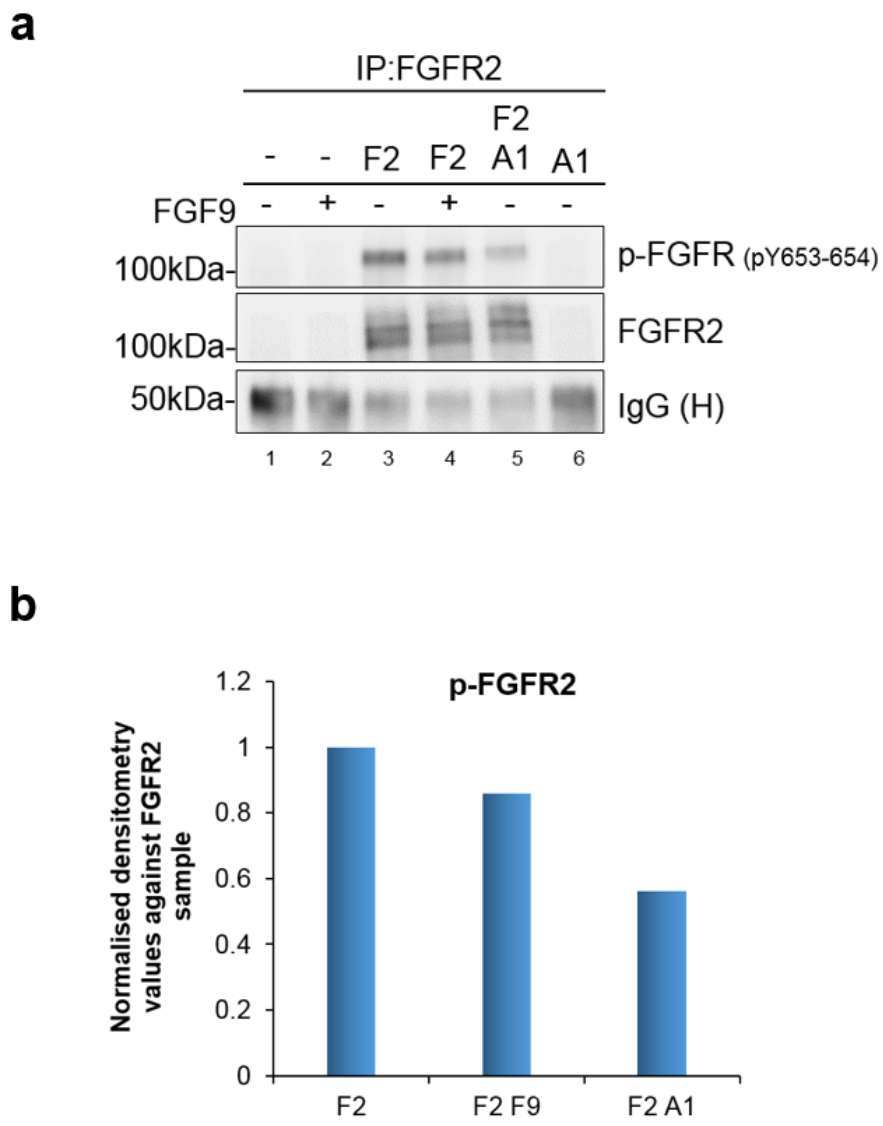

Figure 4. 3: Detection of basal p-FGFR2 levels in the presence of TRPA1. a) Co-IP experiment using an anti-FGFR2 antibody on un-transfected and FGFR2-FLAG and/or tGFP-TRPA1-transfected HEK-293T cells. Results were analysed by western blot for p-FGFR. b) Quantification of co-IP results in a bar graph illustrating the p-FGFR2/total FGFR2 ratio normalised against the FGFR2 sample (n = 1).

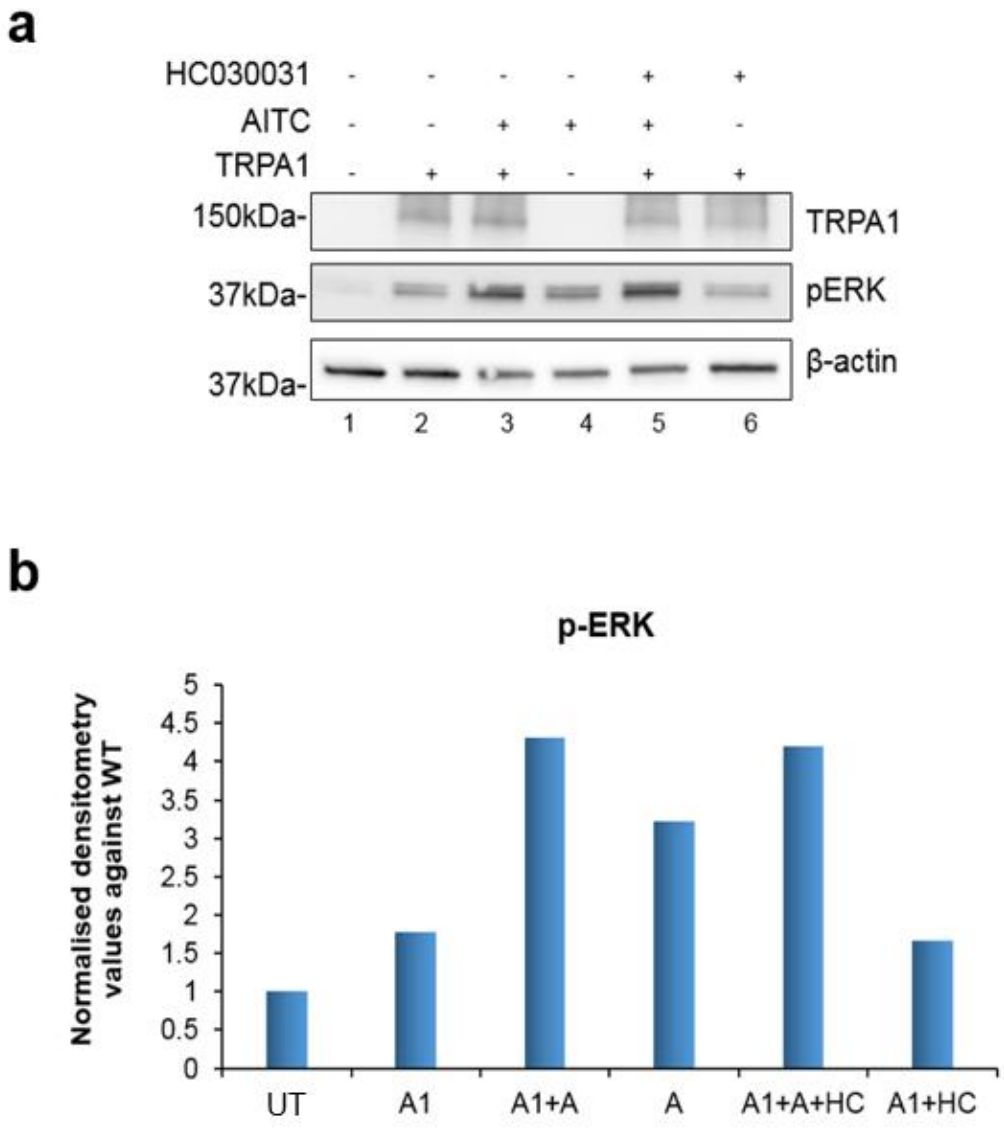

Figure 4. 4: TRPA1 increases p-ERK. a) Western blot on un-transfected (UT) or tGFP-TRPA1-transfected HEK-293T cells that were serum starved or treated with AITC and/or HC030031 using antibodies against the indicated proteins. Treatment with AITC or HC030031 and TRPA1 transfection are indicated by – and +. β-actin was used as a loading control. b) Quantification of the western blot by densitometry using ImageJ. Densitometry values were normalised against β-actin and presented as a fold-change compared to the control (un-transfected cells) (n = 1).

4.2.2. The FGFR2-TRPA1 co-expression affects FGFR2 dimerisation

The canonical RTK activation mechanism requires dimerisation between two receptor monomers prior to kinase activation, and subsequent increase in phosphorylated tyrosine residues (p-FGFR2). In the previous section, it was demonstrated that the basal p-FGFR2 levels are decreased in the presence of TRPA1 and therefore, it was hypothesised that the TRPA1 binding can influence FGFR2 dimerisation. To investigate the effect of TRPA1 on FGFR2 dimerisation, PLA experiments, specifically designed for receptor dimerization, were performed.

HEK-293T cells were double transfected with two differentially-tagged FGFR2 constructs: FGFR2-STREP and FGFR2-FLAG. Anti-STREP and anti-FLAG antibodies were utilised to detect the two different FGFR2 molecules and create PLA signal if located in proximity. In this case, proximity between the FGFR2 molecules is translated to dimer formation. The PLA signal was analysed in the presence and absence of TRPA1.

Firstly, it was crucial to confirm the efficiency of the triple transfection (FGFR2-STREP, FGFR2-FLAG and tGFP-TRPA1). Immunofluorescence staining of triple transfected cells (Figure 4.5) revealed that there are cells expressing all three proteins (yellow circle), as well as cells that miss the expression of TRPA1 (yellow arrows) or one of the FGFR2 receptors (red circle). Therefore, only GFP-positive cells (TRPA1 expression) with PLA signal (both FGFR2 expression) were analysed.

The PLA signal (n = 41 cells for FGFR2 only and n = 34 cells for FGFR2+TRPA1) corresponding to FGFR2 dimers was approximately 50%

lower (p-value ≤ 0.001 by Mann Whitney U test) in the presence of TRPA1 indicating inhibition of receptor dimerization (Figure 4.6).

Moreover, to verify the PLA results, FGFR2 dimerisation was studied by comparing the dimers/monomers ratio in the presence (reducing) and absence (non-reducing) of β-mercaptoethanol (β-ME) by Western blot. The ratio of FGFR2 dimers/monomers in FGFR2-expressing cells was approximately three times lower (n = 3, p-value ≤ 0.0001 by 2-way ANOVA with Tukey's post-hoc) in the presence of β-ME, a chemical agent reducing the disulphide bonds which could possibly stabilise the dimer (lane 1 and 2). When the cells were co-transfected with TRPA1, the dimers/monomers ratio in absence of β-ME was significantly decreased by approximately 40% (n = 3, p-value ≤ 0.0001 by 2-way ANOVA with Tukey's post-hoc) which indicates TRPA1 has an inhibitory effect on FGFR2 dimerisation (Figure 4.7a, lane 1 and 3, and b). Similar to the FGFR2 condition, β-ME decreased the ratio in FGFR2+TRPA1-expressing cells by three-fold (lane 3 and 4). Cells expressing FGFR2 and treated with FGF9 were used as a positive control however, no differences were observed between treated and non-treated ratios (Figure 4.7a, lanes 1 and 5, and c).

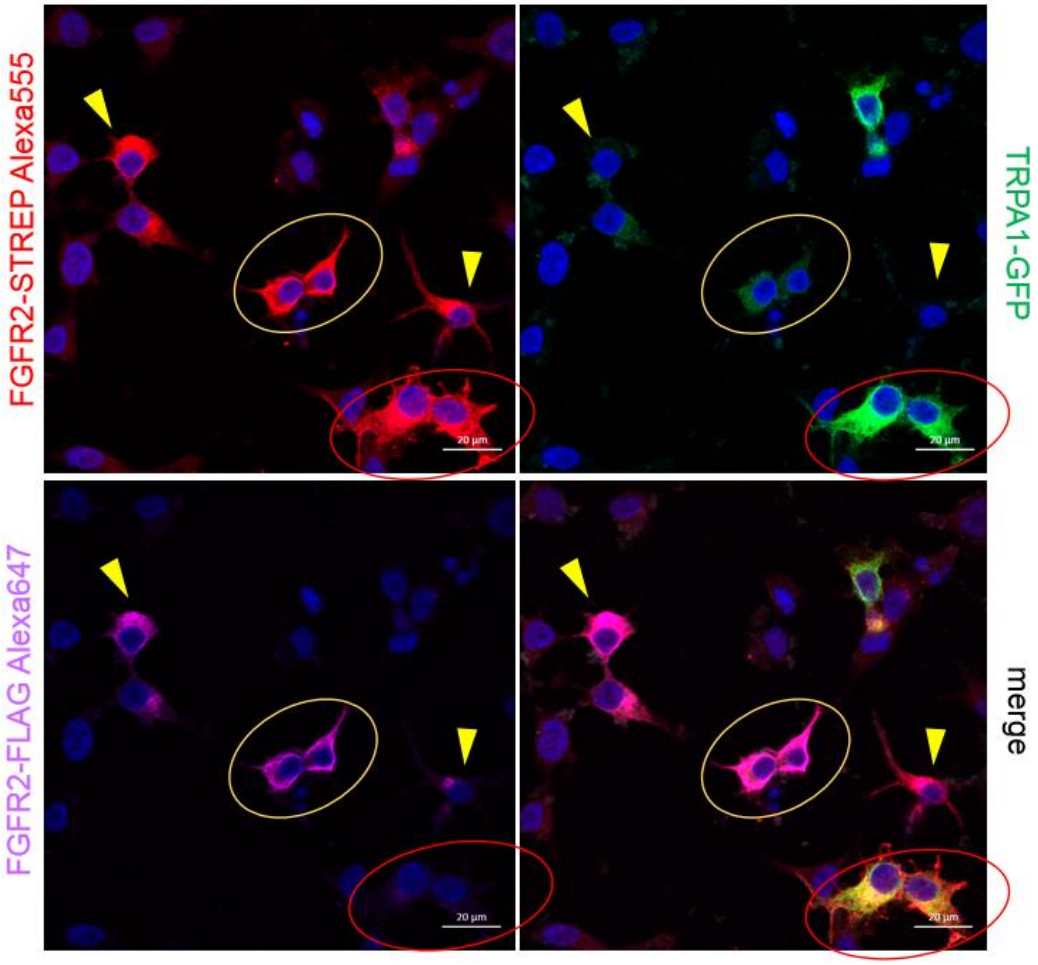

Figure 4. 5: Efficiency of triple transfection for tGFP-TRPA1, FGFR2-FLAG and FGFR2-STREP by Immunofluorescence. Immunofluorescence staining of HEK-293T cells transfected with tGFP-TRPA1 (green), FGFR2-FLAG (magenta) and FGFR2-STREP (red). Cells expressing all three proteins are indicated by a yellow circle. Cells expressing both FGFR2 constructs but no TRPA1 are indicated by the yellow arrow. Cells expressing TRPA1 and FGFR2-STREP, but no FGFR2-FLAG are indicated by a red circle. Representative images are presented. Scale bar = 20µm.

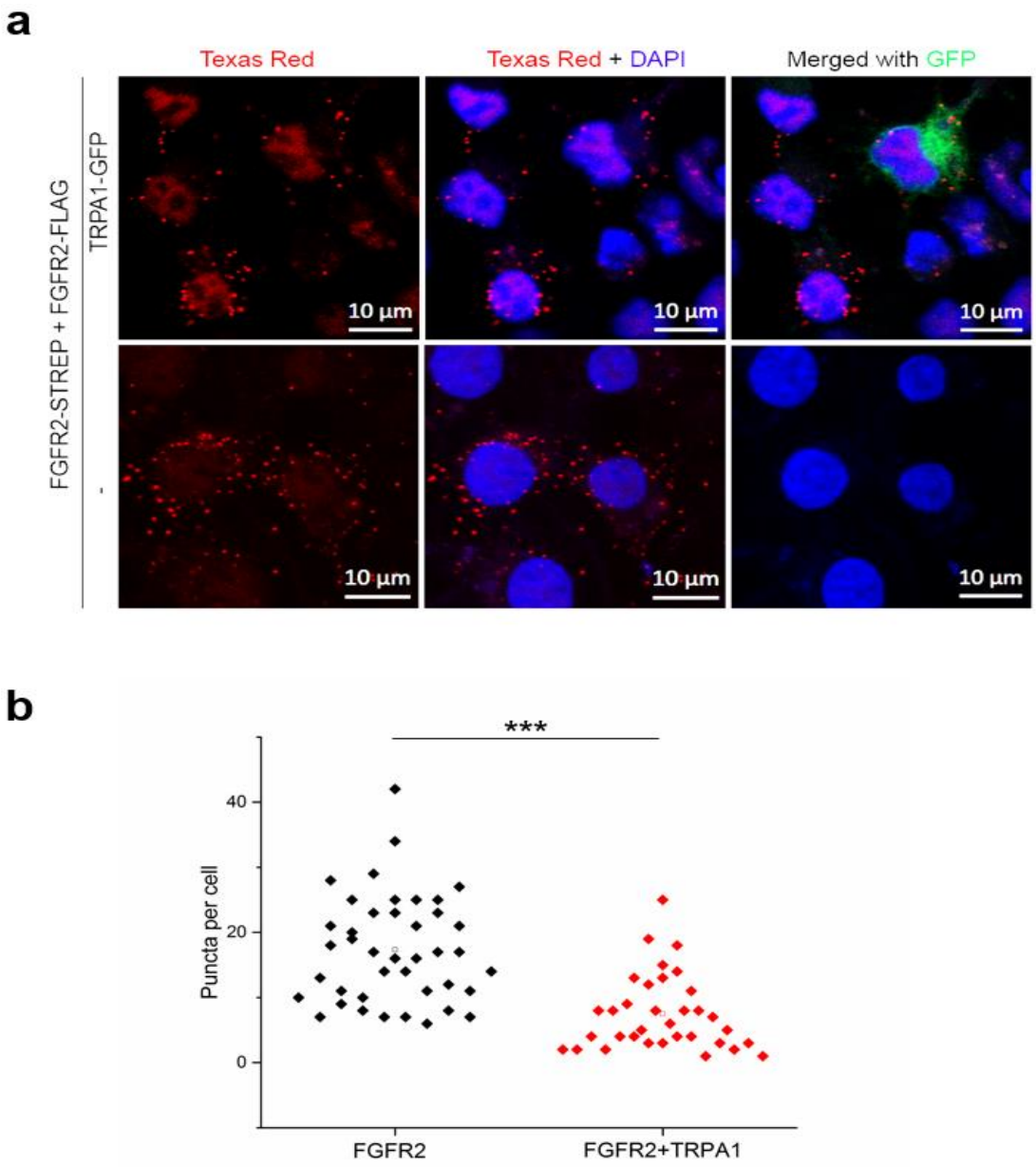

Figure 4. 6: TRPA1 inhibits FGFR2 dimerisation as shown by PLA. a) Representative images of PLA on FGFR2-STREP and FGFR2-FLAG in the presence and absence of tGFP-TRPA1. PLA is indicated with Texas Red, DAPI = nucleus, GFP = TRPA1. Scale bar = 10µm. b) Quantification of three technical replicates from this PLA experiment (n = 1). The scatter blot illustrates the number of PLA puncta per cell in the presence and absence of TRPA1. Significant difference is indicated by *** (p-value ≤ 0.0001, by non-parametric Mann Whitney U test). FGFR2 = 41 cells, mean = 17.3 puncta per cell. FGFR2+TRPA1 = 34 cells, mean = 7.5 puncta per cell.

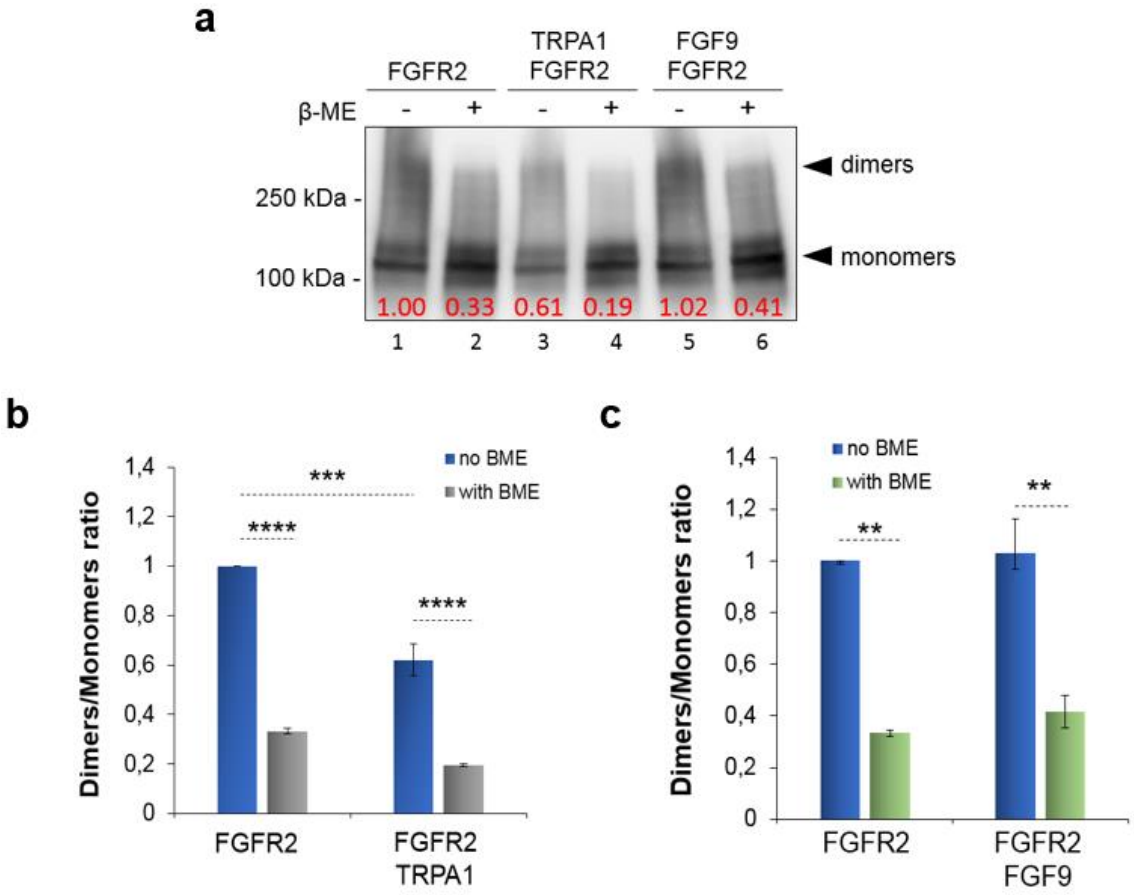

Figure 4. 7: FGFR2 dimers are decreased in the presence of TRPA1. a) Lysates from HEK-293T cells transfected with FGFR2-FLAG and FGFR2-FLAG+tGFP-TRPA1, were subject to SDS-PAGE and mixed with SDS loading buffer in the presence or absence of β-mercaptoethanol (β-ME). Results were visualised by a Western blot against total FGFR2. FGFR2 monomers and dimers are indicated by black arrows. The average normalised dimers/monomers ratio for each condition is shown in red. b) and c) Quantification of the dimers and monomers by densitometry using ImageJ. Dimers densitometry values were divided by the monomers values creating the dimers/monomers ratio which was normalised against the FGFR2 without β-ME sample. ns = non-significant. Significant differences are indicated by asterisks (2-WAY ANOVA with Tukey's multiple comparisons analysis, n = 3). Error bars = S.E.M.

4.2.3. Reduced PLCγ1-FGFR2 interaction in the presence of TRPA1

The experiments, so far, suggest that the FGFR2-TRPA1 interaction inhibits basal receptor dimerization (Figure 4.6), activation and FGFR2-mediated PLCγ1 phosphorylation (Figure 4.1). Based on the literature, PLCγ1 directly interacts with the FGFR2 receptor and acts as a substrate for phosphorylation that will eventually activate the phospholipase (Huang et al., 2016). To study the FGFR2-PLCγ1 binding in the presence and absence of TRPA1, co-IP experiments were performed. Anti-FGFR2 antibody was utilised to precipitate FGFR2 and the presence of PLCγ1 was detected with an anti-PLCγ1 antibody by western blot. PLCγ1 was precipitated with FGFR2, confirming interaction between the two proteins. However, there was an approximately 30% reduction when cells were co-transfected with TRPA1 which indicates TRPA1-mediated inhibition of the FGFR2-PLCγ1 interaction (figure 4.8).

Reduced FGFR2-PLCγ1 interaction can be translated into lower levels of p-PLCγ1 bound to FGFR2. Similar co-IP experiment was performed to detect differences in the p-PLCγ1 levels that are bound to FGFR2. As shown in Figure 4.9, p-PLCγ1 levels, precipitated by FGFR2, were approximately 50% reduced in the presence of TRPA1. Notably, p-PLCγ1 levels were not increased following FGF9 stimulation.

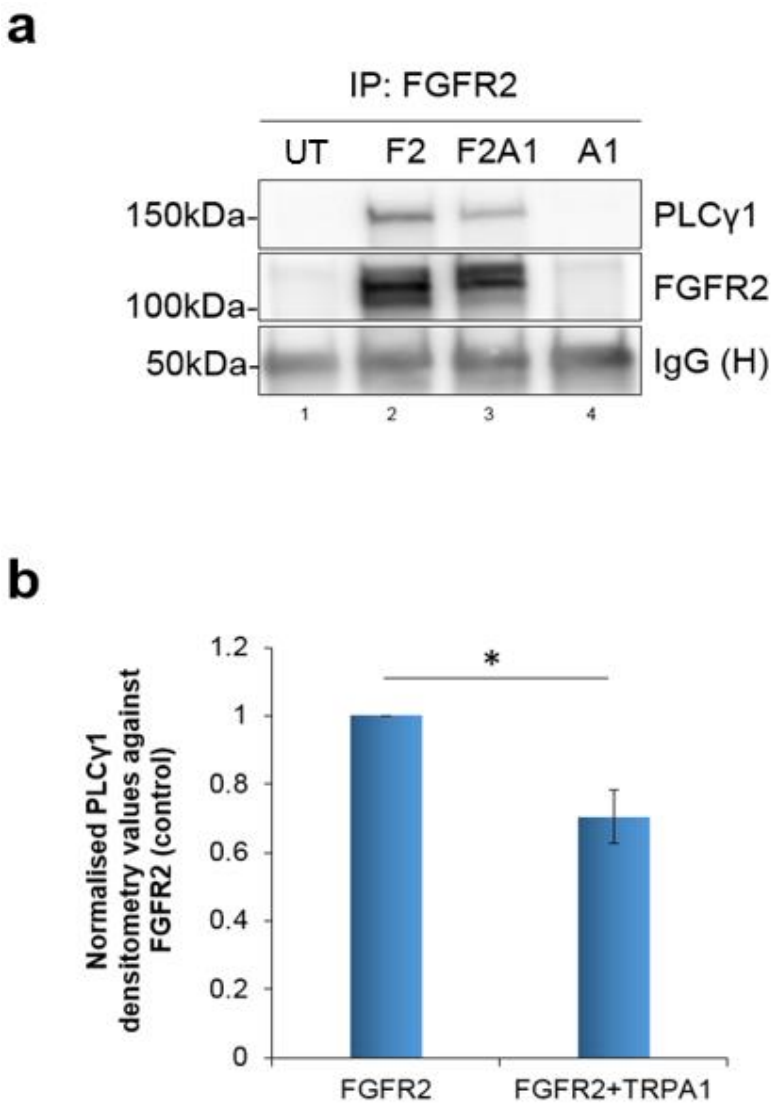

Figure 4. 8: TRPA1 inhibits basal PLCγ1-FGFR2 binding as shown by co-IP. a) Co-IP on un-transfected (UT) and FGFR2-FLAG and/or tGFP-TRPA1-transfected HEK-293T cells using an anti-FGFR2 antibody (Santa Cruz). Results were visualised by Western blot for the indicated proteins. b) Quantification of western blot by densitometry using ImageJ. PLCγ1 densitometry values were normalised against FGFR2 levels. Bar Graph illustrates the fold-change in the PLCγ1 precipitation in the presence compared to the absence of TRPA1 (n = 3), Error bars = S.E.M.

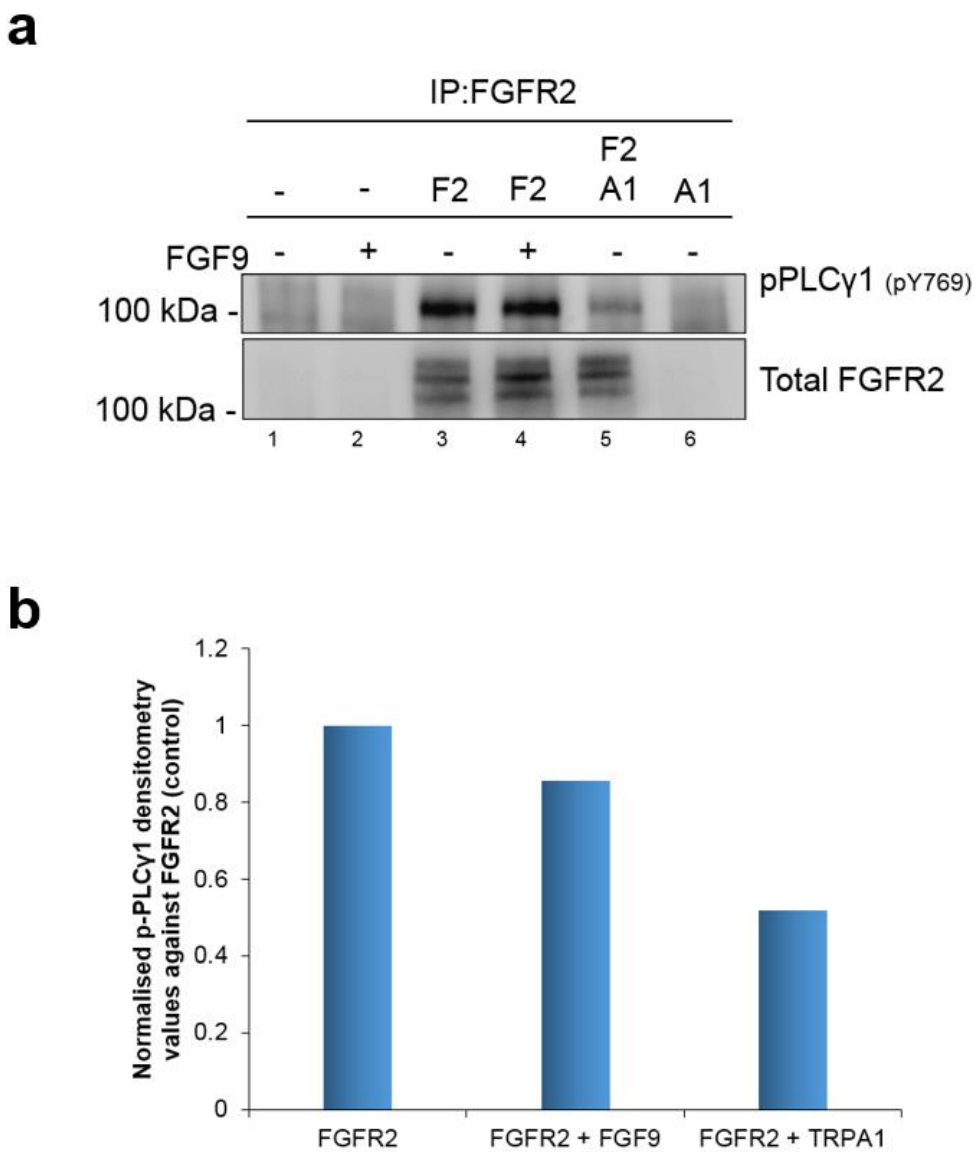

Figure 4. 9: Reduced p-PLCγ1 bound to FGFR2 in the presence of TRPA1. a) Co-IP on non-transfected and FGFR2-FLAG and/or TRPA1-tGFP-transfected HEK-293T cells using an anti-FGFR2 antibody (Santa Cruz). Results were visualised by Western blot for the indicated antibodies. b) Quantification of western blot by densitometry using ImageJ. p-PLCγ1 densitometry values were normalised against FGFR2 levels. Bar Graph illustrates the fold-change in the p-PLCγ1 precipitation in the presence compared to the absence of TRPA1 (n = 1).

4.2.4. TRPA1 allows FGFR2 activation under stimulating conditions but hinders PLCγ1 binding to the receptor

To further understand the mechanism by which TRPA1 inhibits PLCγ1 binding to FGFR2, it was important to monitor the phosphorylation levels of Y769 on FGFR2, which is the PLCγ1 binding site (Huang et al., 2016). Co-IP experiments were performed on HEK-293T cells transfected with FGFR2-STREP in the presence and absence of tGFP-TRPA1 (Figure 4.10). An anti-FGFR2 antibody was used to precipitate FGFR2 and the phosphorylation levels of both FGFR2 A-loop (Y653-654) and Y769 were detected by an anti-p-FGFR and anti-pY769 antibody, respectively. The binding of PLCγ1 and TRPA1 was also detected by an anti-PLCγ1 and anti-TRPA1 antibody, respectively. As shown in previous experiments, PLCγ1 binding and p-FGFR levels were drastically reduced in the presence of TRPA1 (lanes 3 and 5). According to the densitometry values, pY769 levels were also reduced in the presence of TRPA1, which could suggest a mechanism for the TRPA1-mediated PLCγ1 binding reduction (Figure 4.10). However, due to the poor quality of the antibody as well as the single repeat of the experiment, pY769 levels cannot be identified with certainty.

Based on the general RTK signalling, receptor stimulation by a ligand causes increased tyrosine phosphorylation and activation of the receptor. To test this phenomenon in the presence of TRPA1, cells treated with FGF9 were also included in the previous co-IP experiment. Firstly, the interaction between FGFR2 and TRPA1 under stimulating conditions was confirmed by detection of precipitated TRPA1 in both the absence and presence of FGF9 (Figure 4.10, lanes 5 and 6, TRPA1 panel). p-FGFR2 (A-loop) as well as pY769 levels were also studied. Interestingly, p-FGFR (A-loop) levels, in this

one experiment, were increased upon stimulation in cells expressing FGFR2-STREP+tGFP-TRPA1, which could suggest that FGFR2 can be activated by its ligand in the presence of TRPA1 (lane 5). However, more repeats are necessary to fully understand the regulation of the receptor in the presence of stimulation. Once again, the pY679 levels in the presence of FGF9 could not be identified with certainty due to the poor signal to noise ratio in the western blot. Interestingly, PLCγ1 binding to FGFR2 did not increase in the presence of FGF9 compared to no FGF9 stimulation even though A-loop tyrosine residues seemed to be phosphorylated (lanes 5 and 6).

Therefore, the IP in Figure 4.10 suggests that the FGFR2-TRPA1 interaction still occurs following FGF9 stimulation possibly resulting in receptor activation, yet TRPA1 still inhibits PLCγ1 binding. One possible explanation could be that TRPA1 physically hinders the binding of PLCγ1 to the receptor. To test this hypothesis, co-IP experiments were performed with an anti-TRPA1 antibody on FGFR2-FLAG+tGFP-TRPA1-expressing cells (Figure 4.11). If FGFR2, interacting with TRPA1 through the C-terminal domain, can still interact with PLCγ1, then TRPA1 would be able to precipitate PLCγ1, because they would all form a complex. The ability of TRPA1 to co-precipitate PLCγ1 indirectly and through FGFR2 was tested by probing for PLCγ1 in the western blot. TRPA1 precipitated FGFR2 but not PLCγ1. This result could suggest that TRPA1, FGFR2 and PLCγ1 do not form a complex all together and that TRPA1 may therefore physically occlude the binding site for PLCγ1 (lane 3). As a negative control TRPA1-expressing cells were used to show that TRPA1 does not interact with PLCγ1 in the absence of FGFR2 (lane 4).

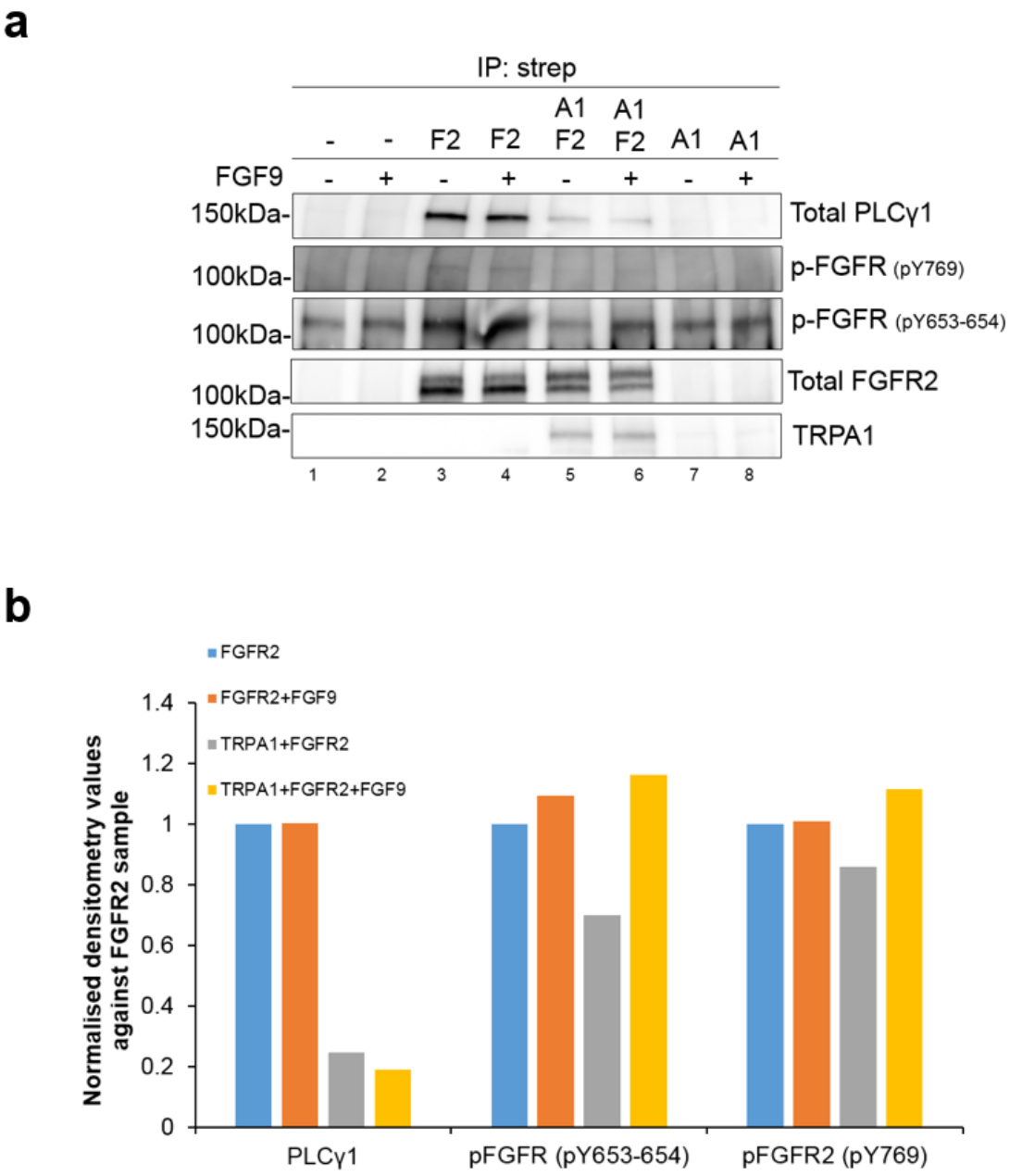

Figure 4. 10: FGFR2 phosphorylation in the presence of TRPA1 and FGF9. a) Co-IP on un-transfected and FGFR2-STREP and/or tGFP-TRPA1-transfected HEK-293T cells using an anti-FGFR2 antibody (Santa Cruz). Results were visualised by Western blot for the indicated proteins. b) Quantification of western blot by densitometry using ImageJ. All densitometry values were normalised against FGFR2 levels. Bar Graph illustrates the fold-change in the PLCγ1, p-FGFR and p-Y769 levels in the

presence and absence of TRPA1 and FGF9 compared to the control sample (FGFR2-expressing cells) (n = 1).

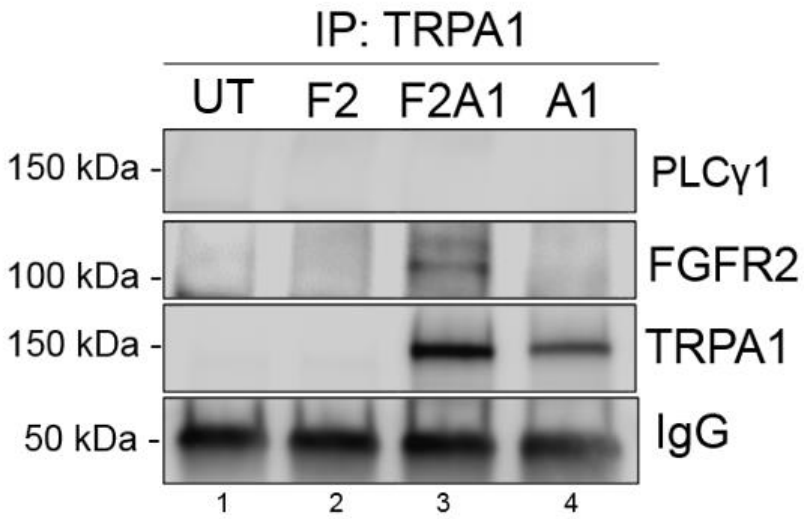

Figure 4. 11: TRPA1 does not form a complex with FGFR2-PLCγ1 through FGFR2. Co-IP on un-transfected (UT) and FGFR2-STREP and/or TRPA1-tGFP-transfected HEK-293T cells using an anti-TRPA1 antibody. Results were visualised by Western blot for the indicated antibodies.

4.3. Discussion

4.3.1. FGF9 as an agonist of FGFR2 signalling

FGF9 is a ligand that recognises the IIIc splice variant of FGFR2, FGFR1 and FGFR3 (Ornitz and Itoh, 2015). Throughout this chapter, FGF9 treatment has been used as a positive control that will activate FGFR2 and downstream signalling pathways. However, FGF9-treated cells over-expressing FGFR2, consistently lack increased levels of p-FGFR2 and p-PLCγ1, while exhibiting elevated levels of p-ERK, compared to un-treated cells (e.g. Figure 4.1).

The fact that FGFR2 forms pre-dimers even in the absence of extracellular stimulation could possibly explain this phenomenon (Lin et al., 2012). Pre-dimer formation and basal phosphorylated receptor levels have been reported for other RTKs in the past including, EGFR, VEGFR and TrkB (Sarabipour et al., 2016; Shen and Maruyama, 2012; Yu et al., 2002). Only EGFR dimers have been shown to be un-phosphorylated which highlights the unique characteristics of each RTK. Hence, it is speculated that RTKs exist in a monomer-dimer equilibrium prior to ligand stimulation, which eventually fully activates the receptors. In the present study, over-expression may have caused excessive levels of FGFR2 which shifted the equilibrium towards predominantly dimers due to protein abundance. Basal p-FGFR2 levels are probably saturated and no difference can be detected by treatment with FGF9 (Figure 4.1a lane 3 and 4).

An alternative approach to detect differences in the p-FGFR2 levels between FGF9-treated and untreated cells would be to generate a stable cell line

expressing low levels of FGFR2 which would also eliminate variations originating from transient transfections. Chi-Chuan, and colleagues, for instance, were able to detect p-FGFR2 differences, albeit small, by utilising an FGFR2-stable cell line (Lin et al., 2012).

This hypothesis described above is somewhat undermined by the fact that treatment with FGF9 increased p-ERK levels but not p-PLCγ1 in FGFR2-transfected cells (Figure 4.1). Hence, it would be tempting to speculate that FGF9 may have a pathway-specific effect on FGFR2, whereby it activates ERK but not the PLCγ1 pathway. Ming-Min Chang and colleagues have shown that the FGF9/FGFR2 does not activate PLCγ1 in mouse Leydig cancer cells (Chang et al., 2018). Jih-Ing Chuang and colleagues demonstrated similar results for FGF9/FGFR2 in cortical and dopaminergic neurons (Chuang et al., 2015). In contrast, other studies show activation of both pathways in cells including human uterine endometrial stromal cells (Wing et al., 2005), indicating that the downstream signal programming highly depends on the cell type. Timsah and colleagues have also detected higher levels of p-PLCγ1 following FGF9 treatment in HEK cells stably transfected with FGFR2, indicating that it is posing further questions to why PLCγ1 pathway was not activated in the present experiments (Timsah et al., 2014).

One possible explanation for the difference in pathway activation is that the PLCγ1 pathway was already fully activated prior to stimulation, the same way the FGFR2 phosphorylation was saturated. This hypothesis contradicts previously published studies demonstrating that RTK pre-dimer formation on its own does not activate downstream signalling (Lin et al., 2012; Timsah et

al., 2014). However, these studies were emphasised on the MAPK pathway and showed no further activation prior to ligand stimulation - they did not investigate p-PLCγ1 levels before and after stimulation. The results in the present study suggest that FGFR2 pre-dimers, even though unable to fully activate the MAPK pathway (only basal levels), are still able to induce PLCγ1 signalling, even in the absence of FGF9.

The reason behind differences in activation of ERK and PLCγ1 downstream pathways observed in this chapter is still unclear. Chi-Chuan and colleagues proposed that dimeric GRB2, that binds to the C-terminal proline-rich motif of FGFR2 promoting receptor dimerization, inhibits downstream signalling by masking key residues. With that said, it is likely for PLCγ1 to not be affected by this regulation, since PLCγ1 is a direct substrate of FGFR2 and there are less regulatory points into activating the pathway compared to ERK, which is located further downstream in the cascade. Further experiments are needed to understand the basal and stimulated FGFR2 signalling.

4.3.2. FGFR2-TRPA1 interaction affects p-FGFR2 and p-PLCγ1 but not p-ERK levels

Western blot experiments revealed that the basal p-FGFR2 levels were decreased by approximately 50% in the presence of TRPA1 (Figure 4.1, 4.2, 4.3, lane 3 and 5). The antibody used recognises phosphorylated Tyrosine residues (pY653-654) in the activation loop of FGF Receptors which are important for catalytic activity. Phosphorylation of Y653 increases kinase activity by 50 to 100-fold, while phosphorylation of Y654 increases it by an extra 10-fold (Lew et al., 2009). Therefore, decreased p-FGFR levels are an

indication of decreased FGFR kinase activity. Here, the results suggest that interaction of TRPA1 with FGFR2 results in reduced phosphorylation and consequently, lower kinase activity. The exact mechanism of inhibition is not investigated. However, it could be hypothesised that either TRPA1 dissociates FGFR2 dimers or has an interaction-induced allosteric effect on the FGFR2 kinase activity.

Following p-FGFR2 levels, downstream signalling pathways were also investigated. Firstly, p-PLCγ1 levels were decreased by approximately 60% (Figure 4.1, lane 3 and 5) indicating lower phospholipase activity and pathway activation. Since PLCγ1 is a direct substrate of FGFR2, reduced phosphorylated levels are expected as a result of lower FGFR2 kinase activity.

Normally, lower p-FGFR2 levels lead to lower p-ERK however, this is not the case in the present experiment. The MAPK pathway was not altered by the presence of TRPA1 (Figure 4.1-4.2, lane 3 and 5). However, it is likely that the FGFR2-mediated ERK phosphorylation is actually inhibited by TRPA1 but at the same time, the presence of TRPA1 alone could be causing MAPK activation which compensates for the actual reduction caused by the FGFR2-TRPA1 interaction.

Indeed, the western blot in Figure 4.4 shows that TRPA1 alone can increase p-ERK levels (lane 1 and 2). Additional treatment with AITC increases p-ERK even further (lane 2 and 3) which is consistent with previous studies (J.-L. Chen et al., 2017; Schaefer et al., 2013; Takahashi et al., 2018). However, it is not clear whether the increase is TRPA1-mediated because AITC alone can still activate non-TRPA1-expressing HEK cells (lane 1 and

4). These data are similar with studies showing that AITC treatment increases p-ERK levels in different cell types including the MDA-MB-468 human breast adenocarcinoma cells and PC-3 prostate cancer cells (Tsai et al., 2012; C. Xu et al., 2006). The use of HC030031 as a specific TRPA1 inhibitor did not have an effect on p-ERK levels indicating that either the inhibition was not sufficient or p-ERK increase is calcium-independent (lane 5 and 6). Based on previously mentioned studies, p-ERK increase is calcium-induced. The experiment was performed once, and more repeats are needed to ensure significant differences. Alternatively, the same experiment can be performed with cells cultured in presence and absence of EGTA (calcium chelator) that will abrogate calcium influx from the extracellular space and therefore, calcium-mediated effects can be detected. Similar information can be obtained from experiments using a pore mutant of TRPA1 that will not be capable of current conductance and thus, show whether the p-ERK increase is an indirect effect of TRPA1 expression or TRPA1 current-dependent.

Nevertheless, results from this western blot (Figure 4.4) in combination with literature suggest that it is plausible for TRPA1 to induce ERK phosphorylation indicating that p-ERK levels are both FGFR2- and TRPA1-dependent, further complicating the interpretation of the results (Figure 4.1, lane 3 and 5, p-ERK panel).

In conclusion, western blots on transfected HEK-293T cells suggest that TRPA1 inhibits FGFR2 phosphorylation and subsequent kinase activity that results in a decrease in PLCγ1 phosphorylation, while maintaining levels of p-ERK unaffected.

4.3.3. TRPA1 binding to FGFR2 affects receptor dimerisation

FGFR2 dimerisation was investigated by PLA in the presence and absence of TRPA1. PLA signal was approximately 50% lower in the presence of TRPA1 suggesting inhibition of dimerization (Figure 4.7). This result could possibly justify the TRPA1-mediated reduction in p-FGFR2 levels detected by western blot (Figure 4.1). However, there are certain limitations deriving from the protein expression levels that should be considered prior to any conclusions.

The main limitation is the variability of protein expression due to transient transfections. It was noticed that not all cells express all three transfected proteins, let alone similar levels. Cells stably transfected with proteins of interest would be more suitable for this experiment. Apart from the variability derived from transient transfections, possible competition for the transcriptional machinery could have created variability too, since FGFR2-FLAG and tGFP-TRPA1 are under the control of CMV promoter. Taken together with the findings in Figure 4.7, reduced PLA signal could originate from lower expression of one of the receptors (STREP or FLAG tagged) when co-expressed with TRPA1, instead of actual inhibition of dimerization by TRPA1.

However, FGFR2 multimer separation in non-reducing conditions (no β-ME) in an SDS-PAGE revealed similar results. The FGFR2 dimer/monomer ratio was 40% lower in the presence of TRPA1 suggesting that TRPA1 inhibits dimerization of the receptor (Figure 4.7).

Cell lysates are usually loaded and resolved in a native polyacrylamide gel without detergents (no SDS) or reducing agents (no β-ME) to compare

monomer and dimer levels between treatments (Yu et al., 2002). In our case, the samples were resolved in the presence of SDS so that any FGFR2-TRPA1 complexes are dissociated and thus, strictly FGFR2 dimers and monomers are analysed and fully resolved. Therefore, the comparison was made between presence and absence of β-ME. However, not clear and distinctive bands for dimers were formed and therefore, additional experiments could enhance this interpretation. For example, comparing the pull down between FGFR2-FLAG and FGFR2-STREP in the presence and absence of TRPA1 would also show whether there is an inhibition in the dimerization/interaction between the two receptor versions.

Another important finding from this experiment could be that disulphide bonds are crucial for FGFR2 dimerisation since their disruption reduces FGFR2 dimers in all samples (FGFR2, FGFR2+TRPA1, FGFR2+FGF9). The importance of disulphide bonds in RTK dimerisation including TrkB and p75 receptors has been proposed in the past (Nadezhdin et al., 2016; Shen et al., 2019). The present results are also consistent with studies on FGFR2 and FGFR3 Cysteine mutants that cause increased dimerisation through formation of intermolecular disulphide bonds (Adar et al., 2002; Liao et al., 2013; Plotnikov et al., 2000; Sarabipour and Hristova, 2016).

Even though inhibition of dimerisation is consistent with lower p-FGFR2 and p-PLCγ1 levels, it does not explain the unaffected levels of p-ERK. Therefore, it is speculated that TRPA1 promotes ERK activation through an FGFR2-independent mechanism that masks the actual MAPK signalling inhibition derived from their interaction, as discussed in the section 4.3.2. This would also imply that TRPA1 does not inhibit FGFR2 allosterically.

It can be speculated that TRPA1 passively inhibits FGFR2 dimerisation due to competition with GRB2. Dimeric GRB2 binding on the C-terminal proline-rich motif, causes FGFR2 dimerisation in unstimulated conditions. Therefore, TRPA1 being highly expressed, overtakes the binding site for GRB2 resulting in an indirect prevention of pre-dimer formation.

4.3.4. TRPA1 physically hinders PLCγ1 binding to FGFR2

The results obtained so far reveal lower levels of p-PLCγ1 as a result of TRPA1 binding to FGFR2. Moreover, co-IP experiments show reduced PLCγ1 and p-PLCγ1 binding to FGFR2 in the presence of TRPA1, which explains the lower phosphorylation levels (Figure 4.8 and 4.9). However, it is not clear how TRPA1 achieves reduced FGFR2-PLCγ1 binding. To address that, the PLCγ1-FGFR2 binding was studied upon stimulation with FGF9.

A co-IP experiment suggested that TRPA1 and FGFR2 can still interact even in the presence of stimulation by FGF9 (Figure 4.10). Results from one experiment showed that even if FGFR2 can possibly be activated by FGF9 in the presence of TRPA1 (increased A-loop phosphorylation), PLCγ1 binding to the receptor is still reduced. Therefore, the FGF9/FGFR2-mediated PLCγ1 pathway is inhibited in the presence of TRPA1. However, this hypothesis is based on one repeat and more repeats are necessary to validate this preliminary result. On the other hand, due to poor signal to noise ratio, results for pY769 levels (PLCγ1 binding site) could not be interpreted with certainty.

An additional preliminary co-IP experiment (Figure 4.11) could suggest that TRPA1 sterically hinders the binding of PLCγ1 to FGFR2 because an anti-TRPA1 antibody was not able to indirectly co-precipitate PLCγ1 through the

FGFR2-TRPA1 interaction. This result could mean that they cannot form a PLCγ1-FGFR2-TRPA1 complex in the presence of TRPA1, most likely because both PLCγ1 and TRPA1 share adjacent binding sites on FGFR2 (Figure 4.11). The two PLCγ1 binding sites on FGFR2 (p-Y769 and Proline-rich motif) are likely covered by TRPA1. If this hypothesis is valid, it could be plausible for PLCγ1, TRPA1 as well as GRB2 to complete for the binding site on FGFR2, since they all bind in adjacent areas located in the C-terminal domain. Therefore, the equilibrium between these proteins could regulate FGFR2 signaling. Competition experiments would shed more light into the dynamics of this network of interactions and validate this hypothesis.

More repeats are necessary to verify significant results and to achieve more certainty in conclusions. However, a hypothetical model of FGFR2-TRPA1 physical and functional interaction can be constructed based on the findings so far combined with literature on FGFR2 signalling (Figure 4. 12). In summary, TRPA1 directly interacts with the C-terminal domain of FGFR2 through the ARD (1-10 repeats). The interaction causes inhibition of basal FGFR2 phosphorylation levels. The mechanism behind FGFR2 inhibition is not clear however, it is most likely due to inhibition of basal dimerization induced by GRB2.

Reduced basal p-FGFR2 levels result in lower downstream signaling including the MAPK and the PLCγ1 pathway. Activation of the MAPK pathway, however, could be rescued by an FGFR2-independent and TRPA1-mediated mechanism. However, further experiments are needed to elaborate on the MAPK pathway regulation and validate the hypothesis.

TRPA1 inhibits the binding of PLCγ1 to FGFR2, most likely by physically hindering the binding site for PLCγ1, causing the inhibition of the pathway.

In contrast, only preliminary hypothesis can be made regarding stimulating conditions due to lack of experimental repeats. Therefore, TRPA1 and FGFR2 interaction could occur under FGF9 stimulation and could cause FGFR2 activation and phosphorylation (A-loop at least) while maintaining PLCγ1 inhibition. A proposed model is shown in Figure 4.12. Nevertheless, more experimental repeats are needed to ensure significant effects.

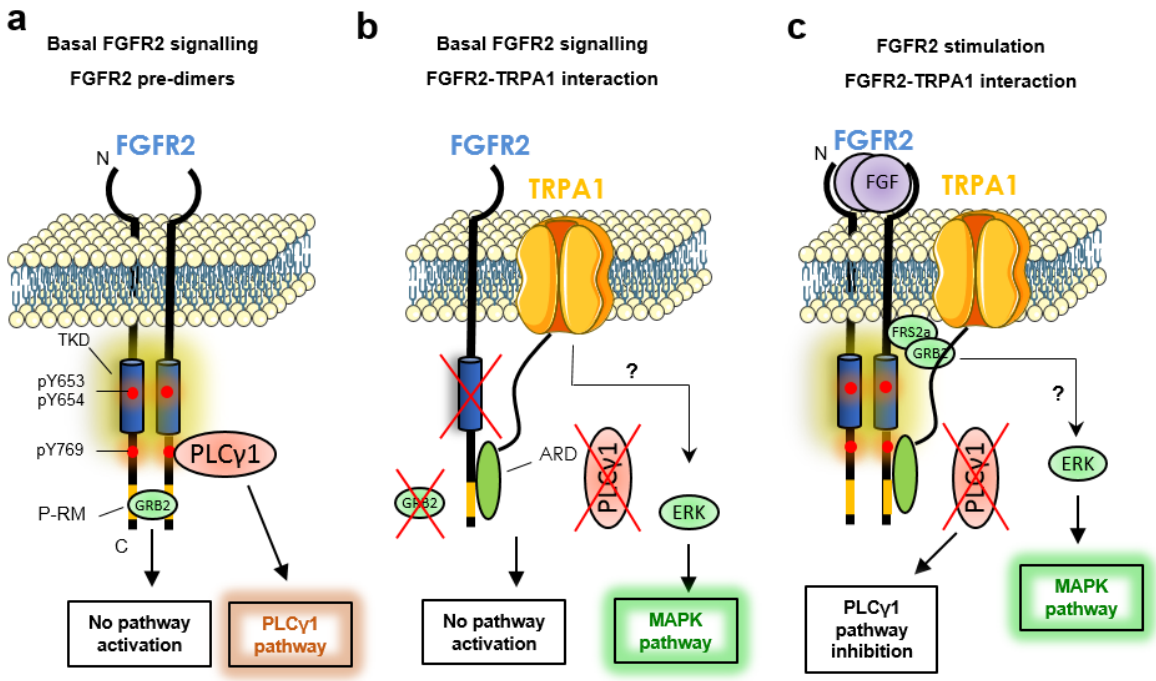

Figure 4. 12: Schematic of the hypothetical FGFR2-TRPA1 model of interaction.

a) Basal/Unstimulated conditions: Dimeric GRB2 binds to the proline-rich motif of FGFR2 causing receptor pre-dimers that cannot activate the MAPK pathway, as previously shown in the literature. However, pY769 is possibly still accessible to PLCγ1 and could result in phosphorylation by FGFR2 and activation of the PLCγ1 pathway.

b) Basal FGFR2 in Presence of TRPA1: the TRPA1 ARD binds to the C-terminal domain of FGFR2 possibly preventing GRB2 from binding and causing receptor dimerization. Thus, tyrosines on FGFR2 monomers are no longer phosphorylated and no downstream pathway is activated. TRPA1 likely masks the proline-rich motif (second PLCγ1 binding site), preventing PLCγ1 from being phosphorylated and activated by the receptor. There is a possibility that TRPA1 itself can induce MAPK activation in an FGFR2-independent manner.

c) FGFR2 stimulation in TRPA1 presence: FGF9 stimulates FGFR2 dimerisation and complete activation of the kinase domain that can potentially induce downstream pathways including the MAPK and PLCγ1 pathway. However, based on co-IP experiments, FGFR2-bound TRPA1 could still block the binding site for PLCγ1 (pY769) as well as the proline-rich motif (second binding site), completely inhibiting PLCγ1 activation. Activation of the MAPK pathway in stimulating conditions was not investigated.

4.3.5. The effect of TRPA1 on FGFR2 activation: comparison with published model

Notably, there are differences between the model described in this thesis and the model we published 2 years ago (Berrout et al., 2017). Even though both models involve the interaction of FGFR2 and TRPA1, the findings from our publication supported the activation of basal FGFR2 and downstream signalling by TRPA1 rather than inhibition, as described here. Particularly, TRPA1 was suggested to act as a molecular scaffold that brings two FGFR2 monomers in proximity causing receptor dimerization and activation. Differences in methodology as well as use of different cells could possibly be the reason for this discrepancy.

As mentioned before, FGFR2 was expressed in high levels, as a result of the transient transfection, which saturated the activation state of the receptor. No further activation could be detected as seen using FGF9 and therefore, potential activation by TRPA1 would not be detected either. The binding of TRPA1 to FGFR2 could then induce the internalisation of the receptor as a response to activation, resulting in less p-FGFR2 in the western blot. Next, FGF9 effect on FGFR2 signalling was potentiated when

cells overexpressed TRPA1 suggesting that lower levels of FGFR2 are crucial for studying activation. Therefore, the FGFR2 levels can potentially affect the fate of FGFR2 signalling.

Another important observation was the fact that total FGFR2 levels were increased when HEK-293T cells were co-transfected with TRPA1 (western blot results not shown), suggesting that TRPA1 somehow induces FGFR2 expression. TRPA1 increases ERK and p38 pathway activation. These pathways can positively regulate FGFR2 expression through phosphorylation of pRb and subsequent release of E2F1 to the nucleus resulting in FGFR2 gene activation (D'Amici et al., 2013; Kondo et al., 2013). Another possible TRPA1-mediated mechanism of FGFR2 overexpression could be via the increased p-ERK and subsequent CREB activation that binds to the CRE (CREB Response Element) position on the CMV promoter located in the plasmid used for transient transfection (Chen and Stinski, 2002).

Therefore, to obtain equal amounts of total FGFR2 between single and double transfected cells, half the amount of FGFR2 plasmid was used for co-transfection with TRPA1. Phosphorylated FGFR2 levels were always normalised against the total FGFR2 levels to obtain an accurate result in the experiments presented herein. Therefore, it is possible that the detected increase in p-FGFR2 levels and FGFR2 activation, described in our publication, was a consequence of the TRPA1-induced FGFR2 gene overexpression.

Another possible explanation for our contradicting results is the use of different sub-cultures of HEK-293T cells ("older" cells). HEK-293T cells are

characterised by extreme chromosomal instability and karyotype diversity, reviewed by A.A. Stepanenko and V.V.Dmitrenko (Stepanenko and Dmitrenko, 2015). HEK-293 cells cultured in different banks or labs exhibit a variety of copy number alterations and numerical chromosome instability. For instance, HEK-293 cells from ATCC are hypotriploid with 30% of the cells having 64 chromosomes while HEK-293 cells from the European Collection of Cell Cultures (ECACC) have 62-70 chromosomes. Therefore, cells derived from different sources or undergone long-term culturing can exhibit chromosomal diversification which occurs due to expression of the E6/E7 oncoproteins of Papilloma virus 16, dysregulation of genes involved in genomic and chromosome stability, occasional lack of telomerase and rare multipolar mitosis.

Furthermore, transfection of HEK-293 cells with oncogenes or even empty vectors has been reported to affect chromosomal stability. Therefore, it is difficult to discriminate whether results are a consequence of the product of the transfected gene or a result of the chromosomal changes caused by the gene transfer (Stepanenko and Dmitrenko, 2015).

In our case, the use of a cell line with unstable genome over the period of 3.5 years would have caused enough genetic variations that were eventually able to alter the biological process. Taken together, it is likely that both activation and inhibition of FGFR2 signalling can occur depending on a third-party factor that has not been identified yet. Nevertheless, further experiments with various expression levels between components (competition experiments) as well as use of different cell types are

necessary to understand the true biological phenomenon and add information into our previous publication.

5. Chapter 5
Summary and Conclusion

This study provided the first indication of direct interaction between FGFR2 and TRPA1. Experimental evidence indicates that this interaction is mediated by the C-terminal domain of FGFR2 and the ARD of TRPA1 (AR1-10).

Preliminary super-resolution microscopy experiments suggested that the majority of the complexes exist in 1:1 and 2:1 stoichiometry (FGFR2:TRPA1). However, formation of higher order complexes cannot be excluded.

The role of the TRPA1 ARD in protein-protein interaction and channel regulation remains elusive. Here, we propose a novel role for the ARD which involves direct interaction with an RTK. According to our publication, FGFR2 inhibits TRPA1 activation highlighting the regulatory role of the ARD in channel activation (Berrout et al., 2017).

Protein expression of FGFR2 and TRPA1 was shown in a LUAD cell line. The endogenous FGFR2-TRPA1 complex formation was detectable in HCC-515 cells which implies a possible role in tumorigenic signal regulation.

To further understand the effect of TRPA1 on cancer signalling, the FGFR2 activity and downstream signalling pathways were subject to extensive investigation using over-expressed proteins. The major findings revealed that the site of interaction is very critical for the FGFR2 signal regulation in both the absence and presence of FGFR2 stimulation.

According to the literature as well as our findings, it is conceivable that TRPA1 could compete for the C-terminal domain of FGFR2 with GRB2 in basal conditions. This prevents GRB2 from binding resulting in inhibition of basal FGFR2 dimerisation as well as phosphorylation and downstream signal transduction.

Co-IP and western blot experiments (e.g. Figure 4.1, 4.8 and 4.10) also suggest that high levels of TRPA1 prevent PLCγ1 binding to the same C-terminal domain of FGFR2 upon stimulation, resulting in PLCγ1 pathway inhibition.

Taken together, our data could suggest a protective role of TRPA1 against FGFR2-mediated cancer metastasis. Activation of the PLCγ1 pathway by RTKs has been shown to increase cell motility and invasion and is linked to worse disease-free survival (Lattanzio et al., 2013; Timsah et al., 2014). Therefore, inhibition of the FGFR2-mediated PLCγ1 pathway activation by TRPA1 could abrogate invasion-related cellular responses. Functional assays including migration and invasion assays would strengthen this hypothesis.

In contrast, studies have also proposed that TRPA1 favours cancer progression. For instance, Takahashi and colleagues recently proposed that TRPA1 promotes cancer cell survival by activating anti-apoptotic mechanisms that overcome the oxidative stress conditions. These mechanisms involve calcium dependent activation of the RAS-ERK/AKT/mTOR pathways (Takahashi et al., 2018). Furthermore, our publication demonstrates FGFR2-mediated inhibition of TRPA1 activation as a result of direct interaction with the ARD (Berrout et al., 2017).

Consequently, our study indicates that the use of TRPA1 or FGFR2 levels alone as a prognostic marker is not adequate and proposes the combinatorial use of FGFR2, TRPA1, GRB2 and PLCγ1 expression level as prognostic markers for cancer progression. High levels of FGFR2 and TRPA1, in combination with low levels of PLCγ1 and GRB2, are likely to be protective due to the reciprocal negative regulation between FGFR2 and TRPA1 (Timsah et al., 2015).

Exploiting the interaction between FGFR2 and TRPA1 as a drug that mimics the binding could potentially combat FGFR2-related malignancies including head and neck, lung, gastric, bladder and breast cancer (Commissioner, 2019; Fletcher et al., 2013; Kim et al., 2019; McDermott et al., 2018; Timsah et al., 2015). The design of a non-conventional FGFR2 inhibitor that can bind to the C-terminal domain of FGFR2 and mimic the TRPA1 inhibitory effect provides a specific and targeted therapeutic against FGFR2. Ankyrin Repeat Proteins (DARPins), developed as a binding platform that is superior to conventional antibody recognition, are already investigated as potential inhibitors in therapeutics (e.g. DARPin H10-2-G3 against HER2 and breast cancer) (Epa et al., 2013; Houlihan et al., 2015).

However, additional studies are necessary to fully understand and verify the results presented in this thesis. Firstly, competition experiments between TRPA1 and PLCγ1 as well as GRB2 will confirm our interpretation and model of interaction between FGFR2 and TRPA1. Functional assays such as proliferation and invasion assays will also be informative regarding cellular responses induced by the FGFR2-TRPA1 complex. It will also be beneficial to investigate alternative signalling pathways that are activated by

FGFR2 such as the PI3K/AKT pathway, which is mainly involved in cell survival. Identification of the exact binding sites on both proteins will also have a therapeutic interest.

So far, the direct interaction between an RTK and a TRP channel has not been reported and future investigations on this phenomenon will determine whether it is a unique characteristic of FGFR2, or a mechanism widely used by RTKs and TRP channels. Apart from TRPA1, TRPC and TRPV channels carry 4-6 ankyrin repeats in their N-terminal domain and therefore, interaction between other TRP subfamilies with FGFR2 or other RTKs would be possible (Gaudet, 2008).

In conclusion, our study was a first attempt to characterise a novel interaction between FGFR2 and TRPA1 and determine the mechanisms of reciprocal regulation and role in cancer signalling. Our previous publication suggests an activating role of TRPA1 towards the FGFR2 signalling which contradicts the findings of the present thesis. Further research is needed to identify whether TRPA1 has a negative and/or a positive effect on FGFR2 activation and downstream signalling, as well as whether the outcome depends on the cell type, third-party molecules or even expression levels of the components. Nevertheless, it is evident that TRPA1 plays a key regulatory role on FGFR2 signalling, a phenomenon that is worth investigating.

6. List of References

Abbaspour Babaei, M., Kamalidehghan, B., Saleem, M., Huri, H.Z., Ahmadipour, F., 2016. Receptor tyrosine kinase (c-Kit) inhibitors: a potential therapeutic target in cancer cells. Drug Des Devel Ther 10, 2443–2459. https://doi.org/10.2147/DDDT.S89114

Adar, R., Monsonego-Ornan, E., David, P., Yayon, A., 2002. Differential activation of cysteine-substitution mutants of fibroblast growth factor receptor 3 is determined by cysteine localization. J. Bone Miner. Res. 17, 860–868. https://doi.org/10.1359/jbmr.2002.17.5.860

Ahmad, I., Iwata, T., Leung, H.Y., 2012. Mechanisms of FGFR-mediated carcinogenesis. Biochimica et Biophysica Acta (BBA) - Molecular Cell Research 1823, 850–860. https://doi.org/10.1016/j.bbamcr.2012.01.004

Ahmed, Z., George, R., Lin, C.-C., Suen, K.M., Levitt, J.A., Suhling, K., Ladbury, J.E., 2010. Direct binding of Grb2 SH3 domain to FGFR2 regulates SHP2 function. Cell. Signal. 22, 23–33. https://doi.org/10.1016/j.cellsig.2009.08.011

Ahn, S., Lee, J., Hong, M., Kim, S.T., Park, S.H., Choi, M.G., Lee, J.-H., Sohn, T.S., Bae, J.M., Kim, S., Jung, S.-H., Kang, W.K., Kim, K.-M., 2016. FGFR2 in gastric cancer: protein overexpression predicts gene amplification and high H-index predicts poor survival. Mod. Pathol. 29, 1095–1103. https://doi.org/10.1038/modpathol.2016.96

Alvarenga, E.M., Souza, L.K.M., Araújo, T.S.L., Nogueira, K.M., Sousa, F.B.M., Araújo, A.R., Martins, C.S., Pacífico, D.M., de C. Brito, G.A., Souza, E.P., Sousa, D.P., Medeiros, J.V.R., 2016. Carvacrol reduces irinotecan-induced intestinal mucositis through inhibition of inflammation and oxidative damage via TRPA1 receptor activation. Chemico-Biological Interactions 260, 129–140. https://doi.org/10.1016/j.cbi.2016.11.009

Artim, S.C., Mendrola, J.M., Lemmon, M.A., 2012. Assessing the range of kinase autoinhibition mechanisms in the insulin receptor family. Biochem J 448, 213–220. https://doi.org/10.1042/BJ20121365

Asuthkar, S., Velpula, K.K., Elustondo, P.A., Demirkhanyan, L., Zakharian, E., 2015. TRPM8 channel as a novel molecular target in androgen-regulated prostate cancer cells. Oncotarget 6, 17221–17236. https://doi.org/10.18632/oncotarget.3948

Ay, A.-S., Benzerdjerb, N., Sevestre, H., Ahidouch, A., Ouadid-Ahidouch, H., 2013. Orai3 Constitutes a Native Store-Operated Calcium Entry That Regulates Non Small Cell Lung Adenocarcinoma Cell Proliferation. PLoS One 8. https://doi.org/10.1371/journal.pone.0072889

Babina, I.S., Turner, N.C., 2017. Advances and challenges in targeting FGFR signalling in cancer. Nat. Rev. Cancer 17, 318–332. https://doi.org/10.1038/nrc.2017.8

Bahia, P.K., Parks, T.A., Stanford, K.R., Mitchell, D.A., Varma, S., Stevens, S.M., Taylor-Clark, T.E., 2016. The exceptionally high reactivity of Cys 621 is critical for electrophilic activation of the sensory nerve ion

channel TRPA1. J Gen Physiol 147, 451–465. https://doi.org/10.1085/jgp.201611581

Ball, L.J., Kühne, R., Schneider-Mergener, J., Oschkinat, H., 2005. Recognition of proline-rich motifs by protein-protein-interaction domains. Angew. Chem. Int. Ed. Engl. 44, 2852–2869. https://doi.org/10.1002/anie.200400618

Bandell, M., Story, G.M., Hwang, S.W., Viswanath, V., Eid, S.R., Petrus, M.J., Earley, T.J., Patapoutian, A., 2004. Noxious cold ion channel TRPA1 is activated by pungent compounds and bradykinin. Neuron 41, 849–857. https://doi.org/10.1016/s0896-6273(04)00150-3

Bang, S., Hwang, S.W., 2009. Polymodal Ligand Sensitivity of TRPA1 and Its Modes of Interactions. J Gen Physiol 133, 257–262. https://doi.org/10.1085/jgp.200810138

Bargmann, C.I., Weinberg, R.A., 1988. Oncogenic activation of the neu-encoded receptor protein by point mutation and deletion. EMBO J. 7, 2043–2052.

Bautista, D.M., Jordt, S.-E., Nikai, T., Tsuruda, P.R., Read, A.J., Poblete, J., Yamoah, E.N., Basbaum, A.I., Julius, D., 2006. TRPA1 mediates the inflammatory actions of environmental irritants and proalgesic agents. Cell 124, 1269–1282. https://doi.org/10.1016/j.cell.2006.02.023

Bautista, D.M., Siemens, J., Glazer, J.M., Tsuruda, P.R., Basbaum, A.I., Stucky, C.L., Jordt, S.-E., Julius, D., 2007. The menthol receptor TRPM8 is the principal detector of environmental cold. Nature 448, 204–208. https://doi.org/10.1038/nature05910

Bender, F.L.P., Mederos Y Schnitzler, M., Li, Y., Ji, A., Weihe, E., Gudermann, T., Schäfer, M.K.-H., 2005. The temperature-sensitive ion channel TRPV2 is endogenously expressed and functional in the primary sensory cell line F-11. Cell. Physiol. Biochem. 15, 183–194. https://doi.org/10.1159/000083651

Benzerdjeb, N., Sevestre, H., Ahidouch, A., Ouadid-Ahidouch, H., 2016. Orai3 is a predictive marker of metastasis and survival in resectable lung adenocarcinoma. Oncotarget 7, 81588–81597. https://doi.org/10.18632/oncotarget.13149

Bernichtein, S., Pigat, N., Barry Delongchamps, N., Boutillon, F., Verkarre, V., Camparo, P., Reyes-Gomez, E., Méjean, A., Oudard, S.M., Lepicard, E.M., Viltard, M., Souberbielle, J.-C., Friedlander, G., Capiod, T., Goffin, V., 2017. Vitamin D3 Prevents Calcium-Induced Progression of Early-Stage Prostate Tumors by Counteracting TRPC6 and Calcium Sensing Receptor Upregulation. Cancer Res. 77, 355–365. https://doi.org/10.1158/0008-5472.CAN-16-0687

Berrout, J., Kyriakopoulou, E., Moparthi, L., Hogea, A.S., Berrout, L., Ivan, C., Lorger, M., Boyle, J., Peers, C., Muench, S., Gomez, J.E., Hu, X., Hurst, C., Hall, T., Umamaheswaran, S., Wesley, L., Gagea, M., Shires, M., Manfield, I., Knowles, M.A., Davies, S., Suhling, K., Gonzalez, Y.T., Carragher, N., Macleod, K., Abbott, N.J., Calin, G.A., Gamper, N., Zygmunt, P.M., Timsah, Z., 2017. TRPA1–FGFR2 binding event is a regulatory oncogenic driver modulated by miRNA-142-3p. Nat Commun 8, 947. https://doi.org/10.1038/s41467-017-00983-w

Bhullar, K.S., Lagarón, N.O., McGowan, E.M., Parmar, I., Jha, A., Hubbard, B.P., Rupasinghe, H.P.V., 2018. Kinase-targeted cancer therapies:

progress, challenges and future directions. Mol. Cancer 17, 48. https://doi.org/10.1186/s12943-018-0804-2

Borrelli, F., Pagano, E., Romano, B., Panzera, S., Maiello, F., Coppola, D., De Petrocellis, L., Buono, L., Orlando, P., Izzo, A.A., 2014. Colon carcinogenesis is inhibited by the TRPM8 antagonist cannabigerol, a Cannabis-derived non-psychotropic cannabinoid. Carcinogenesis 35, 2787–2797. https://doi.org/10.1093/carcin/bgu205

Brackley, A.D., Gomez, R., Guerrero, K.A., Akopian, A.N., Glucksman, M.J., Du, J., Carlton, S.M., Jeske, N.A., 2017. A-Kinase Anchoring Protein 79/150 Scaffolds Transient Receptor Potential A 1 Phosphorylation and Sensitization by Metabotropic Glutamate Receptor Activation. Sci Rep 7, 1842. https://doi.org/10.1038/s41598-017-01999-4

Brône, B., Peeters, P.J., Marrannes, R., Mercken, M., Nuydens, R., Meert, T., Gijsen, H.J.M., 2008. Tear gasses CN, CR, and CS are potent activators of the human TRPA1 receptor. Toxicol. Appl. Pharmacol. 231, 150–156. https://doi.org/10.1016/j.taap.2008.04.005

Buchanan, P.J., McCloskey, K.D., 2016. CaV channels and cancer: canonical functions indicate benefits of repurposed drugs as cancer therapeutics. Eur Biophys J 45, 621–633. https://doi.org/10.1007/s00249-016-1144-z

Burgess, A.W., Cho, H.-S., Eigenbrot, C., Ferguson, K.M., Garrett, T.P.J., Leahy, D.J., Lemmon, M.A., Sliwkowski, M.X., Ward, C.W., Yokoyama, S., 2003. An open-and-shut case? Recent insights into the activation of EGF/ErbB receptors. Mol. Cell 12, 541–552. https://doi.org/10.1016/s1097-2765(03)00350-2

Byron, S.A., Gartside, M.G., Wellens, C.L., Mallon, M.A., Keenan, J.B., Powell, M.A., Goodfellow, P.J., Pollock, P.M., 2008. Inhibition of activated fibroblast growth factor receptor 2 in endometrial cancer cells induces cell death despite PTEN abrogation. Cancer Res. 68, 6902–6907. https://doi.org/10.1158/0008-5472.CAN-08-0770

Campbell, T.M., Castro, M.A.A., de Santiago, I., Fletcher, M.N.C., Halim, S., Prathalingam, R., Ponder, B.A.J., Meyer, K.B., 2016. FGFR2 risk SNPs confer breast cancer risk by augmenting oestrogen responsiveness. Carcinogenesis 37, 741–750. https://doi.org/10.1093/carcin/bgw065

Cancer of the Lung and Bronchus - Cancer Stat Facts [WWW Document], n.d. . SEER. URL https://seer.cancer.gov/statfacts/html/lungb.html (accessed 11.22.19).

Cao, R., Meng, Z., Liu, T., Wang, G., Qian, G., Cao, T., Guan, X., Dan, H., Xiao, Y., Wang, X., 2016. Decreased TRPM7 inhibits activities and induces apoptosis of bladder cancer cells via ERK1/2 pathway. Oncotarget 7, 72941–72960. https://doi.org/10.18632/oncotarget.12146

Caterina, M., Schumacher, M.A., Tominaga, M., Rosen, T.A., Levine, J.D., Julius, D., 1997. The capsaicin receptor: A heat-activated ion channel in the pain pathway. NATURE 389, 816–824. https://doi.org/10.1038/39807

Caterina, M.J., Rosen, T.A., Tominaga, M., Brake, A.J., Julius, D., 1999. A capsaicin-receptor homologue with a high threshold for noxious heat. Nature 398, 436–441. https://doi.org/10.1038/18906

Cha, J.Y., Lambert, Q.T., Reuther, G.W., Der, C.J., 2008. Involvement of fibroblast growth factor receptor 2 isoform switching in mammary oncogenesis. Mol. Cancer Res. 6, 435–445. https://doi.org/10.1158/1541-7786.MCR-07-0187

Cha, J.Y., Maddileti, S., Mitin, N., Harden, T.K., Der, C.J., 2009. Aberrant receptor internalization and enhanced FRS2-dependent signaling contribute to the transforming activity of the fibroblast growth factor receptor 2 IIIb C3 isoform. J. Biol. Chem. 284, 6227–6240. https://doi.org/10.1074/jbc.M803998200

Chaffer, C.L., Brennan, J.P., Slavin, J.L., Blick, T., Thompson, E.W., Williams, E.D., 2006. Mesenchymal-to-epithelial transition facilitates bladder cancer metastasis: role of fibroblast growth factor receptor-2. Cancer Res. 66, 11271–11278. https://doi.org/10.1158/0008-5472.CAN-06-2044

Chan, P.M., Ilangumaran, S., La Rose, J., Chakrabartty, A., Rottapel, R., 2003. Autoinhibition of the kit receptor tyrosine kinase by the cytosolic juxtamembrane region. Mol. Cell. Biol. 23, 3067–3078. https://doi.org/10.1128/mcb.23.9.3067-3078.2003

Chang, M.-M., Lai, M.-S., Hong, S.-Y., Pan, B.-S., Huang, H., Yang, S.-H., Wu, C.-C., Sun, H.S., Chuang, J.-I., Wang, C.-Y., Huang, B.-M., 2018. FGF9/FGFR2 increase cell proliferation by activating ERK1/2, Rb/E2F1, and cell cycle pathways in mouse Leydig tumor cells. Cancer Sci. 109, 3503–3518. https://doi.org/10.1111/cas.13793

Chen, H., Huang, Z., Dutta, K., Blais, S., Neubert, T.A., Li, X., Cowburn, D., Traaseth, N.J., Mohammadi, M., 2013. Cracking the Molecular Origin of Intrinsic Tyrosine Kinase Activity through Analysis of Pathogenic Gain-of-Function Mutations. Cell Reports 4, 376–384. https://doi.org/10.1016/j.celrep.2013.06.025

Chen, H., Ma, J., Li, W., Eliseenkova, A.V., Xu, C., Neubert, T.A., Miller, W.T., Mohammadi, M., 2007. A ‘Molecular Brake’ in the Kinase Hinge Region Regulates the Activity of Receptor Tyrosine Kinases. Mol Cell 27, 717–730. https://doi.org/10.1016/j.molcel.2007.06.028

Chen, J., Stinski, M.F., 2002. Role of regulatory elements and the MAPK/ERK or p38 MAPK pathways for activation of human cytomegalovirus gene expression. J. Virol. 76, 4873–4885. https://doi.org/10.1128/jvi.76.10.4873-4885.2002

Chen, J.-L., Ping, Y.-H., Tseng, M.-J., Chang, Y.-I., Lee, H.-C., Hsieh, R.-H., Yeh, T.-S., 2017. Notch1-promoted TRPA1 expression in erythroleukemic cells suppresses erythroid but enhances megakaryocyte differentiation. Scientific Reports 7, 42883. https://doi.org/10.1038/srep42883

Chen, Z., Tang, C., Zhu, Yaodan, Xie, M., He, D., Pan, Q., Zhang, P., Hua, D., Wang, T., Jin, L., Qi, X., Zhu, Yifei, Yao, X., Jin, J., Ma, X., 2017a. TrpC5 regulates differentiation through the Ca2+/Wnt5a signalling pathway in colorectal cancer. Clin Sci (Lond) 131, 227–237. https://doi.org/10.1042/CS20160759

Chen, Z., Zhu, Y., Dong, Y., Zhang, P., Han, X., Jin, J., Ma, X., 2017b. Overexpression of TrpC5 promotes tumor metastasis via the HIF-1α-Twist signaling pathway in colon cancer. Clin. Sci. 131, 2439–2450. https://doi.org/10.1042/CS20171069

Chiara, F., Bishayee, S., Heldin, C.-H., Demoulin, J.-B., 2004. Autoinhibition of the platelet-derived growth factor beta-receptor tyrosine kinase by its C-terminal tail. J. Biol. Chem. 279, 19732–19738. https://doi.org/10.1074/jbc.M314070200

Chuang, H., Neuhausser, W.M., Julius, D., 2004. The super-cooling agent icilin reveals a mechanism of coincidence detection by a temperature-sensitive TRP channel. Neuron 43, 859–869. https://doi.org/10.1016/j.neuron.2004.08.038

Cioffi, D.L., Wu, S., Chen, H., Alexeyev, M., St Croix, C.M., Pitt, B.R., Uhlig, S., Stevens, T., 2012. Orai1 determines calcium selectivity of an endogenous TRPC heterotetramer channel. Circ. Res. 110, 1435–1444. https://doi.org/10.1161/CIRCRESAHA.112.269506

Commissioner, O. of the, 2019. FDA approves first targeted therapy for metastatic bladder cancer [WWW Document]. FDA. URL http://www.fda.gov/news-events/press-announcements/fda-approves-first-targeted-therapy-metastatic-bladder-cancer (accessed 10.19.19).

Cordero-Morales, J.F., Gracheva, E.O., Julius, D., 2011. Cytoplasmic ankyrin repeats of transient receptor potential A1 (TRPA1) dictate sensitivity to thermal and chemical stimuli. Proc. Natl. Acad. Sci. U.S.A. 108, E1184-1191. https://doi.org/10.1073/pnas.1114124108

Corey, D.P., García-Añoveros, J., Holt, J.R., Kwan, K.Y., Lin, S.-Y., Vollrath, M.A., Amalfitano, A., Cheung, E.L.-M., Derfler, B.H., Duggan, A., Géléoc, G.S.G., Gray, P.A., Hoffman, M.P., Rehm, H.L., Tamasauskas, D., Zhang, D.-S., 2004. TRPA1 is a candidate for the mechanosensitive transduction channel of vertebrate hair cells. Nature 432, 723–730. https://doi.org/10.1038/nature03066

Cosens, D.J., Manning, A., 1969. Abnormal electroretinogram from a Drosophila mutant. Nature 224, 285–287. https://doi.org/10.1038/224285a0

Cuajungco, M.P., Grimm, C., Heller, S., 2007. TRP channels as candidates for hearing and balance abnormalities in vertebrates. Biochim. Biophys. Acta 1772, 1022–1027. https://doi.org/10.1016/j.bbadis.2007.01.002

Cui, C., Merritt, R., Fu, L., Pan, Z., 2017. Targeting calcium signaling in cancer therapy. Acta Pharm Sin B 7, 3–17. https://doi.org/10.1016/j.apsb.2016.11.001

Dai, Y., Wang, S., Tominaga, M., Yamamoto, S., Fukuoka, T., Higashi, T., Kobayashi, K., Obata, K., Yamanaka, H., Noguchi, K., 2007. Sensitization of TRPA1 by PAR2 contributes to the sensation of inflammatory pain. J. Clin. Invest. 117, 1979–1987. https://doi.org/10.1172/JCI30951

D'Amici, S., Ceccarelli, S., Vescarelli, E., Romano, F., Frati, L., Marchese, C., Angeloni, A., 2013. TNFα modulates Fibroblast Growth Factor Receptor 2 gene expression through the pRB/E2F1 pathway: identification of a non-canonical E2F binding motif. PLoS ONE 8, e61491. https://doi.org/10.1371/journal.pone.0061491

Dela Cruz, C.S., Tanoue, L.T., Matthay, R.A., 2011. Lung cancer: epidemiology, etiology, and prevention. Clin. Chest Med. 32, 605–644. https://doi.org/10.1016/j.ccm.2011.09.001

Deng, N., Goh, L.K., Wang, H., Das, K., Tao, J., Tan, I.B., Zhang, S., Lee, M., Wu, J., Lim, K.H., Lei, Z., Goh, G., Lim, Q.-Y., Tan, A.L.-K., Sin

Poh, D.Y., Riahi, S., Bell, S., Shi, M.M., Linnartz, R., Zhu, F., Yeoh, K.G., Toh, H.C., Yong, W.P., Cheong, H.C., Rha, S.Y., Boussioutas, A., Grabsch, H., Rozen, S., Tan, P., 2012. A comprehensive survey of genomic alterations in gastric cancer reveals systematic patterns of molecular exclusivity and co-occurrence among distinct therapeutic targets. Gut 61, 673–684. https://doi.org/10.1136/gutjnl-2011-301839

Derouiche, S., Mariot, P., Warnier, M., Vancauwenberghe, E., Bidaux, G., Gosset, P., Mauroy, B., Bonnal, J.-L., Slomianny, C., Delcourt, P., Dewailly, E., Prevarskaya, N., Roudbaraki, M., 2017. Activation of TRPA1 Channel by Antibacterial Agent Triclosan Induces VEGF Secretion in Human Prostate Cancer Stromal Cells. Cancer Prev Res (Phila) 10, 177–187. https://doi.org/10.1158/1940-6207.CAPR-16-0257

Deschout, H., Shivanandan, A., Annibale, P., Scarselli, M., Radenovic, A., 2014. Progress in quantitative single-molecule localization microscopy. Histochem. Cell Biol. 142, 5–17. https://doi.org/10.1007/s00418-014-1217-y

Dhillon, A.S., Hagan, S., Rath, O., Kolch, W., 2007. MAP kinase signalling pathways in cancer. Oncogene 26, 3279–3290. https://doi.org/10.1038/sj.onc.1210421

Didkowska, J., Wojciechowska, U., Mańczuk, M., Łobaszewski, J., 2016. Lung cancer epidemiology: contemporary and future challenges worldwide. Ann Transl Med 4, 150. https://doi.org/10.21037/atm.2016.03.11

Doerner, J.F., Gisselmann, G., Hatt, H., Wetzel, C.H., 2007. Transient Receptor Potential Channel A1 Is Directly Gated by Calcium Ions. J. Biol. Chem. 282, 13180–13189. https://doi.org/10.1074/jbc.M607849200

Du, G.-J., Li, J.-H., Liu, W.-J., Liu, Y.-H., Zhao, B., Li, H.-R., Hou, X.-D., Li, H., Qi, X.-X., Duan, Y.-J., 2014. The combination of TRPM8 and TRPA1 expression causes an invasive phenotype in lung cancer. Tumour Biol. 35, 1251–1261. https://doi.org/10.1007/s13277-013-1167-3

Du, J., Xie, J., Yue, L., 2009. Intracellular calcium activates TRPM2 and its alternative spliced isoforms. PNAS 106, 7239–7244. https://doi.org/10.1073/pnas.0811725106

Dubois, C., Vanden Abeele, F., Lehen'kyi, V., Gkika, D., Guarmit, B., Lepage, G., Slomianny, C., Borowiec, A.S., Bidaux, G., Benahmed, M., Shuba, Y., Prevarskaya, N., 2014. Remodeling of channel-forming ORAI proteins determines an oncogenic switch in prostate cancer. Cancer Cell 26, 19–32. https://doi.org/10.1016/j.ccr.2014.04.025

Endicott, J.A., Noble, M.E.M., Johnson, L.N., 2012. The structural basis for control of eukaryotic protein kinases. Annu. Rev. Biochem. 81, 587–613. https://doi.org/10.1146/annurev-biochem-052410-090317

Epa, V.C., Dolezal, O., Doughty, L., Xiao, X., Jost, C., Plückthun, A., Adams, T.E., 2013. Structural model for the interaction of a designed Ankyrin Repeat Protein with the human epidermal growth factor receptor 2. PLoS ONE 8, e59163. https://doi.org/10.1371/journal.pone.0059163

Eswarakumar, V.P., Lax, I., Schlessinger, J., 2005. Cellular signaling by fibroblast growth factor receptors. Cytokine Growth Factor Rev. 16, 139–149. https://doi.org/10.1016/j.cytogfr.2005.01.001

Faouzi, M., Hague, F., Geerts, D., Ay, A.-S., Potier-Cartereau, M., Ahidouch, A., Ouadid-Ahidouch, H., 2016. Functional cooperation between KCa3.1 and TRPC1 channels in human breast cancer: Role in cell proliferation and patient prognosis. Oncotarget 7, 36419–36435. https://doi.org/10.18632/oncotarget.9261

Faouzi, M., Hague, F., Potier, M., Ahidouch, A., Sevestre, H., Ouadid-Ahidouch, H., 2011. Down-regulation of Orai3 arrests cell-cycle progression and induces apoptosis in breast cancer cells but not in normal breast epithelial cells. J. Cell. Physiol. 226, 542–551. https://doi.org/10.1002/jcp.22363

Faouzi, M., Kischel, P., Hague, F., Ahidouch, A., Benzerdjeb, N., Sevestre, H., Penner, R., Ouadid-Ahidouch, H., 2013. ORAI3 silencing alters cell proliferation and cell cycle progression via c-myc pathway in breast cancer cells. Biochim. Biophys. Acta 1833, 752–760. https://doi.org/10.1016/j.bbamcr.2012.12.009

Fish, K.N., 2009. Total internal reflection fluorescence (TIRF) microscopy. Curr Protoc Cytom Chapter 12, Unit12.18. https://doi.org/10.1002/0471142956.cy1218s50

Fixemer, T., Wissenbach, U., Flockerzi, V., Bonkhoff, H., 2003. Expression of the Ca2+-selective cation channel TRPV6 in human prostate cancer: a novel prognostic marker for tumor progression. Oncogene 22, 7858–7861. https://doi.org/10.1038/sj.onc.1206895

Fletcher, M.N.C., Castro, M.A.A., Wang, X., de Santiago, I., O'Reilly, M., Chin, S.-F., Rueda, O.M., Caldas, C., Ponder, B.A.J., Markowetz, F., Meyer, K.B., 2013. Master regulators of FGFR2 signalling and breast cancer risk. Nat Commun 4, 2464. https://doi.org/10.1038/ncomms3464

Furdui, C.M., Lew, E.D., Schlessinger, J., Anderson, K.S., 2006. Autophosphorylation of FGFR1 kinase is mediated by a sequential and precisely ordered reaction. Mol. Cell 21, 711–717. https://doi.org/10.1016/j.molcel.2006.01.022

Gachons, C.P. des, Uchida, K., Bryant, B., Shima, A., Sperry, J.B., Dankulich-Nagrudny, L., Tominaga, M., Smith, A.B., Beauchamp, G.K., Breslin, P.A.S., 2011. Unusual Pungency from Extra-Virgin Olive Oil Is Attributable to Restricted Spatial Expression of the Receptor of Oleocanthal. J. Neurosci. 31, 999–1009. https://doi.org/10.1523/JNEUROSCI.1374-10.2011

Gackière, F., Warnier, M., Katsogiannou, M., Derouiche, S., Delcourt, P., Dewailly, E., Slomianny, C., Humez, S., Prevarskaya, N., Roudbaraki, M., Mariot, P., 2013. Functional coupling between large-conductance potassium channels and Cav3.2 voltage-dependent calcium channels participates in prostate cancer cell growth. Biology open 2, 941–51. https://doi.org/10.1242/bio.20135215

Gambarotto, D., Zwettler, F.U., Cernohorska, M., Fortun, D., Borgers, S., Heine, J., Schloetel, J.G., Reuss, M., Unser, M., Boyden, E.S., Sauer, M., Hamel, V., Guichard, P., 2018. Imaging beyond the super-resolution limits using ultrastructure expansion microscopy (UltraExM). bioRxiv 308270. https://doi.org/10.1101/308270

Gao, S.-L., Kong, C.-Z., Zhang, Z., Li, Z.-L., Bi, J.-B., Liu, X.-K., 2017. TRPM7 is overexpressed in bladder cancer and promotes

proliferation, migration, invasion and tumor growth. Oncol. Rep. 38, 1967–1976. https://doi.org/10.3892/or.2017.5883

Garrett, T.P.J., McKern, N.M., Lou, M., Elleman, T.C., Adams, T.E., Lovrecz, G.O., Zhu, H.-J., Walker, F., Frenkel, M.J., Hoyne, P.A., Jorissen, R.N., Nice, E.C., Burgess, A.W., Ward, C.W., 2002. Crystal structure of a truncated epidermal growth factor receptor extracellular domain bound to transforming growth factor alpha. Cell 110, 763–773. https://doi.org/10.1016/s0092-8674(02)00940-6

Gaudet, R., 2008. A primer on ankyrin repeat function in TRP channels and beyond. Mol Biosyst 4, 372–379. https://doi.org/10.1039/b801481g

Genova, T., Grolez, G.P., Camillo, C., Bernardini, M., Bokhobza, A., Richard, E., Scianna, M., Lemonnier, L., Valdembri, D., Munaron, L., Philips, M.R., Mattot, V., Serini, G., Prevarskaya, N., Gkika, D., Pla, A.F., 2017. TRPM8 inhibits endothelial cell migration via a non-channel function by trapping the small GTPase Rap1. J. Cell Biol. 216, 2107–2130. https://doi.org/10.1083/jcb.201506024

Goetz, R., Mohammadi, M., 2013. Exploring mechanisms of FGF signalling through the lens of structural biology. Nat Rev Mol Cell Biol 14, 166–180. https://doi.org/10.1038/nrm3528

Gotoh, N., 2008. Regulation of growth factor signaling by FRS2 family docking/scaffold adaptor proteins. Cancer Sci. 99, 1319–1325. https://doi.org/10.1111/j.1349-7006.2008.00840.x

Grandl, J., Kim, S.E., Uzzell, V., Bursulaya, B., Petrus, M., Bandell, M., Patapoutian, A., 2010. Temperature-induced opening of TRPV1 ion channel is stabilized by the pore domain. Nat. Neurosci. 13, 708–714. https://doi.org/10.1038/nn.2552

Griffith, J., Black, J., Faerman, C., Swenson, L., Wynn, M., Lu, F., Lippke, J., Saxena, K., 2004. The structural basis for autoinhibition of FLT3 by the juxtamembrane domain. Mol. Cell 13, 169–178. https://doi.org/10.1016/s1097-2765(03)00505-7

Guéguinou, M., Harnois, T., Crottes, D., Uguen, A., Deliot, N., Gambade, A., Chantôme, A., Haelters, J.P., Jaffrès, P.A., Jourdan, M.L., Weber, G., Soriani, O., Bougnoux, P., Mignen, O., Bourmeyster, N., Constantin, B., Lecomte, T., Vandier, C., Potier-Cartereau, M., 2016. SK3/TRPC1/Orai1 complex regulates SOCE-dependent colon cancer cell migration: a novel opportunity to modulate anti-EGFR mAb action by the alkyl-lipid Ohmline. Oncotarget 7, 36168–36184. https://doi.org/10.18632/oncotarget.8786

Gui, L., Wang, Z., Han, J., Ma, H., Li, Z., 2016. High Expression of Orai1 Enhances Cell Proliferation and is Associated with Poor Prognosis in Human Colorectal Cancer. Clin. Lab. 62, 1689–1698. https://doi.org/10.7754/Clin.Lab.2016.160131

Guilbert, A., Dhennin-Duthille, I., Hiani, Y.E., Haren, N., Khorsi, H., Sevestre, H., Ahidouch, A., Ouadid-Ahidouch, H., 2011. Expression of TRPC6 channels in human epithelial breast cancer cells-4. https://doi.org/10.6084/m9.figshare.26528.v1

Gupta, R., Saito, S., Mori, Y., Itoh, S.G., Okumura, H., Tominaga, M., 2016. Structural basis of TRPA1 inhibition by HC-030031 utilizing species-specific differences. Scientific Reports 6, 1–14. https://doi.org/10.1038/srep37460

Hajicek, N., Charpentier, T.H., Rush, J.R., Harden, T.K., Sondek, J., 2013. Autoinhibition and Phosphorylation-Induced Activation of Phospholipase C-γ Isozymes. Biochemistry 52, 4810–4819. https://doi.org/10.1021/bi400433b

Hallinan, N., Finn, S., Cuffe, S., Rafee, S., O'Byrne, K., Gately, K., 2016. Targeting the fibroblast growth factor receptor family in cancer. Cancer Treat. Rev. 46, 51–62. https://doi.org/10.1016/j.ctrv.2016.03.015

Hanahan, D., Weinberg, R.A., 2011. Hallmarks of cancer: the next generation. Cell 144, 646–674. https://doi.org/10.1016/j.cell.2011.02.013

Hardie, R.C., Minke, B., 1992. The trp gene is essential for a light-activated Ca2+ channel in Drosophila photoreceptors. Neuron 8, 643–651. https://doi.org/10.1016/0896-6273(92)90086-S

Hasan, R., Leeson-Payne, A.T.S., Jaggar, J.H., Zhang, X., 2017. Calmodulin is responsible for Ca 2+ -dependent regulation of TRPA1 Channels. Scientific Reports 7, 1–13. https://doi.org/10.1038/srep45098

Heldin, C.-H., Lennartsson, J., Westermark, B., 2018. Involvement of platelet-derived growth factor ligands and receptors in tumorigenesis. J. Intern. Med. 283, 16–44. https://doi.org/10.1111/joim.12690

Hers, I., Vincent, E.E., Tavaré, J.M., 2011. Akt signalling in health and disease. Cell. Signal. 23, 1515–1527. https://doi.org/10.1016/j.cellsig.2011.05.004

Hibi, M., Kaneda, H., Tanizaki, J., Sakai, K., Togashi, Y., Terashima, M., De Velasco, M.A., Fujita, Y., Banno, E., Nakamura, Y., Takeda, M., Ito, A., Mitsudomi, T., Nakagawa, K., Okamoto, I., Nishio, K., 2016. FGFR gene alterations in lung squamous cell carcinoma are potential targets for the multikinase inhibitor nintedanib. Cancer Sci. 107, 1667–1676. https://doi.org/10.1111/cas.13071

Hinman, A., Chuang, H., Bautista, D.M., Julius, D., 2006. TRP channel activation by reversible covalent modification. PNAS 103, 19564–19568. https://doi.org/10.1073/pnas.0609598103

Hochstrate, P., 1989. Lanthanum mimicks the trp photoreceptor mutant of Drosophila in the blowfly Calliphora. J Comp Physiol A 166, 179–187. https://doi.org/10.1007/BF00193462

Hoenderop, J.G.J., Vennekens, R., Müller, D., Prenen, J., Droogmans, G., Bindels, R.J.M., Nilius, B., 2001. Function and expression of the epithelial Ca2+ channel family: comparison of mammalian ECaC1 and 2. J Physiol 537, 747–761. https://doi.org/10.1111/j.1469-7793.2001.00747.x

Houlihan, G., Gatti-Lafranconi, P., Lowe, D., Hollfelder, F., 2015. Directed evolution of anti-HER2 DARPins by SNAP display reveals stability/function trade-offs in the selection process. Protein Eng. Des. Sel. 28, 269–279. https://doi.org/10.1093/protein/gzv029

Hsu, C.-C., Lee, L.-Y., 2015. Role of calcium ions in the positive interaction between TRPA1 and TRPV1 channels in bronchopulmonary sensory neurons. J Appl Physiol (1985) 118, 1533–1543. https://doi.org/10.1152/japplphysiol.00043.2015

Huang, Z., Marsiglia, W.M., Basu Roy, U., Rahimi, N., Ilghari, D., Wang, H., Chen, H., Gai, W., Blais, S., Neubert, T.A., Mansukhani, A., Traaseth, N.J., Li, X., Mohammadi, M., 2016. Two FGF Receptor Kinase

Molecules Act in Concert to Recruit and Transphosphorylate Phospholipase Cγ. Molecular Cell 61, 98–110. https://doi.org/10.1016/j.molcel.2015.11.010

Hubbard, S.R., 1997. Crystal structure of the activated insulin receptor tyrosine kinase in complex with peptide substrate and ATP analog. EMBO J 16, 5572–5581. https://doi.org/10.1093/emboj/16.18.5572

Huff, J., 2015. The Airyscan detector from ZEISS: confocal imaging with improved signal-to-noise ratio and super-resolution. Nat Methods 12, i–ii. https://doi.org/10.1038/nmeth.f.388

Hunter, J.J., Shao, J., Smutko, J.S., Dussault, B.J., Nagle, D.L., Woolf, E.A., Holmgren, L.M., Moore, K.J., Shyjan, A.W., 1998. Chromosomal localization and genomic characterization of the mouse melastatin gene (Mlsn1). Genomics 54, 116–123. https://doi.org/10.1006/geno.1998.5549

Huse, M., Kuriyan, J., 2002. The conformational plasticity of protein kinases. Cell 109, 275–282. https://doi.org/10.1016/s0092-8674(02)00741-9

Hynkova, A., Marsakova, L., Vaskova, J., Vlachova, V., 2016. N-terminal tetrapeptide T/SPLH motifs contribute to multimodal activation of human TRPA1 channel. Scientific Reports 6, 1–16. https://doi.org/10.1038/srep28700

Inada, H., Procko, E., Sotomayor, M., Gaudet, R., 2012. Structural and Biochemical Consequences of Disease-Causing Mutations in the Ankyrin Repeat Domain of the Human TRPV4 Channel. Biochemistry 51, 6195–206. https://doi.org/10.1021/bi300279b

Jaquemar, D., Schenker, T., Trueb, B., 1999. An Ankyrin-like Protein with Transmembrane Domains Is Specifically Lost after Oncogenic Transformation of Human Fibroblasts. J. Biol. Chem. 274, 7325–7333. https://doi.org/10.1074/jbc.274.11.7325

Jerabek-Willemsen, M., André, T., Wanner, R., Roth, H.M., Duhr, S., Baaske, P., Breitsprecher, D., 2014. MicroScale Thermophoresis: Interaction analysis and beyond. Journal of Molecular Structure, Fluorescence studies of biomolecular association processes. 1077, 101–113. https://doi.org/10.1016/j.molstruc.2014.03.009

Jiang, H.-N., Zeng, B., Zhang, Y., Daskoulidou, N., Fan, H., Qu, J.-M., Xu, S.-Z., 2013. Involvement of TRPC channels in lung cancer cell differentiation and the correlation analysis in human non-small cell lung cancer. PLoS ONE 8, e67637. https://doi.org/10.1371/journal.pone.0067637

Jin, P., Bulkley, D., Guo, Y., Zhang, W., Guo, Z., Huynh, W., Wu, S., Meltzer, S., Cheng, T., Jan, L.Y., Jan, Y.-N., Cheng, Y., 2017. Electron cryo-microscopy structure of the mechanotransduction channel NOMPC. Nature 547, 118–122. https://doi.org/10.1038/nature22981

Jin, X., Touhey, J., Gaudet, R., 2006. Structure of the N-terminal Ankyrin Repeat Domain of the TRPV2 Ion Channel. The Journal of biological chemistry 281, 25006–10. https://doi.org/10.1074/jbc.C600153200

Jordt, S.-E., Bautista, D.M., Chuang, H.-H., McKemy, D.D., Zygmunt, P.M., Högestätt, E.D., Meng, I.D., Julius, D., 2004. Mustard oils and cannabinoids excite sensory nerve fibres through the TRP channel ANKTM1. Nature 427, 260–265. https://doi.org/10.1038/nature02282

Julius, D., 2013. TRP channels and pain. Annu. Rev. Cell Dev. Biol. 29, 355–384. https://doi.org/10.1146/annurev-cellbio-101011-155833

Kaabeche, K., Lemonnier, J., Mée, S.L., Caverzasio, J., Marie, P.J., 2004. Cbl-mediated Degradation of Lyn and Fyn Induced by Constitutive Fibroblast Growth Factor Receptor-2 Activation Supports Osteoblast Differentiation. J. Biol. Chem. 279, 36259–36267. https://doi.org/10.1074/jbc.M402469200

Kallioniemi, O.P., Kallioniemi, A., Kurisu, W., Thor, A., Chen, L.C., Smith, H.S., Waldman, F.M., Pinkel, D., Gray, J.W., 1992. ERBB2 amplification in breast cancer analyzed by fluorescence in situ hybridization. Proc Natl Acad Sci U S A 89, 5321–5325.

Kawase, R., Ishiwata, T., Matsuda, Y., Onda, M., Kudo, M., Takeshita, T., Naito, Z., 2010. Expression of fibroblast growth factor receptor 2 IIIc in human uterine cervical intraepithelial neoplasia and cervical cancer. International journal of oncology 36, 331–40. https://doi.org/10.3892/ijo_00000504

Kim, H.S., Kim, J.H., Jang, H.J., Han, B., Zang, D.Y., 2019. Pathological and Prognostic Impacts of FGFR2 Overexpression in Gastric Cancer: A Meta-Analysis. J Cancer 10, 20–27. https://doi.org/10.7150/jca.28204

Kobori, T., Smith, G.D., Sandford, R., Edwardson, J.M., 2009. The transient receptor potential channels TRPP2 and TRPC1 form a heterotetramer with a 2:2 stoichiometry and an alternating subunit arrangement. J. Biol. Chem. 284, 35507–35513. https://doi.org/10.1074/jbc.M109.060228

Kondo, T., Sakurai, J., Miwa, H., Noguchi, K., 2013. Activation of p38 MAPK through transient receptor potential A1 in a rat model of gastric distension-induced visceral pain. Neuroreport 24, 68–72. https://doi.org/10.1097/WNR.0b013e32835c7df2

Koulen, P., Cai, Y., Geng, L., Maeda, Y., Nishimura, S., Witzgall, R., Ehrlich, B.E., Somlo, S., 2002. Polycystin-2 is an intracellular calcium release channel. Nat. Cell Biol. 4, 191–197. https://doi.org/10.1038/ncb754

Kunii, K., Davis, L., Gorenstein, J., Hatch, H., Yashiro, M., Di Bacco, A., Elbi, C., Lutterbach, B., 2008. FGFR2-amplified gastric cancer cell lines require FGFR2 and Erbb3 signaling for growth and survival. Cancer Res. 68, 2340–2348. https://doi.org/10.1158/0008-5472.CAN-07-5229

Kwan, K.Y., Allchorne, A.J., Vollrath, M.A., Christensen, A.P., Zhang, D.-S., Woolf, C.J., Corey, D.P., 2006. TRPA1 contributes to cold, mechanical, and chemical nociception but is not essential for hair-cell transduction. Neuron 50, 277–289. https://doi.org/10.1016/j.neuron.2006.03.042

Lattanzio, R., Piantelli, M., Falasca, M., 2013. Role of phospholipase C in cell invasion and metastasis. Adv Biol Regul 53, 309–318. https://doi.org/10.1016/j.jbior.2013.07.006

Lau, J.K., Brown, K.C., Dom, A.M., Witte, T.R., Thornhill, B.A., Crabtree, C.M., Perry, H.E., Brown, J.M., Ball, J.G., Creel, R.G., Damron, C.L., Rollyson, W.D., Stevenson, C.D., Hardman, W.E., Valentovic, M.A., Carpenter, A.B., Dasgupta, P., 2014. Capsaicin Induces Apoptosis in Human Small Cell Lung Cancer via the TRPV6 Receptor and the Calpain Pathway. Apoptosis 19, 1190–1201. https://doi.org/10.1007/s10495-014-1007-y

Lawrence, M.C., McKern, N.M., Ward, C.W., 2007. Insulin receptor structure and its implications for the IGF-1 receptor. Curr. Opin. Struct. Biol. 17, 699–705. https://doi.org/10.1016/j.sbi.2007.07.007

Leanza, L., Managò, A., Zoratti, M., Gulbins, E., Szabo, I., 2016. Pharmacological targeting of ion channels for cancer therapy: In vivo evidences. Biochim. Biophys. Acta 1863, 1385–1397. https://doi.org/10.1016/j.bbamcr.2015.11.032

Lee, H.J., Kang, H.J., Kim, K.M., Yu, E.S., Kim, K.H., Kim, S.-M., Kim, T.W., Shim, J.H., Lim, Y.-S., Lee, H.C., Chung, Y.-H., Lee, Y.S., 2015. Fibroblast growth factor receptor isotype expression and its association with overall survival in patients with hepatocellular carcinoma. Clin Mol Hepatol 21, 60–70. https://doi.org/10.3350/cmh.2015.21.1.60

Lee, H.J., Seo, A.N., Park, S.Y., Kim, J.Y., Park, J.Y., Yu, J.H., Ahn, J.-H., Gong, G., 2014. Low prognostic implication of fibroblast growth factor family activation in triple-negative breast cancer subsets. Ann. Surg. Oncol. 21, 1561–1568. https://doi.org/10.1245/s10434-013-3456-x

Lee, S.P., Buber, M.T., Yang, Q., Cerne, R., Cortés, R.Y., Sprous, D.G., Bryant, R.W., 2008. Thymol and related alkyl phenols activate the hTRPA1 channel. Br J Pharmacol 153, 1739–1749. https://doi.org/10.1038/bjp.2008.85

Lee, W.H., Choong, L.Y., Jin, T.H., Mon, N.N., Chong, S., Liew, C.S., Putti, T., Lu, S.Y., Harteneck, C., Lim, Y.P., 2017. TRPV4 plays a role in breast cancer cell migration via Ca2+-dependent activation of AKT and downregulation of E-cadherin cell cortex protein. Oncogenesis 6, e338. https://doi.org/10.1038/oncsis.2017.39

Lehen'Kyi, V., Flourakis, M., Skryma, R., Prevarskaya, N., 2007. TRPV6 channel controls prostate cancer cell proliferation via Ca2+/NFAT-dependent pathways. Oncogene 26, 7380–7385. https://doi.org/10.1038/sj.onc.1210545

Lemmon, M.A., Schlessinger, J., 2010. Cell signaling by receptor tyrosine kinases. Cell 141, 1117–1134. https://doi.org/10.1016/j.cell.2010.06.011

Lew, E.D., Furdui, C.M., Anderson, K.S., Schlessinger, J., 2009. The precise sequence of FGF receptor autophosphorylation is kinetically driven and is disrupted by oncogenic mutations. Sci Signal 2, ra6. https://doi.org/10.1126/scisignal.2000021

Li, E., Hristova, K., 2010. Receptor tyrosine kinase transmembrane domains: Function, dimer structure and dimerization energetics. Cell Adh Migr 4, 249–254. https://doi.org/10.4161/cam.4.2.10725

Li, S., Covino, N.D., Stein, E.G., Till, J.H., Hubbard, S.R., 2003. Structural and biochemical evidence for an autoinhibitory role for tyrosine 984 in the juxtamembrane region of the insulin receptor. J. Biol. Chem. 278, 26007–26014. https://doi.org/10.1074/jbc.M302425200

Li, X., Zhang, Q., Fan, K., Li, B., Li, H., Qi, H., Guo, J., Cao, Y., Sun, H., 2016. Overexpression of TRPV3 Correlates with Tumor Progression in Non-Small Cell Lung Cancer. Int J Mol Sci 17. https://doi.org/10.3390/ijms17040437

Li, Y., Mangasarian, K., Mansukhani, A., Basilico, C., 1997. Activation of FGF receptors by mutations in the transmembrane domain. Oncogene 14, 1397–1406. https://doi.org/10.1038/sj.onc.1200983

Liao, R.G., Jung, J., Tchaicha, J., Wilkerson, M.D., Sivachenko, A., Beauchamp, E.M., Liu, Q., Pugh, T.J., Pedamallu, C.S., Hayes, D.N., Gray, N.S., Getz, G., Wong, K.-K., Haddad, R.I., Meyerson, M., Hammerman, P.S., 2013. Inhibitor-sensitive FGFR2 and FGFR3 mutations in lung squamous cell carcinoma. Cancer Res. 73, 5195–5205. https://doi.org/10.1158/0008-5472.CAN-12-3950

Lieu, T., Jayaweera, G., Zhao, P., Poole, D.P., Jensen, D., Grace, M., McIntyre, P., Bron, R., Wilson, Y.M., Krappitz, M., Haerteis, S., Korbmacher, C., Steinhoff, M.S., Nassini, R., Materazzi, S., Geppetti, P., Corvera, C.U., Bunnett, N.W., 2014. The Bile Acid Receptor TGR5 Activates the TRPA1 Channel to Induce Itch in Mice. Gastroenterology 147, 1417–1428. https://doi.org/10.1053/j.gastro.2014.08.042

Lin, C.-C., Melo, F.A., Ghosh, R., Suen, K.M., Stagg, L.J., Kirkpatrick, J., Arold, S.T., Ahmed, Z., Ladbury, J.E., 2012. Inhibition of Basal FGF Receptor Signaling by Dimeric Grb2. Cell 149, 1514–1524. https://doi.org/10.1016/j.cell.2012.04.033

Lisabeth, E.M., Falivelli, G., Pasquale, E.B., 2013. Eph receptor signaling and ephrins. Cold Spring Harb Perspect Biol 5. https://doi.org/10.1101/cshperspect.a009159

Lishko, P.V., Procko, E., Jin, X., Phelps, C.B., Gaudet, R., 2007. The ankyrin repeats of TRPV1 bind multiple ligands and modulate channel sensitivity. Neuron 54, 905–918. https://doi.org/10.1016/j.neuron.2007.05.027

Litan, A., Langhans, S.A., 2015. Cancer as a channelopathy: ion channels and pumps in tumor development and progression. Front Cell Neurosci 9, 86. https://doi.org/10.3389/fncel.2015.00086

Liu, X., Zou, J., Su, J., Lu, Y., Zhang, J., Li, L., Yin, F., 2016. Downregulation of transient receptor potential cation channel, subfamily C, member 1 contributes to drug resistance and high histological grade in ovarian cancer. Int. J. Oncol. 48, 243–252. https://doi.org/10.3892/ijo.2015.3254

Lo Russo, G., Imbimbo, M., Corrao, G., Proto, C., Signorelli, D., Vitali, M., Ganzinelli, M., Botta, L., Zilembo, N., de Braud, F., Garassino, M.C., 2017. Concomitant EML4-ALK rearrangement and EGFR mutation in non-small cell lung cancer patients: a literature review of 100 cases. Oncotarget 8, 59889–59900. https://doi.org/10.18632/oncotarget.17431

Lonic, A., Barry, E.F., Quach, C., Kobe, B., Saunders, N., Guthridge, M.A., 2008. Fibroblast growth factor receptor 2 phosphorylation on serine 779 couples to 14-3-3 and regulates cell survival and proliferation. Mol. Cell. Biol. 28, 3372–3385. https://doi.org/10.1128/MCB.01837-07

Luo, Y., Yang, C., Jin, C., Wang, F., McKeehan, W.L., 2009. Novel phosphotyrosine targets of FGFR2IIIb signaling. Cell Signal 21, 1370–1378. https://doi.org/10.1016/j.cellsig.2009.04.004

Macpherson, L.J., Dubin, A.E., Evans, M.J., Marr, F., Schultz, P.G., Cravatt, B.F., Patapoutian, A., 2007. Noxious compounds activate TRPA1 ion channels through covalent modification of cysteines. Nature 445, 541–545. https://doi.org/10.1038/nature05544

Macpherson, L.J., Geierstanger, B.H., Viswanath, V., Bandell, M., Eid, S.R., Hwang, S., Patapoutian, A., 2005. The pungency of garlic: activation

of TRPA1 and TRPV1 in response to allicin. Curr. Biol. 15, 929–934. https://doi.org/10.1016/j.cub.2005.04.018

Macpherson, L.J., Patapoutian, A., 2010. Flies feel your pain. Nature Chemical Biology 6, 252–253. https://doi.org/10.1038/nchembio.339

Manning, G., Whyte, D.B., Martinez, R., Hunter, T., Sudarsanam, S., 2002. The protein kinase complement of the human genome. Science 298, 1912–1934. https://doi.org/10.1126/science.1075762

Markovic-Mueller, S., Stuttfeld, E., Asthana, M., Weinert, T., Bliven, S., Goldie, K.N., Kisko, K., Capitani, G., Ballmer-Hofer, K., 2017. Structure of the Full-length VEGFR-1 Extracellular Domain in Complex with VEGF-A. Structure 25, 341–352. https://doi.org/10.1016/j.str.2016.12.012

Marsakova, L., Barvik, I., Zima, V., Zimova, L., Vlachova, V., 2017. The First Extracellular Linker Is Important for Several Aspects of the Gating Mechanism of Human TRPA1 Channel. Front Mol Neurosci 10. https://doi.org/10.3389/fnmol.2017.00016

Martínez-Delgado, G., Felix, R., 2017. Emerging Role of CaV1.2 Channels in Proliferation and Migration in Distinct Cancer Cell Lines. Oncology 93, 1–10. https://doi.org/10.1159/000464293

Matsuda, Y., Hagio, M., Seya, T., Ishiwata, T., 2012. Fibroblast Growth Factor Receptor 2 IIIc as a Therapeutic Target for Colorectal Cancer Cells. Mol Cancer Ther 11, 2010–2020. https://doi.org/10.1158/1535-7163.MCT-12-0243

Matsuda, Y., Yoshimura, H., Suzuki, T., Uchida, E., Naito, Z., Ishiwata, T., 2014. Inhibition of fibroblast growth factor receptor 2 attenuates proliferation and invasion of pancreatic cancer. Cancer Sci 105, 1212–1219. https://doi.org/10.1111/cas.12470

McDermott, S.C., Rodriguez-Ramirez, C., McDermott, S.P., Wicha, M.S., Nör, J.E., 2018. FGFR signaling regulates resistance of head and neck cancer stem cells to cisplatin. Oncotarget 9, 25148–25165. https://doi.org/10.18632/oncotarget.25358

Meents, J.E., Fischer, M.J.M., McNaughton, P.A., 2017. Sensitization of TRPA1 by Protein Kinase A. PLOS ONE 12, e0170097. https://doi.org/10.1371/journal.pone.0170097

Minke, B., Wu, C., Pak, W.L., 1975. Induction of photoreceptor voltage noise in the dark in Drosophila mutant. Nature 258, 84–87. https://doi.org/10.1038/258084a0

Monteith, G.R., Prevarskaya, N., Roberts-Thomson, S.J., 2017. The calcium-cancer signalling nexus. Nat. Rev. Cancer 17, 367–380. https://doi.org/10.1038/nrc.2017.18

Montell, C., 2005. Drosophila TRP channels. Pflugers Arch. 451, 19–28. https://doi.org/10.1007/s00424-005-1426-2

Montell, C., Birnbaumer, L., Flockerzi, V., Bindels, R.J., Bruford, E.A., Caterina, M.J., Clapham, D.E., Harteneck, C., Heller, S., Julius, D., Kojima, I., Mori, Y., Penner, R., Prawitt, D., Scharenberg, A.M., Schultz, G., Shimizu, N., Zhu, M.X., 2002. A unified nomenclature for the superfamily of TRP cation channels. Mol. Cell 9, 229–231. https://doi.org/10.1016/s1097-2765(02)00448-3

Montell, C., Rubin, G.M., 1989. Molecular characterization of the Drosophila trp locus: a putative integral membrane protein required for

phototransduction. Neuron 2, 1313–1323. https://doi.org/10.1016/0896-6273(89)90069-x

Moparthi, L., Survery, S., Kreir, M., Simonsen, C., Kjellbom, P., Högestätt, E.D., Johanson, U., Zygmunt, P.M., 2014. Human TRPA1 is intrinsically cold- and chemosensitive with and without its N-terminal ankyrin repeat domain. PNAS 111, 16901–16906. https://doi.org/10.1073/pnas.1412689111

Moqrich, A., Hwang, S.W., Earley, T.J., Petrus, M.J., Murray, A.N., Spencer, K.S.R., Andahazy, M., Story, G.M., Patapoutian, A., 2005. Impaired thermosensation in mice lacking TRPV3, a heat and camphor sensor in the skin. Science 307, 1468–1472. https://doi.org/10.1126/science.1108609

Mosavi, L.K., Cammett, T.J., Desrosiers, D.C., Peng, Z., 2004. The ankyrin repeat as molecular architecture for protein recognition. Protein Sci 13, 1435–1448. https://doi.org/10.1110/ps.03554604

Motiani, R.K., Abdullaev, I.F., Trebak, M., 2010. A novel native store-operated calcium channel encoded by Orai3: selective requirement of Orai3 versus Orai1 in estrogen receptor-positive versus estrogen receptor-negative breast cancer cells. J. Biol. Chem. 285, 19173–19183. https://doi.org/10.1074/jbc.M110.102582

Motiani, R.K., Hyzinski-García, M.C., Zhang, X., Henkel, M.M., Abdullaev, I.F., Kuo, Y.-H., Matrougui, K., Mongin, A.A., Trebak, M., 2013. STIM1 and Orai1 mediate CRAC channel activity and are essential for human glioblastoma invasion. Pflugers Arch. 465, 1249–1260. https://doi.org/10.1007/s00424-013-1254-8

Muller, I.B., de Langen, A.J., Giovannetti, E., Peters, G.J., 2017. Anaplastic lymphoma kinase inhibition in metastatic non-small cell lung cancer: clinical impact of alectinib. Onco Targets Ther 10, 4535–4541. https://doi.org/10.2147/OTT.S109493

Nadezhdin, K.D., García-Carpio, I., Goncharuk, S.A., Mineev, K.S., Arseniev, A.S., Vilar, M., 2016. Structural Basis of p75 Transmembrane Domain Dimerization. J. Biol. Chem. 291, 12346–12357. https://doi.org/10.1074/jbc.M116.723585

Nagata, K., Duggan, A., Kumar, G., García-Añoveros, J., 2005. Nociceptor and Hair Cell Transducer Properties of TRPA1, a Channel for Pain and Hearing. J. Neurosci. 25, 4052–4061. https://doi.org/10.1523/JNEUROSCI.0013-05.2005

Nakashima, S., Shiozaki, A., Ichikawa, D., Hikami, S., Kosuga, T., Konishi, H., Komatsu, S., Fujiwara, H., Okamoto, K., Kishimoto, M., Konishi, E., Otsuji, E., 2017. Transient Receptor Potential Melastatin 7 as an Independent Prognostic Factor in Human Esophageal Squamous Cell Carcinoma. Anticancer Res 37, 1161–1167.

Nan, X., Collisson, E.A., Lewis, S., Huang, J., Tamgüney, T.M., Liphardt, J.T., McCormick, F., Gray, J.W., Chu, S., 2013. Single-molecule superresolution imaging allows quantitative analysis of RAF multimer formation and signaling. Proc Natl Acad Sci U S A 110, 18519–18524. https://doi.org/10.1073/pnas.1318188110

Nielsen, N., Kondratska, K., Ruck, T., Hild, B., Kovalenko, I., Schimmelpfennig, S., Welzig, J., Sargin, S., Lindemann, O., Christian, S., Meuth, S.G., Prevarskaya, N., Schwab, A., 2017. TRPC6 channels modulate the response of pancreatic stellate cells to

hypoxia. Pflugers Arch. 469, 1567–1577. https://doi.org/10.1007/s00424-017-2057-0

Nilius, B., Owsianik, G., 2011. The transient receptor potential family of ion channels. Genome Biol. 12, 218. https://doi.org/10.1186/gb-2011-12-3-218

Ogiso, H., Ishitani, R., Nureki, O., Fukai, S., Yamanaka, M., Kim, J.-H., Saito, K., Sakamoto, A., Inoue, M., Shirouzu, M., Yokoyama, S., 2002. Crystal structure of the complex of human epidermal growth factor and receptor extracellular domains. Cell 110, 775–787. https://doi.org/10.1016/s0092-8674(02)00963-7

Ohkubo, T., Yamazaki, J., 2012. T-type voltage-activated calcium channel Cav3.1, but not Cav3.2, is involved in the inhibition of proliferation and apoptosis in MCF-7 human breast cancer cells. Int. J. Oncol. 41, 267–275. https://doi.org/10.3892/ijo.2012.1422

Okada, T., Inoue, R., Yamazaki, K., Maeda, A., Kurosaki, T., Yamakuni, T., Tanaka, I., Shimizu, S., Ikenaka, K., Imoto, K., Mori, Y., 1999. Molecular and functional characterization of a novel mouse transient receptor potential protein homologue TRP7. Ca(2+)-permeable cation channel that is constitutively activated and enhanced by stimulation of G protein-coupled receptor. J. Biol. Chem. 274, 27359–27370. https://doi.org/10.1074/jbc.274.39.27359

Olsen, S.K., Ibrahimi, O.A., Raucci, A., Zhang, F., Eliseenkova, A.V., Yayon, A., Basilico, C., Linhardt, R.J., Schlessinger, J., Mohammadi, M., 2004. Insights into the molecular basis for fibroblast growth factor receptor autoinhibition and ligand-binding promiscuity. PNAS 101, 935–940. https://doi.org/10.1073/pnas.0307287101

Ong, S.H., Guy, G.R., Hadari, Y.R., Laks, S., Gotoh, N., Schlessinger, J., Lax, I., 2000. FRS2 proteins recruit intracellular signaling pathways by binding to diverse targets on fibroblast growth factor and nerve growth factor receptors. Mol. Cell. Biol. 20, 979–989. https://doi.org/10.1128/mcb.20.3.979-989.2000

Ornitz, D.M., Itoh, N., 2015. The Fibroblast Growth Factor signaling pathway. Wiley Interdiscip Rev Dev Biol 4, 215–266. https://doi.org/10.1002/wdev.176

Pao, W., Miller, V.A., Politi, K.A., Riely, G.J., Somwar, R., Zakowski, M.F., Kris, M.G., Varmus, H., 2005. Acquired resistance of lung adenocarcinomas to gefitinib or erlotinib is associated with a second mutation in the EGFR kinase domain. PLoS Med. 2, e73. https://doi.org/10.1371/journal.pmed.0020073

Park, J., Shim, M.K., Jin, M., Rhyu, M.-R., Lee, Y., 2016. Methyl syringate, a TRPA1 agonist represses hypoxia-induced cyclooxygenase-2 in lung cancer cells. Phytomedicine 23, 324–329. https://doi.org/10.1016/j.phymed.2016.01.009

Park, Y.R., Chun, J.N., So, I., Kim, H.J., Baek, S., Jeon, J.-H., Shin, S.-Y., 2016. Data-driven Analysis of TRP Channels in Cancer: Linking Variation in Gene Expression to Clinical Significance. Cancer Genomics Proteomics 13, 83–90.

Paulsen, C.E., Armache, J.-P., Gao, Y., Cheng, Y., Julius, D., 2015. Structure of the TRPA1 ion channel suggests regulatory mechanisms. Nature 520, 511–517. https://doi.org/10.1038/nature14367

Peiris, M.N., Li, F., Donoghue, D.J., 2019. BCR: a promiscuous fusion partner in hematopoietic disorders. Oncotarget 10, 2738–2754. https://doi.org/10.18632/oncotarget.26837

Pellegrini, L., Burke, D.F., von Delft, F., Mulloy, B., Blundell, T.L., 2000. Crystal structure of fibroblast growth factor receptor ectodomain bound to ligand and heparin. Nature 407, 1029–1034. https://doi.org/10.1038/35039551

Peng, M., Wang, Z., Yang, Z., Tao, L., Liu, Q., Yi, L.U., Wang, X., 2015. Overexpression of short TRPM8 variant α promotes cell migration and invasion, and decreases starvation-induced apoptosis in prostate cancer LNCaP cells. Oncol Lett 10, 1378–1384. https://doi.org/10.3892/ol.2015.3373

Pera, E., Kaemmerer, E., Milevskiy, M.J.G., Yapa, K.T.D.S., O'Donnell, J.S., Brown, M.A., Simpson, F., Peters, A.A., Roberts-Thomson, S.J., Monteith, G.R., 2016. The voltage gated Ca2+-channel Cav3.2 and therapeutic responses in breast cancer. Cancer Cell International 16, 24. https://doi.org/10.1186/s12935-016-0299-0

Peters, A.A., Simpson, P.T., Bassett, J.J., Lee, J.M., Silva, L.D., Reid, L.E., Song, S., Parat, M.-O., Lakhani, S.R., Kenny, P.A., Roberts-Thomson, S.J., Monteith, G.R., 2012. Calcium Channel TRPV6 as a Potential Therapeutic Target in Estrogen Receptor–Negative Breast Cancer. Mol Cancer Ther 11, 2158–2168. https://doi.org/10.1158/1535-7163.MCT-11-0965

Phillips, A.M., Bull, A., Kelly, L.E., 1992. Identification of a Drosophila gene encoding a calmodulin-binding protein with homology to the trp phototransduction gene. Neuron 8, 631–642. https://doi.org/10.1016/0896-6273(92)90085-R

Piao, L.H., Fujita, T., Jiang, C.Y., Liu, T., Yue, H.Y., Nakatsuka, T., Kumamoto, E., 2009. TRPA1 activation by lidocaine in nerve terminals results in glutamate release increase. Biochem Biophys Res Commun 379, 980–984. https://doi.org/10.1016/j.bbrc.2008.12.183

Plotnikov, A.N., Hubbard, S.R., Schlessinger, J., Mohammadi, M., 2000. Crystal structures of two FGF-FGFR complexes reveal the determinants of ligand-receptor specificity. Cell 101, 413–424. https://doi.org/10.1016/s0092-8674(00)80851-x

Pollock, P., Gartside, M., Dejeza, L., Powell, M., Mallon, M., Davies, H., Mohammadi, M., Futreal, P., Stratton, M., Trent, J., Goodfellow, P., 2007. Frequent activating FGFR2 mutations in endometrial carcinomas parallel germline mutations associated with craniosynostosis and skeletal dysplasia syndromes. Oncogene 26, 7158–7162. https://doi.org/10.1038/sj.onc.1210529

Poulin, B., Sekiya, F., Rhee, S.G., 2005. Intramolecular interaction between phosphorylated tyrosine-783 and the C-terminal Src homology 2 domain activates phospholipase C-gamma1. Proc. Natl. Acad. Sci. U.S.A. 102, 4276–4281. https://doi.org/10.1073/pnas.0409590102

Prawitt, D., Monteilh-Zoller, M.K., Brixel, L., Spangenberg, C., Zabel, B., Fleig, A., Penner, R., 2003. TRPM5 is a transient Ca2+-activated cation channel responding to rapid changes in [Ca2+]i. Proc. Natl. Acad. Sci. U.S.A. 100, 15166–15171. https://doi.org/10.1073/pnas.2334624100

Puchner, E.M., Walter, J.M., Kasper, R., Huang, B., Lim, W.A., 2013. Counting molecules in single organelles with superresolution microscopy allows tracking of the endosome maturation trajectory. Proc. Natl. Acad. Sci. U.S.A. 110, 16015–16020. https://doi.org/10.1073/pnas.1309676110

Pyrski, M., Eckstein, E., Schmid, A., Bufe, B., Weiss, J., Chubanov, V., Boehm, U., Zufall, F., 2017. Trpm5 expression in the olfactory epithelium. Mol. Cell. Neurosci. 80, 75–88. https://doi.org/10.1016/j.mcn.2017.02.002

Qian, X., Karpova, T., Sheppard, A.M., McNally, J., Lowy, D.R., 2004. E-cadherin-mediated adhesion inhibits ligand-dependent activation of diverse receptor tyrosine kinases. EMBO J. 23, 1739–1748. https://doi.org/10.1038/sj.emboj.7600136

Rader, K., Orlando, R.A., Lou, X., Farquhar, M.G., 2000. Characterization of ANKRA, a novel ankyrin repeat protein that interacts with the cytoplasmic domain of megalin. J. Am. Soc. Nephrol. 11, 2167–2178.

Ranieri, D., Belleudi, F., Magenta, A., Torrisi, M.R., 2015a. HPV16 E5 expression induces switching from FGFR2b to FGFR2c and epithelial-mesenchymal transition. Int. J. Cancer 137, 61–72. https://doi.org/10.1002/ijc.29373

Ranieri, D., Rosato, B., Nanni, M., Magenta, A., Belleudi, F., Torrisi, M.R., 2015b. Expression of the FGFR2 mesenchymal splicing variant in epithelial cells drives epithelial-mesenchymal transition. Oncotarget 7, 5440–5460. https://doi.org/10.18632/oncotarget.6706

Raphaël, M., Lehen'kyi, V., Vandenberghe, M., Beck, B., Khalimonchyk, S., Vanden Abeele, F., Farsetti, L., Germain, E., Bokhobza, A., Mihalache, A., Gosset, P., Romanin, C., Clézardin, P., Skryma, R., Prevarskaya, N., 2014. TRPV6 calcium channel translocates to the plasma membrane via Orai1-mediated mechanism and controls cancer cell survival. Proc. Natl. Acad. Sci. U.S.A. 111, E3870-3879. https://doi.org/10.1073/pnas.1413409111

Redler, A., Di Rocco, G., Giannotti, D., Frezzotti, F., Bernieri, M.G., Ceccarelli, S., D'Amici, S., Vescarelli, E., Mitterhofer, A.P., Angeloni, A., Marchese, C., 2013. Fibroblast Growth Factor Receptor-2 Expression in Thyroid Tumor Progression: Potential Diagnostic Application. PLoS One 8. https://doi.org/10.1371/journal.pone.0072224

Regad, T., 2015. Targeting RTK Signaling Pathways in Cancer. Cancers (Basel) 7, 1758–1784. https://doi.org/10.3390/cancers7030860

Reshetnyak, A.V., Opatowsky, Y., Boggon, T.J., Folta-Stogniew, E., Tome, F., Lax, I., Schlessinger, J., 2015. The strength and cooperativity of KIT ectodomain contacts determine normal ligand-dependent stimulation or oncogenic activation in cancer. Mol. Cell 57, 191–201. https://doi.org/10.1016/j.molcel.2014.11.021

Ries, J., Kaplan, C., Platonova, E., Eghlidi, H., Ewers, H., 2012. A simple, versatile method for GFP-based super-resolution microscopy via nanobodies. Nat. Methods 9, 582–584. https://doi.org/10.1038/nmeth.1991

Robinson, D.R., Wu, Y.M., Lin, S.F., 2000. The protein tyrosine kinase family of the human genome. Oncogene 19, 5548–5557. https://doi.org/10.1038/sj.onc.1203957

Rubin, G.M., Yandell, M.D., Wortman, J.R., Gabor Miklos, G.L., Nelson, C.R., Hariharan, I.K., Fortini, M.E., Li, P.W., Apweiler, R., Fleischmann, W., Cherry, J.M., Henikoff, S., Skupski, M.P., Misra, S., Ashburner, M., Birney, E., Boguski, M.S., Brody, T., Brokstein, P., Celniker, S.E., Chervitz, S.A., Coates, D., Cravchik, A., Gabrielian, A., Galle, R.F., Gelbart, W.M., George, R.A., Goldstein, L.S., Gong, F., Guan, P., Harris, N.L., Hay, B.A., Hoskins, R.A., Li, J., Li, Z., Hynes, R.O., Jones, S.J., Kuehl, P.M., Lemaitre, B., Littleton, J.T., Morrison, D.K., Mungall, C., O'Farrell, P.H., Pickeral, O.K., Shue, C., Vosshall, L.B., Zhang, J., Zhao, Q., Zheng, X.H., Lewis, S., 2000. Comparative genomics of the eukaryotes. Science 287, 2204–2215. https://doi.org/10.1126/science.287.5461.2204

Ruparel, S., Bendele, M., Wallace, A., Green, D., 2015. Released lipids regulate Transient Receptor Potential Channel (TRP)-dependent oral cancer pain. Mol Pain 11. https://doi.org/10.1186/s12990-015-0016-3

Russo, A., Franchina, T., Ricciardi, G.R.R., Smiroldo, V., Picciotto, M., Zanghì, M., Rolfo, C., Adamo, V., 2017. Third generation EGFR TKIs in EGFR-mutated NSCLC: Where are we now and where are we going. Crit. Rev. Oncol. Hematol. 117, 38–47. https://doi.org/10.1016/j.critrevonc.2017.07.003

Rybarczyk, P., Vanlaeys, A., Brassart, B., Dhennin-Duthille, I., Chatelain, D., Sevestre, H., Ouadid-Ahidouch, H., Gautier, M., 2017. The Transient Receptor Potential Melastatin 7 Channel Regulates Pancreatic Cancer Cell Invasion through the Hsp90α/uPA/MMP2 pathway. Neoplasia 19, 288–300. https://doi.org/10.1016/j.neo.2017.01.004

Sarabipour, S., Ballmer-Hofer, K., Hristova, K., n.d. VEGFR-2 conformational switch in response to ligand binding. eLife 5. https://doi.org/10.7554/eLife.13876

Sarabipour, S., Hristova, K., 2016. Pathogenic Cysteine Removal Mutations in FGFR Extracellular Domains Stabilize Receptor Dimers and Perturb the TM Dimer Structure. J. Mol. Biol. 428, 3903–3910. https://doi.org/10.1016/j.jmb.2016.08.026

Scaltriti, M., Rojo, F., Ocaña, A., Anido, J., Guzman, M., Cortes, J., Di Cosimo, S., Matias-Guiu, X., Ramon y Cajal, S., Arribas, J., Baselga, J., 2007. Expression of p95HER2, a truncated form of the HER2 receptor, and response to anti-HER2 therapies in breast cancer. J. Natl. Cancer Inst. 99, 628–638. https://doi.org/10.1093/jnci/djk134

Schaefer, E.A.M., Stohr, S., Meister, M., Aigner, A., Gudermann, T., Buech, T.R.H., 2013. Stimulation of the chemosensory TRPA1 cation channel by volatile toxic substances promotes cell survival of small cell lung cancer cells. Biochem. Pharmacol. 85, 426–438. https://doi.org/10.1016/j.bcp.2012.11.019

Scheible, M.B., Tinnefeld, P., 2018. Quantifying Expansion Microscopy with DNA Origami Expansion Nanorulers. bioRxiv 265405. https://doi.org/10.1101/265405

Schermelleh, L., Ferrand, A., Huser, T., Eggeling, C., Sauer, M., Biehlmaier, O., Drummen, G.P.C., 2019. Super-resolution microscopy demystified. Nat Cell Biol 21, 72–84. https://doi.org/10.1038/s41556-018-0251-8

Schildhaus, H.-U., Nogova, L., Wolf, J., Buettner, R., 2013. FGFR1 amplifications in squamous cell carcinomas of the lung: diagnostic

and therapeutic implications. Translational Lung Cancer Research 2, 92-100–100.

Schlessinger, J., 2000. Cell signaling by receptor tyrosine kinases. Cell 103, 211–225. https://doi.org/10.1016/s0092-8674(00)00114-8

Selli, C., Erac, Y., Kosova, B., Erdal, E.S., Tosun, M., 2015. Silencing of TRPC1 regulates store-operated calcium entry and proliferation in Huh7 hepatocellular carcinoma cells. Biomed. Pharmacother. 71, 194–200. https://doi.org/10.1016/j.biopha.2015.02.024

Shapovalov, G., Ritaine, A., Skryma, R., Prevarskaya, N., 2016. Role of TRP ion channels in cancer and tumorigenesis. Semin Immunopathol 38, 357–369. https://doi.org/10.1007/s00281-015-0525-1

Sheard, T.M.D., Hurley, M.E., Colyer, J., White, E., Norman, R., Pervolaraki, E., Narayanasamy, K.K., Hou, Y., Kirton, H.M., Yang, Z., Hunter, L., Shim, J., Clowsley, A.H., Smith, A.J., Baddeley, D., Soeller, C., Colman, M.A., Jayasinghe, I., 2019. Three-Dimensional and Chemical Mapping of Intracellular Signaling Nanodomains in Health and Disease with Enhanced Expansion Microscopy. ACS Nano 13, 2143–2157. https://doi.org/10.1021/acsnano.8b08742

Shen, J., Maruyama, I.N., 2012. Brain-derived neurotrophic factor receptor TrkB exists as a preformed dimer in living cells. J Mol Signal 7, 2. https://doi.org/10.1186/1750-2187-7-2

Shen, J., Sun, D., Shao, J., Chen, Y., Pang, K., Guo, W., Lu, B., 2019. Extracellular Juxtamembrane Motif Critical for TrkB Preformed Dimer and Activation. Cells 8. https://doi.org/10.3390/cells8080932

Shewchuk, L.M., Hassell, A.M., Ellis, B., Holmes, W.D., Davis, R., Horne, E.L., Kadwell, S.H., McKee, D.D., Moore, J.T., 2000. Structure of the Tie2 RTK Domain: Self-Inhibition by the Nucleotide Binding Loop, Activation Loop, and C-Terminal Tail. Structure 8, 1105–1113. https://doi.org/10.1016/S0969-2126(00)00516-5

Shoji, K., Teishima, J., Hayashi, T., Ohara, S., Mckeehan, W.L., Matsubara, A., 2014. Restoration of fibroblast growth factor receptor 2IIIb enhances the chemosensitivity of human prostate cancer cells. Oncology Reports 32, 65–70. https://doi.org/10.3892/or.2014.3200

Sia, D., Losic, B., Moeini, A., Cabellos, L., Hao, K., Revill, K., Bonal, D., Miltiadous, O., Zhang, Z., Hoshida, Y., Cornella, H., Castillo-Martin, M., Pinyol, R., Kasai, Y., Roayaie, S., Thung, S.N., Fuster, J., Schwartz, M.E., Waxman, S., Cordon-Cardo, C., Schadt, E., Mazzaferro, V., Llovet, J.M., 2015. Massive parallel sequencing uncovers actionable FGFR2-PPHLN1 fusion and ARAF mutations in intrahepatic cholangiocarcinoma. Nat Commun 6, 6087. https://doi.org/10.1038/ncomms7087

Skrzypski, M., Kołodziejski, P.A., Mergler, S., Khajavi, N., Nowak, K.W., Strowski, M.Z., 2016. TRPV6 modulates proliferation of human pancreatic neuroendocrine BON-1 tumour cells. Biosci Rep 36. https://doi.org/10.1042/BSR20160106

Smith, G.D., Gunthorpe, M.J., Kelsell, R.E., Hayes, P.D., Reilly, P., Facer, P., Wright, J.E., Jerman, J.C., Walhin, J.-P., Ooi, L., Egerton, J., Charles, K.J., Smart, D., Randall, A.D., Anand, P., Davis, J.B., 2002. TRPV3 is a temperature-sensitive vanilloid receptor-like protein. Nature 418, 186–190. https://doi.org/10.1038/nature00894

So, K., Tei, Y., Zhao, M., Miyake, T., Hiyama, H., Shirakawa, H., Imai, S., Mori, Y., Nakagawa, T., Matsubara, K., Kaneko, S., 2016. Hypoxia-induced sensitisation of TRPA1 in painful dysesthesia evoked by transient hindlimb ischemia/reperfusion in mice. Scientific Reports 6, 1–12. https://doi.org/10.1038/srep23261

Soda, M., Choi, Y.L., Enomoto, M., Takada, S., Yamashita, Y., Ishikawa, S., Fujiwara, S., Watanabe, H., Kurashina, K., Hatanaka, H., Bando, M., Ohno, S., Ishikawa, Y., Aburatani, H., Niki, T., Sohara, Y., Sugiyama, Y., Mano, H., 2007. Identification of the transforming EML4-ALK fusion gene in non-small-cell lung cancer. Nature 448, 561–566. https://doi.org/10.1038/nature05945

Söderberg, O., Gullberg, M., Jarvius, M., Ridderstråle, K., Leuchowius, K.-J., Jarvius, J., Wester, K., Hydbring, P., Bahram, F., Larsson, L.-G., Landegren, U., 2006. Direct observation of individual endogenous protein complexes in situ by proximity ligation. Nat. Methods 3, 995–1000. https://doi.org/10.1038/nmeth947

Song, C., Bae, Y., Jun, J., Lee, H., Kim, N.D., Lee, K.-B., Hur, W., Park, J.-Y., Sim, T., 2017. Identification of TG100-115 as a new and potent TRPM7 kinase inhibitor, which suppresses breast cancer cell migration and invasion. Biochim Biophys Acta Gen Subj 1861, 947–957. https://doi.org/10.1016/j.bbagen.2017.01.034

Stepanenko, A.A., Dmitrenko, V.V., 2015. HEK293 in cell biology and cancer research: phenotype, karyotype, tumorigenicity, and stress-induced genome-phenotype evolution. Gene 569, 182–190. https://doi.org/10.1016/j.gene.2015.05.065

Stewart, A., Smith, G., Sandford, R., Edwardson, J., 2010. Atomic Force Microscopy Reveals the Alternating Subunit Arrangement of the TRPP2-TRPV4 Heterotetramer. Biophysical journal 99, 790–7. https://doi.org/10.1016/j.bpj.2010.05.012

Story, G.M., Peier, A.M., Reeve, A.J., Eid, S.R., Mosbacher, J., Hricik, T.R., Earley, T.J., Hergarden, A.C., Andersson, D.A., Hwang, S.W., McIntyre, P., Jegla, T., Bevan, S., Patapoutian, A., 2003. ANKTM1, a TRP-like channel expressed in nociceptive neurons, is activated by cold temperatures. Cell 112, 819–829. https://doi.org/10.1016/s0092-8674(03)00158-2

Strübing, C., Krapivinsky, G., Krapivinsky, L., Clapham, D.E., 2001. TRPC1 and TRPC5 form a novel cation channel in mammalian brain. Neuron 29, 645–655. https://doi.org/10.1016/s0896-6273(01)00240-9

Studier, F.W., Moffatt, B.A., 1986. Use of bacteriophage T7 RNA polymerase to direct selective high-level expression of cloned genes. J. Mol. Biol. 189, 113–130. https://doi.org/10.1016/0022-2836(86)90385-2

Sun, M., Goldin, E., Stahl, S., Falardeau, J.L., Kennedy, J.C., Acierno, J.S., Bove, C., Kaneski, C.R., Nagle, J., Bromley, M.C., Colman, M., Schiffmann, R., Slaugenhaupt, S.A., 2000. Mucolipidosis type IV is caused by mutations in a gene encoding a novel transient receptor potential channel. Hum. Mol. Genet. 9, 2471–2478. https://doi.org/10.1093/hmg/9.17.2471

Suss-Toby, E., Selinger, Z., Minke, B., 1991. Lanthanum reduces the excitation efficiency in fly photoreceptors. The Journal of General Physiology 98, 849–868. https://doi.org/10.1085/jgp.98.4.849

Tajeddine, N., Gailly, P., 2012. TRPC1 Protein Channel Is Major Regulator of Epidermal Growth Factor Receptor Signaling. J Biol Chem 287, 16146–16157. https://doi.org/10.1074/jbc.M112.340034

Takahashi, N., Chen, H.-Y., Harris, I.S., Stover, D.G., Selfors, L.M., Bronson, R.T., Deraedt, T., Cichowski, K., Welm, A.L., Mori, Y., Mills, G.B., Brugge, J.S., 2018. Cancer Cells Co-opt the Neuronal Redox-Sensing Channel TRPA1 to Promote Oxidative-Stress Tolerance. Cancer Cell 33, 985-1003.e7. https://doi.org/10.1016/j.ccell.2018.05.001

Takahashi, N., Kuwaki, T., Kiyonaka, S., Numata, T., Kozai, D., Mizuno, Y., Yamamoto, S., Naito, S., Knevels, E., Carmeliet, P., Oga, T., Kaneko, S., Suga, S., Nokami, T., Yoshida, J., Mori, Y., 2011. TRPA1 underlies a sensing mechanism for O2. Nat. Chem. Biol. 7, 701–711. https://doi.org/10.1038/nchembio.640

Takahashi, N., Mizuno, Y., Kozai, D., Yamamoto, S., Kiyonaka, S., Shibata, T., Uchida, K., Mori, Y., 2008. Molecular characterization of TRPA1 channel activation by cysteine-reactive inflammatory mediators. Channels (Austin) 2, 287–298. https://doi.org/10.4161/chan.2.4.6745

TAMURA, T., KURISHIMA, K., NAKAZAWA, K., KAGOHASHI, K., ISHIKAWA, H., SATOH, H., HIZAWA, N., 2015. Specific organ metastases and survival in metastatic non-small-cell lung cancer. Mol Clin Oncol 3, 217–221. https://doi.org/10.3892/mco.2014.410

Tanaka, K., Nosaki, K., Otsubo, K., Azuma, K., Sakata, S., Ouchi, H., Morinaga, R., Wataya, H., Fujii, A., Nakagaki, N., Tsuruta, N., Takeshita, M., Iwama, E., Harada, T., Nakanishi, Y., Okamoto, I., 2017. Acquisition of the T790M resistance mutation during afatinib treatment in EGFR tyrosine kinase inhibitor-naïve patients with non-small cell lung cancer harboring EGFR mutations. Oncotarget 8, 68123–68130. https://doi.org/10.18632/oncotarget.19243

Tchaicha, J.H., Akbay, E.A., Altabef, A., Mikse, O.R., Kikuchi, E., Rhee, K., Liao, R.G., Bronson, R.T., Sholl, L.M., Meyerson, M., Hammerman, P.S., Wong, K.-K., 2014. Kinase domain activation of FGFR2 yields high-grade lung adenocarcinoma sensitive to a Pan-FGFR inhibitor in a mouse model of NSCLC. Cancer Res. 74, 4676–4684. https://doi.org/10.1158/0008-5472.CAN-13-3218

Terasawa, H., Kohda, D., Hatanaka, H., Tsuchiya, S., Ogura, K., Nagata, K., Ishii, S., Mandiyan, V., Ullrich, A., Schlessinger, J., Inagaki, F., 1994. Structure of the N-terminal SH3 domain of GRB2 complexed with a peptide from the guanine nucleotide releasing factor Sos. Nature Structural Biology 1, 891–897. https://doi.org/10.1038/nsb1294-891

The top 10 causes of death [WWW Document], n.d. URL https://www.who.int/news-room/fact-sheets/detail/the-top-10-causes-of-death (accessed 11.22.19).

Theelen, W.S., Mittempergher, L., Willems, S.M., Bosma, A.J., Peters, D.D., van der Noort, V., Japenga, E.J., Peeters, T., Koole, K., Šuštić, T., Blaauwgeers, J.L., van Noesel, C.J., Bernards, R., van den Heuvel, M.M., 2016. FGFR1, 2 and 3 protein overexpression and molecular aberrations of FGFR3 in early stage non-small cell lung cancer. J Pathol Clin Res 2, 223–233. https://doi.org/10.1002/cjp2.51

Till, J.H., Becerra, M., Watty, A., Lu, Y., Ma, Y., Neubert, T.A., Burden, S.J., Hubbard, S.R., 2002. Crystal structure of the MuSK tyrosine kinase:

insights into receptor autoregulation. Structure 10, 1187–1196. https://doi.org/10.1016/s0969-2126(02)00814-6

Timsah, Z., Ahmed, Z., Lin, C.-C., Melo, F.A., Stagg, L.J., Leonard, P.G., Jeyabal, P., Berrout, J., O'Neil, R.G., Bogdanov, M., Ladbury, J.E., 2014. Competition between Grb2 and Plcγ1 for FGFR2 regulates basal phospholipase activity and invasion. Nature Structural & Molecular Biology 21, 180–188. https://doi.org/10.1038/nsmb.2752

Timsah, Z., Berrout, J., Suraokar, M., Behrens, C., Song, J., Lee, J.J., Ivan, C., Gagea, M., Shires, M., Hu, X., Vallien, C., Kingsley, C.V., Wistuba, I., Ladbury, J.E., 2015. Expression pattern of FGFR2, Grb2 and Plcγ1 acts as a novel prognostic marker of recurrence recurrence-free survival in lung adenocarcinoma. Am J Cancer Res 5, 3135–3148.

Torre, L.A., Bray, F., Siegel, R.L., Ferlay, J., Lortet-Tieulent, J., Jemal, A., 2015. Global cancer statistics, 2012. CA Cancer J Clin 65, 87–108. https://doi.org/10.3322/caac.21262

Trevisan, G., Materazzi, S., Fusi, C., Altomare, A., Aldini, G., Lodovici, M., Patacchini, R., Geppetti, P., Nassini, R., 2013. Novel therapeutic strategy to prevent chemotherapy-induced persistent sensory neuropathy by TRPA1 blockade. Cancer Res. 73, 3120–3131. https://doi.org/10.1158/0008-5472.CAN-12-4370

Truckenbrodt, S., Maidorn, M., Crzan, D., Wildhagen, H., Kabatas, S., Rizzoli, S.O., 2018. X10 expansion microscopy enables 25-nm resolution on conventional microscopes. EMBO Rep. 19. https://doi.org/10.15252/embr.201845836

Tsai, S.-C., Huang, W.-W., Huang, W.-C., Lu, C.-C., Chiang, J.-H., Peng, S.-F., Chung, J.-G., Lin, Y.-H., Hsu, Y.-M., Amagaya, S., Yang, J.-S., 2012. ERK-modulated intrinsic signaling and G(2)/M phase arrest contribute to the induction of apoptotic death by allyl isothiocyanate in MDA-MB-468 human breast adenocarcinoma cells. Int. J. Oncol. 41, 2065–2072. https://doi.org/10.3892/ijo.2012.1640

Tuteja, N., 2009. Signaling through G protein coupled receptors. Plant Signal Behav 4, 942–947.

Ulăreanu, R., Chiriţoiu, G., Cojocaru, F., Deftu, A., Ristoiu, V., Stănică, L., Mihăilescu, D.F., Cucu, D., 2017. N-glycosylation of the transient receptor potential melastatin 8 channel is altered in pancreatic cancer cells. Tumour Biol. 39, 1010428317720940. https://doi.org/10.1177/1010428317720940

Vancauwenberghe, E., Noyer, L., Derouiche, S., Lemonnier, L., Gosset, P., Sadofsky, L.R., Mariot, P., Warnier, M., Bokhobza, A., Slomianny, C., Mauroy, B., Bonnal, J.-L., Dewailly, E., Delcourt, P., Allart, L., Desruelles, E., Prevarskaya, N., Roudbaraki, M., 2017. Activation of mutated TRPA1 ion channel by resveratrol in human prostate cancer associated fibroblasts (CAF). Mol. Carcinog. 56, 1851–1867. https://doi.org/10.1002/mc.22642

Vashisht, A., Trebak, M., Motiani, R.K., 2015. STIM and Orai proteins as novel targets for cancer therapy. A Review in the Theme: Cell and Molecular Processes in Cancer Metastasis. Am. J. Physiol., Cell Physiol. 309, C457-469. https://doi.org/10.1152/ajpcell.00064.2015

Veldhuisen, B., Spruit, L., Dauwerse, H.G., Breuning, M.H., Peters, D.J., 1999. Genes homologous to the autosomal dominant polycystic

kidney disease genes (PKD1 and PKD2). Eur. J. Hum. Genet. 7, 860–872. https://doi.org/10.1038/sj.ejhg.5200383

Velghe, A.I., Van Cauwenberghe, S., Polyansky, A.A., Chand, D., Montano-Almendras, C.P., Charni, S., Hallberg, B., Essaghir, A., Demoulin, J.-B., 2014. PDGFRA alterations in cancer: characterization of a gain-of-function V536E transmembrane mutant as well as loss-of-function and passenger mutations. Oncogene 33, 2568–2576. https://doi.org/10.1038/onc.2013.218

Venkatachalam, K., Montell, C., 2007. TRP channels. Annu. Rev. Biochem. 76, 387–417. https://doi.org/10.1146/annurev.biochem.75.103004.142819

Voets, T., Talavera, K., Owsianik, G., Nilius, B., 2005. Sensing with TRP channels. Nat. Chem. Biol. 1, 85–92. https://doi.org/10.1038/nchembio0705-85

Voronin, D.A., Kiseleva, E.V., 2008. Functional role of proteins containing ankyrin repeats. Cell Tiss. Biol. 2, 1–12. https://doi.org/10.1134/S1990519X0801001X

Wan, X., Lu, Y., Chen, X., Xiong, J., Zhou, Y., Li, P., Xia, B., Li, M., Zhu, M.X., Gao, Z., 2014. Bimodal voltage dependence of TRPA1: mutations of a key pore helix residue reveal strong intrinsic voltage-dependent inactivation. Pflugers Arch - Eur J Physiol 466, 1273–1287. https://doi.org/10.1007/s00424-013-1345-6

Wang, S., Dai, Y., Fukuoka, T., Yamanaka, H., Kobayashi, K., Obata, K., Cui, X., Tominaga, M., Noguchi, K., 2008. Phospholipase C and protein kinase A mediate bradykinin sensitization of TRPA1: a molecular mechanism of inflammatory pain. Brain 131, 1241–1251. https://doi.org/10.1093/brain/awn060

Wang, T., Ning, K., Lu, T.-X., Hua, D., 2017a. Elevated expression of TrpC5 and GLUT1 is associated with chemoresistance in colorectal cancer. Oncology Reports 37, 1059–1065. https://doi.org/10.3892/or.2016.5322

Wang, T., Ning, K., Lu, T.-X., Sun, X., Jin, L., Qi, X., Jin, J., Hua, D., 2017b. Increasing circulating exosomes-carrying TRPC5 predicts chemoresistance in metastatic breast cancer patients. Cancer Sci. 108, 448–454. https://doi.org/10.1111/cas.13150

Wang, Y.Y., Chang, R.B., Waters, H.N., McKemy, D.D., Liman, E.R., 2008. The nociceptor ion channel TRPA1 is potentiated and inactivated by permeating calcium ions. J. Biol. Chem. 283, 32691–32703. https://doi.org/10.1074/jbc.M803568200

Ward, C.W., Lawrence, M.C., Streltsov, V.A., Adams, T.E., McKern, N.M., 2007. The insulin and EGF receptor structures: new insights into ligand-induced receptor activation. Trends Biochem. Sci. 32, 129–137. https://doi.org/10.1016/j.tibs.2007.01.001

Wassie, A.T., Zhao, Y., Boyden, E.S., 2019. Expansion microscopy: principles and uses in biological research. Nat Methods 16, 33–41. https://doi.org/10.1038/s41592-018-0219-4

Watanabe, H., Vriens, J., Janssens, A., Wondergem, R., Droogmans, G., Nilius, B., 2003. Modulation of TRPV4 gating by intra- and extracellular Ca2+. Cell Calcium 33, 489–495. https://doi.org/10.1016/s0143-4160(03)00064-2

Webster, M.K., Donoghue, D.J., 1996. Constitutive activation of fibroblast growth factor receptor 3 by the transmembrane domain point mutation found in achondroplasia. EMBO J. 15, 520–527.

Wehrman, T., He, X., Raab, B., Dukipatti, A., Blau, H., Garcia, K.C., 2007. Structural and mechanistic insights into nerve growth factor interactions with the TrkA and p75 receptors. Neuron 53, 25–38. https://doi.org/10.1016/j.neuron.2006.09.034

Wei, W., Huang, W., Lin, Y., Becker, E.B.E., Ansorge, O., Flockerzi, V., Conti, D., Cenacchi, G., Glitsch, M.D., 2017. Functional expression of calcium-permeable canonical transient receptor potential 4-containing channels promotes migration of medulloblastoma cells. J Physiol 595, 5525–5544. https://doi.org/10.1113/JP274659

Wes, P.D., Chevesich, J., Jeromin, A., Rosenberg, C., Stetten, G., Montell, C., 1995. TRPC1, a human homolog of a Drosophila store-operated channel. PNAS 92, 9652–9656. https://doi.org/10.1073/pnas.92.21.9652

Williamson, M.P., 1994. The structure and function of proline-rich regions in proteins. Biochem. J. 297 (Pt 2), 249–260. https://doi.org/10.1042/bj2970249

Wilson, R.I., Corey, D.P., 2010. The force be with you: a mechanoreceptor channel in proprioception and touch. Neuron 67, 349–351. https://doi.org/10.1016/j.neuron.2010.07.022

Wilson, S.R., Gerhold, K.A., Bifolck-Fisher, A., Liu, Q., Patel, K.N., Dong, X., Bautista, D.M., 2011. TRPA1 is required for histamine-independent, Mas-related G protein-coupled receptor-mediated itch. Nat. Neurosci. 14, 595–602. https://doi.org/10.1038/nn.2789

Wilson, S.R., Thé, L., Batia, L.M., Beattie, K., Katibah, G.E., McClain, S.P., Pellegrino, M., Estandian, D.M., Bautista, D.M., 2013. The epithelial cell-derived atopic dermatitis cytokine TSLP activates neurons to induce itch. Cell 155, 285–295. https://doi.org/10.1016/j.cell.2013.08.057

Wing, L.-Y.C., Chen, H.-M., Chuang, P.-C., Wu, M.-H., Tsai, S.-J., 2005. The mammalian target of rapamycin-p70 ribosomal S6 kinase but not phosphatidylinositol 3-kinase-Akt signaling is responsible for fibroblast growth factor-9-induced cell proliferation. J. Biol. Chem. 280, 19937–19947. https://doi.org/10.1074/jbc.M411865200

Wong, R., Turlova, E., Feng, Z.-P., Rutka, J.T., Sun, H.-S., 2017. Activation of TRPM7 by naltriben enhances migration and invasion of glioblastoma cells. Oncotarget 8, 11239–11248. https://doi.org/10.18632/oncotarget.14496

Woo, J.S., Lee, K.J., Huang, M., Cho, C.-H., Lee, E.H., 2014. Heteromeric TRPC3 with TRPC1 formed via its ankyrin repeats regulates the resting cytosolic Ca2+ levels in skeletal muscle. Biochem. Biophys. Res. Commun. 446, 454–459. https://doi.org/10.1016/j.bbrc.2014.02.127

Wu, S., Fowler, D.K., Shaffer, F.J., Lindberg, J.E.M., Peters, J.H., 2017. Ethyl Vanillin Activates TRPA1. J Pharmacol Exp Ther 362, 368–377. https://doi.org/10.1124/jpet.116.239384

Wu, Y.-M., Su, F., Kalyana-Sundaram, S., Khazanov, N., Ateeq, B., Cao, X., Lonigro, R.J., Vats, P., Wang, R., Lin, S.-F., Cheng, A.-J., Kunju, L.P., Siddiqui, J., Tomlins, S.A., Wyngaard, P., Sadis, S., Roychowdhury,

S., Hussain, M.H., Feng, F.Y., Zalupski, M.M., Talpaz, M., Pienta, K.J., Rhodes, D.R., Robinson, D.R., Chinnaiyan, A.M., 2013. Identification of targetable FGFR gene fusions in diverse cancers. Cancer Discov 3, 636–647. https://doi.org/10.1158/2159-8290.CD-13-0050

Wu, Y.-T., Yen, S.-L., Li, C.-F., Chan, T.-C., Chen, T.-J., Lee, S.-W., He, H.-L., Chang, I.-W., Hsing, C.-H., Shiue, Y.-L., 2016. Overexpression of Transient Receptor Protein Cation Channel Subfamily A Member 1, Confers an Independent Prognostic Indicator in Nasopharyngeal Carcinoma. J Cancer 7, 1181–1188. https://doi.org/10.7150/jca.15326

Wybenga-Groot, L.E., Baskin, B., Ong, S.H., Tong, J., Pawson, T., Sicheri, F., 2001. Structural Basis for Autoinhibition of the EphB2 Receptor Tyrosine Kinase by the Unphosphorylated Juxtamembrane Region. Cell 106, 745–757. https://doi.org/10.1016/S0092-8674(01)00496-2

Xia, J., Wang, H., Huang, H., Sun, L., Dong, S., Huang, N., Shi, M., Bin, J., Liao, Y., Liao, W., 2016. Elevated Orai1 and STIM1 expressions upregulate MACC1 expression to promote tumor cell proliferation, metabolism, migration, and invasion in human gastric cancer. Cancer letters 381, 31–40. https://doi.org/10.1016/j.canlet.2016.07.014

Xiao, N., Jiang, L.M., Ge, B., Zhang, T.Y., Zhao, X.K., Zhou, X., 2014. Over-expression of TRPM8 is associated with poor prognosis in urothelial carcinoma of bladder. Tumour Biol. 35, 11499–11504. https://doi.org/10.1007/s13277-014-2480-1

Xu, C., Shen, G., Yuan, X., Kim, J.-H., Gopalkrishnan, A., Keum, Y.-S., Nair, S., Kong, A.-N.T., 2006. ERK and JNK signaling pathways are involved in the regulation of activator protein 1 and cell death elicited by three isothiocyanates in human prostate cancer PC-3 cells. Carcinogenesis 27, 437–445. https://doi.org/10.1093/carcin/bgi251

Xu, H., Delling, M., Jun, J.C., Clapham, D.E., 2006. Oregano, thyme and clove-derived flavors and skin sensitizers activate specific TRP channels. Nat. Neurosci. 9, 628–635. https://doi.org/10.1038/nn1692

Yang, L.-L., Liu, B.-C., Lu, X.-Y., Yan, Y., Zhai, Y.-J., Bao, Q., Doetsch, P.W., Deng, X., Thai, T.L., Alli, A.A., Eaton, D.C., Shen, B.-Z., Ma, H.-P., 2016. Inhibition of TRPC6 reduces non-small cell lung cancer cell proliferation and invasion. Oncotarget 8, 5123–5134. https://doi.org/10.18632/oncotarget.14034

Ye, Y., Dang, D., Zhang, J., Viet, C.T., Lam, D.K., Dolan, J.C., Gibbs, J.L., Schmidt, B.L., 2011. Nerve growth factor links oral cancer progression, pain, and cachexia. Mol. Cancer Ther. 10, 1667–1676. https://doi.org/10.1158/1535-7163.MCT-11-0123

Yee, N.S., 2017. Role of TRPM7 in Cancer: Potential as Molecular Biomarker and Therapeutic Target. Pharmaceuticals (Basel) 10. https://doi.org/10.3390/ph10020039

Yee, N.S., 2016. TRPM8 Ion Channels as Potential Cancer Biomarker and Target in Pancreatic Cancer. Adv Protein Chem Struct Biol 104, 127–155. https://doi.org/10.1016/bs.apcsb.2016.01.001

Yee, N.S., 2015. Roles of TRPM8 Ion Channels in Cancer: Proliferation, Survival, and Invasion. Cancers (Basel) 7, 2134–2146. https://doi.org/10.3390/cancers7040882

Yokoyama, N., Ischenko, I., Hayman, M.J., Miller, W.T., 2005. The C terminus of RON tyrosine kinase plays an autoinhibitory role. J. Biol. Chem. 280, 8893–8900. https://doi.org/10.1074/jbc.M412623200

Yu, K., Herr, A.B., Waksman, G., Ornitz, D.M., 2000. Loss of fibroblast growth factor receptor 2 ligand-binding specificity in Apert syndrome. Proc Natl Acad Sci U S A 97, 14536–14541.

Yu, S., Zhang, Y., Pan, Y., Cheng, C., Sun, Y., Chen, H., 2017. The non-small cell lung cancer EGFR extracellular domain mutation, M277E, is oncogenic and drug-sensitive. Onco Targets Ther 10, 4507–4515. https://doi.org/10.2147/OTT.S131999

Yu, X., Sharma, K.D., Takahashi, T., Iwamoto, R., Mekada, E., 2002. Ligand-independent dimer formation of epidermal growth factor receptor (EGFR) is a step separable from ligand-induced EGFR signaling. Mol. Biol. Cell 13, 2547–2557. https://doi.org/10.1091/mbc.01-08-0411

Yuzawa, S., Opatowsky, Y., Zhang, Z., Mandiyan, V., Lax, I., Schlessinger, J., 2007. Structural basis for activation of the receptor tyrosine kinase KIT by stem cell factor. Cell 130, 323–334. https://doi.org/10.1016/j.cell.2007.05.055

Zarich, N., Oliva, J.L., Martínez, N., Jorge, R., Ballester, A., Gutiérrez-Eisman, S., García-Vargas, S., Rojas, J.M., 2006. Grb2 Is a Negative Modulator of the Intrinsic Ras-GEF Activity of hSos1. Mol Biol Cell 17, 3591–3597. https://doi.org/10.1091/mbc.E05-12-1104

Zarrinpar, A., Bhattacharyya, R.P., Lim, W.A., n.d. The Structure and Function of Proline Recognition Domains 10.

Zhang, S., al-Maghout, T., Bissinger, R., Zeng, N., Pelzl, L., Salker, M.S., Cheng, A., Singh, Y., Lang, F., 2017. Epigallocatechin-3-gallate (EGCG) up-regulates miR-15b expression thus attenuating store operated calcium entry (SOCE) into murine CD4+ T cells and human leukaemic T cell lymphoblasts. Oncotarget 8, 89500–89514. https://doi.org/10.18632/oncotarget.20032

Zhang, X.-F., Chen, J., Faltynek, C.R., Moreland, R.B., Neelands, T.R., 2008. Transient receptor potential A1 mediates an osmotically activated ion channel. Eur. J. Neurosci. 27, 605–611. https://doi.org/10.1111/j.1460-9568.2008.06030.x

Zhang, Y., Cruickshanks, N., Yuan, F., Wang, B., Pahuski, M., Wulfkuhle, J., Gallagher, I., Koeppel, A.F., Hatef, S., Papanicolas, C., Lee, J., Bar, E.E., Schiff, D., Turner, S.D., Petricoin, E.F., Gray, L.S., Abounader, R., 2017. Targetable T-type Calcium Channels Drive Glioblastoma. Cancer Res. 77, 3479–3490. https://doi.org/10.1158/0008-5472.CAN-16-2347

Zhang, Z., Wang, J., He, J., Zeng, X., Chen, X., Xiong, M., Zhou, Q., Guo, M., Li, D., Lu, W., 2016. Identification of TRPCs genetic variants that modify risk for lung cancer based on the pathway and two-stage study. Meta Gene 9, 191–196. https://doi.org/10.1016/j.mgene.2016.07.005

Zhao, Q., Caballero, O.L., Davis, I.D., Jonasch, E., Tamboli, P., Yung, W.K.A., Weinstein, J.N., Kenna Shaw for TCGA research network, Strausberg, R.L., Yao, J., 2013. Tumor-specific isoform switch of the fibroblast growth factor receptor 2 underlies the mesenchymal and malignant phenotypes of clear cell renal cell carcinomas. Clin. Cancer

Res. 19, 2460–2472. https://doi.org/10.1158/1078-0432.CCR-12-3708

Zhu, X., Chu, P.B., Peyton, M., Birnbaumer, L., 1995. Molecular cloning of a widely expressed human homologue for the Drosophila trp gene. FEBS Letters 373, 193–198. https://doi.org/10.1016/0014-5793(95)01038-G

Zhu, X., Jiang, M., Peyton, M., Boulay, G., Hurst, R., Stefani, E., Birnbaumer, L., 1996. trp, a Novel Mammalian Gene Family Essential for Agonist-Activated Capacitative Ca2+ Entry. Cell 85, 661–671. https://doi.org/10.1016/S0092-8674(00)81233-7

Zurborg, S., Yurgionas, B., Jira, J.A., Caspani, O., Heppenstall, P.A., 2007. Direct activation of the ion channel TRPA1 by Ca2+. Nat. Neurosci. 10, 277–279. https://doi.org/10.1038/nn1843

7. Appendix

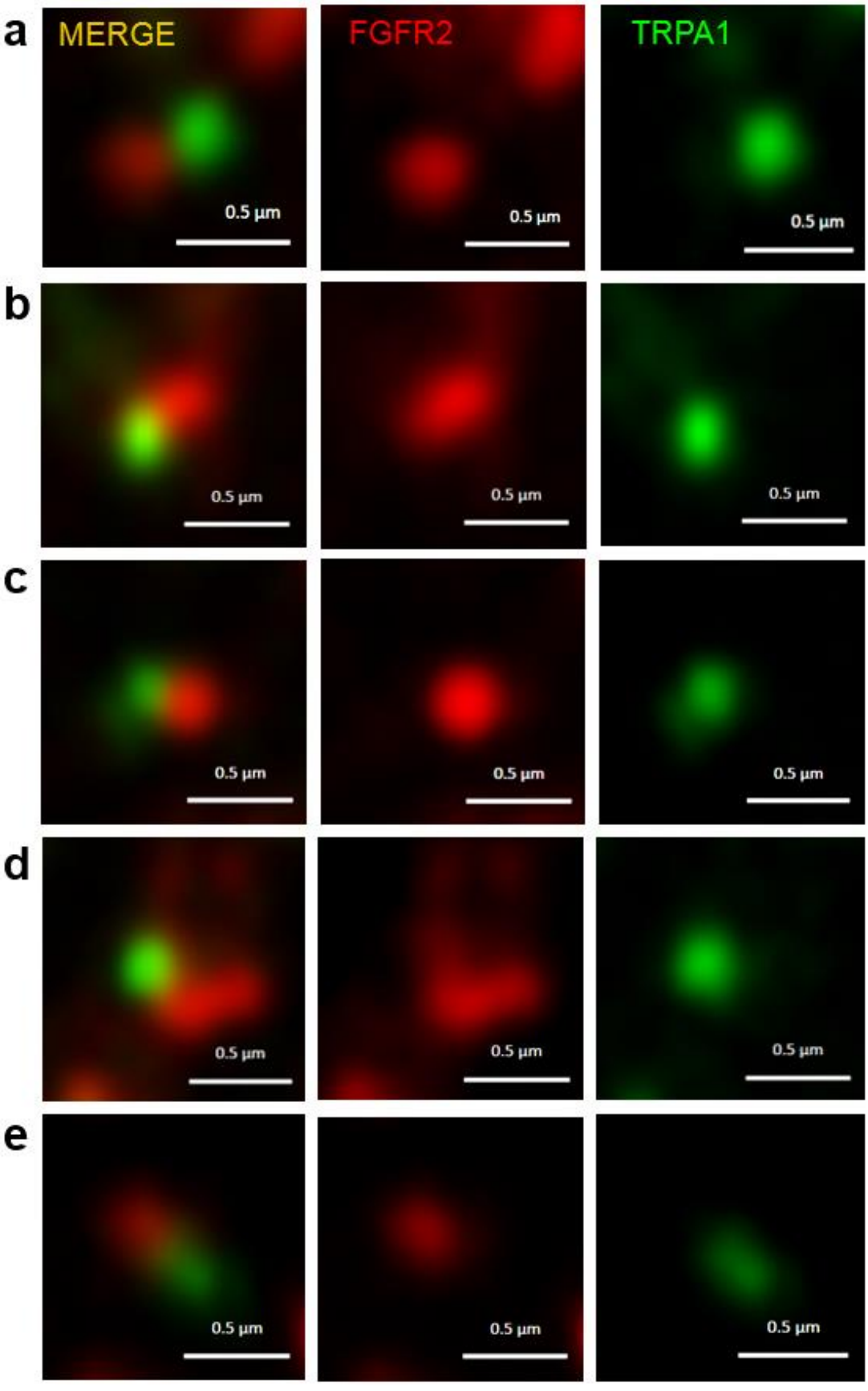

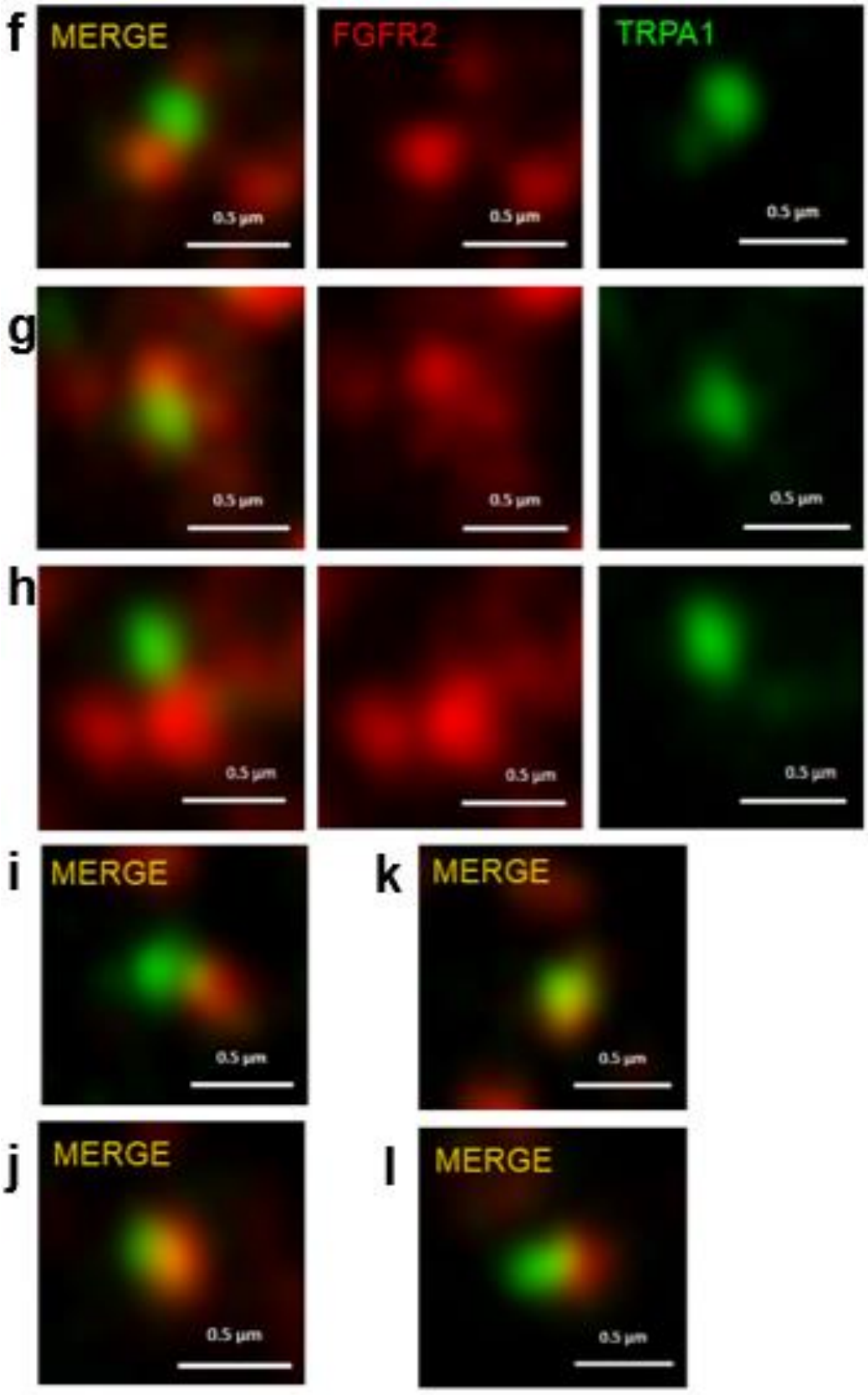

Appendix 1: Representative FGFR2-TRPA1 complexes as captured by ExM 10X. Scale bars represent 500nm/10 (expansion factor) = 50nm.